

NOAA
Professional Paper 13



Climatological Atlas of the World Ocean

Rockville, Md.
December 1982

U.S. Department of Commerce
National Oceanic and Atmospheric Administration

ERRATA SHEET for: "Climatological Atlas of the World Ocean" NOAA
Professional Paper No. 13

- 1) Page 108, Table 65, column 5. Potential density should have units of (10^{-3}g/cm^3).
- 2) Page 23, Equation 17. There should be a square root operator enclosing the entire right side of this equation.
- 3) Throughout the atlas the quantity Brunt-Väisälä frequency is specified as having units of cycles/hour. This is incorrect. The correct units are radians/hour.

Contents

Foreword	xiv
Preface	xv
Abstract	
1. Introduction	
2. Data and data distribution	2
2.1 Data sources	2
2.2 Data reduction and quality control	4
2.2a Range checking	4
2.2b Static stability check	4
2.2c Statistical check	4
2.2d Elimination of spurious data	5
2.2e An example of quality control problems with legitimate data	5
2.2f Modification and elimination of existing data	6
2.2g Positional errors	6
2.3 Representativeness of the data	6
3. Objective analysis procedures	8
3.1 Method of analysis	8
3.1a Derivation of weight function	9
3.1b Response function	9
3.1c Choice of influence radii	10
3.1d First-guess field determination	11
3.2 Additional comments on the objective analysis procedures	11
3.2a Use of dynamic parameters for determining influence radii	11
3.2b Possible need for additional smoothing	12
3.2c Choice of resolution	12
3.2d Modification of the analyses	13
4. Introduction to results	13
5. Basic analyses	13
5.1 Annual mean potential temperature	13
5.2 Annual mean salinity	15
5.3 Annual mean dissolved oxygen and percent oxygen-saturation	17
6. Derived quantities	19
6.1 Depth and characteristics of the annual mean absolute oxygen minimum surface	19
6.2 Annual mean anomaly of geopotential thickness	20
6.3 Annual mean Brunt-Väisälä frequency	23
6.4 Depth and characteristics of the annual mean 27.7 potential density surface	24
6.5 Seasonal density distributions	25
6.6 Depth and salinity of the annual mean 4 °C potential temperature surface	25
6.7 Mixed-layer distributions	26
7. Zonal averages	28
8. Basin mean profiles and volume means	29
9. Summary	31
10. Recommendations and future work	31
11. References	32

Contents

12. Appendix A: The effect of smoothing on a sea surface temperature field	35
13. Appendix B: The effect of the first-guess field on a sea surface temperature field	36
14. Appendix C: Definitions of potential temperature and density parameters	36
15. Appendix D: Objective analyses of the standard deviation of temperature	37
16. Appendix E: User's guide to microfiche	38

List of Tables

- Table 1. Distribution with depth of the number of one-degree square of ocean (Ocean ODSQS), the total number (N) of temperature, salinity, and oxygen observations; and the number of one-degree squares (ODSQS) containing observations of each of these parameters.
- Table 2. Number of surface salinity observations in the ten most densely sampled Marsden squares.
- Table 3. Range of acceptable temperature and salinity values as a function of depth.
- Table 4a. Annual mean potential temperature ($^{\circ}\text{C}$) area-weighted means over five-degree latitude belts for the world ocean as a function of depth, Southern Hemisphere.
- Table 4b. Annual mean potential temperature ($^{\circ}\text{C}$) area-weighted means over five-degree latitude belts for the world ocean as a function of depth, Northern Hemisphere.
- Table 5a. Annual mean potential temperature ($^{\circ}\text{C}$) area-weighted r.m.s. deviations over five-degree latitude belts for the world ocean as a function of depth, Southern Hemisphere.
- Table 5b. Annual mean potential temperature ($^{\circ}\text{C}$) area weighted r.m.s. deviations over five-degree latitude belts for the world ocean as a function of depth, Northern Hemisphere.
- Table 6a. Annual mean salinity ($^{\circ}/\text{.}$) area-weighted means over five-degree latitude belts for the world ocean as a function of depth, Southern Hemisphere.
- Table 6b. Annual mean salinity ($^{\circ}/\text{.}$) area-weighted means over five-degree latitude belts for the world ocean as a function of depth, Northern Hemisphere.
- Table 7a. Annual mean salinity ($^{\circ}/\text{.}$) area-weighted r.m.s. deviations over five-degree latitude belts for the world ocean as a function of depth, Southern Hemisphere.
- Table 7b. Annual mean salinity ($^{\circ}/\text{.}$) area-weighted r.m.s. deviations over five-degree latitude belts for the world ocean as a function of depth, Northern Hemisphere.
- Table 8a. Annual mean potential density ($10^{-3}\text{g}/\text{cm}^3$) area-weighted means over five-degree latitude belts for the world ocean as a function of depth, Southern Hemisphere.
- Table 8b. Annual mean potential density ($10^{-3}\text{g}/\text{cm}^3$) area-weighted means over five-degree latitude belts for the world ocean as a function of depth, Northern Hemisphere.
- Table 9a. Annual mean potential density ($10^{-3}\text{g}/\text{cm}^3$) area-weighted r.m.s. deviations over five-degree latitude belts for the world ocean as a function of depth, Southern Hemisphere.
- Table 9b. Annual mean potential density ($10^{-3}\text{g}/\text{cm}^3$) area-weighted r.m.s. deviations over five-degree latitude belts for the world ocean as a function of depth, Northern Hemisphere.
- Table 10a. Annual mean Brunt-Väisälä frequency (cycles/hr) area-weighted means over five-degree latitude belts for the world ocean as a function of depth, Southern Hemisphere.
- Table 10b. Annual mean Brunt-Väisälä frequency (cycles/hr) area-weighted means over five-degree latitude belts for the world ocean as a function of depth, Northern Hemisphere.
- Table 11a. Annual mean Brunt-Väisälä frequency (cycles/hr) area-weighted r.m.s. deviations over five-degree latitude belts for the world ocean as a function of depth, Southern Hemisphere.
- Table 11b. Annual mean Brunt-Väisälä frequency (cycles/hr) area-weighted r.m.s. deviations over five-degree latitude belts for the world ocean as a function of depth, Northern Hemisphere.
- Table 12a. Annual mean dissolved oxygen (ml/l) area-weighted means over five-degree latitude belts for the world ocean as a function of depth, Southern Hemisphere.
- Table 12b. Annual mean dissolved oxygen (ml/l) area-weighted means over five-degree latitude belts for the world ocean as a function of depth, Northern Hemisphere.
- Table 13a. Annual mean dissolved oxygen (ml/l) area-weighted r.m.s. deviations over five-degree latitude belts for the world ocean as a function of depth, Southern Hemisphere.
- Table 13b. Annual mean dissolved oxygen (ml/l) area-weighted r.m.s. deviations over five-degree latitude belts for the world ocean as a function of depth, Northern Hemisphere.
- Table 14a. Annual mean oxygen-saturation (%) area-weighted means over five-degree latitude belts for the world ocean as a function of depth, Southern Hemisphere.
- Table 14b. Annual mean oxygen-saturation (%) area-weighted means over five-degree latitude belts for the world ocean as a function of depth, Northern Hemisphere.
- Table 15a. Annual mean oxygen-saturation (%) area-weighted r.m.s. deviations over five-degree latitude belts for the world ocean as a function of depth, Southern Hemisphere.
- Table 15b. Annual mean oxygen-saturation (%) area-weighted r.m.s. deviations over five-de-

Contents

- Table 16a. Annual mean potential temperature ($^{\circ}\text{C}$) area-weighted means over five-degree latitude belts for the Pacific Ocean as a function of depth, Southern Hemisphere.
- Table 16b. Annual mean potential temperature ($^{\circ}\text{C}$) area-weighted means over five-degree latitude belts for the Pacific Ocean as a function of depth, Northern Hemisphere.
- Table 17a. Annual mean potential temperature ($^{\circ}\text{C}$) area-weighted r.m.s. deviations over five-degree latitude belts for the Pacific Ocean as a function of depth, Southern Hemisphere.
- Table 17b. Annual mean potential temperature ($^{\circ}\text{C}$) area-weighted r.m.s. deviations over five-degree latitude belts for the Pacific Ocean as a function of depth, Northern Hemisphere.
- Table 18a. Annual mean salinity ($^{\circ}/\text{.}$) area-weighted means over five-degree latitude belts for the Pacific Ocean as a function of depth, Southern Hemisphere.
- Table 18b. Annual mean salinity ($^{\circ}/\text{.}$) area-weighted means over five-degree latitude belts for the Pacific Ocean as a function of depth, Northern Hemisphere.
- Table 19a. Annual mean salinity ($^{\circ}/\text{.}$) area-weighted r.m.s. deviations over five-degree latitude belts for the Pacific Ocean as a function of depth, Southern Hemisphere.
- Table 19b. Annual mean salinity ($^{\circ}/\text{.}$) area-weighted r.m.s. deviations over five-degree latitude belts for the Pacific Ocean as a function of depth, Northern Hemisphere.
- Table 20a. Annual mean potential density ($10^{-3}\text{g}/\text{cm}^3$) area-weighted means over five-degree latitude belts for the Pacific Ocean as a function of depth, Southern Hemisphere.
- Table 20b. Annual mean potential density ($10^{-3}\text{g}/\text{cm}^3$) area-weighted means over five-degree latitude belts for the Pacific Ocean as a function of depth, Northern Hemisphere.
- Table 21a. Annual mean potential density ($10^{-3}\text{g}/\text{cm}^3$) area-weighted r.m.s. deviations over five-degree latitude belts for the Pacific Ocean as a function of depth, Southern Hemisphere.
- Table 21b. Annual mean potential density ($10^{-3}\text{g}/\text{cm}^3$) area-weighted r.m.s. deviations over five-degree latitude belts for the Pacific Ocean as a function of depth, Northern Hemisphere.
- Table 22a. Annual mean Brunt-Väisälä frequency (cycles/hr) area-weighted means over five-degree latitude belts for the Pacific Ocean as a function of depth, Southern Hemisphere.
- Table 22b. Annual mean Brunt-Väisälä frequency (cycles/hr) area-weighted means over five-degree latitude belts for the Pacific Ocean as a function of depth, Northern Hemisphere.
- Table 23a. Annual mean Brunt-Väisälä frequency (cycles/hr) area-weighted r.m.s. deviations over five-degree latitude belts for the Pacific Ocean as a function of depth, Southern Hemisphere.
- Table 23b. Annual mean Brunt-Väisälä frequency (cycles/hr) area-weighted r.m.s. deviations over five-degree latitude belts for the Pacific Ocean as a function of depth, Northern Hemisphere.
- Table 24a. Annual mean dissolved oxygen (ml/l) area-weighted means over five-degree latitude belts for the Pacific Ocean as a function of depth, Southern Hemisphere.
- Table 24b. Annual mean dissolved oxygen (ml/l) area-weighted means over five-degree latitude belts for the Pacific Ocean as a function of depth, Northern Hemisphere.
- Table 25a. Annual mean dissolved oxygen (ml/l) area-weighted r.m.s. deviations over five-degree latitude belts for the Pacific Ocean as a function of depth, Southern Hemisphere.
- Table 25b. Annual mean dissolved oxygen (ml/l) area-weighted r.m.s. deviations over five-degree latitude belts for the Pacific Ocean as a function of depth, Northern Hemisphere.
- Table 26a. Annual mean oxygen-saturation (%) area-weighted means over five-degree latitude belts for the Pacific Ocean as a function of depth, Southern Hemisphere.
- Table 26b. Annual mean oxygen-saturation (%) area-weighted means over five-degree latitude belts for the Pacific Ocean as a function of depth, Northern Hemisphere.
- Table 27a. Annual mean oxygen-saturation (%) area-weighted r.m.s. deviations over five-degree latitude belts for the Pacific Ocean as a function of depth, Southern Hemisphere.
- Table 27b. Annual mean oxygen-saturation (%) area-weighted r.m.s. deviations over five-degree latitude belts for the Pacific Ocean as a function of depth, Northern Hemisphere.
- Table 28a. Annual mean potential temperature ($^{\circ}\text{C}$) area-weighted means over five-degree latitude belts for the Atlantic Ocean as a function of depth, Southern Hemisphere.
- Table 28b. Annual mean potential temperature ($^{\circ}\text{C}$) area-weighted means over five-degree latitude belts for the Atlantic Ocean as a function of depth, Northern Hemisphere.
- Table 29a. Annual mean potential temperature ($^{\circ}\text{C}$) area-weighted r.m.s. deviations over five-degree latitude belts for the Atlantic Ocean as a function of depth, Southern Hemisphere.
- Table 29b. Annual mean potential temperature ($^{\circ}\text{C}$) area-weighted r.m.s. deviations over five-degree latitude belts for the Atlantic Ocean as a function of depth, Northern Hemisphere.

Contents

- Table 30a. Annual mean salinity (‰) area-weighted means over five-degree latitude belts for the Atlantic Ocean as a function of depth, Southern Hemisphere.
- Table 30b. Annual mean salinity (‰) area-weighted means over five-degree latitude belts for the Atlantic Ocean as a function of depth, Northern Hemisphere.
- Table 31a. Annual mean salinity (‰) area-weighted r.m.s. deviations over five-degree latitude belts for the Atlantic Ocean as a function of depth, Southern Hemisphere.
- Table 31b. Annual mean salinity (‰) area-weighted r.m.s. deviations over five-degree latitude belts for the Atlantic Ocean as a function of depth, Northern Hemisphere.
- Table 32a. Annual mean potential density (10^{-3}g/cm^3) area-weighted means over five-degree latitude belts for the Atlantic Ocean as a function of depth, Southern Hemisphere.
- Table 32b. Annual mean potential density (10^{-3}g/cm^3) area-weighted means over five-degree latitude belts for the Atlantic Ocean as a function of depth, Northern Hemisphere.
- Table 33a. Annual mean potential density (10^{-3}g/cm^3) area-weighted r.m.s. deviations over a five-degree latitude belts for the Atlantic Ocean as a function of depth, Southern Hemisphere.
- Table 33b. Annual mean potential density (10^{-3}g/cm^3) area-weighted r.m.s. deviations over a five-degree latitude belts for the Atlantic Ocean as a function of depth, Northern Hemisphere.
- Table 34a. Annual mean Brunt-Väisälä frequency (cycles/hr) area-weighted means over five-degree latitude belts for the Atlantic Ocean as a function of depth, Southern Hemisphere.
- Table 34b. Annual mean Brunt-Väisälä frequency (cycles/hr) area-weighted means over five-degree latitude belts for the Atlantic Ocean as a function of depth, Northern Hemisphere.
- Table 35a. Annual mean Brunt-Väisälä frequency (cycles/hr) area-weighted r.m.s. deviations over five-degree latitude belts for the Atlantic Ocean as a function of depth, Southern Hemisphere.
- Table 35b. Annual mean Brunt-Väisälä frequency (cycles/hr) area-weighted r.m.s. deviations over five-degree latitude belts for the Atlantic Ocean as a function of depth, Northern Hemisphere.
- Table 36a. Annual mean dissolved oxygen (ml/l) area-weighted means over five-degree latitude belts for the Atlantic Ocean as a function of depth, Southern Hemisphere.
- Table 36b. Annual mean dissolved oxygen (ml/l) area-weighted means over five-degree latitude belts for the Atlantic Ocean as a function of depth, Northern Hemisphere.
- Table 37a. Annual mean dissolved oxygen (ml/l) area-weighted r.m.s. deviations over five-degree belts for the Atlantic Ocean as a function of depth, Southern Hemisphere.
- Table 37b. Annual mean dissolved oxygen (ml/l) area-weighted r.m.s. deviations over five-degree belts for the Atlantic Ocean as a function of depth, Northern Hemisphere.
- Table 38a. Annual mean oxygen-saturation (%) area-weighted means over five-degree belts for the Atlantic Ocean as a function of depth, Southern Hemisphere.
- Table 38b. Annual mean oxygen-saturation (%) area-weighted means over five-degree belts for the Atlantic Ocean as a function of depth, Northern Hemisphere.
- Table 39a. Annual mean oxygen-saturation (%) area-weighted r.m.s. deviations over five-degree latitude belts for the Atlantic Ocean as a function of depth, Southern Hemisphere.
- Table 39b. Annual mean oxygen-saturation (%) area-weighted r.m.s. deviations over five-degree latitude belts for the Atlantic Ocean as a function of depth, Northern Hemisphere.
- Table 40a. Annual mean potential temperature ($^{\circ}\text{C}$) area-weighted means over five-degree latitude belts for the Indian Ocean as a function of depth, Southern Hemisphere.
- Table 40b. Annual mean potential temperature ($^{\circ}\text{C}$) area-weighted means over five-degree latitude belts for the Indian Ocean as a function of depth, Northern Hemisphere.
- Table 41a. Annual mean potential temperature ($^{\circ}\text{C}$) area-weighted r.m.s. deviations over five-degree latitude belts for the Indian Ocean as a function of depth, Southern Hemisphere.
- Table 41b. Annual mean potential temperature ($^{\circ}\text{C}$) area-weighted r.m.s. deviations over five-degree latitude belts for the Indian Ocean as a function of depth, Northern Hemisphere.
- Table 42a. Annual mean salinity (‰) area-weighted means over five-degree latitude belts for the Indian Ocean as a function of depth, Southern Hemisphere.

- Table 42b. Annual mean salinity ($^{\circ}/\text{‰}$) area-weighted means over five-degree latitude belts for the Indian Ocean as a function of depth, Northern Hemisphere.
- Table 43a. Annual mean salinity ($^{\circ}/\text{‰}$) area-weighted r.m.s. deviations over five-degree latitude belts for the Indian Ocean as a function of depth, Southern Hemisphere.
- Table 43b. Annual mean salinity ($^{\circ}/\text{‰}$) area-weighted r.m.s. deviations over five-degree latitude belts for the Indian Ocean as a function of depth, Northern Hemisphere.
- Table 44a. Annual mean potential density ($10^{-3}\text{g}/\text{cm}^3$) area-weighted means over five-degree latitude belts for the Indian Ocean as a function of depth, Southern Hemisphere.
- Table 44b. Annual mean potential density ($10^{-3}\text{g}/\text{cm}^3$) area-weighted means over five-degree latitude belts for the Indian Ocean as a function of depth, Northern Hemisphere.
- Table 45a. Annual mean potential density ($10^{-3}\text{g}/\text{cm}^3$) area-weighted r.m.s. deviations over five-degree latitude belts for the Indian Ocean as a function of depth, Southern Hemisphere.
- Table 45b. Annual mean potential density ($10^{-3}\text{g}/\text{cm}^3$) area-weighted r.m.s. deviations over five-degree latitude belts for the Indian Ocean as a function of depth, Northern Hemisphere.
- Table 46a. Annual mean Brunt-Väisälä frequency (cycles/hr) area-weighted means over five-degree latitude belts for the Indian Ocean as a function of depth, Southern Hemisphere.
- Table 46b. Annual mean Brunt-Väisälä frequency (cycles/hr) area-weighted means over five-degree latitude belts for the Indian Ocean as a function of depth, Northern Hemisphere.
- Table 47a. Annual mean Brunt-Väisälä frequency (cycles/hr) area-weighted r.m.s. deviations over five-degree latitude belts for the Indian Ocean as a function of depth, Southern Hemisphere.
- Table 47b. Annual mean Brunt-Väisälä frequency (cycles/hr) area-weighted r.m.s. deviations over five-degree latitude belts for the Indian Ocean as a function of depth, Northern Hemisphere.
- Table 48a. Annual mean dissolved oxygen (ml/l) area-weighted means over five-degree latitude belts for the Indian Ocean as a function of depth, Southern Hemisphere.
- Table 48b. Annual mean dissolved oxygen (ml/l) area-weighted means over five-degree latitude belts for the Indian Ocean as a function of depth, Northern Hemisphere.
- Table 49a. Annual mean dissolved oxygen (ml/l) area-weighted r.m.s. deviations over five-degree latitude belts for the Indian Ocean as a function of depth, Southern Hemisphere.
- Table 49b. Annual mean dissolved oxygen (ml/l) area-weighted r.m.s. deviations over five-degree latitude belts for the Indian Ocean as a function of depth, Northern Hemisphere.
- Table 50a. Annual mean oxygen-saturation (%) area-weighted means over five-degree latitude belts for the Indian Ocean as a function of depth, Southern Hemisphere.
- Table 50b. Annual mean oxygen-saturation (%) area-weighted means over five-degree latitude belts for the Indian Ocean as a function of depth, Northern Hemisphere.
- Table 51a. Annual mean oxygen-saturation (%) area-weighted r.m.s. deviations over five-degree latitude belts for the Indian Ocean as a function of depth, Southern Hemisphere.
- Table 51b. Annual mean oxygen-saturation (%) area-weighted r.m.s. deviations over five-degree latitude belts for the Indian Ocean as a function of depth, Northern Hemisphere.
- Table 52a. Total area (10^4km^2) of five-degree latitude belts as a function of depth for the world ocean, Southern Hemisphere.
- Table 52b. Total area (10^4km^2) of five-degree latitude belts as a function of depth for the world ocean, Northern Hemisphere.
- Table 53a. Total area (10^4km^2) of five-degree latitude belts as a function of depth for the Pacific Ocean, Southern Hemisphere.
- Table 53b. Total area (10^4km^2) of five-degree latitude belts as a function of depth for the Pacific Ocean, Northern Hemisphere.
- Table 54a. Total area (10^4km^2) of five-degree latitude belts as a function of depth for the Atlantic Ocean, Southern Hemisphere.
- Table 54b. Total area (10^4km^2) of five-degree latitude belts as a function of depth for the Atlantic Ocean, Northern Hemisphere.
- Table 55a. Total area (10^4km^2) of five-degree latitude belts as a function of depth for the Indian Ocean, Southern Hemisphere.
- Table 55b. Total area (10^4km^2) of five-degree latitude belts as a function of depth for the Indian Ocean, Northern Hemisphere.
- Table 56a. Annual mean potential temperature ($^{\circ}\text{C}$) basin means and standard errors for the world ocean and Atlantic Ocean as a function of depth.

Contents

- Table 56b. Annual mean potential temperature ($^{\circ}\text{C}$) basin means and standard errors for the Pacific Ocean and Indian Ocean as a function of depth.
- Table 57a. Annual mean salinity ($^{\circ}/\text{.}$) basin means and standard errors for the world ocean and Atlantic Ocean as a function of depth.
- Table 57b. Annual mean salinity ($^{\circ}/\text{.}$) basin means and standard errors for the Pacific Ocean and Indian Ocean as a function of depth.
- Table 58a. Annual mean potential density ($10^{-3}\text{g}/\text{cm}^3$) basin means and standard errors for the world ocean and the Atlantic Ocean as a function of depth.
- Table 58b. Annual mean potential density ($10^{-3}\text{g}/\text{cm}^3$) basin means and standard errors for the Pacific Ocean and Indian Ocean as a function of depth.
- Table 59a. Annual mean dissolved oxygen (ml/l) basin means and standard errors for the world ocean and Atlantic Ocean as a function of depth.
- Table 59b. Annual mean dissolved oxygen (ml/l) basin means and standard errors for the Pacific Ocean and Atlantic Ocean as a function of depth.
- Table 60a. Annual mean oxygen-saturation (%) basin means and standard errors for the world ocean and Atlantic Ocean as a function of depth.
- Table 60b. Annual mean oxygen-saturation (%) basin means and standard errors for the Pacific Ocean and Indian Ocean as a function of depth.
- Table 61. Area, volume, percent volume contribution of each standard level to total basin volume, and the number of points (N_p) used in the standard error computation for the world ocean as a function of depth.
- Table 62. Area, volume, percent volume contribution of each standard level to total basin volume, and the number of points (N_p) used in the standard error computation for the Atlantic Ocean as a function of depth.
- Table 63. Area, volume, percent volume contribution of each standard level to total basin volume, and the number of points (N_p) used in the standard error computation for the Pacific Ocean as a function of depth.
- Table 64. Area, volume, percent volume contribution of each standard level to total basin volume, and the number of points (N_p) used in the standard error computation for the Indian Ocean as a function of depth.
- Table 65. Volume means of potential temperature, salinity, potential density, oxygen, and oxygen-saturation for the major ocean basins and the volume of each basin. Values in parentheses are those computed by Montgomery (1958), Cochrane (1958), and Pollack (1958).
- Table A1. Response function of the test analysis.
- Table E1. Listing of microfiche contents.

List of Figures

- Figure 1. Distribution of (a) SD temperature observations, (b) MBT observations, and (c) XBT observations as a function of depth for the globe and the Northern and Southern Hemispheres.
- Figure 2. Time series of Station Data temperature observations.
- Figure 3. Time series of Station Data oxygen observations.
- Figure 4. Time series of MBT casts.
- Figure 5. Time series of XBT casts.
- Figure 6. Sea surface distribution of one-degree squares containing temperature observations from the merged temperature data set ($SD+MBT+XBT$) for Northern Hemisphere winter (February, March, April). A small dot indicates a one-degree square containing 1-4 observations, a large dot indicates 5 or more observations.
- Figure 7. Sea surface distribution of one-degree squares containing temperature observations from the merged temperature data set ($SD+MBT+XBT$) for Northern Hemisphere summer (August, September, October). A small dot indicates a one-degree square containing 1-4 observations, a large dot indicates 5 or more observations.
- Figure 8. Sea surface distribution of one-degree squares containing salinity observations for Northern Hemisphere summer (August, September, October). A small dot indicates a one-degree square containing 1-4 observations, a large dot indicates 5 or more observations.
- Figure 9. Distribution of one-degree squares containing salinity observations at a depth of 2000 m for the annual period. A small dot indicates a one-degree square containing 1-9 observations, a large dot indicates 10 or more observations.
- Figure 10. Sea surface distribution of one-degree squares containing oxygen observations for the annual period. A small dot indicates a square containing 1-9 observations, a large dot indicates 10 or more observations.
- Figure 11. Response function of the objective analysis.
- Figure 12. Annual mean potential temperature ($^{\circ}\text{C}$) at the sea surface.
- Figure 13. Annual mean potential temperature ($^{\circ}\text{C}$) at 150 m depth.
- Figure 14. Annual mean potential temperature ($^{\circ}\text{C}$) at 500 m depth.
- Figure 15. Annual mean potential temperature ($^{\circ}\text{C}$) at 1000 m depth.
- Figure 16. Annual mean potential temperature ($^{\circ}\text{C}$) at 1500 m depth.
- Figure 17. Annual mean potential temperature ($^{\circ}\text{C}$) at 2000 m depth.
- Figure 18. Annual mean potential temperature ($^{\circ}\text{C}$) at 2500 m depth.
- Figure 19. Annual mean potential temperature ($^{\circ}\text{C}$) at 3000 m depth.
- Figure 20. Annual mean potential temperature ($^{\circ}\text{C}$) at 3500 m depth.
- Figure 21. Annual mean potential temperature ($^{\circ}\text{C}$) at 4000 m depth.
- Figure 22. Annual mean salinity ($^{\circ}/\text{‰}$) at the sea surface.
- Figure 23. Annual mean salinity ($^{\circ}/\text{‰}$) at 150 m depth.
- Figure 24. Annual mean salinity ($^{\circ}/\text{‰}$) at 500 m depth.
- Figure 25. Annual mean salinity ($^{\circ}/\text{‰}$) at 1000 m depth.
- Figure 26. Annual mean salinity ($^{\circ}/\text{‰}$) at 1500 m depth.
- Figure 27. Annual mean salinity ($^{\circ}/\text{‰}$) at 2000 m depth.
- Figure 28. Annual mean salinity ($^{\circ}/\text{‰}$) at 2500 m depth.
- Figure 29. Annual mean salinity ($^{\circ}/\text{‰}$) at 3000 m depth.
- Figure 30. Annual mean salinity ($^{\circ}/\text{‰}$) at 3500 m depth.
- Figure 31. Annual mean salinity ($^{\circ}/\text{‰}$) at 4000 m depth.
- Figure 32. Annual mean oxygen (ml/l) at the sea surface.
- Figure 33. Annual mean oxygen-saturation (%) at the sea surface.
- Figure 34. Annual mean oxygen (ml/l) at 150 m depth.
- Figure 35. Annual mean oxygen-saturation (%) at 150 m depth.
- Figure 36. Annual mean oxygen (ml/l) at 500 m depth.
- Figure 37. Annual mean oxygen-saturation (%) at 500 m depth.
- Figure 38. Annual mean oxygen (ml/l) at 1000 m depth.
- Figure 39. Annual mean oxygen-saturation (%) at 1000 m depth.
- Figure 40. Annual mean oxygen (ml/l) at 1500 m depth.

List of Tables

- Table 1. Distribution with depth of the number of one-degree square of ocean (Ocean ODSQS), the total number (N) of temperature, salinity, and oxygen observations; and the number of one-degree squares (ODSQS) containing observations of each of these parameters.
- Table 2. Number of surface salinity observations in the ten most densely sampled Marsden squares.
- Table 3. Range of acceptable temperature and salinity values as a function of depth.
- Table 4a. Annual mean potential temperature ($^{\circ}\text{C}$) area-weighted means over five-degree latitude belts for the world ocean as a function of depth, Southern Hemisphere.
- Table 4b. Annual mean potential temperature ($^{\circ}\text{C}$) area-weighted means over five-degree latitude belts for the world ocean as a function of depth, Northern Hemisphere.
- Table 5a. Annual mean potential temperature ($^{\circ}\text{C}$) area-weighted r.m.s. deviations over five-degree latitude belts for the world ocean as a function of depth, Southern Hemisphere.
- Table 5b. Annual mean potential temperature ($^{\circ}\text{C}$) area weighted r.m.s. deviations over five-degree latitude belts for the world ocean as a function of depth, Northern Hemisphere.
- Table 6a. Annual mean salinity ($^{\circ}/\text{‰}$) area-weighted means over five-degree latitude belts for the world ocean as a function of depth, Southern Hemisphere.
- Table 6b. Annual mean salinity ($^{\circ}/\text{‰}$) area-weighted means over five-degree latitude belts for the world ocean as a function of depth, Northern Hemisphere.
- Table 7a. Annual mean salinity ($^{\circ}/\text{‰}$) area-weighted r.m.s. deviations over five-degree latitude belts for the world ocean as a function of depth, Southern Hemisphere.
- Table 7b. Annual mean salinity ($^{\circ}/\text{‰}$) area-weighted r.m.s. deviations over five-degree latitude belts for the world ocean as a function of depth, Northern Hemisphere.
- Table 8a. Annual mean potential density ($10^{-3}\text{g}/\text{cm}^3$) area-weighted means over five-degree latitude belts for the world ocean as a function of depth, Southern Hemisphere.
- Table 8b. Annual mean potential density ($10^{-3}\text{g}/\text{cm}^3$) area-weighted means over five-degree latitude belts for the world ocean as a function of depth, Northern Hemisphere.
- Table 9a. Annual mean potential density ($10^{-3}\text{g}/\text{cm}^3$) area-weighted r.m.s. deviations over five-degree latitude belts for the world ocean as a function of depth, Southern Hemisphere.
- Table 9b. Annual mean potential density ($10^{-3}\text{g}/\text{cm}^3$) area-weighted r.m.s. deviations over five-degree latitude belts for the world ocean as a function of depth, Northern Hemisphere.
- Table 10a. Annual mean Brunt-Väisälä frequency (cycles/hr) area-weighted means over five-degree latitude belts for the world ocean as a function of depth, Southern Hemisphere.
- Table 10b. Annual mean Brunt-Väisälä frequency (cycles/hr) area-weighted means over five-degree latitude belts for the world ocean as a function of depth, Northern Hemisphere.
- Table 11a. Annual mean Brunt-Väisälä frequency (cycles/hr) area-weighted r.m.s. deviations over five-degree latitude belts for the world ocean as a function of depth, Southern Hemisphere.
- Table 11b. Annual mean Brunt-Väisälä frequency (cycles/hr) area-weighted r.m.s. deviations over five-degree latitude belts for the world ocean as a function of depth, Northern Hemisphere.
- Table 12a. Annual mean dissolved oxygen (ml/l) area-weighted means over five-degree latitude belts for the world ocean as a function of depth, Southern Hemisphere.
- Table 12b. Annual mean dissolved oxygen (ml/l) area-weighted means over five-degree latitude belts for the world ocean as a function of depth, Northern Hemisphere.
- Table 13a. Annual mean dissolved oxygen (ml/l) area-weighted r.m.s. deviations over five-degree latitude belts for the world ocean as a function of depth, Southern Hemisphere.
- Table 13b. Annual mean dissolved oxygen (ml/l) area-weighted r.m.s. deviations over five-degree latitude belts for the world ocean as a function of depth, Northern Hemisphere.
- Table 14a. Annual mean oxygen-saturation (%) area-weighted means over five-degree latitude belts for the world ocean as a function of depth, Southern Hemisphere.
- Table 14b. Annual mean oxygen-saturation (%) area-weighted means over five-degree latitude belts for the world ocean as a function of depth, Northern Hemisphere.
- Table 15a. Annual mean oxygen-saturation (%) area-weighted r.m.s. deviations over five-degree latitude belts for the world ocean as a function of depth, Southern Hemisphere.
- Table 15b. Annual mean oxygen-saturation (%) area-weighted r.m.s. deviations over five-degree latitude belts for the world ocean as a function of depth, Northern Hemisphere.

Contents

- Figure 41. Annual mean oxygen-saturation (%) at 1500 m depth.
- Figure 42. Annual mean oxygen (ml/l) at 2000 m depth.
- Figure 43. Annual mean oxygen-saturation (%) at 2000 m depth.
- Figure 44. Annual mean oxygen (ml/l) at 2500 m depth.
- Figure 45. Annual mean oxygen-saturation (%) at 2500 m depth.
- Figure 46. Annual mean oxygen (ml/l) at 3000 m depth.
- Figure 47. Annual mean oxygen-saturation (%) at 3000 m depth.
- Figure 48. Annual mean oxygen (ml/l) at 3500 m depth.
- Figure 49. Annual mean oxygen-saturation (%) at 3500 m depth.
- Figure 50. Annual mean oxygen (ml/l) at 4000 m depth.
- Figure 51. Annual mean oxygen-saturation (%) at 4000 m depth.
- Figure 52. Annual mean depth (m) of the absolute oxygen minimum surface with respect to the vertical.
- Figure 53. Annual mean oxygen (ml/l) on the absolute oxygen minimum surface. Hatching indicates areas where gradients are too large to contour.
- Figure 54. Annual mean oxygen-saturation (%) on the absolute oxygen minimum surface. Hatching indicates areas where gradients are too large to contour.
- Figure 55. Annual mean potential density (10^{-3}g/cm^3) on the absolute oxygen minimum surface. Hatching indicates areas where gradients are too large to contour.
- Figure 56. Annual mean anomaly of geopotential thickness ($10\text{ m}^2/\text{sec}^2$) of the 0-500 m layer.
- Figure 57. Annual mean anomaly of geopotential thickness ($10\text{ m}^2/\text{sec}^2$) of the 500-1000 m layer.
- Figure 58. Annual mean anomaly of geopotential thickness ($10\text{ m}^2/\text{sec}^2$) of the 1000-1500 m layer.
- Figure 59. Annual mean anomaly of geopotential thickness ($10\text{ m}^2/\text{sec}^2$) of the 1500-2000 m layer.
- Figure 60. Annual mean anomaly of geopotential thickness ($10\text{ m}^2/\text{sec}^2$) of the 2000-2500 m layer.
- Figure 61. Annual mean anomaly of geopotential thickness ($10\text{ m}^2/\text{sec}^2$) of the 2500-3000 m layer.
- Figure 62. Annual mean anomaly of geopotential thickness ($10\text{ m}^2/\text{sec}^2$) of the 3000-3500 m layer.
- Figure 63. Annual mean anomaly of geopotential thickness ($10\text{ m}^2/\text{sec}^2$) of the 3500-4000 m layer.
- Figure 64. Annual mean anomaly of geopotential thickness ($10\text{ m}^2/\text{sec}^2$) of the 1000-2000 m layer.
- Figure 65. Annual mean anomaly of geopotential thickness ($10\text{ m}^2/\text{sec}^2$) of the 2000-3000 m layer.
- Figure 66. Annual mean anomaly of geopotential thickness ($10\text{ m}^2/\text{sec}^2$) of the 3000-4000 m layer.
- Figure 67. Annual mean anomaly of geopotential thickness ($10\text{ m}^2/\text{sec}^2$) of the 0-2000 m layer.
- Figure 68. Planetary vorticity (f/H) ($10^{-3}\text{m}^{-1}\text{sec}^{-1}$).
- Figure 69. Depth of the world ocean (meters).
- Figure 70. Annual mean Brunt-Väisälä frequency (cycles/hr) at 150 m depth.
- Figure 71. Annual mean Brunt-Väisälä frequency (cycles/hr) at 500 m depth.
- Figure 72. Annual mean Brunt-Väisälä frequency (cycles/hr) at 1000 m depth.
- Figure 73. Annual mean Brunt-Väisälä frequency (cycles/hr) at 1500 m depth.
- Figure 74. Annual mean Brunt-Väisälä frequency (cycles/hr) at 2000 m depth.
- Figure 75. Annual mean Brunt-Väisälä frequency (cycles/hr) at 2500 m depth.
- Figure 76. Annual mean Brunt-Väisälä frequency (cycles/hr) at 3000 m depth.
- Figure 77. Annual mean Brunt-Väisälä frequency (cycles/hr) at 3500 m depth.
- Figure 78. Annual mean depth (meters) of the 27.7 potential density surface.
- Figure 79. Potential temperature ($^{\circ}\text{C}$) on the annual mean 27.7 potential density surface.
- Figure 80. Oxygen (ml/l) on the annual mean 27.7 potential density surface.
- Figure 81. Northern Hemisphere winter (February, March, April) depth (meters) of the 24.5 potential density surface.
- Figure 82. Salinity ($^{\circ}/\text{.}$) on the Northern Hemisphere winter (February, March, April) 24.5 potential density surface.
- Figure 83. Northern Hemisphere winter (February, March, April) depth (meters) of the 26.0 potential density surface.
- Figure 84. Salinity ($^{\circ}/\text{.}$) on the Northern Hemisphere winter (February, March, April) 26.0 potential density surface.
- Figure 85. Northern Hemisphere summer (August, September, October) depth (meters) of the 24.5 potential density surface.
- Figure 86. Salinity ($^{\circ}/\text{.}$) on the Northern Hemisphere summer (August, September, October) 24.5 potential density surface.
- Figure 87. Northern Hemisphere summer (August, September, October) depth (meters) of the 26.0 potential density surface.

Contents

- Figure 88. Salinity ($^{\circ}/\text{.}$) on the Northern Hemisphere summer (August, September, October) 26.0 potential density surface.
- Figure 89. Northern Hemisphere winter (February, March, April) sea surface density, $\sigma\text{-t}$ ($10^{-3}\text{g}/\text{cm}^3$).
- Figure 90. Northern Hemisphere spring (May, June, July) sea surface density, $\sigma\text{-t}$ ($10^{-3}\text{g}/\text{cm}^3$).
- Figure 91. Northern Hemisphere summer (August, September, October) sea surface density, $\sigma\text{-t}$ ($10^{-3}\text{g}/\text{cm}^3$).
- Figure 92. Northern Hemisphere fall (November, December, January) sea surface density, $\sigma\text{-t}$ ($10^{-3}\text{g}/\text{cm}^3$).
- Figure 93. Annual mean depth (meters) of the 4°C potential temperature surface.
- Figure 94. Salinity ($^{\circ}/\text{.}$) on the annual mean 4°C potential temperature surface.
- Figure 95a. March mixed-layer depths based on a temperature criterion of 0.5°C .
- Figure 95b. March mixed-layer depths based on a $\sigma\text{-t}$ criterion of 0.125.
- Figure 96a. September mixed-layer depths based on a temperature criterion of 0.5°C .
- Figure 96b. September mixed-layer depths based on a $\sigma\text{-t}$ criterion of 0.125.
- Figure 97. Annual cycle of mixed-layer depths based on temperature for selected regions in the world ocean.
- Figure 98. Annual mean global zonal average (by one-degree squares) of potential temperature ($^{\circ}\text{C}$).
- Figure 99. Annual mean global zonal average (by one-degree squares) of salinity ($^{\circ}/\text{.}$).
- Figure 100. Annual mean global zonal average (by one-degree squares) of potential density ($10^{-3}\text{g}/\text{cm}^3$).
- Figure 101. Annual mean global zonal average (by one-degree squares) of Brunt-Väisälä frequency (cycles/hr).
- Figure 102. Annual mean global zonal average (by one-degree squares) of oxygen (ml/l).
- Figure 103. Annual mean global zonal average (by one-degree squares) of oxygen-saturation (%).
- Figure 104. Annual mean Pacific zonal average (by one-degree squares) of potential temperature ($^{\circ}\text{C}$).
- Figure 105. Annual mean Pacific zonal average (by one-degree squares) of salinity ($^{\circ}/\text{.}$).
- Figure 106. Annual mean Pacific zonal average (by one-degree squares) of potential density ($10^{-3}\text{g}/\text{cm}^3$).
- Figure 107. Annual mean Pacific zonal average (by one-degree squares) of Brunt-Väisälä frequency (cycles/hr).
- Figure 108. Annual mean Pacific zonal average (by one-degree squares) of oxygen (ml/l).
- Figure 109. Annual mean Pacific zonal average (by one-degree squares) of oxygen-saturation (%).
- Figure 110. Annual mean Atlantic zonal average (by one-degree squares) of potential temperature ($^{\circ}\text{C}$).
- Figure 111. Annual mean Atlantic zonal average (by one-degree squares) of salinity ($^{\circ}/\text{.}$).
- Figure 112. Annual mean Atlantic zonal average (by one-degree squares) of potential density ($10^{-3}\text{g}/\text{cm}^3$).
- Figure 113. Annual mean Atlantic zonal average (by one-degree squares) of Brunt-Vaisala frequency (cycles/hr).
- Figure 114. Annual mean Atlantic zonal average (by one-degree squares) of oxygen (ml/l).
- Figure 115. Annual mean Atlantic zonal average (by one-degree squares) of oxygen-saturation (%).
- Figure 116. Annual mean Indian zonal average (by one-degree squares) of potential temperature ($^{\circ}\text{C}$).
- Figure 117. Annual mean Indian zonal average (by one-degree squares) of salinity ($^{\circ}/\text{.}$).
- Figure 118. Annual mean Indian zonal average (by one-degree squares) of potential density ($10^{-3}\text{g}/\text{cm}^3$).
- Figure 119. Annual mean Indian zonal average (by one-degree squares) of Brunt-Väisälä frequency (cycles/hr).
- Figure 120. Annual mean Indian zonal average (by one-degree squares) of oxygen (ml/l).
- Figure 121. Annual mean Indian zonal average (by one-degree squares) of oxygen-saturation (%).
- Figure 122. Division of world ocean into individual basins.
- Figure 123. Basin means of potential temperature ($^{\circ}\text{C}$) as a function of depth.
- Figure 124. Basin means of salinity ($^{\circ}/\text{.}$) as a function of depth.

- Figure 125. Basin means of potential density (10^{-3}g/cm^3) as a function of depth.
Figure 126. Basin means of dissolved oxygen (ml/l) as a function of depth.
Figure 127. Basin means of saturation of dissolved oxygen (%) as a function of depth.

APPENDIX A

- Figure A1. Standard summer sea surface temperature ($^{\circ}\text{C}$) analysis.
Figure A2. Test summer sea surface temperature ($^{\circ}\text{C}$) analysis.
Figure A3. Test analysis minus standard analysis ($^{\circ}\text{C}$).

APPENDIX B

- Figure B1. First guess summer sea surface test analysis ($^{\circ}\text{C}$).
Figure B2. First guess summer sea surface test analysis minus standard analysis ($^{\circ}\text{C}$).

APPENDIX D

- Figure D1. Annual mean standard deviation of temperature ($^{\circ}\text{C}$) at 150 m.
Figure D2. Annual mean standard deviation of temperature ($^{\circ}\text{C}$) at 500 m.
Figure D3. Annual mean standard deviation of temperature ($^{\circ}\text{C}$) at 1000 m.
Figure D4. Annual mean standard deviation of temperature ($^{\circ}\text{C}$) at 1500 m.

Foreword

For many years there has been a need for an atlas of the world ocean, illustrating its various characteristics on a global scale from the sea surface to abyssal depths. Data have been accumulating for more than a hundred years, but only in about the last eighty years have the temperature measurements been accurate enough to provide more than a rudimentary picture of the abyssal waters. Salinity measurements dating from the early part of the century revealed the major large-scale patterns of the field in the Atlantic but could not provide a clear pattern for the weaker fields in the abyssal Pacific and Indian Oceans. Only in the 1950's did the salinity-measuring instruments allow accuracies sufficient to estimate even the large-scale density fields from top to bottom.

Strangely, methods of measuring dissolved oxygen in the ocean ran ahead of both temperature and salinity in quality until well after the turn of the century, and of all of the non-conservative characteristics, including nutrients, oxygen provides the most nearly complete data set.

Many expeditions and investigators have contributed to the data set available now, but the accumulation has been slow. Some atlases were prepared in the 1920's and 1930's from the data then at hand. The outstanding case is that of the *Meteor* Atlas, that was based upon the *Meteor Expedition* data over most of the Equatorial and South Atlantic; the North Atlantic sector was a composite of data from many expeditions. Most atlases of this period were limited, either by the material at hand, or the purposes of the investigator, to smaller areas or to the upper ocean, or to temperature and salinity alone. Major steps forward were taken beginning in the 1950's when several atlases of sectors of the Atlantic resulted from the collaborative oceanographic programs of the International Geophysical Year 1957-1958, and when several atlases and compilations of data were produced by Soviet investigators. One of the outstanding results of international collaborative expeditions is Klaus Wyrtki's atlas of the Indian Ocean.

Until now, however, no one had carried out so ambitious a project as a global ocean atlas, in such detail. The catalogue of oceanographic atlases prepared recently by Stommel and Fieux (1978) lists no such undertaking.

The present work is particularly ambitious in that the raw materials provided were not collected systematically with such a global project in mind: they are scattered irregularly in time and space, and unfortunately vary also in quality. The task of selecting, testing for quality, arraying and analyzing is described briefly in the text, but only those who have undertaken to use parts of this heterogeneous mass of material can understand fully the difficulty of the work.

However, making such an atlas is not simply a toilsome exercise in statistics. It is also an exploration. Many of the figures and tables herein are the first views we have ever had of some important aspects of the ocean. They are enlightening for all of us. For those who think they are already well informed, they may clarify or offer surprises. For those who have dealt with a narrower area or range of characteristics, they offer a revelation of the large-scale order of the ocean, and a general framework against which problems can be examined and in which solutions may be sought.

Best of all, perhaps, for those who are new to the field and not already committed to one concept or another, it may offer an entry unencumbered by the stretchings, extrapolations and warpings that have been inevitable in less complete arrays.

We have long needed such an atlas and its accompanying tables. This is a really major contribution to knowledge of the global ocean.

Joseph L. Reid
Scripps Institute of Oceanography
La Jolla, CA
November 11, 1981

Stommel, Henry, and Michele Fieux. 1978. *Oceanographic Atlases, A Guide to Their Geographic Coverage and Contents*. Woods Hole Press, Woods Hole, MA, 97 pp.

Preface

Observations of temperature, salinity, and oxygen in the world ocean have been accumulating over the past eighty years to the point where global objective analyses of these data are feasible. The purpose of the project represented by this atlas is to provide an objectively analyzed, gridded set of fields for use in studying the world ocean.

The existence of the observations upon which this atlas is based is due to the efforts of many individuals and we acknowledge their contribution to this atlas. Scientists and technicians studying the world ocean have undertaken the arduous task of collecting and processing the data. Without their efforts this atlas would not have been possible. In addition, the analyses of these data by various scientists have provided valuable references in the preparation of this atlas. The National Oceanographic Data Center, Washington, D.C. has been responsible for collecting the data and storing them on magnetic tape in uniform formats. This effort is invaluable, as these tapes serve as the starting point for the work described in this atlas.

Dr. Abraham Oort initiated this project, and his experience in the analysis and study of global meteorological data sets has been invaluable for my own efforts. This atlas can be considered to be an oceanographic counterpart to the work by Abraham Oort and Gene Rasmusson, "Atmospheric Circulation Statistics," NOAA Professional Paper No. 5, U.S. Department of Commerce, Washington, D.C.

I thank Dr. Joseph Smagorinsky for creating an environment where a long-term project of this nature can be conducted. The encouragement of many individuals is also appreciated.

I also thank M. Cox, Y. Kurihara, J. L. Reid, M. Tsuchiya, H. Stommel and in particular, A. Oort, for their comments on the manuscript.

P. Tunison, W. Ellis, and M. Zadworny prepared the drafted figures and J. Conner performed the photographic work. Ms. J. Kennedy typed the manuscript. M. Rosenstein and A. Oort investigated the use of microfiche as a means of presenting data. Jim Welsh provided valuable programming suggestions during the early part of this study.

The processing and analysis of the data were initially performed on an IBM 360-195 computer and subsequently on a Texas Instruments Advanced Scientific Computer (TI-ASC).

Sydney Levitus

Climatological Atlas of the World Ocean

Sydney Levitus

Geophysical Fluid Dynamics Laboratory

Princeton, N.J.

ABSTRACT

This atlas contains maps of objectively analyzed fields of temperature, salinity, dissolved oxygen, and percent oxygen-saturation at standard oceanographic observation levels on a one-degree latitude-longitude grid for the world ocean. Maps of derived quantities such as geopotential thickness, Brunt-Väisälä frequency, and mixed-layer depths are also presented. The sources of data used in preparation of this atlas were the Station Data, Mechanical Bathythermograph, and Expendable Bathythermograph files of the National Oceanographic Data Center, Washington, D.C. Meridional cross-sections of the zonal averages of the objectively analyzed data are presented both in the form of figures and tables. Statistics on the number of observations, mean, and root-mean-square deviation of temperature, salinity, dissolved oxygen, percent oxygen-saturation, potential density, and specific volume on a five-degree grid are presented in the microfiche section of this atlas. Some discussion of the major oceanographic features observed in the various fields is given.

1. INTRODUCTION

This atlas represents a synthesis of all temperature, salinity, and oxygen data available from the National Oceanographic Data Center (NODC), Washington, D.C. These parameters have been analyzed in a consistent, objective manner at standard oceanographic analysis levels on a one-degree latitude-longitude grid between the surface and ocean bottom with a maximum depth of 5500 m. Annual, seasonal, and in some cases monthly analyses have been computed. Because of a lack of data we are forced to examine the annual cycle by compositing all data, regardless of the year of observation.

The analyses and statistical information presented are intended primarily for use in the study of the role of the oceans in controlling the earth's climate, but they can be used for other scientific investigations also. The objective analyses shown in this atlas have certain limitations owing to the nature of the data base (non-synoptic, scattered in space) and to the characteristics of the objective analysis techniques and the particular grid which we used. These limitations and characteristics will be discussed in the text. The analyses presented are viewed as another tool for studying the world ocean. Preliminary results have already been used in a variety of ways. For example, Oort and Vonder Haar (1976) and Ellis et al. (1977) have used the ocean temperature analyses in conjunction with atmospheric and earth radiation budget data for diagnostic studies of the role of the oceans in the global heat balance. Manabe et al.

(1979) have used the oceanic heat storage computed from the monthly temperature fields in a comparison with heat storage values derived from a joint ocean-atmosphere general circulation model. Cox (1980) has used the analyses as internal boundary conditions in a model of the tropical Pacific Ocean for a study of tropical waves. Mellor et al. (1982) have used the analyses for diagnostic computations of the general circulation of the Atlantic Ocean.

In addition to the analyses presented in the text five-degree square statistics of the observed data for 3-month seasons are given for the upper ocean, and annual statistics at all depths are given in the microfiche packet attached to this atlas.

A description of the early results from this project was given by Levitus and Oort (1977) herein referred to as L&O. Some changes have been made in the analysis scheme since the publication by L&O, and these will be described. Most importantly there has been approximately a 30 percent increase in the total amount of data available, and for some parts of the tropical oceans there is now four times as much temperature data as was previously available. As was done in L&O, we will first discuss the data used and their distribution, the quality control applied, the method of analysis, and the problems encountered. Sections and charts shown in the text can be compared to earlier results. Additional examples will show new uses to which the analyses can

be applied. A large number of maps, cross sections, and tables that were produced in the project cannot be shown in the main text because of space limitations, but have been included in the microfiche appendix.

Even with the additional data we have incorporated, the work presented here is hampered in a number of ways by a lack of data. For example, in some areas quality control is made difficult by the limited number of data. Data may exist in an area for only one season, thus precluding any representative annual analysis. In some areas there may be a reasonable spatial distribution of data points on which to base an analysis, but there may be only a few or perhaps only one datum in the one-degree squares that do contain data.

2. DATA AND DATA DISTRIBUTION

2.1 Data sources

The data used in this project were obtained from the National Oceanographic Data Center (NODC), Washington, D.C. and represent all the data available in the Oceanographic Station Data (SD) file as of the first quarter of 1978, the Expendible Bathythermograph (XBT) as of the first quarter of 1977, and the Mechanical Bathythermograph (MBT) as of the first quarter of 1977.

Our data files as described in L&O were completed through the 1977-1978 period through updates obtained from NODC. Besides the new data obtained, there were some corrections to older data, and some duplicates of earlier stations. The corrections were incorporated into our data files and the duplicates eliminated. The procedure to do this made use of the unique reference number assigned by the NODC to each cast in a file. This procedure also identified numerous duplicate mechanical bathythermograph casts that erroneously had been placed on separate update tapes. The description of the total number of observations used in this study for temperature, salinity, and oxygen and the number of one-degree squares containing observations of these parameters is given in table 1 for each analysis level. Also given in table 1 is the number of one-degree squares over the globe that contain ocean. Note that the number of ocean one-degree squares has changes compared to the same table in L&O. This is due to revisions in the topography used such as the exclusion of marginal seas and lakes and the correction of a few ocean depth figures that now appear to have been in serious error.

The SD file contained ~500,000 hydrographic stations and consisted primarily of Nansen cast data of temperature, salinity, and oxygen. Data from several thousand salinity-temperature-depth (STD) casts are also included in this file. The SD file contained both observed level data for each cast as well as an NODC interpolation to standard levels. We used the NODC standard level values in the work presented in this atlas. Data at the 3500, 4500, and 5500 m levels used in this atlas were interpolated by us from observed levels using the same Lagrange

interpolation procedure as used by NODC (NOAA, 1974). The distribution of the number of temperature observations in this file as a function of depth (standard level) for the globe and individual hemispheres is given in figure 1a. The figure shows that the Station Data file is composed mainly of Northern Hemisphere data. There is a decrease in the number of observations with increasing depth in both hemispheres. The number of salinity observations is generally a few percent less at each level than the number of temperature observations. Time series of the number of Station Data temperature measurements at the sea surface and at 1000m, from year 1900 to the present, are shown in figures 2a and b, respectively. Similar time series plots are shown in figures 3a and b for the oxygen observations. Because of the bias in the distribution of stations towards shallow coastal areas (more than 13 percent of the SD casts occur in the Baltic and North Seas) the time series at 1000 m are presented in addition to those at the surface. The ordinate on these maps represents the number of observations per month. The vertical marks on the abscissa represent January of each year. The time series plots show a number of interesting features. There is a distinct seasonal cycle, indicating that more observations were gathered during the Northern Hemisphere summer season than in the Northern Hemisphere winter season. Since 90 percent of the Station Data file consists of Northern Hemisphere data the observed pattern is dominated by the Northern Hemisphere observations. Minima in the number of observations are associated with the two world wars. Beginning in the late 1940's the number of observations increases to a maximum during the 1960's and then decreases to zero in 1976. In discussing this feature the first point to note is that the NODC Station Data file we have used is complete up to the first quarter of 1978, as previously mentioned. The tailing off of observations from the 1960's to 1978 may be due primarily to the lag between the time observations were taken and the time the data were entered into the NODC file. The data must first be processed by the observer, entered into a format suitable for incorporation into the NODC file, and then incorporated by the NODC. Another possible cause of the tailing off is that investigators may be using CTD instruments to gather data as opposed to taking discrete bottle samples. (The CTD is an instrument that yields continuous measurements of salinity and temperature with depth. The STD was an early version of the CTD.) A file for STD and CTD data has not yet been established at NODC (NOAA, 1980) and so many of these observations are not available.

Besides the bias toward shallow coastal stations there is a bias toward a large number of stations in the western boundary currents such as the Gulf Stream and Kuroshio. To illustrate further these exceptionally strong biases the number of surface salinity observations for the ten most data-dense Marsden squares (ten-degree squares) are presented in table 2. Approximately 40 percent of

the surface salinity observations occur in only ten Marsden squares. For the ocean interior the Station Data observations can be described only as sparse. If one examines in the microfiche appendix the maps of the distribution of observations, these biases are obvious.

The MBT file contained ~785,000 soundings, of which ~103,000 were from weather ship stations. The maximum observation depth for the MBT soundings is 295 m, so that the deepest standard level for which MBT data are available is 250 m. The MBT data we received from NODC came digitized at 5 m intervals and standard level values were simply taken from each cast. The distribution with depth of the total number of MBT observations for the globe and individual hemispheres is shown in figure 1b. This figure shows that the majority of MBT observations occur in the Northern Hemisphere. The observed decrease in the number of observations with depth has a discontinuity at 125 m, which can be attributed to the use of MBT instruments that had measured to a maximum depth of 140 m (Pickard, 1975, p. 92). A monthly time series of the number of MBT observations at the sea surface is shown in figure 4. The plot shows an increase in MBT observations from the 1940's to the 1960's and then a decrease to near zero in 1974. This tailing off can be attributed to the replacement of MBT instruments by XBT instruments, which came into use in the 1960's. As noted by NODC (NOAA, 1980), the XBT has essentially superseded the MBT, although NODC still incorporates digitized MBT data into its file. The large number of MBT casts shown for July 1966 were taken during a NATO exercise in the eastern Atlantic. The data from this multi-ship multi-national survey are identified by the cruise number "MILOC-66." Most of the data from this survey occur in Marsden Squares 182 and 183.

The XBT file contained ~300,000 soundings. Some XBT measurements extended to depths of 1800 m but the deepest observations we used were at 400 m. The reason for this is the systematic error in XBT measurements noted by Flierl and Robinson (1974) and McDowell (1977). The XBT data received from NODC were in the form of values digitized from strip charts. We linearly interpolated these values to standard levels. The distribution with depth of the total number of XBT observations is given in figure 1c. The dropoff in XBT observations between 400 and 500 m and again at 700 meters is due to the use of instruments with different maximum-depth capabilities. The monthly time series for the number of XBT observations at the sea surface is shown in figure 5. The number of XBT casts reaches a maximum in the early 1970's and then decreases. This dropoff is most probably due to the time lag involved in entering new data.

To illustrate further the biases just discussed we present the following maps of distribution of observations. Figures 6 and 7 are maps of the distribution of observations of the merged SD, MBT, and XBT data sets at the sea surface for Northern Hemisphere winter and

summer, respectively. Figure 8 shows the distribution of surface salinity observations for Northern Hemisphere summer. Figure 9 shows the distribution of salinity observations for the annual period at a depth of 2000 m and figure 10 shows the distribution of oxygen observations for the annual period at the sea surface. Clearly the XBT and MBT data add considerably to the total number of temperature observations when we compare the summer distributions of the merged temperature data with the salinity data. Comparison of the merged temperature data distributions shows the relative lack of data in each hemisphere during the respective winter season. The distribution of salinity observations at 2000 m depth shows the bias of data having been gathered in western boundary current regimes. A reasonable amount of data exists in the rest of the world ocean upon which to base an analysis, although more data would provide additional detail and increase the reliability of any analysis. The distribution of oxygen observations at the sea surface shown in figure 10 also illustrates the bias toward more data having been gathered in western boundary current regimes and coastal areas in general. An additional set of maps in the microfiche appendix shows the distribution of observations for the various parameters at standard analysis levels and for various averaging periods. The maps are intended to give the reader a quick feel for the amount of data used in the analyses, particularly as they indicate areas where the lack of data precludes a representative analysis, but where our analysis has filled in. The maps also represent to some degree the state of observational progress in physical oceanography. We emphasize the phrase "to some degree," because some of the older measurements represented by these maps are not as accurate as the newer measurements. For instance, with the use of electrical conductivity techniques, salinity can now be measured to an accuracy of .002 ‰ which is an order of magnitude more accurate than the titration technique. Worthington (1981) has presented a map showing the distribution of high quality hydrographic cast data in the world ocean in which salinity has been measured to this precision. Since the electrical conductivity technique was not in use until the late 1950's (Schleicher and Bradshaw, 1956) we have used nearly all the available historical data in our analyses. Furthermore some observations have simply never been incorporated into the NODC data files.

Another feature of the atlas is the presentation of five-degree square statistics of the observed data as part of the microfiche appendix. We emphasize that these data are not statistics of our analyzed fields; they are raw data, received from NODC, to which our quality control has been applied. The five-degree statistics presented are the number of observations, mean, and root-mean-square deviation. In five-degree squares that contain both ocean and land or sub-ocean floor areas the number of one-degree squares containing ocean is also given. The reasons for the presentation

of these statistics are as follows: 1) we have received requests for these numerical values by investigators who need a quick look at this kind of information without having to resort to computer processing. Up to now this information has not been easily accessible, and the microfiche presentation should help alleviate this problem. 2) The statistics are of much physical interest in themselves, since they represent mean values and temporal variability of the various parameters.

Additional information concerning the NODC data files can be found in the User's Guide to NODC's Data Services (NOAA, 1974).

2.2 Data Reduction and Quality Control

By far the biggest problem faced in this project concerned quality control of the data. The problems encountered relate directly to the general lack in some areas of data upon which to base statistical checks. Consequently certain empirical criteria were applied and, in some cases, subjective judgment was used.

2.2a Range checking

Range checking was performed on all data as a first error check to eliminate the relatively few data that were grossly in error. The ranges used were rather coarse for much of the world ocean, particularly with respect to the deeper levels. The reason for the coarse range is that we included adjacent seas, such as the Mediterranean, which have water mass properties that are highly atypical of most of the world ocean. Even had we not included the adjacent seas, the range of acceptable values would still have been relatively large because of the extreme values that can occur in the ocean near these seas. Various range criteria were tested and the decision made to use the coarse values and check the entire world ocean with these values. This check was successful in that it eliminated the relatively few data that, in some cases, are physically unrealistic. Table 3 gives the ranges allowed for temperature and salinity as a function of depth ranging from -3.0°C to 35.0°C and 0.0 to 40.0 ‰ at the surface to -1.5°C to 3.0°C and 34.3 to 35.5 ‰ at 5500 m depth. The range of acceptable oxygen values was 0 to 14 ml/l at all depths.

2.2b Static stability check

Each hydrographic cast was checked for static stability using the definition of stability defined by Hesselberg and Sverdrup (1914). Neumann and Pierson (1966, p. 139) review the definition. The computation is a "local" one in the sense that adiabatic displacements between adjacent temperature-salinity measurements in the vertical are considered rather than displacements to the sea surface. Lynn and Reid (1968) discuss the reasons for use of the local stability computation. The procedure for computation follows that used by Lynn and Reid (1968) and is given by

$$E = \lim_{\partial z \rightarrow 0} \frac{1}{\rho_0} \frac{\delta \rho}{\partial z}$$

in which $\rho_0 = 1.02 \text{ g/cm}^3$. As noted by Lynn and Reid the term "is the individual density gradient defined by vertical displacement of a water parcel (as opposed to the geometric density gradient). For discrete samples the density difference ($\delta \rho$) between two samples is taken after one is adiabatically displaced to the depth of the other." For the results at any standard level (k) the computation was performed by displacing parcels at the next deeper standard level ($k+1$) to level k . Instabilities have been reported over large areas of the tropical oceans. Based on results from the Meteor Expedition Schubert (1935) computed maps of stability for the Atlantic Ocean between 0 and 25m and 25 and 50m which are reproduced in the text by Neumann and Pierson (1966, p 141). In the 0-25m layer Schubert shows a basin wide area of instability in the subtropics of the South Atlantic with the largest instability being $10^3 E = -2600$. This corresponds to a density inversion of $50 \times 10^{-5} \text{ g/cm}^3$. In the 25-50m layer the lowest value shown is $10^3 E = -317$. To our knowledge, the processes which could maintain such large inversions over such large geographical areas and thick layers have never been explained. Therefore we assume the observations to be in error. Inversions of less than $2 \times 10^{-5} \text{ g/cm}^3$ can be considered to be within the measurement error of salinity ($\sim .02\%$) using the titration technique or measurement errors of $\sim .1^{\circ}\text{C}$ in temperature. One possible explanation for the relatively large number of density inversions involving the surface layer is that samples may have been gathered by a bucket containing residual sea water from a previous sample subjected to evaporation.

The actual procedure for using stability checks to eliminate sets of data points was as follows. To a depth of 30 m inversions in excess of $3 \times 10^{-5} \text{ g/cm}^3$ were eliminated, and below this depth down to the 400 m level, inversions in excess of $2 \times 10^{-5} \text{ g/cm}^3$ were eliminated. Below 400 m any inversion was eliminated. To eliminate an inversion both temperature and salinity were eliminated from further use at both standard levels involved in the computation. In the actual processing a count was kept of the number of inversions in each cast. If a cast had two or more unacceptable inversions, as defined above, then the entire cast was eliminated from further use. About 10,800 casts were eliminated in this way, approximately 2 percent of all casts in the data set.

2.2c Statistical check

Statistical checks were performed to eliminate data as follows. All data for each parameter (irrespective of seasons) and at each standard level were averaged by Marsden Square (ten-degree square) to produce a record of the number of observations, mean, and standard deviation in each square. For temperature, the statistics included the data from the SD, MBT, and XBT files merged together. In the preliminary work presented in L&O a five-standard-deviation criterion was used to eliminate gross errors. In other words, after the statistics were computed each individual observation was

eliminated if it deviated five standard deviations or more from the mean. In the present study this check was modified and extended as follows. Below 50 m, a three-standard-deviation criterion was used rather than the five-standard-deviation criterion. Above 50 m depth, a five-standard-deviation criterion was used in Marsden squares that contained any land area; and in selected Marsden squares that came close to land areas a four-standard-deviation check was used. In all other squares a three-standard-deviation criterion was used. The reason for the weaker criterion in coastal and near-coastal regions was the exceptionally large variability in the coastal Marsden square statistics, particularly for the salinity data. Salinity variability can be related to river runoff, and large samples are needed to compute representative means. Also, frequency distributions in some coastal regions are observed to be skewed or bimodal so that they do not resemble normal distributions which is the basic hypothesis underlying this kind of check. Thus to avoid eliminating good data the standard deviation criteria were weakened as given above. The total number of salinity, temperature, and oxygen measurements in each cast, as well as the total number of observations exceeding the criterion, were recorded. If 20 percent of the data in a cast were found to exceed the standard deviation criterion, then the entire cast was eliminated. This check was imposed after tests indicated that surface data from particular casts (which upon inspection appeared to be erroneous) were being eliminated but deeper data were not. Other situations were found where erroneous data from the deeper portion of a cast were eliminated, while near-surface data from the same cast were not eliminated because of larger natural variability in surface layers. One reason for this was the decrease of data with depth and resulting change in sample statistics. The standard deviation check was applied twice to the data set.

In summary, first the Marsden Square statistics were computed, and the elimination procedure described above was used to provide a preliminary data set. Next, new Marsden-square statistics were computed from this preliminary data set and used with the same statistical check to produce a new, clean data set. The purpose for applying the statistical check twice was to eliminate in the first round any grossly erroneous or nonrepresentative data from the data set that artificially increased the variances. The second check then should be more effective in eliminating smaller but probably still erroneous observations. The statistical checking just described eliminates from one to four percent of the data of each parameter at each standard level with the larger percentages being at the deeper levels. A cautionary note and further explanation of the statistical checking is warranted here. One example of interest is that during the initial checking most of the oxygen data in two particular Marsden squares were found to be seriously in error (values were too low by a factor of eight to ten), which rendered the original statistical checks

useless in these squares. The problem was first detected in the preliminary analyses. The original casts were examined, the cruise was noted, and a paper was found in the literature that showed the original data. This example indicates one of the quality control problems encountered in this work.

As previously noted there is a general lack of data in the mid-ocean regions, particularly at great depths, and also there is some seasonal bias toward more observations being taken during summer than winter. For these reasons we included all data regardless of season in our statistical checking and computed statistics over relatively large areas, ten-degree squares.

2.2d Elimination of spurious data

Finally the data were averaged by one-degree squares for input to the objective analysis program. After initial objective analyses were computed, it was found, not unexpectedly, that the input set of one-degree means still contained suspicious data contributing to unrealistic distributions, appearing as a few intense bull's-eyes. Examination of these features indicated that some of them were due to particular oceanographic cruises. Many U.S.S.R. salinity data were found to be associated with these features and also to be responsible for other quality control problems. Therefore the suspicious cruises and all U.S.S.R. salinity data below 400 m were eliminated from the data set. In addition, some one-degree squares were eliminated due to the unrealistic features they produced. The analyses were then recomputed without the U.S.S.R. salinity data and the other suspicious data just mentioned. The exclusion of all U.S.S.R. salinity data may not have been necessary, but lack of time prohibited us from making the necessary checks to determine the reliability of each particular cast and cruise. In essence, the decision was made to risk elimination of some good data rather than produce analyses in which numerous unrealistic features appeared. This applies to the selected cruises eliminated as well as to the U.S.S.R. data. It is only with the addition of many more data that one will be able to determine if some of the discarded data are usable.

2.2e An example of quality control problems with legitimate data

In connection with the above discussion, we will give a specific example of recent observations that would not have passed our quality control criteria but which do represent valid oceanographic phenomena. McDowell and Rossby (1978) observed with both XBT and CTD casts an anticyclonic subsurface lens of relatively warm, saline water at 25°N, 70°W. The water mass properties of the eddy indicated that it was of Mediterranean Sea origin. According to their paper, values of approximately 35.5 ‰ and 10°C represent the salinity and temperature at the center of the eddy at a depth of approximately 1000 m. The statistics of the historical data for Marsden square 79 (20°N–30°N, 60°W–70°W) containing 471 temperature and 417 salinity observations

at this depth are such that the observed temperature at the center of the eddy is over seven standard deviations from the Marsden square mean and the salinity value is over six standard deviations from the mean. McDowell and Rossby took a series of background measurements around the central core of the eddy and found the central salinity value of the eddy to be twenty standard deviations from the mean of the background stations. They noted that 1) based on the atlas of Worthington and Wright (1970), observations in the western Atlantic of Mediterranean and eastern Atlantic water are rare, and 2) the station spacing and vertical resolution of standard hydrographic surveys, approximately 100 km and 100 m, respectively, are such that it is possible that other eddies in this region could have avoided detection. The point we would like to make is that if only one eddy with anomalous properties is observed in a data-rich region and is based on a few casts or just a single cast, then it would probably be eliminated in our statistical checking. If an eddy with anomalous properties appears in a data-sparse region, then it might not be eliminated but appear as what we believe to be an error or nonrepresentative piece of data. Even if real, the data from the eddy would affect a relatively large area of our analysis. For example, McDowell and Rossby indicate a diameter of 20 km for the eddy they described. Features on this length scale simply cannot be accurately represented on a one-degree grid. As discussed later, the smallest scale that can be represented is a two-gridpoint wave. In relation to the statistical features of the eddy phenomenon just discussed, we wish to point out that the five-degree square statistics we present in the microfiche section of this atlas are based on our edited data set. Legitimate values representing eddies may have been eliminated. These statistics should be interpreted accordingly.

2.2f Modification and elimination of existing data

Only data from one set of cruises were modified from the original data before averaging into one-degree squares. These were the oxygen measurements from the Discovery Expedition prior to 1952, which were increased by a factor of 1.1 following J. L. Reid (personal communication); Gordon (1966) and Wyrski (1971).

One-degree square salinity means near the mouths of rivers flowing into the Arctic Ocean were as low as 3.0‰ . These data produced an unreasonable distribution over an area extending several degrees of latitude. Therefore all salinity one-degree square means with values less than 27.0‰ were eliminated from use in the final objective analyses. Coachman and Aagaard (1974) note that in the Arctic Ocean "salinities are never much below about 27‰ , except very close to a river mouth, because this fresh water is efficiently mixed with more saline deeper water on the shallow continental shelf by the action of winds, tides, and currents."

2.2g Positional Errors

Consideration had to be given also to problems stemming from positional errors in the reports. If an error in

location was such that the sounding was placed in the wrong Marsden square, then, depending on the number of observations in the square and the difference between the value of the erroneous sounding and the mean of the correctly located soundings, the erroneous sounding would or would not be eliminated through our error checking. If an error in location was such that an observation was placed in a one-degree square defined as land, the observation was not used in the analyses.

Ocean depths for each one-degree square on the globe were based on the report by Smith et al. (1966). In regions poleward of 49° latitude, their topography was based on regions larger than one-degree squares, so that an interpolation had to be performed to produce a one-degree square topography for this region. Smith et al. (1966) discussed the methods used in determining ocean depths and possible sources of error.

One other type of positional error we encountered was detected in the following way. With each cast the latitude and longitude are given as part of the master record describing the cast. The master record also gives a location via a geographical numbering system such as the Marsden, Canadian, or WMO systems that are described in NOAA (1974, p. 32). We received the Station Data and MBT files with the Marsden system as the geographical numbering system and with the data sorted geographically by ascending Marsden square number. As a check, we computed the Marsden ten-degree and one-degree square numbers from the given latitude and longitude and then compared our computed values with those given in the master record. Interesting results were obtained. Sometimes disagreement was found between our computed values and those given in the master record. In some cases, and these were relatively few but of great importance, we found that the latitude of a station indicated a northern (southern) hemisphere location while the NODC Marsden square assignment indicated a southern (northern) location. The same type of error was sometimes found in longitude. When these errors were encountered the casts were simply eliminated from use. It would have been too time consuming to save and correct every possible error of any nature encountered. In some other cases disagreement was found because data fell exactly on a ten-degree or one-degree square boundary which represented an ambiguity in the NODC assignment of Marsden square numbers. Inspection revealed that there was no consistent assignment in these cases. In the computer program used to check this we assigned the ten-degree and one-degree square numbers that occurred furthest from the origin of the Marsden system ($0^\circ, 0^\circ$) to any observation that fell on a square boundary. We note this situation because before we checked in detail as to what was occurring we eliminated (temporarily) numerous casts that had this ambiguity.

2.3 Representativeness of the Data

Another problem that arises in conjunction with quality control is the representativeness of the data. The general paucity of data forces us to use all historical

data. This implies that in any given one-degree square there may be data from a month or season of one particular year, while in the same or a nearby square there may be data from an entirely different year. If there is large interannual variability in a region where scattered sampling in time has occurred, then one can expect the analysis to reflect this. Because the observations are scattered with respect to time, except for a few limited areas, the results cannot, in a strict sense, be considered a true long-term climatological average.

What we have attempted to produce for each parameter with the data now available are analyses of the monthly, seasonal, and annual fields that show the dominant variations in the large-scale permanent or semi-permanent features of the field. A good example of the large-scale interannual variability one must be concerned with is given in the work of Smed (1943). This work was an investigation of interannual variability in the surface salinities of the North Atlantic. One might consult the work of Tabata (1965) for information and references on interannual variability in the Pacific Ocean as observed at ocean weather stations. Mosby (1959) examined interannual variability at ocean weather station "M" in the Norwegian Sea at intermediate and deep levels, while Helland (1963) discussed interannual variability in the upper ocean at station "M". Monin et al. (1977) review, in part, the oceanographic literature regarding interannual variability. Obviously the El Nino phenomenon must be cited as another example of large-scale interannual variability. One of the earlier references concerning the representativeness of single hydrographic casts is Seiwel (1939). He presents time series measurements made over a period of several days that show the effect of internal waves on dynamic height computations. Another early reference that discusses ocean variability appears in the text of Sverdrup et. al. (1942, p. 681) where they discuss the results of the International Gulf Stream Expedition of 1938 (Defant and Helland-Hansen, 1939). They describe large-amplitude, small-scale features and variability observed from two ships occupying 159 stations in an area less than 10,000 square miles and from hourly time series measurements made by one of the ships for a ninety-hour period. In view of these observations Sverdrup et. al. note the need for care in interpreting scattered observations. Defant (1950) also discusses the interpretation of oceanographic data that is contaminated by internal waves.

Another possible source of bias may arise from measurements having intentionally been taken in an area experiencing anomalous conditions. An example of this would be the repeated sampling of certain warm or cold eddies. An example of interannual variability on small scales involving eddies is given by Uda (1964). He reviews results showing the Kuroshio to have a path that is essentially bimodal. This bimodality is further described by several investigators in Stommel and Yoshida (1972). In particular, Taft (1972) shows frequency distributions of the path of the Kuroshio that describe the

bimodality. Obviously if the Kuroshio tends to occupy two different positions, statistics of water properties in this area can be expected to reflect this. Winterfeld and Stommel (1972) present statistics that show bimodality in the temperature field at intermediate depths in this region. The bimodality discussed here provides another reason for smoothing the historical data. The change in the path of the Kuroshio is on the order of a few degrees of latitude, and it is precisely features of this scale that we attempt to eliminate by smoothing. If one had access to synoptic data with high resolution then one could examine such small-scale features; or if one knew that the smaller scale features were permanent then analyzing these features on a finer grid would be reasonable. There are other examples of bimodality in oceanographic data. For example Kim and Rossby (1979) examined the statistics of data taken in the North Atlantic where Gulf Stream rings occur and suggested the flow and statistics to be bimodal. An example of the danger of using data that is unrepresentative is given by Leetmaa et al. (1977).

Our discussion of representativeness of the data is meant to provide a perspective on our knowledge of the oceans as presented in this atlas. We present smoothed analyses of historical means based in certain areas on relatively few observations with some sampling biases. We do believe, however, that useful information about the oceans can be gained through our procedures and that the large-scale features are representative of the real ocean. In other words, we believe that, if a hypothetical global synoptic set of ocean data (temperature, salinity, or oxygen) existed and one were to smooth this data to the same degree as we have smoothed the historical means overall, the large-scale features would be similar. However, some local differences would certainly occur because of interannual variability. Fuglister (1960) noted that hydrographic sections observed during the I.G.Y. in the South Atlantic were virtually identical to those observed thirty years earlier during the Meteor Expedition. He found that relatively small differences existed, but the major features were identical. Furthermore, despite the fact that the data are not synoptic, we note that there are large-scale features in individual oceans that are so similar that their very existence suggests that they are permanent or semipermanent features. There is no question that interannual variability is of great importance but its study would require special observing systems. Satellite measurements are required for global ocean monitoring of interannual variability.

To clarify the discussions of the amount of available data, quality control techniques, and representativeness of the data, the reader should examine in detail the maps of the distribution of data presented in the microfiche section of this atlas. These maps are provided to give the reader a quick, simple way of examining the sampling problem. Basically for the all-data annual mean analyses the data diminish with increasing depth. In the upper ocean, the all-data annual mean distributions

are quite good for defining large-scale features, but for the seasonal periods the data base for some regions is inadequate. With respect to the deep ocean, in some areas the distribution of observations may be adequate for some diagnostic computations but inadequate for other purposes. Obviously if an isolated deep basin or some region of the deep ocean has only one observation, then no horizontal gradient computations are meaningful. However useful information is provided by the observation in the computation of e.g., a volumetric mean over a major ocean basin.

3. OBJECTIVE ANALYSIS PROCEDURES

3.1 Method of analysis

An objective analysis scheme of the iterative difference-correction type (Cressman, 1959) was used to analyze the data. Input to the analysis scheme were the observed one-degree square means of data for whatever period was being analyzed and a first-guess value for each square. For instance, the one-degree square means for our annual analysis were computed using all available data regardless of the date of observation. If we were computing an analysis of temperature for the month of July, we used all the historical July data.

The analysis scheme was the same for all levels and proceeded as follows. Each one-degree square value was defined as being representative of the center of that particular one-degree square. The 360×180 gridpoints are located at the intersection of half-degree lines of latitude and longitude. An influence radius was then specified. At those grid points where there was an observed mean value, the difference between the mean and the first-guess field was computed. A correction to the first-guess value at all gridpoints was next computed as a distance-weighted mean of all gridpoint difference values that lie within the area around the gridpoint defined by the influence radius. Mathematically, the correction factor is given by the expression

$$C_{i,j} = \frac{\sum_{s=1}^n W_s Q_s}{\sum_{s=1}^n W_s} \quad (1)$$

in which

- $C_{i,j}$ = the correction factor at point (i,j)
- i,j = coordinates of a gridpoint in the east-west and north-south directions, respectively
- n = the number of observations that fall within the area around the point i,j defined by the influence radius
- Q_s = the difference between the observed mean and the first guess at the s^{th} point in the influence area
- W_s = $\exp(-Er^2/R^2)$ for $r \leq R$

$$W_s = 0 \text{ for } r > R$$

r = distance of the observation from the gridpoint

R = influence radius

$$E = 4.$$

The derivation of the weight function, W_s , will be presented later in this section. At each gridpoint we computed an analyzed value $G_{i,j}$ as the sum of the first guess, $F_{i,j}$ and the correction $C_{i,j}$ at the point. The expression for this is

$$G_{i,j} = F_{i,j} + C_{i,j} \quad (2)$$

If there were no data points within the area defined by the influence radius, then the correction was zero, the first-guess field was left unchanged, and the analyzed value was simply the first-guess value. This correction procedure was applied at all gridpoints to produce an analyzed field. This field was then used as the new first-guess field, and the procedure was repeated until a certain response function had been achieved. The number of iterations required depends on the disparity between the first-guess field and the observed input data. The smaller the difference is, the fewer iterations that are required. After each iteration, the resulting field was smoothed with a five-point smoother of the type described by Shuman (1957).

The analysis scheme is set up so that the influence radius, and the number of five-point smoothing passes can be varied with each iteration. The strategy used is to begin the analysis with a large influence radius and decrease it with each iteration. This technique allows us to analyze progressively smaller scale phenomena with each iteration.

The analysis scheme is based on the work of several researchers whose efforts were directed toward the analysis of meteorological data. Bergthörsson and Döös (1955) computed corrections to a first-guess field using various techniques. One of these techniques was to assume that the difference between a first-guess value and an analyzed value at a gridpoint was the same as the difference between an observation and a first-guess value at a nearby observing station. All the observed differences in an area surrounding the gridpoint were then averaged and added to the gridpoint first guess value to produce an analyzed value. Cressman (1959) modified this method by applying a distance-related weight function to each observation used in the correction in order to give more weight to observations that occur closest to the gridpoint. In addition, Cressman introduced the method of performing several iterations of the analysis scheme using the analysis produced in each iteration as the first-guess field for the next iteration. He also suggested beginning the analysis with a relatively large influence radius and decreasing it with successive iterations so as to analyze smaller scale phenomena with each pass.

Sasaki (1960) introduced a weight function that was specifically related to the density of observations, and

Barnes (1964) extended the work of Sasaki. It is the weight function presented by Barnes that has been used in our analysis. The derivation of the weight function which we present for completeness follows the work of Sasaki (1960) and Barnes (1964). Barnes (1973) further developed the technique but these results have not been incorporated into the analysis procedures used in producing this atlas.

3.1a Derivation of weight function

The principle upon which the weight function was derived was given succinctly by Barnes and is that "the two-dimensional distribution of an atmospheric variable can be represented by the summation of an infinite number of independent harmonic waves, that is, by a Fourier integral representation." If $f(x,y)$ is the variable to be represented, then in polar coordinates (r,θ) , a smoothed or filtered function $g(x,y)$ can be defined as follows

$$g(x, y) = \frac{1}{2\pi} \int_0^{2\pi} \int_0^{\infty} \eta f(x + r \cos \theta, y + r \sin \theta) d(r^2/4K) d\theta \quad (3)$$

in which r is the radial distance from a gridpoint whose coordinates are (x,y) . The weight function is defined as

$$\eta = \exp(-r^2/4K), \quad (4)$$

which resembles the Gaussian distribution in form. The exact shape of the weight function is determined by the value of K , which is dependent on the distribution of data. The determination of K follows.

The weight function has the property that

$$\frac{1}{2\pi} \int_0^{2\pi} \int_0^{\infty} \eta d(r^2/4K) d\theta = 1. \quad (5)$$

This property is desirable because in the continuous case (3) the application of the weight function to the distribution $f(x,y)$ will not change the mean of the distribution. However, in the discrete case (1), we only sum the contributions to within the distance R . This introduces an error in the evaluation of the filtered function, because the condition given by (5) does not apply. The error can be pre-determined and set to a reasonably small value in the following manner. If one carries out the integration in (5) with respect to θ , the remaining integral can be rewritten as

$$\int_0^R \eta d(r^2/4K) + \int_R^{\infty} \eta d(r^2/4K) = 1. \quad (6)$$

Defining the second integral as ϵ yields

$$\int_0^R \exp(-r^2/4K) d(r^2/4K) = 1 - \epsilon, \quad (7)$$

where

$$\epsilon = \exp(-R^2/4K)$$

In our analyses we have chosen $\epsilon=0.02$, which implies with respect to (6) the representation of 98 percent of the influence of any data around the gridpoint in the area defined by the influence radius, R . In terms of the weight function used in the evaluation of (1) this choice leads to a value of $E=4$ since

$$E = R^2/4K = -\ln \epsilon.$$

The choice of ϵ and the specification of R now determine the shape of the weight function.

3.1b Response function

It is desirable to know the response of a data set to the interpolation procedure applied to it. Following Barnes (1964, 1973), we let

$$f(x) = A \sin(ax) \quad (8)$$

in which $\alpha=2\pi/\lambda$ with λ being the wavelength of a particular Fourier component, and substitute this function into equation (3) along with the expression for η in equation (4). Then

$$g(x) = D(A \sin ax) = D f(x), \quad (9)$$

in which

$$D = \exp(-\pi^2 R^2/4\lambda^2).$$

The quantity D is the response function for one application of the analysis. We note that the phase of each Fourier component is not changed by the interpolation procedure. As previously noted, the results of an analysis pass are used as the first-guess for the next analysis pass in an iterative fashion. The response function after N iterations as derived by Barnes is

$$g_N(x) = f(x)D \sum_{n=1}^N (1 - D)^{n-1}. \quad (10)$$

Equation (10) differs trivially from that given by Barnes. The difference is due to the fact that our first-guess field was defined as a zonal average, annual mean, or seasonal mean, whereas Barnes used the first application of the analysis as a first-guess. Barnes (1964) also showed that applying the analysis scheme in an iterative fashion will result in convergence of the analyzed field to the observed data field. However, we do not wish to approach the observed data too closely because, as previously noted, we believe the smallest scale features to be artifacts of the averaging of historical data and, in addition, at least seven or eight gridpoints are needed to represent a Fourier component.

The response function given in (10) is useful in two ways. The first is that it is informative to know what Fourier components make up the analyses. The second is that the computer programs used in generating the analyses can be checked for correctness by comparison with (10). This was done in the following manner. A "perfect" set of observations was generated on our latitude-longitude grid by using the sum of all those Fourier components whose wavelengths are divisible into 360 an integral number of times. This perfect data

set consisted simply of one dimensional waves. The perfect data set was then analyzed with the objective procedures just described. A first-guess field was defined as the zonal average in one-degree latitude belts. Values of the influence radius R were prescribed and several iterations performed. The resulting analysis was then Fourier analyzed, and the amplitude of each Fourier component was compared with that computed from (10) for the same values of R . Agreement between the two was within 2 percent. The disagreement was because (10) is based on integration to infinity, whereas in the analysis we only integrate out to distance R .

3.1c Choice of influence radii

In the preliminary results discussed in L&O, an influence radius was chosen as a multiple of the average distance between gridpoints containing data. We will term this distance the average separation distance. For the first iteration the influence radius was set to a relatively large multiple of the average separation distance. With each additional iteration the influence radius was decreased. The reason for computing the influence radius as a multiple of the average separation distance was this: if ungridded data are regularly spaced with an average separation of 200 km, the smallest wavelength that can be analyzed from the data is 400 km. It then follows that a grid to which the data will be interpolated should not have a resolution finer than 200 km spacing. One should also note that short wavelengths will contain a great deal of noise. Thus the influence radius needs to be at least seven or eight times the average separation distance. If we inspect the distribution of observations given in the microfiche section for the various parameters at different depths and for the different averaging periods, it becomes clear that the data are not regularly distributed in space or by season. At one extreme, regions exist in which every one-degree square contains data and no interpolation needs to be performed. At the other extreme, we note regions in which no data exist. Thus with variable data spacing the separation distance is a function of geographical position and averaging period. However if we computed and used a different average separation distance for each parameter at each depth and each averaging period, we would be generating analyses in which the wavelengths of observed phenomena might differ from one depth level to another and from one season to another. Therefore we chose to use a fixed set of influence radii which allows us to analyze each parameter at every depth and season in exactly the same way. We also note that at least seven or eight grid points are needed to accurately represent a Fourier component that makes up a field, particularly for the computation of derivatives. The need to damp small scales also accounts for the amount of smoothing performed, as seen in the response function for this analysis. This function is given in figure 11 and will be derived and discussed in more detail shortly.

Inspection of (1) shows that the physical premise upon which the analysis is based is that the difference between the analyzed field and the first-guess at any gridpoint is proportional to the sum of the weighted differences between the observed mean and first-guess at all gridpoints containing data within the influence area.

Each analysis consisted of four iterations applied to a first-guess field. The influence radii on the four iterations were respectively 1541, 1211, 881, and 771 km. After each iteration a five-point smoother of the type described by Shuman (1957) was applied. The response function of the five-point smoother was chosen to approximate the response function of the objective analysis scheme. There is, however, a difference in the amount of smoothing performed by the gridpoint smoother as compared with the smoothing inherent in the objective analysis scheme. The objective analysis is performed in physical space, and the smoothing as given by equation (10) is invariant with respect to latitude. For example, if our influence radius is 770 km, then in the equatorial region our influence region extends seven gridpoints to the east and west of the gridpoint being analyzed. At 30° latitude from the Equator our influence region extends out fourteen gridpoints to the east and west of the gridpoint being analyzed. The amount of smoothing remains the same in each region but the east-west resolution has increased in moving poleward. The smoothing performed by the five-point smoother, however, does not remain invariant to changes in latitude. Because the longitudinal distances between gridpoints decrease with increasing latitude, the five-point smoother does less smoothing with increasing latitude. In data-dense areas this decrease in smoothing will be unimportant since the gridpoint smoother is applied after the objective analysis has already smoothed the data. The reason for using the five-point smoother is that our data is not evenly distributed in space. As the analysis moves from regions containing data to data void regions, small-scale discontinuities may develop. The five-point smoother is used to eliminate these discontinuities. The five-point smoother does not affect the phase of the waves in the data.

At gridpoints where no observed data points fall within the influence area one could expand the influence radius until some minimum number of data points were found. We did not use this procedure, because it implies an analysis with different maximum length scales in different regions, and we wish to minimize differences of this type.

The response function for the analyses presented in this atlas is shown in figure 11. The response function represents the smoothing inherent in the objective analysis with four iterations, with the previously noted influence radii, plus the smoothing of the five-point smoother applied after each analysis pass. The response function without the effect of the five-point smoother does not differ from figure 11 by more than five percent at any wavelength.

One additional point needs to be noted. The analysis in terms of a Fourier integral representation of the data field depends on the assumption that the region analyzed is continuous in space. We note however that there are ocean basins separated by narrow sills with water mass properties substantially different on each side of the sill. Analysis of each region should be carried out independently of the adjacent region. The separate analysis of each region, however, is an arduous task and has been carried out only in part. The details of this procedure will be discussed in the following section.

3.1d First-guess field determination

As previously noted, there are gaps in the data coverage. We wish to avoid creating spurious features in these gaps. Our method of providing first-guess fields has been chosen in an attempt to avoid the creation of such features. Another requirement for selecting first-guess fields is that although the objective analysis scheme will converge after a sufficient number of iterations, we desire the first-guess field to be reasonably close to the final analysis so as to reduce the amount of computer time required for convergence to our desired response function. Also as previously noted, we have adjacent basins whose water mass properties are individually nearly homogeneous but whose properties differ considerably. Spurious features can be created when an influence area extends over two basins of this nature. Our choice of first-guess field attempts to minimize the creation of these features.

To provide a first-guess field for the annual analysis at any standard level we first zonally averaged the observed data in each one-degree latitude belt by individual ocean basins. The Mediterranean and Red Seas were treated as individual basins. The Venezuela Basin and the Sulu Sea were treated as individual basins below their sill depths. The Norwegian Sea and Arctic Ocean were treated separately below the sill depth of the Greenland-Iceland-Shetland ridge. The zonal average computed at every one-degree belt in every individual ocean basin was used as the first guess for all one-degree squares in the belt. The reason for computing a separate first-guess in each individual basin can be explained with the aid of equations (1) and (2). We have at any grid point (i,j) an analyzed value as defined by

$$G_{i,j} = F_{i,j} + \sum_{S=1}^n W_s Q_s / \sum_{S=1}^n W_s. \quad (11)$$

For simplicity, we will use the case in which only one observed data point falls within the influence area. The coordinates of this point will be denoted by i',j' on our grid. If we let $OB_{i',j'}$ denote the observed one-degree square mean at this point then (11) becomes

$$G_{i,j} = F_{i,j} + (OB_{i',j'} - F_{i',j'}). \quad (12)$$

Thus for this case the difference between the analyzed point and the first-guess at point (i,j) is assumed to equal the difference between the observed data point

and the first-guess at the point i',j' . We note that, if the observed mean at a gridpoint is equal to the first-guess at that gridpoint, then the correction is obviously zero, and this gridpoint will affect no other gridpoint. For the situations where we have adjacent basins with individually nearly homogeneous properties, then defining a separate first-guess field for each basin means that the observed means in each basin are closer to their first-guess field than if this separation of basins had not been performed. Thus when the influence area extends across basins the corrections are relatively small. We observed, in experimenting, that this procedure greatly reduced spurious features around these basins and incorporated the procedure into our analysis scheme. We do note that it is a time consuming procedure to define a separate first-guess field for each basin, and therefore it could not be done for every area or parameter.

Once the annual analyses were completed they were used as first-guess fields for each of the four seasonal analyses. In the case of temperature, the seasonal analyses were used as first-guess fields for the monthly temperature analyses. In the preliminary work described in L&O semester analyses were computed, but these intermediate analyses were not computed or used in the present work. The reason for using the annual analyses as a first-guess and then the seasonal analyses is this. We recognize that fairly large data-void regions exist, in some cases to such an extent that a seasonal or monthly analysis in these regions is not meaningful. We are interested in computing integral quantities such as heat storage that are deviations from annual means. The geographic distribution of observations for the all-data annual periods (see microfiche maps) is excellent for the upper layers of the ocean. By using an all-data annual mean first-guess field and keeping the influence radius relatively small, regions where data exists for only one season or month will show no contribution to the annual cycle. By contrast, if we used a zonal average for each season or month then, in those latitudes where gaps exist, the first-guess field would be heavily biased by the few data points that exist. If these are anomalous data in some way, an entire basin wide belt may be affected. In the future, when sufficient data become available, the analysis of each seasonal and monthly field should be computed independently of data from any other season or month. In a data-dense area the choice of the first-guess field does not have a substantial effect on the final result. We have performed calculations to quantify this statement, and the results are given in Appendix B.

3.2 Additional comments on the objective analysis procedures

3.2a Use of dynamic parameters for determining influence radii

Some further comments concerning the choice of analysis procedures are in order here. Since the publication of L&O we have received suggestions that the influence

radius in the analysis procedure should be based on some dynamical quantity such as the internal Rossby radius of deformation. We disagree with this suggestion. Our stated goal is to examine the large-scale distributions of various parameters. To do this we must composite all of the historical data. With this stated purpose it is questionable to us that basing our analysis scheme on a length scale associated with baroclinic waves is at all relevant. Moreover even if we had synoptic data, it is not clear that the internal radius of deformation is the only relevant length scale of importance. For the synoptic surface salinity field a length scale associated with atmospheric precipitation patterns might be of importance in some areas, such as the Intertropical Convergence Zone. The distribution of oxygen might have length scales associated with biological activity such as the distribution of plankton. We also note that with an internal radius of deformation on the order of 100 km one would need synoptic data with a resolution on the order of 12 km to properly resolve a feature of this scale. Clearly, to investigate a phenomena of this type an expedition planned for this purpose (such as Mode or Polymode) must be carried out. Since the internal radius of deformation is a function of stratification, ocean depth, and latitude, and since it can be smaller or larger than 100 km an observation network must take this into account. In summary, we have not built any physical assumption into our analysis scheme, except that which results from smoothing. Therefore the analyses may be used to determine the relative importance of various physical processes, taking into account the smoothing that has been performed.

3.2b Possible need for additional smoothing

Additional smoothing may be required in certain regions. We have smoothed the data to the degree shown in the response function in figure 6. In computations that involve taking derivatives, additional smoothing may be required, particularly in data-sparse regions. Besides the five-point smoother used in the computation of the analyzed fields presented in this atlas, a median smoother proposed by Tukey (1974) has been found useful in eliminating noise while preserving sharp discontinuities in the analyses. The reader is referred to Rabiner et al. (1975) for a discussion of the properties of the median smoother. The effect of varying the amount of smoothing in the objective analyses is quantified in Appendix A.

Another point to note is that additional smoothing does not necessarily have to be applied to the standard level analyses. If one is working with fields interpolated to potential density surfaces, then smoothing might be applied to the fields of properties on the potential density surface. This procedure would reduce the amount of cross-isopycnal smoothing in regions of steeply sloping isopycnals such as the Gulf Stream.

3.2c Choice of resolution

Having discussed both the objective analysis procedures and the data used in this study, some further com-

ments concerning why particular procedures were chosen are appropriate. Use of a one-degree grid in this project represents a compromise between several factors. For a global analysis, one-degree spacing represents a maximum resolution that could be conveniently handled on the computer systems used in this project. Finer resolution could be accommodated but would have required much additional program effort and resources. For most of the world ocean, the data density does not justify the additional effort and resources. As previously noted, the density of observations depends on parameter type, depth, averaging period, and geographical location. In some regions there are not enough data to support the one-degree resolution, and additional smoothing is required. In regions such as the western boundary current regimes where current-counter-current systems exist we believe that a finer resolution than one-degree is needed to properly resolve features that appear in the historical mean data. The western current regimes also have a high enough data density to support finer resolution.

The resolution chosen to represent oceanographic and meteorological fields is of great importance. Saunders (1976) examined wind stress data on both a one-degree and five-degree grid in part of the North Atlantic. He found that the curl of the wind stress computed on the five-degree grid was 50 percent less than the curl computed on the one-degree grid. This is a substantial difference and is of particular importance when considering balance of force type computations. For example, if one computes the Sverdrup transport on a five-degree grid and compares it with "observed" ocean transports computed on a different-sized grid, then one can expect discrepancies between the two estimates simply because of the different resolutions. Similarly, if one compares satellite data such as altimeter measurements of sea level with the analyses presented in this atlas, one can expect differences simply because the altimeter data represent point measurements and the atlas results represent smoothed fields. To compare the results quantitatively one would need to smooth the altimeter data to the same degree as the analyses. In this particular example one also expects differences because the altimeter data are synoptic and the analyses are based on historical means. Again, we note that for areas such as the western boundary current regimes one should work with high-resolution hydrographic data to properly resolve mesoscale features.

Users of the analyses described in this atlas may have needs that do not require one-degree resolution, or they may be constrained by computer limitations that preclude using the one-degree resolution data. In averaging the data over larger areas one should be aware of the loss of resolution and also be aware that, if one averages data across basin boundaries, spurious features may result. In regions where the analyses are composed of large-scale, relatively flat features, averaging to a coarser grid will probably not result in the loss of much information.

Related to some of the points just discussed and indirectly related to our analysis procedures is the matter of averaging data on an irregular grid to maximize the number of observations used to compute statistics. The averaging areas are defined as regions where the data are nearly homogeneous. This technique has obvious merits but also some disadvantages. With an irregular grid the length scales that can be represented differ from one part of the grid to another as the size of the averaging areas differ. If one interpolates the data on an irregular grid to a regular grid one must take care not to introduce spurious features in the interpolation procedure.

3.2d Modification of the analyses

Modifications to the objectively analyzed fields were made in a few instances. Below 3000 m depth in the Arctic Ocean and Mediterranean Sea, and below 3500 m in the Sulu Sea, no data existed upon which to base an analysis. Therefore the temperature, salinity, oxygen, and oxygen-saturation fields at these levels were set equal to the 3000 m values in the Arctic and Mediterranean and to the 3500 m values in the Sulu Sea.

The objective analysis scheme has the property that it can produce weak relative extrema. Thus in certain locations it produced values of oxygen and oxygen-saturation that were slightly negative. Such negative values occurred only along the eastern boundaries of the ocean at depths of 50 m to 900 m where biological activity produces observed values that are quite small. The total number of these negative values at any particular depth ranged from two to ninety values with the maximum found at a depth of 300 m. These negative values were replaced by the average of the values of adjacent grid points. Also, in the Arctic some values of temperature less than -2.1°C were produced and these values were replaced by a value of -2.1°C .

4. INTRODUCTION TO RESULTS

Drafted results (including the distributions of potential temperature, salinity, dissolved oxygen and percent oxygen-saturation at various levels, as well as derived quantities) are presented in the following sections. These maps and figures are presented for several reasons. The analyses at selected standard levels allow the reader and potential user a quick method to evaluate the results both by comparing with previously published work and also by simple inspection. Further, the analyses present information that is of basic interest. Distributions of these quantities are not always easily obtainable, if indeed they are obtainable at all.

Derived quantities such as the fields of geopotential thickness and Brunt-Väisälä frequency are also of basic interest and give an idea of what integral and derivative quantities look like. In the case of the thickness fields, there are recently published maps for comparison. The maps of the depth and other properties of some constant-density surfaces are presented to allow eval-

uation of interpolated fields. It has long been appreciated that a major feature of the oceanic circulation is that large-scale flow is largely constrained to constant-density surfaces. Thus it is important to examine at least a few examples of these fields. The depth of and salinity on the 4°C potential temperature surface is presented for comparison with previously published work. Mixed-layer distributions are also of basic interest, especially for atmospheric and oceanic modelers, and maps of this quantity are presented. All of the drafted maps have been prepared using computer contoured maps as a guide for drafting. We note that the maps presented here have been slightly edited. Some contours are simply too short to have been drafted. In a very few cases some small-scale features that appeared to be erroneous have not been drafted. In areas where few, if any, data exist, such as parts of the Arctic Ocean, contours have not been drawn. In some areas where gradients are too large to contour, contours have not been entered. Most of the drafted figures presented in the following sections appear in the attached microfiche appendix along with many of the standard level analyses that could not be drafted. One can examine and compare these maps with their drafted counterparts.

Zonal averages over one-degree latitude belts for the world ocean and for individual ocean basins are presented for parameters in the form of figures. These same parameters are presented in tabular form as area-weighted averages over five-degree latitude belts.

Because of the large extremes of gradients of the various quantities presented we have had to use variable contour intervals to delineate many features. We wish to emphasize that in the microfiche section only one contour interval is used. While we present the microfiche maps in order to make available the results of all important analyses, we note that some features on the microfiche maps may not appear simply because of the contour interval used. It is generally not feasible to use finer intervals for selected regions.

We present a limited discussion pointing out major oceanographic features. One should consult the work of Reid (1981) and Warren (1981) for reviews of the mid-depth and deep-water circulations of the world ocean respectively.

5. BASIC ANALYSES

5.1 Annual mean potential temperature

Horizontal distributions of annual mean potential temperature are presented in figures 12 through 21 and were computed as follows. First annual mean fields of in situ temperature were computed as the average of our monthly temperature analyses at standard levels from the sea surface through 1000 m, and as the average of our seasonal temperature analyses at standard levels from 1100 m through 1500 m. Below 1500 m the annual mean in situ temperature fields were simply the analyses of the composited all-data one-degree square means at each standard level. These annual mean in situ temperature fields were then used with the annual

mean salinity fields described in section 5.2 to compute annual mean potential temperature fields. Potential temperature was computed using the polynomial given by Bryden (1973) (see Appendix C for the definition of potential temperature). In the upper 1000 m of the ocean, temperature and potential temperature are practically identical, so we will refer to these upper ocean distributions simply as temperature.

The sea surface temperature distribution in figure 12 is similar to previously published maps. Major features are the relatively low equatorial and tropical temperatures in the eastern Pacific and Atlantic Oceans. These features are generally ascribed to upwelling. In particular, we note that low temperature regions extend from the western coasts of Africa and South America in a northwesterly direction. Wyrki (1965) shows the amplitude and phase of the first two Fourier components of sea surface temperature in the Pacific that show propagation of a thermal wave from the coast of South America to the northwest. Both the phase and amplitude of the first harmonic show tongue-like distributions with phase propagation toward the northwest and with the amplitude of the first harmonic decreasing toward the northwest. Merle et al. (1980) have carried out a similar analysis for the tropical Atlantic and find a similar phenomenon. Philander and Pacanowski (1980), using experimental results from a numerical ocean model, suggest that this phenomenon may be due to wave propagation and advection of coastally upwelled water generated by winds parallel to the coast. Another feature to note in figure 12 is the accumulation of warm water in the western equatorial Pacific Ocean. This feature is not found in the Atlantic nor in the Indian Ocean. The monsoon circulation in the Indian Ocean makes interpretation of an annual mean field for that region suspect in any case.

The distribution of temperature at 150 m in figure 13 shows many interesting features. In both the eastern Pacific and Atlantic Ocean at about 10°N relative temperature minima, with contours elliptical in shape, appear. A similar pattern appears in the Indian Ocean centered at about 8°S. A similar minimum in the Atlantic appeared in the map presented by Sverdrup et al. (1942). Relative minima appeared in the Pacific and Indian Oceans of their map, but the features were not as well defined as in figure 13. For a more detailed comparison one can examine the temperature distribution at 200 m depth in the microfiche appendix. If we examine the annual mean temperature fields presented in the microfiche section of this atlas we see clearly that at shallower depths (30 to 75 m) minima first appear in the eastern parts of the Atlantic and Pacific and extend westward from the coasts with increasing depth. In the Indian Ocean the minima extend eastward from the coast with increasing depth. In the western North Atlantic at about 30°N, and in the western North Pacific at the same latitude, tongue-shaped patterns appear in the temperature distribution. We associate these features with recirculation of the northeastward flow at

these levels and the eastward flow of the subtropical countercurrents. We again note that the maps presented in this atlas are interpolated, smoothed analyses of non-synoptic data. One might consult the work of Yoshida (1970) which is based on synoptic data showing alternating bands of eastward and westward currents in this region (Pacific Ocean). Hasunuma and Yoshida (1978) have also examined synoptic data in this same region of the Pacific and found a system of currents and countercurrents. White et al. (1978) have investigated seasonal and interannual variations of the subtropical front in the North Pacific, and Roden (1975) has investigated the large-scale frontal structures of the North Pacific and processes regarding their formation.

The accumulation of warm water in the western equatorial Pacific Ocean noted at the sea surface is still observed at 150 m, although the absolute maximum in temperature is located east of the surface maximum. An accumulation of warm water is observed in the subtropical gyres of the Indian Ocean at 20°S, 55°E and in the North Pacific, North Atlantic, and South Atlantic at approximately 15° to 20° latitude from the Equator.

The distribution of temperature at 500 m is shown in figure 14. The accumulation of warm water in the subtropical gyres of all the world oceans is distinct at this level. Also apparent is the greater warmth of the North Atlantic compared with the other oceans. The equatorial Pacific exhibits a relative temperature maximum in contrast to the temperature minimum that was found in most of the equatorial Pacific at the sea surface. In the Southern Hemisphere at about 5°S to 10°S in the western Pacific and Indian Oceans, and at 10°S to 20°S in the Atlantic, meridional temperature minima exist. The axes of these minima slope along a southeast-northwest line. As will be discussed later, these regions of minimum temperature appear as regions of cyclonic shear in maps of geopotential thickness. The fact that these features exist in all major oceans suggests a common cause. In the eastern South Pacific the tongue-shaped distribution of temperature is a manifestation of the circulation of Antarctic Intermediate Water. Reid (1965) discusses this circulation.

Figure 15 shows the distribution of potential temperature at 1000 m. The dominant feature is the warm tongue extending from the Mediterranean Sea westward into the Atlantic. The accumulations of warm water in the subtropical gyres remain distinct features. The relative meridional temperature maximum in the equatorial Pacific observed at 500 m still exists and is, in fact, observed down to at least 2500 m. A tongue of relatively warm water southeast of Japan extends to the northeast. A similar feature appeared in the 150 m distribution, and its existence was ascribed to near surface processes. The feature does not appear in the 500 m temperature field but a somewhat larger tongue-like distribution does appear in the 500 m salinity field. It is significant that the feature being discussed in figure 15 does not appear distinctly without the 3.75°C con-

tour being present. If we examine the 1000 m temperature distribution presented by Winterfeld and Stommel (1972) for this region, we note that their contours and those in figure 15 show good agreement. However the 3.75°C contour is not plotted on their map, and as a result the tongue-like nature of the temperature distribution in figure 15 does not appear in their map. The tongue-like distribution represents an example of the contouring difficulties one can encounter. We have attempted to delineate the major oceanographic features that we have observed, but it is possible that some have escaped notice. In the Pacific and Indian Oceans the tropical minima observed at 500 m still appear but have shifted southward. In the Atlantic Ocean a weak minimum exists from 40°W eastward to the African coast along 26°S latitude. Delineation of this feature requires a finer contour interval than the ones used in figure 15.

Figure 16 shows the distribution of potential temperature at 1500 m. Many of the features discussed previously for the upper levels remain nearly unchanged, so we will mainly focus on changes with respect to the 1000 m level distribution. The southern hemisphere tropical temperature minima in the Atlantic and Indian Oceans do not appear, but in the South Pacific a relatively cold mass of water occupies much of the basin. It is not known whether the processes responsible for the minima observed at 500 m or 1000 m are also responsible for this feature. The meridional temperature gradient between 50°S and 60°S delineates the Antarctic Circumpolar Current. Along approximately 115°W from 40°S to 55°S a bifurcation of the temperature field appears. This temperature structure suggests that separate gyres exist at this latitude, with the 120°W meridian as a boundary between them. We will see evidence of this in the deeper temperature and particularly in the 2000 m salinity fields. The geopotential thickness maps presented in section 6.2 clearly show the existence of separate gyres. Their existence was confirmed by the data from the Scorpio Expedition as noted by Reid (1973c) along with some earlier evidence for the existence of separate gyres. The distribution of potential temperature at 2000 m (figure 17) shows significant changes with respect to the 1500 m field. The temperature gradient in the Mediterranean tongue is obviously weaker. In the Indian Ocean at 35°S, 70°E a pool of relatively cold water is observed. This feature also appears in a map of the 2000 m potential temperature distribution field presented by Wyrтки (1971). In the North Pacific at 45°N, 140°W a cold tongue extends westward from the coast.

In figure 18 the potential temperature distribution at 2500 m is shown. The cold tongue in the North Pacific at 45°N now extends much farther westward. A major feature of the North Pacific is that the meridional temperature gradient from the Equator to 30°N is much larger than the gradient from 30°N to 60°N. Maximum temperature in the North Pacific occurs at the Equator. In the North Atlantic the temperature distribution is much different, with maximum temperatures occurring

between 30°N and 50°N. At about 50°S, 115°W a tongue of cold water extends to the north and northwest from the Antarctic Circumpolar Current. This tongue separates the warm cores of the gyres to the east and west.

Figure 19 shows the distribution of potential temperature at 3000 m. At 3000 m the topography of the deep ocean begins to appear as the mid-ocean ridges manifest themselves. Qualitatively most of the features at the 2500 m level remain unchanged at the 3000 m level. One notable change is the filament-like structure of the isotherms in the South Pacific at 120°W between the Equator and 40°S.

The distribution of potential temperature at 3500 m is shown in figure 20. All gradients at this level are noticeably weaker. Some contours in the tropical Pacific have not been included. We believe quality control problems and the lack of data, in general, result in some fictitious features. The distribution of temperature at 4000 m is shown in figure 21. Again we note the weakness of the gradients.

5.2 Annual mean salinity

From the sea surface to 1000 m the annual mean at each standard level represents the average of the four seasonal salinity analyses we have computed. Each seasonal analysis was computed using composited all-data seasonal one-degree square means as input to the objective analysis procedure. Below 1500 m the annual mean at each level was computed using composited all-data one-degree square means as input to the objective analysis procedure.

The distribution of salinity at the sea surface is shown in figure 22. The major features are well known and will be noted only in brief. Subtropical salinity maxima associated with the excess of evaporation over precipitation appear in all the individual oceans. Subpolar regions exhibit low salinities associated with the excess of precipitation over evaporation. Low-salinity tongues associated with runoff from major river basins, such as the Amazon, are apparent as well as low-salinity tongues such as that observed in the Gulf of Panama that is associated with an excess of precipitation over evaporation. Advection of high-salinity water southward is apparent off the eastern coast of South America.

Figure 23 shows the distribution of salinity at 150 m depth. Again the subtropical maxima are common to all oceans. The maxima here represent regions in which high salinity water sinking from the ocean surface along constant density surfaces intersects the 150 m level. Evidence of advective effects appears in the tongue-like nature of the field in the eastern boundary currents of the north and south Pacific Oceans. The subtropical gyres do not penetrate far into the tropics in the eastern Pacific and eastern Atlantic. This lack of penetration partially explains the relative homogeneity observed in these areas. In the eastern part of the North Pacific a region of low salinity is centered at approximately

45°N, 135°W. This area has been termed the Dilute Domain by Favorite et al. (1976). The relative maximum in the Gulf of Alaska is associated with the cyclonic gyre in that area. Between 50°S and 60°S a relative minimum is apparent in the meridional salinity profile. This minimum is associated with the sinking of low salinity Antarctic surface water along the polar front zone. Gordon (1967) and Gordon and Goldberg (1970) have described this feature as well as much other oceanographic information for the Antarctic Ocean. In the North Pacific and South Pacific minima tongues extend from high latitudes first eastward, then southward as part of the eastern boundary currents, and then westward. Reid (1973a) has described these features. Their sources are the low-salinity surface waters of the subpolar regions. In the Indian Ocean at 20°S we note a low-salinity tongue extending westward from the Timor and Banda Seas. Sharma (1972) has described this feature. The salinity distributions at other standard levels show this feature distinctly between 75 m and 1400 m depth.

The distribution of salinity at 500 m is shown in figure 24. The subtropical maxima at this level all coincide fairly well with subtropical anticyclonic gyres as defined by the geopotential thickness field (see figure 57). In the tropical Pacific the Equator is observed to be a relative maximum in salinity with respect to the meridional profile. The minimum in salinity in the north Pacific as outlined by the 34.0‰ contour and the minima in the southeastern Pacific as determined by the large-scale tongue of low-salinity water are associated with the flow of Intermediate Water (Reid, 1965). The relative maxima in the subarctic gyres of the Pacific delineate the gyres observed in the geopotential thickness field. The relative minimum in salinity observed between 50°S and 60°S at 150 m appears more distinctly at 500 m and has shifted northward. A relative maximum in salinity appears around the Antarctic continent at approximately 60°S. This maximum is associated with the Circumpolar Deep Water (CDW) flowing around Antarctica. This water mass shoals towards the south, so as we examine the salinity fields at deeper levels we will observe this feature shifting northward.

The field of salinity at 1000 m is presented in figure 25 and shows substantial differences from the 500 m field. The most obvious of these is the presence of a high-salinity tongue associated with the Mediterranean outflow. Another change is that at 1000 m the centers of the subtropical gyres are relative minima in salinity in contrast to the situation at 500 m where they were maxima. The relative minima in the meridional salinity profile observed at upper levels in latitudes 40°S to 60°S have shifted farther northward and are replaced by a strong meridional gradient in salinity. The northward shift of the minima with increasing depth is also observed at deeper standard levels, and will not be noted again. The high-salinity band associated with the CDW water mass is again noted.

The distribution of salinity at 1500 m (figure 26) exhibits relatively few qualitative differences from the salinity field at 1000 m. One difference is that a high-salinity tongue extends southwestward from the Greenland-Iceland-Scotland ridge. The pattern indicates a flow of high-salinity water from the Norwegian Sea into the Atlantic. A qualitative difference, we note, is the weakened gradients at the greater depth.

At 2000 m the distribution of salinity (figure 27) is quite similar to the 1500 m distribution. One new feature is the splitting of the contours along 115°W in the South Pacific. This feature is a counterpart to the distribution of temperature in this region. The relative zonal salinity maximum along 115°W separates the low-salinity cores of the gyres to the east and west just as the temperature minimum along this meridian separates the warm cores of the gyres to the east and west. This feature will be discussed further in the section describing the geopotential thickness fields. In the North Pacific a low-salinity band extends northeastward from Japan to the coast of North America. This band remains distinct down to 3000 m depth. In reviewing the Antarctic water masses, Gordon and Goldberg (1970) present distributions of temperature, salinity, and oxygen at various standard levels. In discussing the CDW they note that on their 2000 m and 3000 m maps of salinity the "high salinity of the Circumpolar Deep Water extends to the northern boundary of the maps (40°S) except in the southeastern Atlantic Ocean where the higher salinity North Atlantic Deep Water has intruded." They further note that at "shallower levels, the salinity maximum of the Circumpolar Deep Water is isolated from the salinity maximum of the North Atlantic Deep Water by a lower salinity band." They conclude from their maps that "the influx of North Atlantic Deep Water into Circumpolar Deep Water must take place below the 1000 m level" and suggest that the influx occurs east of the Atlantic mid-ocean ridge "and not across the southern section of the Argentine Basin which has little of the highly saline North Atlantic Deep Water." The 2000 m field shown in figure 27 differs from Gordon and Goldberg's field in the southwestern Atlantic. In figure 27 we note that the salinity field does not increase monotonically towards the Equator. A relative maximum is observed extending southeastward from South America at 40°S, 55°W to 45°S, 10°E, and to the north of this relative maximum a relative minimum exists. It is possible that North Atlantic Deep Water (NADW) could be supplying the CDW from this maximum. One other point to note regarding the supply of CDW from NADW is that at 1500 m the salinity field in figure 26 shows a minimum extending across most of the South Atlantic. At the eastern end of this minimum higher salinities exist along the west coast of Africa, but they are not high enough to be considered a source of CDW. Thus regardless of exactly where the CDW is supplied with saline water, it would appear to be at a depth in excess of 1500 m. Callahan (1972) has studied the circulation of the deep water around the Antarctic. He concluded that the source-

es of CDW are to be found in the western South Atlantic and western Indian Ocean. Clowes and Deacon (1935) suggested that North Indian Deep Water flowing south along the east coast of Africa is a source of CDW at 30°E.

The distribution of salinity at 2500 m is shown in figure 28. Some features have changed in comparison to the 2000 m field. We no longer see the distinct relative salinity maximum associated with the subarctic gyres in the North Pacific. A tongue of relatively fresh water extending northward appears in the South Atlantic, bound by the 34.92 contour, but it is less distinct at the 2000 m level. This tongue also appears in the salinity map of the core layer of the intermediate oxygen maximum presented by Wüst (1935). The depth of this core layer is found between 2000 m and 2500 m in the general area of this tongue and so the agreement is as expected. In the Atlantic the CDW is no longer distinguishable as a band of maximum salinity. In the Indian Ocean a relative maximum appears beginning at about 45°S, 45°E and extends eastward. In the Pacific a maximum band occurs which becomes more narrow as it approaches the Drake Passage, so that no maximum band is discernible even at the "entrance" to the Atlantic.

The distribution of salinity at 3000 m, shown in figure 29, is similar to the 2500 m field. One difference is that we no longer observe a distinct outflow from the Mediterranean. The 3500 m distribution, shown in figure 30, differs qualitatively from the 3000 m field in the North Pacific. At 3500 m we do not find an east-west oriented low-salinity band at high latitudes as was the case at 3000 m depth. At 150°W the isohalines are north-south oriented. We observe weak relative maxima in the South Indian and South Pacific Oceans associated with the CDW water mass. At 4000 m (figure 31) the salinity field still shows some structure, but the gradients are quite weak.

5.3 Annual mean dissolved oxygen and percent oxygen-saturation

Figures 32 through 51 show distributions of dissolved oxygen and percent saturation of dissolved oxygen (hereinafter referred to as oxygen and oxygen-saturation, respectively). The annual mean oxygen and oxygen-saturation fields are based on a composite of all data in the Station Data file averaged by one-degree squares.

Percent oxygen-saturation was computed for each hydrographic cast at each standard depth level that had measurements of temperature, salinity, and oxygen. First, potential temperature was computed from the temperature and salinity observations, and next the solubility of the potential temperature-salinity pair was computed, using the formula of Weiss (1970). If we let C represent solubility in ml/l with respect to atmospheric pressure, T represent potential temperature on the Kelvin scale, and S represent salinity in ‰, then

$$\ln C = A_1 + A_2(100/T) + A_3 \ln (T/100) + A_4(T/100) + S[B_1 + B_2(T/100) + B_3(T/100)^2], \quad (13)$$

in which

$A_1 =$	-173.4292
$A_2 =$	249.6339
$A_3 =$	143.3483
$A_4 =$	-21.8492
$B_1 =$	-0.033096
$B_2 =$	0.014259
$B_3 =$	-0.0017000

If O_2 represents the observed oxygen, and P percent oxygen-saturation, then we defined percent oxygen-saturation as

$$P = 100 \cdot (O_2 / C) \quad (14)$$

The oceanographic convention in the computation of percent oxygen-saturation, which we have followed here, is to compute solubility and saturation with respect to atmospheric pressure. The solubility of oxygen in sea water is dependent on pressure (Föyn (1969) notes an increase in the solubility of a gas of about 10 percent per meter of increased depth), but exchange of oxygen with the atmosphere always occurs at atmospheric pressure; hence the convention of computation with respect to atmospheric pressure. Biological production of oxygen in the upper ocean can produce sea water with saturations greater than 100 percent when computed in this way. Shulenberger and Reid (1981) show values of 120 percent in the North Pacific during summer and Codispoti and Richards (1971) found values of 150 percent in the Arctic. Examination of the analyses we have produced do not show values this high, but we have computed only all-data annual mean fields.

The distribution of oxygen and oxygen-saturation are very similar below the ocean's surface layers. The reason for presenting both quantities is that relatively few of these fields have been presented in the literature, and the magnitudes of these quantities are of interest, as are their patterns of distribution.

The distribution of oxygen in the world ocean has been reviewed by Richards (1957). He discusses the sources and sinks of oxygen in the ocean as well as the distribution of oxygen. In particular, he reviews various facets of the long-standing controversy concerning the existence and maintenance of the deep oxygen minimum in the world ocean. Wyrski (1962), Menzel (1974), and Fiadeiro and Craig (1978) also attempt to explain the feature. Shulenberger and Reid (1981) discuss the shallow oxygen maximum in the Pacific Ocean and, in attempting to explain the high saturation values observed in the Pacific, discuss possible controlling physical and biological processes. Kester et al. (1973) and Lambert et al. (1973) discuss observations of oxygen made with continuous profiling instruments which showed oxygen variability with horizontal and vertical length scales

much smaller than can be resolved on the grid used in this study. They also give an example of the time variability of oxygen.

Figure 32 shows the distribution of oxygen at the sea surface. The major features are the increase of oxygen with increasing latitude and the approximate correspondence of the isolines of oxygen with isotherms. Both these features are due to the solubility of oxygen being predominantly a function of temperature. A map of oxygen-saturation at the sea surface is presented in figure 33. This distribution should be interpreted with care, since it is an all-data annual mean and may not be representative of annual mean conditions. Some regions are made up of data from only one season. The map is presented for comparison with deeper distributions. The sea surface is generally close to being saturated. Subsaturations are observed in the upwelling regions of the eastern equatorial Pacific and coastal areas. A future project might be to analyze and present this quantity for seasonal periods, where the data coverage permits.

Figures 34 and 35 show the distribution of oxygen and oxygen-saturation at 150 m depth. There is a strong contrast between the oxygen-saturation at the sea surface and 150 m. Outstanding features at 150 m are the four tongues of relatively low oxygen and oxygen-saturation extending westward from the continents in the tropical Atlantic and Pacific. In these tongues the absolute oxygen minimum with respect to the vertical occurs at depths of 300 to 500 m as shown in figure 52. The value of oxygen and oxygen-saturation at the absolute minimum varies from region to region, as shown in figures 53 and 54. The existence of these tongues has generally been ascribed to upwelling of nutrient-rich water that results in relatively intense primary productivity near the ocean surface. As the organic matter dies and undergoes oxidative reduction while it sinks, nutrients are released into the water column, and oxygen is withdrawn, resulting in an oxygen minimum layer and a nutrient maximum layer. The process repeats itself with the upwelling of the nutrient-rich water. It was pointed out by Richards (1957) that the depth of the oxygen minimum layer and nutrient maximum layers do not coincide, since the nutrient maximum layer is deeper than the oxygen minimum layer. This observation is well illustrated in the meridional sections of oxygen, phosphate, and nitrate presented in the Geosecs Atlantic Expedition Atlas, (Bainbridge, 1980). With regard to this theory one might examine the map of vertical velocity at the base of the Ekman layer in the North Atlantic, presented by Leetma and Bunker (1978). The vertical velocity field shows the same tongue-like distribution as the oxygen fields. Other phenomena may also play a role, or even dominate, in the formation and maintenance of the oxygen minimum tongues. Moreover, upwelling might be due to transient wave phenomena rather than a local one. For example, advection of oxygen-poor water into these regions may be of

importance. Pak et al. (1980) have discussed the offshore transport of oxygen-poor water from the continental shelves off the western coast of South America. In the Indian Ocean south of the Equator there is only a weak relative minimum in the oxygen field at this depth and we hesitate to ascribe this feature to the same processes that form the minimum tongues in the tropical Atlantic and Pacific. We do note, however, that at depths of 50 to 100 m centered at about 7°S and extending from 50°E to 90°E the distribution of oxygen shows closed, elliptically shaped contours (using a contour interval of 0.2 ml/l) that may be due to the same processes in the Atlantic and Pacific. The temperature field shows a relative minimum at these depths, but we also note the large annual cycle in this region. A proper description of the fields awaits seasonal analyses. Other important features at 150 m depth are the minima in the subarctic regions of the North Pacific that are also often assumed to be related to upwelling and organic productivity. These North Pacific minima are in sharp contrast with the high values at corresponding latitudes in the North Atlantic. This difference can be ascribed to the general upwelling and shallowness of any downward convective activity in the Pacific (probably due to low surface salinities, as noted by Reid (1973b)) compared with the deep convection in the North Atlantic that ventilates the deep waters. Large areas in all the oceans with oxygen-saturation greater than 90 percent suggest that the ocean water at 150 m is in direct contact with the sea surface at some time during the year or that oxygen at 150 m is replenished by a certain process such as vertical diffusion.

Examining the distributions at 500 m (figures 36 and 37) we note that only in the northern North Atlantic, and in small regions at 50°S, are saturations in excess of 90 percent. If we compare these figures with the 500-1000 m geopotential thickness field (figure 57) we see approximate agreement in the North Atlantic and North Pacific between the positions of the subtropical gyres and relative maxima in the oxygen and oxygen-saturation fields. In the South Atlantic and South Pacific this agreement does not hold. We have no explanation for this difference between hemispheres but suggest that in the Northern Hemisphere the location of the ventilated regions may be related to the formation of deep mixed-layers. These layers are caused by strong evaporative cooling following the outbreaks of cold, dry, continental polar air (Worthington, 1959, Masuzawa 1969). The relative minimum tongues in the tropics, as well as the subarctic minima, again appear at 500 m depth, but the gradients across their boundaries have been greatly reduced. In comparing the oxygen-saturation map with the 500-1000 m thickness map in figure 57 we note that the 10 percent contour lines define the cyclonic gyres quite well. A notable feature is the reduction of the area with oxygen-saturation in excess of 90 percent at 500 m compared with that of the 150 m level.

The oxygen distributions at 1000 m (figures 38 and 39) show substantial changes with respect to the 500 m patterns. In the North Pacific a series of basin-wide relatively oxygen-rich and oxygen-poor tongues, slope from southwest to northeast. Reid and Mantyla (1978) have reviewed some of the earlier observations of these tongues and ascribe their origin to advection. They present the distribution of oxygen on an isopycnal surface, whose depth in the North Pacific lies between 700 and 1000 m, and also show the relative flow field for the 1000-3500 m thickness layer. Their work indicates that the oxygen-rich tongues coincide with outflow from the western boundary current. Examination of the oxygen-fields at 1000 m with the relative shear flow of the 1000-2000 geopotential thickness map (figure 64) corroborates their conclusion. The flow in the southernmost oxygen-rich tongue separates from the coast in the region around 10°N as part of the circulation of the cyclonic gyre in that region. The shear flow in the northernmost oxygen-rich tongue separates from the coast at about 35°N to 45°N. In the North Atlantic the oxygen-saturation now increases monotonically from south to north. The relative minimum tongue that was found at 500 m in the western Atlantic, oriented from southwest to northeast, no longer exists. There is a change, though, in the slope of the axis of the North Atlantic tongue. The axis lies on an east-west line compared to the northeast-southwest trend at 500 m. This change of slope may be due in part to relatively oxygen-rich Antarctic Intermediate water entering the region as well as to the influence of the Mediterranean outflow. The Southern Hemisphere patterns remain qualitatively the same. The oxygen minimum tongues of the tropics remain distinct.

The oxygen distributions at 1500 m presented in figures 40 and 41 show distinct changes compared with those at 1000 m. The southernmost oxygen-rich tongue in the North Pacific still appears as a basin-wide feature, but on its southern side the magnitude of the gradients of oxygen and oxygen-saturation is reduced. With the exception of the North Atlantic tropical minimum tongue, the tropical minima appear less distinct and the axis of the North Atlantic tongue now slopes from northwest to southeast. In the Southern Hemisphere the closed contours that might be associated with the subtropical gyres have either disappeared or become much smaller. The distribution of oxygen in the South Pacific resembles the patterns produced by Kuo (1978), who used Stommel's (1958) deep circulation model with topographic effects included. In particular, the deflection of contours by the East Pacific Ridge in figure 40 is a feature of Kuo's results when topography is included but does not appear in the results for a flat-bottom model. There are, however, other features in his model that appear to be of topographic origin but do not appear in the distributions presented here.

The oxygen distributions at 2000 m are presented in figures 42 and 43. Qualitatively the distributions re-

semble the 1500 m patterns. One difference is that, in the North Pacific the southernmost oxygen-rich tongue previously discussed does not appear distinctly at 2000 m. Only a suggestion of this tongue appears. However, if one examines the 2000-3000 m geostrophic shear (figure 65) one still sees the eastward flows at both 10°N and 40°N and the westward flow centered along 35°N.

The 2500 m oxygen distributions are shown in figures 44 and 45. In the South Pacific the contours over and around the East Pacific Ridge do not show the same intense distortions as were observed in upper levels.

The distributions of oxygen at 3000 m are shown in figures 46 and 47. In the North Pacific we observe the gradients to be greatly reduced in comparison to those in the upper levels. The distributions show the eastern North Pacific to be lower in oxygen than the western North Pacific. The low-oxygen tongue extending westward from the North American coast that was first noted at 1000 m is still observed. In the mid-latitudes of the North Pacific the oxygen and oxygen-saturation increase in magnitude from the minima they attained at shallower depths. In the South Pacific a relatively strong gradient sloping from northeast of New Zealand toward the southeast appears to separate the waters of the South Pacific from the Antarctic Ocean.

At 3500 m (figures 48 and 49) and 4000 m (figures 50 and 51) the oxygen distributions are broken up by the topography of the sea floor, but qualitatively they resemble the 3000 m distributions. The minimum tongue in the North Atlantic remains a distinct feature. At this depth the presence of the oxygen-rich North Atlantic Deep Water plays a role in maintaining the basin-wide distribution.

6. DERIVED QUANTITIES

6.1 Depth and characteristics of the annual mean absolute oxygen minimum surface

Figure 52 shows the depth of the absolute oxygen minimum (with respect to the vertical) surface. Figures 53, 54 and 55 show the distribution of various properties on this surface namely oxygen, oxygen-saturation, and potential density, respectively. The depth of the absolute oxygen minimum in any one-degree square column is simply defined as the standard level depth at which the minimum oxygen value occurs in the water column. The distributions of other properties on this surface were determined by simply using the values of the parameter at the depth of the oxygen minimum. In some coastal and shelf break regions the gradients of the parameters being presented are exceptionally large. It is not physically practical to present contours in these regions. Examination of the distributions in these regions shows that the depth of the oxygen minimum changes by several standard levels (as much as 900 m) over horizontal distances as short as one-degree of latitude or longitude. What is occurring is that the absolute oxygen minimum is not a continuous feature as the

ocean shoals towards land. The regions where these gradients are particularly strong are the shelf break regions of the northern Bering Sea, western and northern Australia, New Zealand, Argentina, and the eastern coast of North America. Also the absolute oxygen minimum in the open ocean is not a continuous feature. This is because several relative minima can exist in the water column and, as the oxygen field changes on each of these surfaces, the depth of the absolute minimum can change discontinuously. Wyrski (1962) presents several vertical profiles of oxygen that illustrate the existence of multiple extrema. Examining the depth of the absolute oxygen minima in figure 52 we note the sharp depth gradient (denoted by the 500 m and 1000 m depth contours) that begin at the southwest coast of South America and extend across the Pacific to the northwest. Examination of oxygen cross sections indicates that this gradient represents an example of the discontinuity of the absolute oxygen minimum as just discussed. Obviously, care must be taken in interpreting figures 52 through 55.

Some of the major features are the shallow tropical minima at depths of 300 m to 500 m. The Pacific tongues are deficient in oxygen when compared with the Atlantic tongues. Specifically the North Pacific tongue shows values less than .25 ml/l with saturations less than five per cent. The Pacific tongues occur at potential densities less than 26.75, and the Atlantic tongues at less than 27.1. Richards (1957) presented a map of oxygen at the absolute oxygen minimum for the tropical Atlantic. The agreement between his map and figure 53 is excellent. Examining the North Pacific features north of 15°N we see the basin-wide tongues extending eastward from the western boundary that were previously noted in the standard level analyses. The oxygen minimum band between the two maxima tongues is found at depths a few hundred meters below the maximum bands. Saturations in the minima are less than five percent in the eastern region of this band. Comparison of the North Pacific and North Atlantic distributions illustrates the extreme difference in the physical processes and the resulting circulations of these two oceans. Clearly the North Atlantic is well vented by the formation of deep waters at the sea surface, while the North Pacific shows no evidence of direct vertical ventilation and only relatively weak ventilation by horizontal advection.

In the North Atlantic the Labrador Sea can be defined by the deep oxygen minimum that occurs at 2000 m depth. This minimum occurs at a density surface equal to or greater than 27.75. Most of the North Atlantic between 20°N and 40°N exhibits an oxygen minimum between 800 and 900 m depth. At this minimum oxygen ranges from 3.0 to 4.0 ml/l and potential density from 27.20 to 27.5. Seiwel (1937) attempted to describe and explain this feature.

In describing the Southern Hemisphere distributions we note that the maximum depths of the oxygen minimum in each ocean occur between 30°S and 40°S in

regions that approximately coincide with relative extrema in the temperature and salinity fields at these depths. Upon examination of the geopotential thickness maps in Section 6.2, we observe that the absolute oxygen minima occur at or near the centers of subtropical anticyclonic shear. Another major feature of the Southern Hemisphere distributions is delineated by the 500 m contour closest to the Antarctic continent on the map of the depth of the minimum layer. This contour represents the intersection of the relatively de-oxygenated Circumpolar Deep Water with the 55°S to 65°S latitude band.

6.2 Annual mean anomaly of geopotential thickness

In figures 56 through 63 maps of geopotential thickness, which is essentially a measure of the geostrophic shear, are shown for eight 500 m thick layers between the surface and 4000 m depth, i.e., for the 0-500 m layer down to the 3500-4000 m layer. We defined the geopotential thickness, ΔD , between two constant pressure surfaces, p_1 and p_2 , in the ocean as

$$\Delta D = \int_{p_1}^{p_2} [\alpha(S, T, p) - \alpha(35^\circ/\text{‰}, 0^\circ\text{C}, p)] dp \quad (15)$$

in which $\alpha(S, T, p)$ represents specific volume (cm^3/g) at salinity $S(^\circ/\text{‰})$, temperature $T(^\circ\text{C})$, and pressure $p(\text{decibars})$. The quantity $\alpha(35^\circ/\text{‰}, 0^\circ\text{C}, p)$ represents the specific volume of a "standard" ocean that has uniform values of salinity and temperature, $35^\circ/\text{‰}$ and $^\circ\text{C}$, respectively, at pressure p as a function of depth. In the actual procedure we computed the geopotential thickness between surfaces of constant depth. Pressure in units of decibars was replaced by depth in units of meters. The pressure differential dp was replaced by the quantity $\bar{\rho}gdz$, in which $\bar{\rho}$ represents a constant density of magnitude 1.02 and units of g/cm^3 , g had a value of $9.8 \text{ m}/\text{sec}^2$, and dz represents the difference in meters between two surfaces of constant depth. The units of geopotential thickness are those of specific energy, ($10 \text{ m}^2/\text{sec}^2$). In the specific volume (density) computation the Knudsen-Ekman equation of state for sea water has been used as given by Fofonoff (1962). Appendix C contains the formula for the equation of state. The temperature and salinity fields used in the computation of the annual mean anomaly of geopotential thickness fields were the annual mean fields of in situ temperature and salinity described in sections 5.1 and 5.2 respectively.

In the following discussion these maps are used to delineate changes in the large-scale ocean circulation with depth. Some of these maps will be compared with previously published maps. In addition, some maps of geopotential thickness for some 1000 m thick layers, namely the 1000-2000 m and 3000-4000 m layer are presented in figures 64, 65, and 66. Finally, in figure 67 is given a map of the dynamic topography of the sea surface with respect to the 2000 m level, while figures

68 and 69 are maps of planetary vorticity (coriolis parameter divided by ocean depth) and ocean bottom topography that will be useful in our discussion of the deep ocean circulation. The ocean topography on which these maps are based is that of Smith et al. (1966). In figures 68 and 69 some contours have not been entered because of their short length. The arrows on the thickness maps indicate the direction of flow, assuming geostrophy and the deeper level to be a level of no motion. We note that the assumption of a reference level of no motion is not generally valid and can lead to misleading interpretations. Our main interest, however, is in the large-scale flow patterns and how they change with depth. Even with additional information, such as water mass properties, the absolute direction of flow can be difficult to determine. For an example of this the reader is referred to Warren (1973, p.10). An essentially equivalent and no less unambiguous rule for determining the flow direction is to use the thermal wind relation, assuming that velocity always decreases with depth. This procedure then yields the same direction of flow as the assumption that the deepest level of the layer considered is at rest. The absolute velocity field is of prime importance, but its attempted computation through analytical or general circulation modeling techniques is beyond the scope of this paper. Stommel and Schott (1977) and Wunsch (1978) have developed analytical techniques to determine the absolute velocity field from hydrographic station data. Mellor et al. (1982) present mass transports for the North Atlantic Ocean using a diagnostic technique based on the analyses presented in this atlas.

The 0-500 m thickness map in figure 56 shows the subtropical anticyclonic and subarctic cyclonic circulations noted in previously published dynamic topographies. In particular, Wyrтки (1974) published a 0-500 m topography for the Pacific. There is good agreement between Wyrтки's map and figure 56. The tropical current systems are apparent as well as the anticyclonic circulation of the Beaufort Sea. The Mindanao eddy at about 130°E, 7°N described by Wyrтки as the western terminus of the North Pacific equatorial countercurrent trough, is also present. The subtropical countercurrents of the North Pacific (Yoshida and Kidikoro, 1967) and North Atlantic (Voorhis and Hersey, 1964) appear in this annual mean map but appear more prominently in some of the monthly-mean maps. The Southern Ocean distribution agrees quite well with the thickness map presented by Gordon et al. (1981).

The 500-1000 m thickness map in figure 57 shows distinct changes in circulation compared with the 0-500 m map. The tropical current systems in the Atlantic and Pacific have disappeared, indicating their shallowness as noted previously by Wyrтки (1974) for the Pacific. The subtropical gyres appear more distinct, and recirculations are more apparent. Some shear remains in the Indian Ocean, but it is weak compared with the surface distribution. As is well known, the surface flow

itself in the northern Indian Ocean totally reverses from summer to winter, so no discussion is presented for the annual mean surface flow in that region. The main feature in the southern Indian Ocean is the subtropical gyre whose axis lies along 32°S. The Alaskan and Kamchatka gyres still appear and, in fact, will remain noticeable down to great depths. The surface cyclonic gyre of the Labrador Sea is greatly reduced in intensity. The circumpolar current appears on all thickness maps but becomes more distinct with increasing depth. The Northern Hemisphere oceanic polar fronts are shown clearly. One might consult the work of Dietrich (1969) to compare our smoothed maps based on non-synoptic data with the convoluted flow found during the I.G.Y. investigation of 1958 in the northern North Atlantic. In the western portions of the tropical North and South Pacific Oceans, weak cyclonic gyres appear equatorward of the subtropical gyres. Weak cyclonic flow appears in the tropics of the South Atlantic.

Comparing the 1000-1500 m map with the 500-1000 m map we see a substantial weakening of the gradients for all circulation features. In the North Atlantic, weak northward shear flow appears along the western coasts of Africa and Europe, while in the 500-1000 m map the shear flow tends to be southward. Along the northeastern portion of South America the thickness map indicates northwest shear flow parallel to the coast, and this appears to join the northward shear flow at Florida. Another part of this northwest shear flow turns toward the northeast and extends across the entire North Atlantic basin. This northeastward shear flow is totally opposite in direction to the flow indicated by the 500-1000 m map. The South Atlantic shows little change. In the North Pacific the subarctic cyclonic gyres show only a weakening in intensity. There are substantial changes in the rest of the North Pacific. The subtropical gyre is reduced in its equatorial extent. The gyre extends southward to approximately 25°N on the 1000-1500 m map as compared with 15°N on the 500-1000 m map. In the South Pacific the subtropical gyre also has a reduced equatorward extent. In both the North Pacific and South Pacific western tropical regions we find cyclonic gyres. The axes of these gyres lie slightly poleward of their 500-1000 m counterparts.

Comparison of the 1500-2000 m thickness map with the 1000-1500 m map again shows some noticeable changes in the circulation. A weak anticyclonic gyre now appears in the Labrador Sea. Shear flow from the southwest to northeast again starts at the northeast tip of South America as it did on the 1000-1500 m map but turns to the north and then due west to return to the North American coast at Florida. In the western South Atlantic a closed cyclonic gyre appears equatorward of the subtropical gyre. In the North Pacific the subtropical gyre extends to about 150°W, but to the south and east a series of three weak anticyclonic gyres exist, and south of these are three more weak cyclonic gyres. Each set of three gyres might actually consist of one

but, with gradients as weak as those observed, the details of the flow depend considerably on the smoothness of the flow performed and on the data available. The South Pacific shows major changes where topography begins to play a role in determining the shear flow patterns. The flow is continuous, nearly basin wide, subtropical gyre of the upper layers has split into two gyres, probably due to the East Pacific Rise at 115°W. In fact, the shear flow roughly follows lines of constant planetary vorticity as shown in figure 68). The two-gyre nature of the shear flow in this area was previously noted in the discussion of the temperature and salinity fields at this depth. Reid and Arthur (1975) have noted the same nature in their geopotential thickness maps for the Pacific Ocean. The tropical cyclonic gyre in the western tropical North Pacific is similar to that in the 2000-1500 m distribution. The cyclonic circulation previously noted in the western tropics of the South Pacific is no longer present. There exists, however, a nearly basin-wide cyclonic gyre centered at about 25°S, 120°W. In the Indian Ocean north of 25°S weak shear flow dominates, while south of this latitude the subtropical gyre and Antarctic Circumpolar Current remain distinct features. We note in the upper layers, but still more clearly on the 1500-2000 m thickness and the 2000-2500 m thickness maps, that the subtropical gyres of the Southern Hemisphere remain distinct features with increasing depth, but their Northern Hemisphere counterparts weaken considerably or even disappear.

Comparison of the 2000-2500 m map with the 1500-2000 m map shows cyclonic flow to persist at 55°N, 30°W. A more distinct anticyclonic gyre now appears in the North Atlantic, and there is continuous westward shear flow across the basin at 30°N. Eastward shear flow at about 20°N appears to form a cyclonic gyre. In the South Atlantic the circulation is quite similar to that depicted on the 1500-2000 m map. The North Pacific shows interesting changes. The weak anticyclonic gyre of the 1500-2000 m map at 35°N extending eastward from Asia to 150°W, has now been reduced in size to a gyre centered at 42°N, 175°W and is only about 35 degrees of longitude in width. To the north, the cyclonic shear flow of the subpolar regions still remains. To the south and west, cyclonic gyres exist with westward shear flow at about 40°N due to both the cyclonic and anticyclonic gyres. In the South Pacific a major change is that a distinct branch of the eastward flow at 55°S, 120°W turns northward for approximately 2800 kilometers, turns eastward and then southward to its initial latitude, where it continues flowing eastward. Again the flow roughly parallels isolines of planetary vorticity, so that conservation of potential vorticity appears to be a controlling factor. Moreover, the cyclonic flow at 25°S, 120°W is greatly reduced in size. The circulation in the Indian Ocean has not changed qualitatively.

The 2500-3000 m thickness map begins to show the presence of major topographic features such as the

mid-ocean ridges. In comparison with the 2000-2500 m flow the North Atlantic shows little evidence of cyclonic flow in the subpolar region but still shows the anticyclonic gyre north of 30°N. In the South Atlantic the subtropical gyre appears as a small feature at 32°S, snug against the South American coast. Upon comparison with the map of planetary vorticity, the flow at 10°W between 20°S and 40°S appears to be influenced by topography. In the North Pacific the subpolar gyres still appear, but a large, basin-wide, cyclonic gyre to the south replaces the relatively smaller anticyclonic and cyclonic gyres that appeared on the 2000-2500 m map. In the South Pacific, cyclonic gyres appear just south of the Equator, and the subtropical gyre still remains distinct. Some component of the eastward shear flow at 50°S, 120°W turns northward and, after a convoluted trip, returns to its starting latitude and resumes eastward flow. In the Indian Ocean the features may be compared with those on a similar map by Wyrki (1971). However, details of the flow differ. For example, the features of figure 61 north of 40°S are somewhat disjointed as compared with those on Wyrki's map. This probably reflects differences in smoothing between the two analyses. Nevertheless, overall agreement is good.

The 3000-3500 m map shows the broad anticyclonic circulation in the North Atlantic as is observed in the 2500-3000 m map, but it also indicates the existence of two distinct anticyclonic gyres. Shear flow to the northwest now appears northeast of South America and at 15°W north of the Equator. In the South Atlantic there is an anticyclonic gyre centered at 45°S, 50°W. Quite apparent now are the deficiencies of the assumption that the deeper level is one of no motion. Reid et al. (1977) pointed out that the absolute flow in the western part of this gyre flow is actually from the south to the north judging by water mass properties. The North Pacific exhibits an anticyclonic gyre centered at 45°N, 180°E. Just to the south of this gyre is a cyclonic gyre. In the eastern part of the basin a northward shear flow appears, parallel to the coast. In the South Pacific the subtropical gyre is still quite distinct, but to its north another anticyclonic gyre appears.

Finally the 3500-4000 m map shows many of the same features as the 3000-3500 m map, although in a somewhat more disjointed pattern. Some features that appeared to be erroneous, either for lack of data or through other analysis problems, have been eliminated in this presentation. There is still anticyclonic flow in the North Atlantic. Cyclonic shear flow exists in the North African Basin. Southward shear flow is indicated along the western edge of the South Atlantic to about 45°S. The North Pacific shows anticyclonic shear flow at 45°N similar to that observed in the 3000-3500 m map as well as the roughly northern flow along the coast. Other features appear, but the gradients are quite weak and the data quite sparse, and so one should interpret these deeper ocean maps with caution. In the South Pacific

the subtropical gyre persists. The Antarctic Circumpolar Current is still much in evidence at this level.

The maps of the 1000-2000, 2000-3000, and 3000-4000 m thickness fields are presented for comparison with the maps of Wyrтки (1974) for the Pacific Ocean, Wyrтки (1971) for the Indian Ocean, Reid and Arthur (1975) for the Pacific Ocean, and Gordon et al. (1978) for the southern ocean. The only feature that will be noted is that of the alternating eastward and westward shear flows in the North Pacific on the two deeper maps. These patterns were previously noted in the discussion of the oxygen distributions at these depths. The correspondence between the tongues in the oxygen fields and the axes of relative flow as shown in these figures is quite good.

Figure 67 is the 0-2000 m thickness map, and if the 2000 m level is assumed to be a level of no motion, the map represents the topography of the sea surface. As previously noted, this hypothesis is not generally valid, but over such a thick layer the qualitative sense of the circulation should be quite good. For example, Kirwan et al. (1978) have shown that satellite tracked drifters in the eastern North Pacific follow trajectories quite similar to the mean annual dynamic topography (with respect to 1000 m) presented by Wyrтки (1975). Wyrтки et al. (1981) show that buoys placed in the Pacific North Equatorial Countercurrent exhibited trajectories that "verify the coherent character of a current such as the North Equatorial Countercurrent." One should note that in regions of intense mesoscale eddy activity this type of agreement may not hold. Nevertheless it is of interest that the large-scale flow in some parts of the world ocean are successfully mapped, based on non-synoptic data. We could present maps with respect to deeper levels and capture more of the deeper gradients but then we would lose more of the coastal flow. One could discuss the differences in height from ocean to ocean as Reid (1961) has done (based on temperature and salinity differences, water mass formation regions, and geography), but this is beyond the scope of this study. However, tables 56 through 60 and figures 123 through 127 show mean values of water mass properties for individual ocean basins that could be used for such ocean-by-ocean comparisons.

6.3 Annual mean Brunt-Väisälä frequency

The horizontal distributions of annual mean Brunt-Väisälä frequency, N , for selected standard levels are shown in figures 70 through 77. This parameter is of interest for at least two reasons. The first is that the Brunt-Väisälä frequency is of prime importance in the studies of various types of wave motion in the ocean. The second reason is that it is a vertical derivative and thus yields some visual information on the smoothness of the analyses. Alternatively to presenting Brunt-Väisälä frequency we could have presented the Hesselberg-Sverdrup stability parameter, since the two are simply different forms of the same quantity. In fact, in

the discussion we will use the two interchangeably by referring to regions of large (small) N as being regions of high (low) stability. We could also have presented distributions of derived quantities, such as the Rossby radii of deformation, but we leave such computations for later work and only present here one factor that is indicative of stratification. The temperature and salinity fields used in the computation of the annual mean Brunt-Väisälä frequency fields were the annual mean fields of in situ temperature and salinity described in sections 5.1 and 5.2 respectively.

The definition of N for a continuous fluid is

$$N = \sqrt{\frac{g}{\rho_0} \frac{\partial \rho}{\partial z}} \quad (16)$$

in which $g=9.8$ m/sec² and ρ_0 is a constant equal to 1.02 with units of density. For data given at discrete levels in the vertical, the computation (as noted similarly on p. 10 for the stability computation) of N at some depth level k involves computing the vertical density gradient by adiabatically displacing the parcel of water from level $k+1$ to level k , and then taking the density difference between the parcel at the depth level k and the parcel displaced to level k . We have computed annual mean distributions of N from the annual mean objective analyses of in situ temperature and salinity. Thus the finite difference formula for the Brunt-Väisälä frequency at a depth level k and a one-degree square denoted by (i,j) is

$$N_{i,j,k} = \frac{g}{\rho_0} \left[\rho_{i,j,k+1}(S_{i,j,k+1}, T'_{i,j,k+1}, Z_k) - \rho_{i,j,k}(S_{i,j,k}, T_{i,j,k}, Z_k) \right] / (Z_{k+1} - Z_k) \quad (17)$$

in which S, T, ρ , and Z represent salinity, temperature, density, and depth, and T' represents the local potential temperature the water parcel, originally at level $k+1$, has after adiabatic displacement to level k . The formula used for computing the adiabatic temperature change of the displacement parcel is given by Bryden (1973) and is presented here in Appendix C.

In this atlas N will be given in cycles/hr. We recognize that cy/sec or radians/sec represent the standard MKS units for this quantity but prefer units of cy/hr, giving a more "physical feel" to this quantity.

The distribution at the sea surface will not be presented. The only features worthy of mention are the areas of high stability located in the regions of river runoff. Seasonal maps might show areas of varying stability that would be of interest, but much more salinity data would be required. Figure 70 shows the distribution of N at 150 m. The major feature at this level is the area of large values in the tropics, which defines

the region of high stability where the tropical thermocline intersects this depth. In the eastern parts of the tropical Pacific and tropical Atlantic, which are below the thermocline at this level, the values of N are substantially smaller. Minimum bands centered at about 10°N in the Pacific and western Atlantic appear to be associated with the equatorial countercurrents in these regions. The center of the minimum band in each ocean coincides with the northern edge of the countercurrent in each ocean as seen in the 0-500 geopotential thickness map shown in figure 56. Relatively small values are observed in the weakly stratified polar and subpolar regions. A tongue of relatively high stability extends eastward from Japan, and a weaker counterpart to this feature appears to extend eastward from the east coast of the United States.

Figure 71 shows the distribution of N at 500 m. The subtropical gyres are the regions of highest stability. Almost no structure appears in the tropics. Polar and subpolar regions show relatively weak stratification. The Kuroshio Extension is characterized by a gradient in N that weakens with increasing distance from the coast. The same holds for the Gulf Stream system. A relative maximum appears at 50°S to 60°S from 80°E longitude eastward to 75°W longitude that approximately coincides with the axis of the Antarctic Circumpolar Current (ACC) as shown in figure 57.

The distribution of N at 1000 m is shown in figure 72. Major features are again the relative maxima that appear in the subtropical gyres of all the major oceans. The maxima, however, are weaker than their 500 m counterparts and the gradients across the gyres are considerably reduced compared with the gradients at 500 m. Across the entire Southern Hemisphere ocean there is a distinct meridional gradient that appears to be associated with the ACC as delineated in figure 53 but no relative maximum is observed as was the case at the 500 m level. The distribution of N in the subarctic regions of the North Pacific delineates the individual gyres of that region. In the North Atlantic the dominant tongue-shaped distributions of temperature and salinity in the Mediterranean outflow have no counterpart in the distribution of stability.

At a depth of 1500 m the distribution of N (figure 73) shows some major differences from the 1000 m distribution. The gradient associated with the subtropical gyres in both the North Pacific and North Atlantic have disappeared or weakened, but in the southern hemisphere we still observe maxima associated with these features. A relative minimum centered at approximately 170°W along 15°S coincides with a region of cyclonic shear, as observed in the 1000-1500 m geopotential thickness field shown in figure 58. The magnitude of N at 1500 m is for the most part substantially smaller than N at 1000 m. An exception is in the region of the ACC where N has shown only a slight decrease in magnitude. Also the meridional gradient across the ACC shows only a slight decrease as compared with the 1000 m gradient.

Figure 74 shows the distribution of N at 2000 m. The relative lack of change in the magnitude and meridional gradient of N that characterized the comparison of the 1500 m level with the 1000 m level also characterizes the comparison of the 2000 m level with the 1500 m level. In the Southern Hemisphere we still observe the gradients and relative maxima associated with the subtropical gyres. As observed at 1500 m there is correspondence in the stability field as delineated by the minimum centered at $20^{\circ}\text{S}, 130^{\circ}\text{W}$ with the region of cyclonic shear as observed in the 1500-2000 m geopotential thickness field shown in figure 59.

The distributions of N at 2500 m, 3000 m, and 3500 m are shown in figures 75 through 77. These distributions are quite similar and will be discussed as a group. In the North Pacific and North Atlantic the gradients of N are quite weak. In the Southern Hemisphere the major features are, as at upper levels, the relative maxima of the subtropical gyres and the gradient associated with the ACC.

6.4 Depth and characteristics of the annual mean 27.7 potential density surface

Figure 78 shows the depth of the 27.7 annual mean potential density surface and figures 79 and 80 show the respective distributions of potential temperature and oxygen on this surface. To compute these surfaces, first potential density was computed at each gridpoint on each standard level from the equation of state for sea water, (Fofonoff, 1962) (included in Appendix C), using the annual mean potential temperature and salinity analyses previously described in sections 5.1 and 5.2, with pressure set equal to zero. The depth of the 27.7 surface was then computed at each gridpoint by linear interpolation between those two standard levels whose range of potential density bracketed 27.7. The values of oxygen and potential temperature on the 27.7 surface were then computed by linear interpolation at each gridpoint using the values of these parameters at the adjacent standard levels above and below the computed depth of the 27.7 surface.

The 27.7 surface is simply one of many deep constant potential density surfaces that could have been presented. We chose to present an isopycnal surface because it has often been assumed (Reid, 1981) in oceanography that mixing and flow in the oceans predominantly occur along isopycnal surfaces. Much of descriptive physical oceanography has been based on the use of isopycnal surfaces. Kawai (1966) and Reid and Lynn (1971) have improved this technique through the use of several reference surfaces for the computation of local potential density. We present the depth of and distributions on the 27.7 surface simply as an example of an isopycnal surface that can be defined using the objective analyses presented in this atlas. Shading indicates regions where the density surface does not exist in the water column.

The outstanding feature of this surface is its northward descent from 200 to 1800 m in the 45°S to 65°S

circumpolar belt. This annual mean density surface does not intersect the sea surface to any significant extent in the Antarctic Ocean. From examination of the distributions of observations we note that the data in this region represent mainly local summer data, so that in this region the density surface may intersect the sea surface that in fact could be sea ice. Both the oxygen and potential temperature fields show large gradients coincident with the region of sharp descent. In the South Pacific along 115°W a relative minimum exists in the depth of this surface. This minimum is consistent with the relatively low temperatures and high salinities observed along this longitude. The maximum depths of this surface in the southern hemisphere coincide with the centers of the subtropical gyres as observed in the 2000-2500 m geopotential thickness field presented in figure 60.

In the Pacific Ocean from 30°S to 30°N, the depth of the 27.7 surface is approximately 2000 m throughout, so the fields of oxygen and potential temperature on this surface are very similar to the distributions of these quantities at 2000 m. The depth minima of this surface in the subarctic North Pacific are associated with regions of cyclonic shear, as seen in figure 60. In the North Atlantic the surface shoals very steeply in the region northeast of Cape Hatteras. This shoaling is associated with the Gulf Stream flow. The potential temperature field shows the warm tongue associated with the Mediterranean outflow, and the oxygen field shows the tropical minimum tongues previously discussed.

6.5 Seasonal density distributions

Northern Hemisphere winter (February, March, April) and Northern Hemisphere summer (August, September, October) distributions of the depth of and salinity on the 24.5 and 26.0 potential density surfaces are shown in figures 81 through 88. These surfaces were computed using the seasonal fields of potential temperature and potential density computed from the seasonal analyses of in situ temperature and salinity. Comparison of the winter versus summertime distributions clearly shows large seasonal differences in area exposed to direct contact with the atmosphere. In particular, during the summer in the North Pacific there is only a very small region in the northern North Pacific in which the 26.0 surface intersects the sea surface (as denoted by the shaded areas on the maps). This suggests that exchange of properties between this surface and the atmosphere by direct contact is limited during summer. For the winter distribution, however, we see a much larger area of intersection with the sea surface. Clearly, if one is interested in air-sea exchange, then the seasonal variability of density surfaces is of importance. Indeed, direct exchange of properties and materials between the atmosphere and ocean density surfaces may not be the only process by which ocean density surfaces acquire characteristics or materials. Reid (1965), in a study of the

intermediate waters of the Pacific Ocean, has suggested that vertical exchange plays a major role in the formation of the North Pacific intermediate waters. He inferred this because the density surface that is characteristic of this water mass does not appear to intersect the sea surface in the North Pacific to any significant degree.

The greater depths of the density surfaces in the North Pacific then in the North Atlantic reflect the greater warmth of the Atlantic than the Pacific in these regions. One can examine these maps as well as the distributions of temperature and salinity and make similar comparisons for other oceans as well.

One major feature of these maps is the ridge-trough system that appears in the tropical Atlantic and tropical Pacific. The equatorial countercurrents are particularly well delineated by this distribution as observed on the summer depth of the 26.0 surface. The advection of low salinity water southward in the eastern Pacific is a significant feature. Comparing the distributions of depth and salinity where these surfaces have their deepest vertical penetration we perceive relatively little change of these distributions from season to season.

To show the seasonal differences in the surface areas intersected by various ranges of density we present figures 89 through 92 which are seasonal maps of density (σ_t) at the sea surface. These can be used for rough estimates of the seasonal variation of the amount of exposed area for various density ranges.

6.6 Depth and salinity of the annual mean 4°C potential temperature surface

For a comparison of the analyses presented in this atlas with earlier subjective analyses by investigators relying exclusively on high quality Nansen cast data, we present in figures 93 and 94 the depth of and salinity on the 4°C potential temperature surface. A linear interpolation was used for computation of these fields from the annual mean fields of potential temperature and salinity fields described in sections 5.1 and 5.2. Where temperature inversions exist in the water column we used the deepest level at which the isotherm was found for defining the surface. Figures 93 and 94 can be compared with maps of the same quantity presented by Worthington and Wright (1970) for the North Atlantic Ocean. For their study Worthington and Wright used only salinity data measured to an accuracy of three decimal places. The accuracy of their data allowed them to use a fine contour interval and to contour in detail relatively small-scale features where the data was sufficient. In some regions, as they point out, the station spacing is too coarse to draw contours without some ambiguity. Since they used data at the exact station location rather than averaging data by grid squares, as we did, they could contour in finer detail in regions of high station density. By contrast, the results presented in this atlas are based on salinities accurate to two decimal places with data averaged by one-degree squares,

so that the smallest resolvable feature has a wavelength of two degrees. Smoothing of the entire field as described in section 3 further reduces the scale of features that appear in the analyses. Comparing the depths of the 4°C surface between the two maps we find good agreement of the large-scale features. There are noticeably more small-scale features in their maps but this is attributable to the nature of their analysis technique. At 36°N, 73°W we note that in the space of one degree there are three contours and four or five stations to support the analysis. If one were to average the data by one-degree squares before contouring it is clear that this gradient would be greatly reduced in magnitude. This comparison of the two techniques should give some accounting for the differences between the two sets of results.

Also there are some features of special interest in the fields themselves. At about 10°S, 30°W the depth contours converge, and a large meridional salinity gradient appears along this convergence line. These features appear because there is an inversion of the 4°C surface in this region. The inversion is well illustrated in the meridionally oriented temperature profiles presented by Wust (1935), particularly for the western and central Atlantic temperature sections.

6.7 Mixed-layer distributions

As another interesting example of derived quantities that can be computed from our analyses we present distributions of mixed-layer depths for March and September based both on a temperature criterion and a sigma-t (density) criterion, as well as some time-plots of the annual cycle of mixed-layer depths based on a temperature criterion for selected one-degree squares. The mixed-layer fields were determined from our monthly analyzed fields of temperature and monthly fields of sigma-t computed from our monthly analyzed fields of temperature with the appropriate seasonal salinity analyses. In the polar regions contours have been drawn in some areas where ice normally occurs during the winter season. The results in these areas are not based on winter data and simply represent the annual mean first-guess fields. One can examine the distribution of observations in these regions and note that in some cases the results are due mainly to summertime data only.

The criterion for determining the mixed-layer depth based on temperature is as follows. At each one-degree square the surface temperature is used as a reference temperature. Then each succeeding deeper standard level is examined until one is found that has a temperature differing from the surface temperature by more than some chosen value. Except in the cases specifically noted, the value used in the results presented here was 0.5°C. A linear interpolation is then performed between this subsurface level and the preceding level to obtain the depth at which the subsurface temperature differs from the surface temperature by the chosen value. The maximum depth we examined was 1000 m. If the criterion

was not met through this level, the mixed-layer depth was set at 1000 m. A caveat needs to be issued here. It is that a temperature criterion is not adequate for determining mixed-layer depths over the entire world ocean. For example, in subarctic regions one observes isothermal conditions or even temperature profiles with inversions combined with a salinity profile that stabilizes the water column and, in effect, controls the depth of mixing. Examination of some regions in the analyses presented in this atlas show that the temperature is isothermal (to within 0.5°C) to a depth of 1000 m but with a strong halocline existing near the surface. Thus we have also computed mixed-layer depths based on sigma-t (see Appendix C for definition). The procedure for computation is the same as for temperature, with the sigma-t criterion being a value of 0.125 (10⁻³ g/cm³). For brevity we drop the units of sigma-t in future occurrences in the text. This value corresponds approximately to a temperature difference of 0.5°C for a parcel of water with a salinity of 35.0 ‰ and a temperature in the 17°C to 19°C range. Because the coefficient of thermal expansion for sea water is a strongly non-linear function of temperature, a temperature difference of 0.5°C corresponds to a relatively large range of sigma-t differences over the range of temperatures and salinities found in the surface layers of the world ocean. For example, at a salinity of 35.0 ‰ the 0.5°C temperature difference corresponds to sigma-t changes of approximately 0.075 magnitude in the 6°C to 10°C range and to approximately 0.15 magnitude in the 24°C to 26°C range. This property of sea water makes comparison of the mixed-layer depths based solely on a temperature criterion with mixed-layer depths based solely on a sigma-t criterion ambiguous. Using the values of thermal expansion just noted, and neglecting any vertical salinity stratification, the following example is informative. Had we used a sigma-t difference of 0.15 as our criterion in order to obtain mixed-layer depths comparable to the mixed-layer depths found using a temperature criterion of 0.5°C, then the mixed-layer depths in colder regions would not correspond to mixed-layer depths found with the 0.5°C temperature criterion. In the 6°C to 10°C range use of the 0.125 sigma-t criterion corresponds to a 1.0°C criteria in the temperature case. One should keep this phenomena in mind when comparing the mixed-layer maps computed with the temperature and sigma-t criteria that are shown in this section. In regions with a very strong thermocline the phenomena just discussed would not cause a very large change in the mixed-layer depths computed with either criteria, but in other regions it might be of importance. One can conceive of performing the mixed-layer computation with a variable sigma-t criterion that corresponds to a fixed temperature criterion, such as 0.5°C, over the entire world ocean. To do this, the coefficient of thermal expansion would be evaluated with the surface values of temperature and salinity in each one-degree square to determine the sigma-t difference re-

quired to obtain a temperature difference equal to the desired temperature criteria. This procedure is beyond the scope of the present work.

Our primary goal in presenting mixed-layer maps for the same months, but based solely on either a temperature criterion or a sigma-t criterion, is to demonstrate the importance of the salinity stratification on the determination of mixed-layer depths. This effect is known but perhaps not generally appreciated. Mixed-layer computations that appear in the literature are almost always based on a temperature criterion. Temperature measurements are far more abundant than salinity measurements, which may account for this practice.

In computing monthly fields of sigma-t we used our monthly temperature analyses with the appropriate seasonal salinity analysis. The lack of salinity data for large areas of the world ocean necessitated this procedure, and the annual cycle of salinity may not be well represented in some areas. The results, however, do show major differences in some areas between the mixed-layer computations based solely on temperature and those based solely on sigma-t that are due to the presence of haloclines. In particular, the subpolar regions of the North Pacific and Southern Ocean show major differences.

All the mixed-layer distributions here are relatively noisy, probably reflecting the non-synoptic characteristics of the data. Large-scale features do appear, however. A number of small-scale features have not been contoured.

We will first compare the March and September mixed-layer depths determined by using a temperature criterion of 0.5°C (figures 95a and 96a). The most obvious phenomenon is the shallowness of the mixed-layer in summer versus that in winter in each hemisphere. Solar heating produces a shallow summer mixed-layer, while air-sea interactions produce the deeper winter mixed-layers. There are also regions where ocean dynamics appear to play a major role. During March in the eastern equatorial Pacific a minimum tongue is centered along the Equator. Qualitatively this feature, as well as the relative maximum to the north, agrees well with the March map of mixed-layer depth presented by Wyrтки (1964) for this region. Wyrтки's definition of the mixed-layer depth was the average of two procedures based on temperature data alone, and so we can only make qualitative comparisons. The equatorial minimum, as suggested by Wyrтки, can be ascribed to equatorial upwelling. The general zonal character of troughs and ridges in the tropics are related to the presence of equatorial current-counterstream systems. This structure of ridges and troughs also appears in the mixed-layer maps presented by Bathen (1972). Relatively complicated structures appear southeast of Japan and the eastern United States in March. Proceeding eastward from Cape Hatteras the mixed-layer is first shallow, then it increases sharply as part of a relative maximum

tongue that slopes northeast to southwest. Continuing eastward there is a decrease and then an increase before the field becomes relatively flat. In the Pacific there is a minimum east of Japan as delineated by the 75 m contour, and as we move southeastward a relative maximum appears. We will not attempt to explain these features except to note that the outbreak of continental polar air masses as suggested by Worthington (1959, 1972) and Masuzawa (1969) results in relatively deep mixed-layers and must be considered one of the causative factors. In addition, the western boundary currents probably play a role. A relative minimum on the March distribution is centered at $50^{\circ}\text{N}, 38^{\circ}\text{W}$. This could be the result of a cyclonic circulation in this region. To the north and west of this minimum is a relatively narrow maximum band. A similar feature appears in the North Pacific. In both oceans there are relatively small regions in which the mixed-layer depth extends to at least 1000 m, (the deepest level to which we searched), although the contour has not been put on the map. We will show that salinity is a controlling factor in some of these regions. The last feature to be noted on figures 95a and 96a is the occurrence of deep mixed-layers in the 50°S to 60°S latitude band. Data showing deep mixed-layers (based on temperature) at these latitudes have been presented previously. Colborn (1975) and Wyrтки (1971) noted the existence of deep mixed-layers in the Indian Ocean. McCartney (1977) presented additional station data showing the existence of deep mixed-layers for the Indian, Atlantic, and Pacific Oceans. He suggests that Antarctic Intermediate Water is formed in these mixed-layers. Additional data, especially salinity measurements, are needed to define the features of this area.

Comparing the March mixed-layer depth distributions based on a sigma-t criterion of .125 shown in figure 95b with the March mixed-layer distribution based on temperature, the most dramatic difference occurs in the North Pacific Ocean. The deep (>250 m) mixed-layers between 47°N and 57°N in the temperature-based distribution have much more shallow (approximately 100 m) counterparts in the sigma-t based distribution. This is due in major part to the presence of a halocline in this region, a limiting factor for deep mixed-layer formation, as noted by previous investigators. The 150 m contour to the northeast of Japan in figure 95b contains mixed-layers of about 190 m in depth. This region contains the deepest mixed-layers in the North Pacific except for a relatively small area extending eastward from the Kamchatka Peninsula and an even smaller area extending southwestward from the same peninsula. The region bounded by the 150 m contour, then, is a relative maximum in mixed-layer depth with respect to the meridional direction, but it is interesting to note that in figure 95a this geographical region is a relative minimum. In the eastern equatorial Pacific the 10 m and 25 m contours are nearly the same on both maps. In the North Atlantic the minimum observed at 52°N ,

35°W in the temperature based distribution does not appear in the sigma-t-based distribution. A major feature that does appear in both distributions is the relative maximum whose axis occurs along a northeast-southwest sloping line from about 40°N,30°W to about 30°N,60°W. The maximum depth of this feature is much deeper in the sigma-t based distribution than in the temperature-based distribution. In contrast to the North Pacific sigma-t-based distribution, there are areas in the North Atlantic that have mixed-layer depths of 1000 m although these areas are relatively small. They occur in the Labrador Sea, just southeast of Greenland, and at 68°N,5°W. In the Southern Hemisphere the two distributions are fairly similar during March, the summer season.

The September mixed-layer depth distribution based on sigma-t is shown in figure 96b. In both September distributions the North Atlantic and North Pacific features are quite similar, suggesting that, as seen in the Southern Hemisphere summer distributions, the summer heating of the upper ocean is responsible for shallow mixed-layers. In the Southern Ocean, particularly south of 45°S, the mixed-layer depths are much shallower in the sigma-t-based distribution as compared with the temperature-based distribution. In particular, between 170°W and 70°W, where salinity data do exist during the August-September-October period, the 500 m mixed-layer depths observed in the temperature-based distribution have no counterpart in the sigma-t-based distribution, in which mixed-layers for that region are less than 100 m.

Figures 97a and 97b show the annual cycle of mixed-layer depths based on temperature at one-degree squares for selected regions. Considering the previous discussion comparing the sigma-t-based mixed-layer distribution with temperature-based distributions, one might question why we present the annual cycle of mixed-layer depths for selected regions based on a temperature criterion alone. One reason is that we will be comparing our results with previous work that was defined on the basis of temperature alone. Future work might include a more detailed examination of the annual cycle based on a mixed-layer criterion in which a variable sigma-t criterion is used. Figure 97a shows that very similar annual cycles occur southeast of the Kuroshio and the Gulf Stream. The mixed-layer is at its deepest at the end of the winter, and then within two months the mixed-layer shoals to its near-minimum value through solar heating. The mixed-layers presented here are not as deep as those observed synoptically in these regions (Worthington, 1972), but this is to be expected, since we are dealing with climatological means and smoothed fields. Figure 97b shows the annual cycle for subtropical regions, which have a relatively small-amplitude annual cycle. Figures 97c and 97d show mixed-layer depths computed from the data presented in this atlas, but with a criterion of 1.0°C difference with the surface temperature, compared with mixed-layer depths

presented by Colborn (1975). Colborn computed mixed-layer depths with two different techniques, each based solely on temperature, and averaged the two to obtain his final result. He noted that both techniques "gave similar results in most instances." One of these techniques was to find the depth at which subsurface temperature differed from the surface temperature by 1.0°C. Hence our criterion was changed to 1.0°C for purposes of comparison. Figure 97c shows the annual cycle in mixed-layer depth for the southeastern portion of the Southern Indian Ocean region, Area 29, as defined by Colborn (Figure 13 in his text). We find good agreement in the annual cycle in both results. Figure 97d shows the annual cycle in the Central Arabian Sea, Area 3, as defined by Colborn. Both computations show a semiannual cycle associated with the monsoon and the solar cycle. Colborn discusses the formative mechanisms for the semiannual cycle.

7. ZONAL AVERAGES

The zonal averages by one-degree latitude belts of potential temperature, salinity, oxygen, oxygen-saturation, potential density, and Brunt-Väisälä frequency (N) for the world ocean and individual oceans are presented in figures 98 through 121. The large-scale water mass features previously discussed in the standard level analyses are apparent in these figures. We emphasize that some front-like features appearing in these figures are due simply to the averaging of data across basins that individually are relatively homogeneous but different from each other with respect to water mass properties. Nevertheless, the figures represent true zonal averages and are therefore of certain interest. One can examine the standard level distributions to note those regions where averaging occurs across different basins within individual oceans. The boundaries of the individual oceans are given in figure 122. The Atlantic zonal averages do not include the Mediterranean Sea, the Baltic Sea, or Hudson Bay. The Indian Ocean does not include the Red Sea or Persian Gulf. The global averages include all of the world ocean except for the Black Sea, which was excluded from the analysis.

The zonally averaged salinity fields in each ocean at about 60°S to 70°S show a low-salinity tongue extending first downward and northward and then upward again in tropical latitudes. The tongue represents Antarctic Intermediate Water (AAIW). The distribution of AAIW and its counterclockwise, basin-wide flow in the South Pacific has been described by Reid (1965). There are associated tongues of high oxygen content and low temperature that are characteristic of this water mass. At latitudes 50°S to 60°S at depths in excess of 3000 m we note in each ocean low salinity, low temperature, relatively dense, oxygen-rich water that represents Antarctic Bottom Water (AABW). The Atlantic exhibits the lowest salinities of any of the basins in this region. Common in all basins between the AAIW and the AABW

is the upward and northward penetration of a high-salinity, low-oxygen tongue which represents Circumpolar Deep Water (CDW). This water mass is also characterized by a relative maximum in its upper portions in the Brunt-Väisälä frequency with respect to the meridional direction. In the Atlantic and Indian Oceans a relative maximum in potential density also characterizes the CDW. In the Indian Ocean at 40°S, 3000 m depth, the source of the CDW appears as a distinct relative maximum. The northern Indian Ocean exhibits high salinities characteristic of the North Indian Deep Water.

In figure 112 a slight inversion in the Atlantic Ocean zonally averaged potential density field exists from 25°S to about 5°N. An inversion of potential density in the deep ocean is observed in a meridional section through the Atlantic presented by Lynn and Reid (1968) and in a zonal section across the Indian Ocean presented by Warren (1981). The apparent instability can be explained in terms of the thermodynamic properties of sea water, and no real instability exists. Potential density, which is defined as the density a parcel of water would have if adiabatically displaced to the sea surface, cannot be used in the deep ocean for determination of stability. The stability computation is a local one and was described in Section 2.2b of this atlas. Lynn and Reid (1968) also discuss earlier work concerning these deep inversions. That the inversion exists in the zonally averaged potential density field of the Atlantic Ocean could be explained by its widespread nature.

At the surface and near-surface regions in the subtropics of the northern and southern Atlantic and Pacific Oceans, and in the subtropics of the southern Indian Ocean, the high-salinity tongues are associated with an excess of evaporation over precipitation. In the distributions of Brunt-Väisälä frequency, a relative maximum with respect to the vertical is associated with these subtropical salinity features. At a latitude of approximately 10°N in the Pacific and Atlantic we note the low-salinity surface waters associated with the ITCZ. The Indian Ocean shows a surface salinity minimum at about 10°S. On the cross-sections of Brunt-Väisälä frequency the contours do not extend to the sea floor, because the computation involves a displacement from a particular level to the next most shallow level.

The North Pacific exhibits a low-salinity, oxygen-rich tongue associated with the North Pacific Intermediate Water. Below this Intermediate Water the very low oxygen values are associated with the subarctic cyclonic gyres previously noted in the standard level distributions. Also in the North Pacific at about 42°N and in depths in excess of 1000 m, there is a relatively cold, fresh, oxygen-rich extremum with respect to the meridional direction. This feature appears quite distinctly on the standard level distributions.

The high-salinity, oxygen-rich water of the North Atlantic illustrates the ventilation of this ocean compared to that of the North Pacific. In the tropical At-

lantic the shallow oxygen minima appear quite distinctly in the zonal average, but in the Pacific the southern minimum we noted in the standard level distributions does not appear very distinctly.

The outstanding features in the distribution of N are the relative maxima associated with the main ocean thermocline that dominate the distributions. The shoaling of the thermocline in the tropics and its deepening in the subtropics are apparent.

In the global averages the front-like feature centered at about 63°N is due, in part, to the separation of the North Atlantic by the ridge systems between Greenland and Scotland and the different water mass properties of the basins on either side of the ridge.

For convenience we have computed for the same parameters shown in figures 98 through 121, area-weighted means and area-weighted root-mean-square deviations over five-degree belts of latitude for the world ocean and individual oceans. These statistics are shown in tables 4 through 51. The ocean area of each five-degree latitude belt as a function of depth for the world ocean and each individual ocean is given in tables 52 through 55. The formula for defining the area-weighted mean, \bar{X}_N , of a parameter over the N ocean one-degree squares in a five-degree latitude belt was

$$\bar{X}_N = \frac{\sum_{n=1}^N X_n A_n}{\sum_{n=1}^N A_n}, \quad (18)$$

in which X_n represents the value of the parameter at the n^{th} one-degree square in the belt, and A_n represents the area of the n^{th} one-degree square in the belt. The formula for the root-mean-square deviation (R.M.S.D.) of a parameter over a five-degree belt was defined as

$$\text{R.M.S.D.} = \left[\frac{\sum_{n=1}^N X_n^2 A_n}{\sum_{n=1}^N A_n} - \left(\frac{\sum_{n=1}^N X_n A_n}{\sum_{n=1}^N A_n} \right)^2 \right]^{\frac{1}{2}} \quad (19)$$

8. BASIN MEAN PROFILES AND VOLUME MEANS

Area weighted basin means of various parameters have been computed for the world ocean and each of the major ocean basins (Atlantic, Pacific, Indian as defined in figure 122) and for the northern and southern hemisphere portions of these basins. These means are presented as a function of depth in figures 123 through 127. These means and associated standard errors are also tabulated in tables 56 through 60. Information including the area and volume of each standard level over which the means are computed is given in tables 61 through 64. The percentage contribution that each standard level contributes to the volume of each

basin is given in this same table as well as the number of independent points used in the standard error computation. Of course one can construct and display the basin-wide averages in a number of ways to serve various purposes. The present tabulations allow users to graph the information and perform computations in any desired format. Basin volume-weighted means and the total volume in each basin are presented in table 65.

The area-weighted mean of any parameter on a standard level across a basin was computed using equation (18) with N redefined as the total number of one-degree squares in the basin. The volume-weighted mean of a parameter in a basin was similarly computed using (18), with N defined as the total number of one-degree volumes in the basin, and with A_n the area of one-degree square n , replaced by V_n , the volume of a one-degree square box, as will be defined in equation (21) to follow.

The parameters presented in this section are the same as those presented as zonally averaged quantities with the following exception. The basin-wide mean of the Brunt-Väisälä frequency has been left out, as this particular quantity does not appear very useful. Instead, the basin means of potential density have been presented both in graphic and tabular form.

The basin means will be discussed briefly with respect to the comparison of one ocean basin with another, but the global profiles will not be discussed specifically. The profiles of potential temperature show the North Atlantic to be warmer than the South Atlantic at all depths. The North Pacific is warmer than the South Pacific at depths less than 150 m and greater than 1200 m, although at the greater depths the differences are quite small. The division of the Indian Ocean into a North Indian and South Indian Ocean at the Equator does not yield much information with respect to northern versus southern hemisphere distributions, because the volume of the Indian Ocean north of the equator is so small compared with the volume south of the Equator. This division has been computed for consistency and because the North Indian Ocean is of special interest in itself. Being essentially a tropical ocean, the North Indian Ocean is, as expected, much warmer than the South Indian Ocean. In the surface layers the North Pacific Ocean is substantially warmer than any other ocean except the North Indian. In deeper layers the North Atlantic is warmer than the other oceans, which is the contributory factor to its being the warmest of all oceans (excluding the North Indian) in terms of its volume mean.

Examination of the salinity profiles shows that at all depths below 30 meters the North Atlantic is the most saline of all oceans. The North Pacific is less saline than the South Pacific at all depths. The South Indian is saline compared with the South Pacific. At least part of this difference might be ascribed to the North Indian Deep Water (NIDW) described by Clowes and Deacon (1935). The presence of NIDW is clearly seen in the mean salinity profiles for the North Indian Ocean.

Relative maxima in the profiles of all the oceans are observed at depths of 50 to 250 m. These features represent the waters of the subtropical salinity maxima. With the exception of the North Indian Ocean the salinity minima characteristic of Intermediate Waters are observed at depths of 500 to 1000 m in all oceans.

The potential density profiles show the South Atlantic to be denser than the North Atlantic in the upper 100 m of the water column. Below this depth the North Atlantic is denser than the South Atlantic. An inversion occurs in the potential density field of the North Atlantic at the depths of 4000 and 4500 m. Other slight inversions are also observed at the deeper standard levels in the world ocean. We assume these inversions are related to the thermodynamic properties of sea water, as noted in section 7. The South Pacific is more dense than the North Pacific, but at depths greater than 900 m the difference between the two oceans is no more than .03. The South Indian is more dense than the North Indian Ocean from the surface through 500 m. From 500 to 2000 m the reverse is true, and below 2000 m the North Indian is again more dense than the South Indian Ocean.

The profiles of oxygen for the Atlantic Ocean show that the North Atlantic and South Atlantic Oceans have similar mean oxygen values (within 0.2 ml/l) in the surface to 1000 m depth range. Below 1000 m the North Atlantic has an oxygen content that is larger than the South Atlantic by as much as .85 ml/l. As previously noted, this is due to the formation of deep water in the North Atlantic. The South Pacific has a larger dissolved oxygen content than the North Pacific at all depths. Differences between the two oceans are as large as 2.6 ml/l. The greatest difference between the two oceans occurs at a depth of 800 m. The North Indian Ocean has basin means of less than .75 ml/l at some standard levels.

The percent oxygen-saturation profiles show slight supersaturation in the surface layers of all the individual ocean basins. Again, oxygen data are not necessarily well distributed by season so the lack of observations in some areas may bias these results. Both the North Pacific and North Indian Oceans exhibit saturations of less than 20 percent at intermediate depth ranges.

Tables 56 through 60 contain the tabulated basin averaged means shown in figures 123 through 127. A standard error is given with each mean to give the reader some estimate of the variability of each basin mean. Each standard error (S.E.) at a particular level is computed in the following way. The area weighted root-mean-square deviation of all gridpoint values is computed at the standard level and is denoted by σ . The total area of the standard level within the basin is computed and then divided by the area defined by the influence radius on the last pass of the objective analysis scheme. Thus this area is given by πR_1^2 where $R_1=771$ kilometers. The quotient yields a value, N_l , which is used as the number of independent points in N_l estimating the standard error as

$$\text{S.E.} = \sigma / \sqrt{N_I} . \quad (20)$$

The area and value of N_I for each basin are given in tables 61 through 64. In addition, the volume occupied by each standard level and the percent contribution of each standard level volume to the entire volume of the basin is given. The volume of each standard level is defined as follows. Excluding the sea surface and deepest standard level occurring at any one-degree square water column, the depth range, Δz , through which a volume is computed for any standard level (denoted by k) is given as

$$\Delta z_k = .5[z_{k+1} - z_{k-1}] , \quad (21)$$

in which z_{k+1} is the depth of the first standard level deeper than k , and z_{k-1} is the depth of the first standard level shallower than k . The volume of the surface standard level is taken over the 0 to 5 m depth range. The depth range through which a volume is computed for the deepest standard level is given as

$$\Delta z_k = .5[z_k - z_{k-1}] . \quad (21a)$$

Volume means for each basin, along with the total volume of each basin, are presented in table 65. For the purpose of comparison with earlier work, the corresponding values computed by Montgomery (158), Pollak (1958), and Cochrane (1958) are also presented (in parentheses) in table 38. Except for the North Indian Ocean the North Atlantic is the warmest, saltiest, densest and most oxygenated of the major ocean basins. The South Atlantic is the coldest, and the North Pacific (excluding the North Indian Ocean) is the most poorly oxygenated of all the basins. We divided the world ocean into individual oceans in the same manner as Montgomery, Cochrane, and Pollack (hereinafter MCP), and so a direct comparison is possible. Examining the potential temperature means we note that the means computed from the analyses presented in this atlas are warmer than those presented by MCP by .06 to .19°C, with the exception of the Indian Ocean, which is 05°C cooler than that presented by MCP. The salinity means all agree to within .03 ‰.

9. SUMMARY

In the preceding sections we have described the results of a project to analyze objectively the historical oceanographic data base on file at the National Oceanographic Data Center, U.S.A. The techniques used to analyze the data were discussed. To establish a certain confidence level, distributions at standard levels were presented for comparison with work published by other investigators. Most previous results referred to were obtained from subjective analyses. In most cases comparison shows excellent agreement. Differences, such as the example presented in Section 6.6, usually can be explained in terms of differences in data density and in degree of smoothing. However, one should note that the addition of new data may alter the distributions we

have presented. On the other hand, we do not expect changes in the very large scale features that appear.

Another reason for presentation of the analyses in this work is the receipt of many requests for information of the type contained in this publication. Requests for information such as the differences in value of various parameters from ocean to ocean and from one part of an ocean basin to another have been received. This information is often not easily obtained from the literature, and in some cases, it does not exist. The microfiche packet attached to this atlas greatly expands the volume of information available to users, particularly those without access to computers. One major advantage of this atlas compared to subjective analyses is that the basic fields reside on magnetic tape which will be made available in the near future. One is therefore not limited to the use of those fields presented in this atlas but can derive numerous other fields that may be of interest.

One advantage of the analysis techniques used in this atlas resides in the knowledge of the amount of smoothing applied in the objective analyses as given by the response function in figure 11. We believe this to be an important parameter in constructing and describing a climatology of any geophysical parameter. One reason is the practice of computing anomalies from a standard climatology. As noted previously, it is important that the synoptic field be smoothed to the same extent as the climatology to prevent generation of spurious anomalies simply through differences in smoothing. A second reason is that purely diagnostic computations require a minimum of seven or eight gridpoints to represent any Fourier component with accuracy. Higher order derivatives will require more smoothing. The smoothing function of figure 11 informs users how much smoothing has been applied to these fields.

The results presented in this atlas show some features that are suspect and may be due to nonrepresentative or incorrect data that were not eliminated by the quality control techniques used. Although we have attempted to eliminate as many of these features as possible some obviously remain. We have attempted to create a data set that can be used as a "black box," but the lack of data in some regions and the magnitude of the effort needed to eliminate all important problems are limiting factors. Finally, there are some instances in which one simply does not know whether a particular distribution is representative or not. Only additional data will ameliorate this situation.

Additional references that can be used for comparison with the fields represented in this atlas are Barkley (1968), Robinson (1976), and Robinson et al. (1979).

10. RECOMMENDATIONS AND FUTURE WORK

The principal recommendation that can be made is that additional oceanographic data be obtained in order to make better estimates of the annual cycle of temperature, salinity, and oxygen in the upper layers of the world ocean and to fill in data-sparse regions at deeper

levels. This atlas represents one approach and one set of techniques used to analyze the historical ocean data base. We feel that, regardless of technique used or of the purposes for which analyses are used, the lack of data in some areas and for some averaging periods represents the single most important limiting factor in studying the world ocean. Even in some areas where sufficient data exist to define a field there may be a need for more data to improve on the statistical reliability of the field. However, acquisition of oceanographic data is both expensive and time consuming. Since the myriad of physical processes found in the oceans occur over a broad spectrum of time and length scales, some of the research priorities governing the acquisition of new data may not coincide with the type of survey work needed to fill in the data gaps noted here. In any case, it is important that all data be archived for future use. Both the acquiring of new data and the archiving of all data are of great importance for future work.

We will note specifically a few quantities of interest that would benefit from additional data and why these are of importance. The world ocean represents a major component of the Earth's climate system. The annual thermal cycle of the ocean and the meridional transport of heat by the oceans have historically been recognized to be of great potential importance in maintaining the Earth's climate. Jung (1956) reviewed some of the earlier work on the relative importance of the atmosphere and ocean in the meridional transport of heat. Part of his work was reproduced by Neumann and Pierson (1966, p. 244). Oort and Vonder Haar (1976) evoked renewed interest in this subject. The monthly distributions of temperature observations in the microfiche packet indicate a need for more data in the tropics and, in general, in the Southern Hemisphere. Meridional sections would be most appropriate for filling in gaps.

Examination of the seasonal distributions of salinity and oxygen indicate the greater sparsity of these data (compared with the temperature data) to examine the annual cycle. The annual salinity cycle is of general importance in studying the role of the ocean in the hydrological cycle. Surface salinity is of particular importance since, in some areas, it governs the depth of penetrative convection.

At intermediate levels the data distributions are fairly reasonable for producing annual mean all-data analyses. Some data-sparse areas exist, and more data are needed.

In the deep ocean, particularly at depths in excess of 3000 m where topographic barriers and isolated basins appear, there is a great need for additional data. The gradients at these depths are quite weak, calling for high quality data.

We believe that there is a need for analyses of the type presented in this atlas, but with finer resolution in such areas as the western boundary current regimes, where sharp gradients and current-counter-current systems exist. Finer resolution would allow accurate representation of features in these regions.

11. REFERENCES

- Bainbridge, A. E., 1976: Geosecs Atlantic Expedition, Vol. 2, *National Science Foundation*, Washington, D. C., 198 pp.
- Barkley, R. A., 1968: *Oceanographic Atlas of the Pacific Ocean*, University of Hawaii Press, Honolulu, 20pp.
- Barnes, S. L., 1964: A technique for maximizing details in numerical weather map analysis. *J. App. Meteor.*, 3, 396-409.
- , 1973: Mesoscale objective map analysis using weighted time series observations. *NOAA Technical Memorandum ERL NSSL-62*, 60 pp.
- Bathen, K., 1972: On the seasonal changes in the depth of the mixed-layer in the North Pacific Ocean. *J. Geophys. Res.*, 77, 7138-7150.
- Bergthörsson, P., and B. Döös, 1955: Numerical weather map analysis. *Tellus*, 7, 329-340.
- Bryden, H., 1973: New polynomials for thermal expansion, adiabatic temperature gradient and potential temperature of sea water. *Deep Sea Res.*, 20, 401-408.
- Callahan, J. E., 1972: The structure and circulation of Deep Water in the Antarctic. *Deep Sea Res.*, 19, 563-575.
- Clowes, A. J., and G. E. R. Deacon, 1935: The Deep-Water Circulation of the Indian Ocean. *Nature*, 136, 936-938.
- Coachman, L. K., and K. Aagaard, 1974: Physical oceanography of Arctic and Subarctic Seas. *Marine Geology and Oceanography of Arctic Seas*. Edited by Yvonne Herman, Springer-Verlag, N.Y., 397 pp.
- Cochrane, J. D., 1958: The frequency distribution of water characteristics in the Pacific Ocean. *Deep Sea Res.*, 5, 111-127.
- Codispoti, L. A. and F. A. Richards, 1971: Oxygen supersaturations in the Chukchi and East Siberian Seas. *Deep Sea Res.*, 18, 341-351.
- Colborn, J. G., 1975: *The Thermal Structure of the Indian Ocean*. University of Hawaii Press, Honolulu, 173 pp.
- Cox, M. D., 1980: Generation and propagation of 30-day waves in a numerical model of the Pacific. *J. Phys. Oceanogr.*, 10, 1168-1186.
- Cressman, G. P., 1959: An operational objective analysis scheme. *Mon. Wea. Rev.*, 87, 329-340.
- Defant, A., 1950: Reality and illusion in oceanographic survey. *J. Mar. Res.*, 9, 120-138.
- , and B. Helland-Hansen, 1939: Bericht über die oceanographischen Untersuchungen im zentralen und östlichen Teil des Nordatlantischen Ozeans im Frühsommer 1938 (Internationale Golfstrom Expedition). *Preuss. Akad. d. Wiss. Abh.*, Jahrg., 1939, Phys.-Math. Klasse, Nr 5, 64 pp.
- Dietrich, G., 1969: Atlas of the hydrography of the northern North Atlantic Ocean. *Conseil International Pour L'Exploration De La Mer Service Hydrographique*, Charlottenlund Slot - Denmark, 140 pp.
- Ellis, J. S., T. H. Vonder Haar, S. Levitus, and A. Oort, 1978: The annual variation in the global heat balance of the earth. *J. Geophys. Res.*, 83, 1958-1962.

- Favorite, F., A. J. Dodimead, and K. Nasu, 1976: Oceanography of the Subarctic Pacific Region, 1960-71. *International North Pacific Fisheries Commission Bulletin Number 33*, Vancouver, 187 pp.
- Fiadeiro, M. E. and H. Craig, 1978: Three-dimensional modelling of tracers in the deep Pacific Ocean: I Salinity and Oxygen. *J. Mar. Res.*, 36, 323-355.
- Flierl, G., and A. Robinson, 1974: XBT-CTD intercomparison. *In Instrument Description and Intercomparison Report of the MODE-I Intercomparison Group*, 173 pp.
- Fofonoff, N. P., 1962: Physical properties of sea water. *The Sea, Vol. 1*, edited by M. N. Hill, Interscience, New York, 3-30.
- Föyn, E., 1969: The composition of sea water and significance of the chemical components of the marine environment. *Chemical Oceanography*. Edited by R. Lange, Scandinavian University Books, Universitetsforlaget, Oslo/Bergen/Tromsø, 152 pp.
- Fuglister, F. C., 1960: *Atlantic Ocean Atlas*, Woods Hole Oceanographic Institute, Woods Hole, 209 pp.
- Gordon, A. L., 1966: Potential temperature, oxygen, and circulation of bottom water in the Southern Ocean. *Deep Sea Res.*, 13, 1125-1138.
- Gordon, A. L., 1967: Structure of Antarctic waters between 20°W and 170°W. Antarctic Map Folio Series, 6, Am. Geogr. Soc., New York, 10 pp.
- Gordon, A. L., and R. D. Goldberg, 1970: Circumpolar characteristics of Antarctic Waters, 13, Am. Geogr. Soc., New York, 6 pp.
- Gordon, A. L., E. Molinelli, and T. Baker, 1978: Large-scale dynamic topography of the Southern Ocean. *J. Geophys. Res.*, 83, 3023-3032.
- Hasunuma, K. and K. Yoshida, 1978: Splitting of the subtropical gyre in the western North Pacific. *J. Oceanogr. Soc. Japan*, 34, 160-171.
- Helland, P., 1963: Temperature and salinity variations in the upper layers at ocean weather station M (66°N, 2°E). Univ. Bergen, Arbok 1963, Naturv. r. Nr. 16, Bergen, 26 pp.
- Hesselberg, T., and H. U. Sverdrup, 1914: Die Stabilitätsverhältnisse des Seewassers bei Vertikalen Verschiebungen. *Aarb. Bergen Mus.*, No. 14, 17 pp.
- Jung, G. H., 1956: Energy transport by air and sea. Prepared for ONR, Contr. No. N7-onr - 48702, OPNAV P03-8.
- Kawai, H., 1966: A generalized potential vorticity in the oceans. Kyoto University, Geophysical Institute, Special Contribution, 6, 79-83.
- Kester, D. R., K. T. Crocker, and G. R. Miller, 1973: Small-scale oxygen variations in the thermocline. *Deep Sea Res.* 20, 409-412.
- Kim, K., and T. Rossby, 1979: On the eddy statistics in a ring-rich area: a hypothesis of bimodal structure. *J. Mar. Res.*, 37, 201-213.
- Kirwan, A. D., G. D. McNally, E. Reyna, and W. J. Merrell, 1978: The near surface circulation of the Eastern Pacific Ocean. *J. Phys. Oceanogr.*, 8, 937-945.
- Kuo, H. H., 1978: Topographic effect on the deep circulation and the abyssal oxygen distribution. *J. Phys. Oceanogr.*, 8, 428-436.
- Lambert, R. B., D. R. Kester, M.E.Q. Pilson, and K. E. Kenyon, 1973: In situ dissolved oxygen measurements in the North and West Atlantic Ocean. *J. Geophys. Res.*, 78, 1479-1483.
- Leetmaa, A., P. Niiler, and H. Stommel, 1977: Does the Sverdrup Relation account for the Mid-Atlantic circulation? *J. Mar. Res.*, 35, 1-10.
- , and A. F. Bunker, 1978: Updated charts of the mean annual wind stress, convergences in the Ekman layers and Sverdrup transports in the North Atlantic. *J. Mar. Res.* 36, 311-321.
- Legeckis, R., 1978: A survey of worldwide sea surface temperature fronts detected by environmental satellites. *J. Geophys. Res.*, 83, 4501-4522.
- Levitus, S., and A. Oort, 1977: Global analysis of oceanographic data. *Bull. Amer. Meteor. Soc.*, 58, 1270-1284.
- Lynn, R. J., and J. L. Reid, 1968: Characteristics and circulation of deep and abyssal waters. *Deep Sea Res.*, 15, 577-598.
- Manabe, S., K. Bryan, and M. J. Spelman, 1979: A global ocean-atmosphere climate model with seasonal variation for future studies of climate sensitivity. *Dyn. Atmos. Oceans*, 3, 393-426.
- Masuzawa, J., 1969: Subtropical Mode Water. *Deep Sea Res.*, 16, 463-472.
- McCartney, M. S., 1977: Subantarctic Mode Water. *A Voyage of Discovery*. edited by M. Angell, Pergamon Press, New York, 103-119.
- Mc Dowell, S., 1977: A note on XBT accuracy. *Polymode News*, 29.
- Mc Dowell, S., and H. T. Rossby, 1978: Mediterranean water: An intense mesoscale eddy off the Bahamas. *Science*, 202, 1085-1087.
- Mellor, G., C. Mechoso, and E. Keto, 1982: A diagnostic calculation of the general circulation of the Atlantic Ocean. To be published.
- Menzel, D. W., 1974: Primary productivity, dissolved and particulate organic matter, and the sites of oxidation of organic matter. *The Sea, Vol. 5*, edited by M. N. Hill, Wiley Interscience, New York, 659-678.
- Merle, J., M. Fieux, and P. Hisard, 1980: Annual signal and interannual anomalies of sea surface temperature in the eastern equatorial Atlantic Ocean. *Deep Sea Res.*, Supplement II to Vol. 26, 77-102.
- Monin, A. S., V. M. Kamenkovich, and V. G. Kort, 1977: *Variability of the Oceans*. John Wiley and Sons, New York, 241 pp.
- Montgomery, R. B., 1958: Water characteristics of Atlantic Ocean and world ocean. *Deep Sea Res.*, 5, 134-148.
- Mosby, H., 1959: Deep water in the Norwegian Sea. *Geophys. Publ.*, Geophys. Norv., 21 (3), Oslo, 62 pp.
- Neumann, G. and W. J. Pierson, 1966: *Principles of Physical Oceanography*. Prentice Hall Inc., Englewood Cliffs, N.J., 545 pp.

- NOAA, 1974: User's Guide to NODC's Data Services. Environmental Data Service, Washington, D.C.
- NOAA, 1980: National Oceanographic Data Center Annual Report. Environmental Data and Information Service, Washington, D.C.
- Oort, A. H., and T. H. Vonder Haar, 1976: On the observed annual cycle in the ocean-atmosphere heat balance over the northern hemisphere. *J. Phys. Oceanogr.*, 6, 781-800.
- Pak, H., L. A. Codispoti, and R. Zanereld, 1980: On the intermediate particle maxima associated with oxygen poor water off South America. *Deep Sea Res.*, 27A, 783-797.
- Philander, S. G. H., and R. C. Pacanowski, 1981: The oceanic response to cross-equatorial winds (with application to coastal upwelling in low latitudes), *Tellus*, 33, 201-210.
- Pickard, G. L., 1975: *Descriptive Physical Oceanography*. Pergamon Press, New York, 214 pp.
- Pollak, M. J., 1958: Frequency distribution of potential temperatures and salinities in the Indian Ocean. *Deep Sea Res.*, 5, 128-133.
- Rabiner, L. R., M. R. Sambur, and C. E. Schmidt, 1975: Applications of a nonlinear smoothing algorithm to speech processing, *IEEE Trans. on Acoustics, Speech and Signal Processing*, Vol. Assp-23, 552-557.
- Reid, J. L., 1961: On the temperature, salinity, and density differences between the Atlantic and Pacific Oceans in the upper kilometre. *Deep Sea Res.*, 7, 265-275.
- Reid, J. L., 1962: On circulation, phosphate-phosphorous content, and zooplankton volumes in the upper part of the Pacific Ocean. *Limnol. Oceanogr.* 7, 287-306.
- , 1965: *Intermediate Waters of the Pacific Ocean*, Johns Hopkins Oceanogr. Stud. , 2, Johns Hopkins Press, Baltimore, 85 pp.
- , 1973a: The shallow salinity minima of the Pacific Ocean. *Deep Sea Res.*, 20, 51-68.
- , 1973b: *Northwest Pacific Ocean Water in Winter*. *The Johns Hopkins Oceanogr. Stud.* , 5, 96 pp.
- Reid, J. L., 1973c: Transpacific hydrographic sections at Lats. 43°S and 28°S: the Scorpio Expedition-III. Upper water and a note on southward flow at mid-depth. *Deep Sea Res.*, 20, 39-49.
- , 1981: On the mid-depth circulation of the world ocean. *Evolution of Physical Oceanography*. Edited by B. Warren and C. Wunsch, MIT Press, 623 pp.
- , and R. J. Lynn, 1971: On the influence of the Norwegian-Greenland and Weddell Seas upon the bottom waters of the Indian and Pacific Oceans. *Deep Sea Res.*, 18, 1063-1088.
- , and R. S. Arthur, 1975: *J. Mar. Res.*, 33, supplement, 37-52.
- , W. D. Nowlin, and W. C. Patzert, 1977: On the characteristics and circulation of the southwestern Atlantic Ocean. *J. Phys. Oceanogr.*, 7, 62-91.
- , and A. W. Mantyla, 1978: On the mid-depth circulation of the North Pacific Ocean. *J. Phys. Oceanogr.*, 8, 946-951.
- Richards, F. A., 1957: Oxygen in the ocean. *Mem. Geol. Soc. Amer.*, 67, 185-238.
- Robinson, M. K., 1976: Atlas of the North Pacific monthly mean temperatures and mean salinities of the surface layer, U.S. Naval Oceanographic Office, Washington, D.C., 173 pp.
- Robinson, M. K., R. A. Bauer, E. H. Schroeder, 1979: Atlas of North Atlantic-Indian Ocean monthly mean temperatures and salinities of the surface layer, U.S. Naval Oceanographic Office, Washington, D.C., 213 pp.
- Rodén, G. I., 1975: On North Pacific temperature, salinity, sound velocity, and density fronts and their relation to the wind and energy flux fields. *J. Phys. Oceanogr.*, 5, 557-571.
- Sasaki, Y., 1960: An objective analysis for determining initial conditions for the primitive equations. Ref. 60-16T, Atmospheric Research Lab., Univ. of Oklahoma Research Institute, Norman, 23 pp.
- Saunders, P. M., 1976: On the uncertainty of wind stress curl computations. *J. Mar. Res.*, 34, 155-160.
- Schleicher, K. E., and A. L. Bradshaw, 1956: A conductivity bridge for measurements of the salinity of sea water. *J. Cons.*, 22, 9-20.
- Schroeder, E. H., 1965: Average monthly temperatures in the North Atlantic Ocean. *Deep Sea Res.*, 12, 323-343.
- Schubert, O. von, 1935: Die Stabilitätsverhältnisse im Atlantischen Ozean. *Wiss. Ergebn. dt. atlant. Exped. Meteor 1925-1927*, 6 (2), (1), 54 pp.
- Seiwell, H. R., 1937: The minimum oxygen concentration in the western basin of the North Atlantic. *Papers in Physical Oceanography and Meteorology*, V(3), Woods Hole, 24 pp.
- , 1939: The effect of short period variations of temperature and salinity on calculations in dynamic oceanography. *Papers in Phys. Ocean. and Meteor.*, VII(3), Woods Hole, 32 pp.
- Sharma, G. S., 1972: Water characteristics at 200 cl/t in the intertropical Indian Ocean during the southwest monsoon. *J. Mar. Res.*, 30, 102-111.
- Shulenberger, E., and J. L. Reid, 1981: The Pacific shallow oxygen maximum, deep chlorophyll maximum, and primary productivity, reconsidered. *Deep Sea Res.*, 28, 901-918.
- Shuman, F. G., 1957: Numerical methods in weather prediction: II. Smoothing and filtering. *Mon. Wea. Rev.*, 85, 357-361.
- Smed, J., 1943: Annual and seasonal variations in the salinity of the North Atlantic surface water, Conseil Perm. Intern. p. 1 'Expl. de la Mer., Rapp. et Proc.-Verb, 112, Copenhagen, 79-94.
- Smith, S. M., H. W. Menard, and G. Sharman, 1966: Worldwide ocean depths and continental elevations. SIO Ref. G5-8, Scripps Institute of Oceanography, Univ. of California, LaJolla, 17 pp.
- Stommel, H., 1958: The abyssal circulation. *Deep Sea Res.*, 5, 80-82.

- _____, and K. Yoshida (eds.), 1972: *Kuroshio: Physical Aspects of the Japan Current*. University of Washington Press, 517 pp.
- _____, and F. Schott, 1977: The beta spiral and the determination of the absolute velocity field from hydrographic station data. *Deep Sea Res.*, 24, 325-329.
- Sverdrup, H. U., M.W. Johnson, and R. H. Fleming, 1942: *The Oceans*. Prentice Hall Inc., Englewood Cliffs, N.J. 1060 pp.
- Tabata, S., 1965: Variability of Oceanographic conditions at Ocean Station "p" in the Northeast Pacific Ocean. *Transactions of the Royal Society of Canada*, III, 367-418.
- Taft, B., 1972: Characteristics of the flow of the Kuroshio south of Japan. *Physical Aspects of the Japan Current*, edited by H. Stommel and K. Yoshida, University of Washington Press, Seattle, 165-214.
- Tukey, J. W., 1974: Nonlinear (nonsuperposable) methods for smoothing data, in *Cong. Rec.*, 1974 EASCON, pp. 673.
- Uda, M., 1964: On the nature of the Kuroshio, its origins and meanders. *Studies on Oceanography*, edited by K. Yoshida, University of Tokyo Press, Tokyo, 89-107.
- Voorhis, A. D., and J. B. Hersey, 1964: Oceanic thermal fronts in the Sargasso Sea. *J. Geophys. Res.*, 18, 3809-3814.
- Warren, B. A., 1973: Transpacific hydrographic sections at Lats. 43°S and 28°S: the Scorpio Expedition -II. Deep Water. *Deep Sea Res.*, 20, 9-38.
- _____, 1981: Transindian hydrographic section at Lat. 18°S: Property distributions and circulation in the South Indian Ocean. *Deep Sea Res.*, 28, 759-788.
- _____, 1981: Deep circulation of the world ocean. *Evolution of Physical Oceanography*, edited by B. Warren and C. Wunsch, MIT Press, 623 pp.
- Weiss, R.F., 1970: The solubility of nitrogen, oxygen and argon in water and sea water. *Deep Sea Res.*, 17, 721-735.
- White, W. B., K. Hasunuma, and H. Solomon, 1978: Large scale seasonal and secular variability of the subtropical front in the western North Pacific from 1954 to 1974. *J. Geophys. Res.*, 83, 4531-4544.
- Winterfeld, T., and H. Stommel, 1972: Distribution of stations and properties at standard depths in the Kuroshio area. *Kuroshio: Physical Aspects of the Japan Current*, University of Washington Press, 81-93.
- Worthington, L. V., 1959: The 18° water in the Sargasso Sea. *Deep Sea Res.*, 5, 297-305.
- _____, 1972: Anticyclogenesis in the oceans as a result of outbreaks of continental polar air. *Studies in Physical Oceanography*, 1. Gordon and Beach Science Publishers, New York, 169-178.
- _____, 1981: The water masses of the world ocean: some results of a fine scale census. *Evolution of Physical Oceanography*, edited by B. Warren and C. Wunsch, MIT Press, 623 pp.
- _____, and W. R. Wright, 1970: *North Atlantic Ocean Atlas*: Woods Hole Oceanographic Institute, Woods Hole, MA., pp 24.
- Wunsch, C., 1978: Determining the general circulation of the oceans. *Science*, 196, 871-875.
- Wust, G., 1935: *The Stratosphere of the Atlantic Ocean*, English translation edited by W. J. Emery, Aprevind Publishing Co. Pvt. Ltd., New Delhi, India, 112 pp.
- Wyrтки, K., 1962: The oxygen minima in relation to ocean circulation. *Deep Sea Res.*, 9, 11-23.
- _____, 1964: The thermal structure of the eastern Pacific Ocean, *Deutsche Hydrog. Zeits. Ergänzungsheft*, 84 pp.
- _____, 1965: The annual and semiannual variation of sea surface temperature in the North Pacific Ocean. *Limn. and Oceanogr.*, 10, 307-313.
- _____, 1971: *Oceanographic Atlas of the Indian Ocean Expedition*, National Science Foundation, 531 pp.
- _____, 1974: The dynamic topography of the Pacific Ocean and its fluctuations. Rep. H-16-74-S, Hawaii Institute of Geophysics, 19 pp.
- _____, 1975: Fluctuations of dynamic topography in the Pacific Ocean. *J. Phys. Oceanogr.*, 5, 450-459.
- _____, E. Firing, D. Halpern, R. Knox, G. J. McNally, W. C. Patzert, E. D. Stroup, B. A. Taft, R. Williams, 1981: The Hawaii to Tahiti Shuttle Experiment. *Science*, 211, 22-28.
- Yoshida, K., and T. Kidokoro, 1967: A subtropical counter-current in the North Pacific. *J. Oceanogr. Soc. Japan*, 23, 32-35.
- _____, 1970: Subtropical countercurrents: Band Structures revealed from CSK data. *The Kuroshio*, edited by J. C. Marp, East West Center Press, Honolulu, 197-204.

12. APPENDIX A

The Effect of Smoothing on a Sea Surface Temperature Field

As previously discussed, the amount of smoothing applied to the objective analyses shown in this atlas is given by the response function shown in figure 11. We wish now to demonstrate how varying the amount of smoothing affects our results. Therefore an objective analysis of the observed one-degree square summer (Aug-Oct) sea surface temperature means was computed, differing from the usual objective analysis procedures, described in Section 3, only by the amount of smoothing performed. An influence radius of 551 km was used on all four analysis passes, and the five-point smoother was applied less frequently. The response function for this analysis is given by the values in table A1. Note that much less smoothing was performed in this case, compared with the amount of smoothing indicated in figure 11. We will refer to this less smoothed analysis as the "test" analysis or "test" case, while the analysis of the same summer temperature means, but character-

ized by the response function in Section 3, will be called the "standard" analysis. The summer sea surface temperature field for the North Atlantic is presented in figure A1 for the standard case and in figure A2 for the test case. We present only the North Atlantic portion of the global analysis, because the scale of some of the features we wish to discuss are relatively small and are better delineated on a limited area map.

Comparing figures A1 and A2 the effects of differences in smoothing are easily noticed. The gradients of the test analysis (less smoothing) are stronger, and are particularly noticeable in the Gulf Stream system. The tongue-shaped distribution of isotherms that extends to the northwest from the Labrador Sea shows a larger amplitude and tighter gradients in the test analysis. In figure A3 the distribution of test analysis minus the standard analysis is shown. This field quantifies the effect of varying the amount of smoothing. Differences in the open ocean, away from regions of large gradients, are generally less than 0.3°C. In the Gulf Stream system and northwest Labrador Sea differences exceed 1.0°C, and at some points along the east coast of the United States the differences exceed 1.5°C. Figure A3 illustrates the importance of smoothing in the interpretation of anomaly fields from a climatology. By variations only in the amount of smoothing one can generate relatively large differences between objective analyses of the same data set. Consistency in the amount of smoothing between a synoptic field and the climatology to which it is compared is therefore of great importance.

13. APPENDIX B

The Effect of the First-Guess Field on a Sea Surface Temperature Field

To demonstrate the effect of defining a first-guess field for a seasonal analysis based on the zonal average of observed seasonal data rather than using the annual analysis, as was done in this study, we present the following results. Figure B1 shows a summer sea surface temperature analysis made from the same data and analysis parameters as the standard analysis shown in figure A1. The only difference between the two analyses is that the analysis shown in figure B1 was produced using a zonal average of the observed sea surface temperature means as a first guess rather than using the annual analysis. There are differences in the two analyses. However they are more clearly seen in figure B2, which shows the difference field between the two analyses. The differences are quite small between the two fields in mid-ocean, where sea surface temperature gradients are small, but relatively large differences appear in coastal and near-coastal regions, where gradients are large. The difference between the two fields is due to the fact that we began with different first-guess fields and have deliberately not let the analyses converge to the observed data, since we wish to smooth our results.

14. APPENDIX C

Definitions of Potential Temperature and Density Parameters

The equation of state for sea water, the various density functions defined from it, and the definition of potential temperature will be discussed in this section. Our purpose is to provide basic equations and definitions for readers not familiar with these quantities. For more detailed exposition the reader is referred to the references that we shall cite in the course of discussion.

For this discussion we will let T , S , and P represent the in situ temperature (°C), salinity (‰), and pressure (decibars) of a parcel of sea water. The descriptive term "in situ" refers to the value of a parameter measured "in place" as opposed to the value of the parameter after some change such as an adiabatic displacement. For brevity we shall simply refer to in situ temperature as temperature. The oceanographic convention is to assume that pressure at the sea surface is equal to zero, or to be more exact, the pressure at some depth is the total pressure minus one standard atmosphere as noted by Fofonoff (1962).

The potential temperature, θ , of a parcel of sea water is the temperature the parcel would have if it were displaced adiabatically to the sea surface. Computation of potential temperature is done to remove the warming effect of compressibility on sea water thereby allowing for comparison and tracing of water masses in the deep ocean. To compute potential temperature we used the equation formulated by Bryden (1973),

$$\theta = T - \sum_i \sum_j \sum_k A_{ijk} P^i (S - 35)^j T^k \quad (C-1)$$

in which

$$\begin{aligned} A_{100} &= 0.36504 \times 10^{-4} & A_{210} &= -0.41057 \times 10^{-10} \\ A_{101} &= 0.83198 \times 10^{-5} & A_{200} &= 0.89309 \times 10^{-8} \\ A_{102} &= -0.54065 \times 10^{-7} & A_{201} &= -0.31628 \times 10^{-9} \\ A_{103} &= 0.40274 \times 10^{-9} & A_{202} &= 0.21987 \times 10^{-11} \\ A_{110} &= 0.17439 \times 10^{-5} & A_{300} &= -0.16056 \times 10^{-12} \\ A_{111} &= -0.29778 \times 10^{-7} & A_{301} &= 0.50484 \times 10^{-14} \end{aligned}$$

The in situ density of sea water, ρ , is a function of temperature, salinity, and pressure

$$\rho = \rho(S, T, p) \quad (C-2)$$

Density changes due to the compressibility of seawater are much larger than density changes due either to thermal expansion or to saline expansion, over the range of temperature and salinity observed in the world ocean. To isolate the effects of changes in temperature and salinity on the density of a parcel of water, the quantities sigma-t, denoted as σ_t , and potential density, denoted σ_θ are defined. The definition of σ_t of a water parcel of temperature, T , and salinity, S , is simply the density the parcel would have if evaluated at the sea surface, where the pressure is zero, minus a constant equal to 1 and multiplied by 10^3 . The subtraction and multiplication are done for numerical convenience, since

density values for most of the world ocean are greater than 1.0 and less than 1.03 g/cm³. The expression for sigma-t is

$$\sigma_t = [\rho(S, T, 0) - 1] \times 10^3 \quad (C-3)$$

If the potential temperature of the water parcel is θ , then potential density is expressed as

$$\sigma_\theta = [\rho(S, \theta, 0) - 1] \times 10^3 \quad (C-4)$$

An alternate expression for the in situ density of sea water, ρ , is the quantity sigma, σ , expressed as

$$\sigma = [\rho(S, T, p) - 1] \times 10^3 \quad (C-5)$$

The equation for the computation of sigma-t is, following Fofonoff (1962),

$$\sigma_t = \Sigma_t + (\sigma_0 - \Sigma_0)[1 - A_t + B_t(\sigma_0 + \Sigma_0)] \quad (C-6)$$

in which Σ_t and Σ_0 are the specific gravity anomaly of pure water at temperature, t , and 0°C respectively. The value of Σ_0 is -0.1324. The values A_t , B_t are computed from

$$A_t = 4.7867 \times 10^{-3}T + 9.8185 \times 10^{-5}T^2 - 1.0843 \times 10^{-6}T^3 \quad \text{and} \quad (C-7)$$

$$B_t = 1.8030 \times 10^{-5}T - 8.164 \times 10^{-7}T^2 + 1.667 \times 10^{-8}T^3. \quad (C-8)$$

The quantity σ_0 is the density of a parcel of sea water with salinity, S , at a temperature of 0°C and pressure equal to zero and is expressed as

$$\sigma_0 = [\rho(S, 0, 0) - 1] \times 10^3 \quad (C-9)$$

The equation for the computation of σ_0 as given by Neumann and Pierson (1966) is

$$\sigma_0 = -.093 + 0.8149S - 0.000482S^2 + 0.0000068S^3. \quad (C-10)$$

The equation for the computation of the density of a parcel of sea water with temperature, T , salinity, S , and pressure, p , is (following Fofonoff (1962)

$$\rho(S, T, p) = \frac{1 + 10^{-3}\sigma_t}{1 - \mu p}, \quad (C-11)$$

in which

$$\begin{aligned} 10^9\mu = & [4886/(1 + 1.83 \times 10^{-5}p)] \\ & - (227 + 28.33T - 0.551T^2 + 0.004T^3) \\ & + 10^{-4}p(105.5 + 9.50T - 0.158T^2) \\ & - 1.5 \times 10^{-8}Tp^2 \\ & - 10^{-1}(\sigma_0 - 28)[(147.3 - 2.72T + 0.04T^2) \\ & - 10^{-4}p(32.4 - 0.87T + 0.02T^2)] \\ & + 10^{-2}(\sigma_0 - 28)^2[4.5 - 0.1T \\ & - 10^{-4}p(1.8 - 0.06T)] \end{aligned} \quad (C-12)$$

15. APPENDIX D Objective Analyses of the Standard Deviation of Temperature

Standard deviation statistics for the observed temperature, salinity, oxygen, and density data in five-degree squares are tabulated in the microfiche appendix of this atlas. We have also objectively analyzed the one-degree square values of the standard deviations of temperature, salinity, and oxygen in the same way we produced the mean fields presented in this atlas. The one-degree square values were based on a composite of all Station Data file observations regardless of the season. Although there is a lack of data for some regions, the presented fields show many interesting features. Analysis of the one-degree square deviations allows us to resolve these features to a better degree than the five-degree square tabulated data. We have used as input only those one-degree squares that contain four or more observations. We present only the temperature analyses, since the salinity and oxygen fields are generally quite similar. The formula for the computation of the standard deviation (S.D.) in a one-degree square with N observations is

$$\text{S.D.} = \sqrt{\sum_{n=1}^N (T_n - \bar{T})^2 / (N - 1)} \quad (D-1)$$

We recognize that computation of the standard deviation of the depth of isotherms might represent a more useful quantity for some purposes and that detrending of the analyses would present useful information, but these procedures are beyond the scope of this work. We wish only to point out regions of large variability.

The hatched areas on the maps in this section represent areas where there are not enough data in individual one-degree squares to produce a meaningful analysis. The criterion used to determine areas where enough data were available was as follows. Any five-degree square region that contained two or more one-degree squares, each with four or more observations, was defined as a region containing enough data to produce a meaningful result. Five-degree square areas that did not meet this criterion were hatched and no contours drawn. This definition while somewhat arbitrary, does give some measure of the reliability of these fields.

The 150 m distribution shown in figure D1 is shallow enough so that besides eddies, rings, current shifts, and internal waves, the annual temperature cycle as well as penetrative convection may contribute to some of the observed variability. A number of distinct features appear. In the North Atlantic a region of large variability appears to be associated with the Gulf Stream system, and another region of large variability appears off the northeastern coast of South America. In the South Atlantic a region of high variability occurs off the coast of South America at 40°S, 50°W. In the North Pacific a tongue of maximum variability extending eastward from Japan is associated with the Kuroshio Ex-

tension. In the western tropical Pacific a region of maximum variability along an east-west axis may be associated with displacements of the thermocline. In the western Indian Ocean there is a region of large variability off the coast of Somalia. This feature probably reflects variability of upwelling or horizontal currents due to the monsoon regime of this area.

The 500 m and 1000 m distributions presented in figures D2 and D3 show patterns similar to each other. Both the Gulf Stream system and the Kuroshio Extension region are characterized by relative maxima in variability. These maxima may be due to several factors, including shifts in the axes of the current systems, the presence of eddies and rings, and internal waves. We again emphasize that the gradients of these features have been somewhat reduced by the smoothing performed in the objective analysis procedure. Other than the two features just noted, the only other feature that appeared at 150 m and also at the 500 m and 1000 m levels is the maximum off South America at 40°S, 50°W.

At 1500 m the maxima of the Gulf Stream system and Kuroshio Extension are considerably reduced. The major feature at this level is the relative maximum in variability that extends westward from the Straits of Gibraltar. This maximum is undoubtedly associated with the Mediterranean Sea outflow.

16. APPENDIX E

User's Guide to Microfiche

Attached to this atlas are two envelopes containing a total of 17 microfiche. Each of the microfiche is numbered for identification with the first fiche numbered F-01 and the seventeenth numbered F-17. Fiche F-01 through F-14 contain 200 frames per fiche and fiche F-15 through F-17 contain 170 frames per fiche. For identification purposes the frames are numbered consecutively so the first row of frames on a fiche are numbered 1 through 20 or 1 through 17 and the last row of frames on a fiche are numbered 181 through 200 or 154 through 170. The number of each frame is printed in the upper right corner of each frame.

The fiche contain three types of information. The first type is statistics of observed data by five-degree squares at standard levels. The number of observations, mean, and root-mean-square deviation of various parameters are presented for both annual and seasonal periods. We emphasize that these statistics are based on observed data in the NODC Station Data, MBT, and XBT files after exclusion of suspicious data as described in section 2.2. The data are not "analyzed" in any way. For each standard level the globe is divided into sextants of 90° of latitude by 120° of longitude. Each sextant occupies one frame on the microfiche and the sextant number (1 to 6) is given in the upper right corner of the frame beneath the frame number. Five degree squares that are land are denoted by cross-hatching and five-degree squares that are completely

beneath the ocean floor are denoted by dot shading. Five-degree square boxes are formed by the intersection of lines of constant latitude and longitude drawn at five-degree spacing. The number of observations that exist in a particular square is given as the top-most number in the five-degree box, the mean is second from the top, and the root-mean-square deviation is third from the top. A fourth number may appear as "NL=" and represents the number of one-degree squares of land or sub-ocean floor in that five-degree square as computed according to the one-degree land-sea distribution for each standard level used in the objective analyses presented in this atlas. The land-sub-ocean floor-sea distribution at each standard level is based on the ocean topography of Smith et al. (1966).

Fiche F-01 through F-06 contain the five-degree square statistics for the annual period for temperature (in situ temperature from the sea surface through 500 m depth and potential temperature below 500 m depth), salinity, oxygen, oxygen-saturation, potential density, and anomaly of specific volume at all standard levels from the sea surface through 5500 m depth. We again note that these statistics are based on individual hydrocast data with the exception of temperature in the upper 500 m of the ocean which includes MBT and XBT data. By "annual" we mean that all data regardless of date of observation have been used in computing these statistics.

Fiche F-07 through F-14 contain five-degree square statistics of the same parameters given in Fiche F-01 through F-06 but for seasonal periods at standard levels from the sea surface through 250 m depth. The winter season (Northern Hemisphere) is defined as February, March, April and each season uses all data regardless of year of observation.

If one compares the statistics of oxygen and oxygen-saturation (annual or seasonal) there are a very few five-degree squares in which the number of observations of each quantity do not agree. This is because quality control checks eliminated some temperature and or salinity observations in these five-degree squares resulting in oxygen-saturation not being computed. In addition, for a very few five-degree squares the sum of observations for the four seasons does not add up to the total number of observations found in the corresponding five-degree square for the annual period. This is because some data may have been eliminated from a seasonal period but not from the annual period (or vice versa) for quality control reasons.

The second type of information presented on the fiche are the objectively analyzed fields of parameters and derived quantities shown in the text but at all standard levels. Fiche F-15 contains the annual mean objectively analyzed fields of potential temperature, salinity, oxygen, oxygen-saturation, and potential density at all standard levels from the sea surface through 5500 m depth. These represent the same fields discussed in sections 4 and 5 of this atlas. No drafted maps of potential density were

shown in the text. This field was computed from the fields of potential temperature and salinity described in sections 5.1 and 5.2. All these fields are presented for completeness, since it is not feasible to draft every parameter at every standard level. The variation with depth of these fields is of interest. The microfiche maps, however, are not of the same quality for presentation as the drafted fields. The drafted figures shown in the atlas can be compared with their microfiche counterpart.

Fiche F-16 contains the annual mean Brunt-Väisälä frequency at all standard levels, and represents the same fields discussed before in section 6. In addition, F-16 contains the objectively analyzed seasonal fields of in situ temperature and salinity at each standard level from the sea surface through 250 m.

The third type of information contained on the fiche is given on Fiche F-17. This fiche contains maps of the distribution of temperature, salinity, and oxygen observations for the annual period at all standard levels from the sea surface through 5500 m depth on a one-degree latitude-longitude grid. Maps of the seasonal distribution of observations for these same para-

eters are given for the sea surface and 250 m level only. Maps of the monthly distributions of temperature observations at the sea surface and 250 m level and maps of the monthly distribution of salinity observations at the sea surface are also shown. The distribution of observations on all of these maps is given by a dot pattern. Indication of the actual number of observations in each one-degree square is not possible because of limitations of space and optics. The maps indicate the input of data for the one-degree objective analyses presented in this atlas. Information concerning the number of observations can also be found on the fiche containing five-degree square statistics. One point to note is that the five-degree square statistics contain some data that were not used in the objective analyses presented in this atlas. For example, data that occurred in land or sub-ocean floor one-degree squares were not used in the objective analyses but were used in the compilation of the five-degree square statistics.

Table E1 is presented as a guide for finding information on the microfiche. The location of various fields are given by fiche and frame number. Some blank frames are included on the fiche for spacing.

Table 1.—Distribution with depth of the number of one-degree square of ocean (Ocean ODSQS), the total number (N) of temperature, salinity, and oxygen observations; and the number of one-degree squares (ODSQS) containing observations of each of these parameters.

Standard Level	Depth, m	Ocean ODSQS	Temperature		Salinity		Dissolved Oxygen	
			N	ODSQS	N	ODSQS	N	ODSQS
1	0	42 164	1 464 354	31 580	399 429	22 117	150 016	18 346
2	10	42 054	1 436 708	31 563	381 214	21 937	155 413	18 740
3	20	41 936	1 423 482	31 460	373 401	21 865	152 514	18 711
4	30	41 809	1 395 803	31 319	356 286	21 734	148 839	18 646
5	50	41 244	1 329 294	30 761	318 728	21 196	138 255	18 260
6	75	40 945	1 258 820	30 424	285 155	20 888	125 023	17 913
7	100	40 327	1 200 438	29 998	258 484	20 544	114 706	17 599
8	125	40 169	1 153 435	29 819	236 822	20 342	108 774	17 424
9	150	39 858	1 026 604	29 497	224 526	20 129	105 238	17 149
10	200	39 255	950 923	28 919	195 946	19 604	98 070	16 705
11	250	39 058	839 599	28 037	184 459	19 379	92 856	16 434
12	300	38 623	411 915	23 966	173 880	19 078	87 564	16 073
13	400	38 272	376 539	23 352	159 349	18 601	81 064	15 645
14	500	37 849	152 641	18 384	146 046	18 016	75 297	15 252
15	600	37 579	130 872	17 745	109 105	15 535	65 309	14 990
16	700	37 352	120 379	17 409	99 931	15 283	60 916	14 784
17	800	37 059	113 040	17 107	93 659	14 982	57 372	14 455
18	900	36 879	105 504	16 826	87 562	14 695	54 389	14 235
19	1000	36 493	94 155	16 215	77 384	14 004	48 890	13 510
20	1100	36 315	77 789	15 281	64 064	13 105	42 046	12 799
21	1200	36 057	67 792	14 469	56 206	12 299	35 097	11 960
22	1300	35 862	56 713	13 711	46 304	11 340	31 030	11 482
23	1400	35 716	52 541	13 346	42 628	10 970	28 872	11 142
24	1500	35 405	45 863	12 735	36 701	10 439	25 490	10 508
25	1750	34 914	30 271	11 187	23 878	9 167	20 559	9 443
26	2000	33 856	24 411	9 896	19 210	8 086	16 612	8 319
27	2500	32 077	17 317	8 043	14 221	6 769	12 110	6 857
28	3000	29 188	12 666	6 429	10 410	5 396	9 086	5 493
29*	3500	25 089	6 338	3 679	5 307	3 083	4 786	3 123
30	4000	19 718	6 591	3 475	5 393	2 880	4 782	2 921
31*	4500	12 856	2 191	1 346	1 849	1 136	1 687	1 147
32	5000	6 883	1 332	775	1 020	616	936	640
33*	5500	1 847	138	92	113	73	98	76

* These levels are not standard NODC levels. The data presented are interpolations from observed levels above and below the respective level.

Sydney Levitus

Table 2.—Number of surface salinity observations in the ten most densely sampled Marsden squares.

Rank	Marsden square	Marsden square boundaries	Number of surface salinity observations
1	216	0, 10E, 50N, 60N	41 079
2	131	130E, 140E, 30N, 40N	32 345
3	215	10E, 20E, 50N, 60N	23 143
4	181	0, 10W, 50N, 60N	22 231
5	151	60W, 70W, 40N, 50N	19 369
6	157	120W, 130W, 40N, 50N	18 919
7	132	120E, 130E, 30N, 40N	16 475
8	130	140E, 150E, 30N, 40N	14 913
9	166	140E, 150E, 40N, 50N	12 432
10	252	0, 10E, 60N, 70N	11 282

Table 3.—Range of acceptable temperature and salinity values as a function of depth.

Standard Level	Depth (m)	Temperature		Salinity	
		Range of Acceptable Values (°C)		Range of Acceptable Values (‰)	
1	0.	-3.0	- 35.0	0.0	- 40.0
2	10.	-3.0	- 35.0	0.0	- 40.0
3	20.	-3.0	- 35.0	0.0	- 40.0
4	30.	-3.0	- 35.0	0.0	- 40.0
5	50.	-3.0	- 35.0	20.0	- 40.0
6	75.	-3.0	- 35.0	20.0	- 40.0
7	100.	-3.0	- 30.0	30.0	- 40.0
8	125.	-3.0	- 30.0	30.0	- 40.0
9	150.	-3.0	- 30.0	30.0	- 40.0
10	200.	-3.0	- 30.0	30.0	- 40.0
11	250.	-3.0	- 28.0	30.0	- 40.0
12	300.	-3.0	- 28.0	30.0	- 40.0
13	400.	-3.0	- 28.0	33.0	- 40.0
14	500.	-3.0	- 28.0	33.0	- 40.0
15	600.	-3.0	- 20.0	33.0	- 40.0
16	700.	-3.0	- 20.0	33.0	- 40.0
17	800.	-3.0	- 20.0	33.0	- 40.0
18	900.	-3.0	- 20.0	33.0	- 40.0
19	1000.	-3.0	- 18.0	33.0	- 40.0
20	1100.	-3.0	- 18.0	33.0	- 38.0
21	1200.	-3.0	- 18.0	33.0	- 38.0
22	1300.	-3.0	- 18.0	33.0	- 38.0
23	1400.	-3.0	- 18.0	33.0	- 38.0
24	1500.	-3.0	- 18.0	33.0	- 38.0
25	1750.	-3.0	- 13.0	33.0	- 38.0
26	2000.	-3.0	- 13.0	33.0	- 38.0
27	2500.	-3.0	- 13.0	33.0	- 38.0
28	3000.	-3.0	- 7.0	33.0	- 35.5
29	3500.	-3.0	- 7.0	33.0	- 35.5
30	4000.	-1.5	- 7.0	33.0	- 35.5
31	4500.	-1.5	- 7.0	33.0	- 35.5
32	5000.	-1.5	- 7.0	33.0	- 35.5
33	5500.	-1.5	- 3.0	34.3	- 35.5

Table 4a.—Annual mean potential temperature (°C) area-weighted means over five-degree latitude belts for the world ocean as a function of depth, Southern Hemisphere.

Table 4a: Annual mean potential temperature (°C) area-weighted means over five-degree latitude belts for the world ocean as a function of depth, Southern Hemisphere. The table shows temperature values for depths from 0 to 5500m and latitudes from 87.5S to 2.5S.

Table 4b.—Annual mean potential temperature (°C) area-weighted means over five-degree latitude belts for the world ocean as a function of depth, Northern Hemisphere.

Table 4b: Annual mean potential temperature (°C) area-weighted means over five-degree latitude belts for the world ocean as a function of depth, Northern Hemisphere. The table shows temperature values for depths from 0 to 5500m and latitudes from 87.5N to 2.5N.

Table 6a.—Annual mean salinity (‰) area-weighted means over five-degree latitude belts for the world ocean as a function of depth, Southern Hemisphere.

Table with 28 columns for latitude (-87.5 to -2.5) and 28 rows for depth (0 to 5500 M). Values range from approximately 34.18 to 35.71.

Table 6b.—Annual mean salinity (‰) area-weighted means over five-degree latitude belts for the world ocean as a function of depth, Northern Hemisphere.

Table with 28 columns for latitude (2.5 to 87.5) and 28 rows for depth (0 to 5500 M). Values range from approximately 34.12 to 35.71.

Table 7a.—Annual mean salinity (‰) area-weighted r.m.s. deviations over five-degree latitude belts for the world ocean as a function of depth, Southern Hemisphere.

Table 7a: Annual mean salinity area-weighted r.m.s. deviations over five-degree latitude belts for the world ocean as a function of depth, Southern Hemisphere. The table is a grid with depth (0 to 5500m) on the y-axis and latitude (-87.5 to -2.5) on the x-axis. Values represent salinity deviations.

Table 7b.—Annual mean salinity (‰) area-weighted r.m.s. deviations over five-degree latitude belts for the world ocean as a function of depth, Northern Hemisphere.

Table 7b: Annual mean salinity area-weighted r.m.s. deviations over five-degree latitude belts for the world ocean as a function of depth, Northern Hemisphere. The table is a grid with depth (0 to 5500m) on the y-axis and latitude (2.5 to 87.5) on the x-axis. Values represent salinity deviations.

Table 10a.—Annual mean Brunt-Väisälä frequency (cycles/hr) area-weighted means over five-degree latitude belts for the world ocean as a function of depth, Southern Hemisphere.

Table with 26 columns for latitude (from -87.5 to -2.5) and 26 rows for depth (from 0 to 5500). Values represent annual mean Brunt-Väisälä frequency in cycles/hr.

Table 10b.—Annual mean Brunt-Väisälä frequency (cycles/hr) area-weighted means over five-degree latitude belts for the world ocean as a function of depth, Northern Hemisphere.

Table with 16 columns for latitude (from 2.5 to 87.5) and 26 rows for depth (from 0 to 5500). Values represent annual mean Brunt-Väisälä frequency in cycles/hr.

Table 13a.—Annual mean dissolved oxygen (ml/l) area-weighted r.m.s. deviations over five-degree latitude belts for the world ocean as a function of depth, Southern Hemisphere.

Table with columns for LATITUDE (from -87.5 to -2.5) and rows for DEPTH (M) (from 0 to 5500). Values represent annual mean dissolved oxygen area-weighted r.m.s. deviations.

Table 13b.—Annual mean dissolved oxygen (ml/l) area-weighted r.m.s. deviations over five-degree latitude belts for the world ocean as a function of depth, Northern Hemisphere.

Table with columns for LATITUDE (from 2.5 to 87.5) and rows for DEPTH (M) (from 0 to 5500). Values represent annual mean dissolved oxygen area-weighted r.m.s. deviations.

Table 19a.—Annual mean salinity (‰) area-weighted r.m.s. deviations over five-degree latitude belts for the Pacific Ocean as a function of depth, Southern Hemisphere.

Table with columns for Latitude (-87.5 to -2.5) and Depth (0 to 5500 meters). It shows annual mean salinity values and area-weighted r.m.s. deviations for the Southern Hemisphere.

Table 19b.—Annual mean salinity (‰) area-weighted r.m.s. deviations over five-degree latitude belts for the Pacific Ocean as a function of depth, Northern Hemisphere.

Table with columns for Latitude (2.5 to 87.5) and Depth (0 to 5500 meters). It shows annual mean salinity values and area-weighted r.m.s. deviations for the Northern Hemisphere.

Table 23a.—Annual mean Brunt-Väisälä frequency (cycles/hr) area-weighted r.m.s. deviations over five-degree latitude belts for the Pacific Ocean as a function of depth, Southern Hemisphere.

Table with columns for Latitude (ranging from -87.5 to -2.5) and Depth (M) (ranging from 0 to 5500). It contains numerical data representing Brunt-Väisälä frequency and its deviations.

Table 23b.—Annual mean Brunt-Väisälä frequency (cycles/hr) area-weighted r.m.s. deviations over five-degree latitude belts for the Pacific Ocean as a function of depth, Northern Hemisphere.

Table with columns for Latitude (ranging from 2.5 to 87.5) and Depth (M) (ranging from 0 to 5500). It contains numerical data representing Brunt-Väisälä frequency and its deviations.

Table 30a.—Annual mean salinity (‰) area-weighted means over five-degree latitude belts for the Atlantic Ocean as a function of depth, Southern Hemisphere.

Table with 16 columns for Latitude (-87.5 to -2.5) and 20 rows for Depth (0 to 5500 M). Salinity values range from approximately 34.18 to 35.99.

Table 30b.—Annual mean salinity (‰) area-weighted means over five-degree latitude belts for the Atlantic Ocean as a function of depth, Northern Hemisphere.

Table with 16 columns for Latitude (2.5 to 87.5) and 20 rows for Depth (0 to 5500 M). Salinity values range from approximately 34.71 to 35.99.

Table 31a.—Annual mean salinity (‰) area-weighted r.m.s. deviations over five-degree latitude belts for the Atlantic Ocean as a function of depth, Southern Hemisphere.

Table with 26 columns for Latitude (from -87.5 to -2.5) and 30 rows for Depth (from 0 to 5500 M). Values represent r.m.s. deviations of salinity.

Table 31b.—Annual mean salinity (‰) area-weighted r.m.s. deviations over five-degree latitude belts for the Atlantic Ocean as a function of depth, Northern Hemisphere.

Table with 26 columns for Latitude (from 2.5 to 87.5) and 30 rows for Depth (from 0 to 5500 M). Values represent r.m.s. deviations of salinity.

Table 35a.—Annual mean Brunt-Väisälä frequency (cycles/hr) area-weighted r.m.s. deviations over five-degree latitude belts for the Atlantic Ocean as a function of depth, Southern Hemisphere.

Table with columns for Latitude (-87.5 to -2.5) and Depth (0 to 5500 M) showing Brunt-Väisälä frequency data for the Southern Hemisphere.

Table 35b.—Annual mean Brunt-Väisälä frequency (cycles/hr) area-weighted r.m.s. deviations over five-degree latitude belts for the Atlantic Ocean as a function of depth, Northern Hemisphere.

Table with columns for Latitude (2.5 to 87.5) and Depth (0 to 5500 M) showing Brunt-Väisälä frequency data for the Northern Hemisphere.

Table 51a.—Annual mean oxygen-saturation (%) area-weighted r.m.s. deviations over five-degree latitude belts for the Indian Ocean as a function of depth, Southern Hemisphere.

Table with columns for Latitude (-87.5 to -2.5) and Depth (0 to 5500 meters). Values represent oxygen-saturation deviations.

Table 51b.—Annual mean oxygen-saturation (%) area-weighted r.m.s. deviations over five-degree latitude belts for the Indian Ocean as a function of depth, Northern Hemisphere.

Table with columns for Latitude (2.5 to 87.5) and Depth (0 to 5000 meters). Values represent oxygen-saturation deviations.

Table 56a.—Annual mean potential temperature (°C) basin means and standard errors for the world ocean and Atlantic Ocean as a function of depth.

Standard Level	Depth	World Ocean		Southern Hemisphere Ocean		Northern Hemisphere Ocean		Atlantic Ocean		South Atlantic Ocean		North Atlantic Ocean	
		Mean	Standard Error	Mean	Standard Error	Mean	Standard Error	Mean	Standard Error	Mean	Standard Error	Mean	Standard Error
1	0.	18.10	0.72	16.60	0.96	20.15	1.04	15.29	1.41	14.38	2.06	16.00	1.91
2	10.	18.03	0.72	16.54	0.95	20.07	1.05	15.21	1.41	14.32	2.06	15.91	1.93
3	20.	17.89	0.72	16.43	0.95	19.89	1.06	15.06	1.41	14.19	2.04	15.76	1.94
4	30.	17.67	0.72	16.27	0.95	19.60	1.06	14.81	1.40	13.95	2.01	15.50	1.93
5	50.	17.00	0.70	15.73	0.93	18.76	1.05	14.19	1.36	13.30	1.95	14.90	1.87
6	75.	15.99	0.67	14.86	0.89	17.57	0.99	13.34	1.28	12.40	1.84	14.11	1.75
7	100.	14.99	0.63	14.00	0.85	16.40	0.92	12.61	1.20	11.54	1.73	13.52	1.64
8	125.	14.06	0.59	13.24	0.80	15.22	0.84	11.97	1.12	10.83	1.60	12.94	1.53
9	150.	13.24	0.54	12.57	0.74	14.21	0.76	11.48	1.05	10.26	1.49	12.53	1.44
10	200.	11.84	0.46	11.36	0.64	12.55	0.62	10.65	0.93	9.27	1.28	11.88	1.28
11	250.	10.75	0.40	10.31	0.55	11.40	0.55	10.00	0.84	8.56	1.13	11.30	1.18
12	300.	9.88	0.35	9.40	0.47	10.59	0.50	9.42	0.79	7.83	1.02	10.89	1.10
13	400.	8.46	0.29	7.93	0.37	9.24	0.45	8.34	0.70	6.63	0.84	9.93	1.01
14	500.	7.28	0.25	6.79	0.30	8.02	0.40	7.22	0.63	5.47	0.65	8.87	0.93
15	600.	6.38	0.22	5.96	0.26	7.00	0.36	6.25	0.56	4.52	0.50	7.89	0.85
16	700.	5.65	0.19	5.28	0.23	6.20	0.33	5.44	0.50	3.80	0.38	7.02	0.77
17	800.	5.04	0.17	4.71	0.20	5.55	0.30	4.82	0.45	3.32	0.31	6.28	0.70
18	900.	4.54	0.15	4.22	0.17	5.03	0.27	4.37	0.41	3.02	0.27	5.68	0.65
19	1000.	4.12	0.14	3.80	0.14	4.60	0.25	4.03	0.38	2.83	0.26	5.23	0.62
20	1100.	3.78	0.13	3.47	0.13	4.27	0.24	3.83	0.36	2.73	0.26	4.92	0.59
21	1200.	3.50	0.12	3.19	0.11	3.96	0.23	3.65	0.35	2.66	0.26	4.65	0.57
22	1300.	3.26	0.11	2.96	0.10	3.70	0.22	3.49	0.33	2.59	0.26	4.41	0.55
23	1400.	3.04	0.10	2.77	0.09	3.46	0.21	3.35	0.32	2.54	0.26	4.18	0.53
24	1500.	2.85	0.10	2.60	0.09	3.23	0.20	3.21	0.31	2.48	0.26	3.97	0.51
25	1750.	2.47	0.09	2.27	0.08	2.78	0.18	2.93	0.28	2.34	0.26	3.56	0.48
26	2000.	2.18	0.08	2.01	0.08	2.44	0.17	2.69	0.27	2.18	0.25	3.25	0.45
27	2500.	1.79	0.97	1.64	0.07	2.01	0.15	2.32	0.24	1.89	0.24	2.82	0.40
28	3000.	1.50	0.07	1.36	0.07	1.73	0.12	1.98	0.20	1.61	0.24	2.43	0.31
29*	3500.	1.27	0.06	1.09	0.08	1.55	0.08	1.70	0.17	1.28	0.24	2.25	0.10
30	4000.	1.08	0.06	0.82	0.08	1.41	0.07	1.39	0.19	0.88	0.25	2.07	0.10
31*	4500.	0.91	0.08	0.59	0.10	1.30	0.07	1.18	0.24	0.59	0.30	1.94	0.09
32	5000.	0.90	0.10	0.52	0.14	1.23	0.08	1.06	0.32	0.37	0.41	1.81	0.09
33*	5500.	1.02	0.12	0.61	0.24	1.17	0.09	1.18	0.51	-0.10	0.39	1.53	0.21

*These are not standard NODC levels. The data used are interpolations from observed levels.

Table 56b.—Annual mean potential temperature (°C) basin means and standard errors for the Pacific Ocean and Indian Ocean as a function of depth.

Standard Level	Depth	Pacific Ocean			South Pacific Ocean			North Pacific Ocean			Indian Ocean			South Indian Ocean			North Indian Ocean		
		Mean	Standard Error		Mean	Standard Error		Mean	Standard Error		Mean	Standard Error		Mean	Standard Error		Mean	Standard Error	
1	0.	19.87	0.91		18.08	1.32		22.00	1.15		17.91	1.65		16.04	1.78		27.91	0.34	
2	10.	19.79	0.91		18.00	1.31		21.92	1.15		17.85	1.65		15.99	1.78		27.82	0.35	
3	20.	19.64	0.91		17.91	1.31		21.70	1.17		17.75	1.64		15.89	1.77		27.67	0.39	
4	30.	19.42	0.91		17.78	1.31		21.38	1.19		17.58	1.64		15.75	1.77		27.42	0.46	
5	50.	18.68	0.91		17.30	1.30		20.33	1.21		16.95	1.60		15.19	1.72		26.61	0.58	
6	75.	17.57	0.89		16.47	1.27		18.91	1.19		15.91	1.49		14.26	1.61		24.95	0.56	
7	100.	16.52	0.85		15.71	1.24		17.50	1.13		14.64	1.37		13.25	1.48		22.42	0.43	
8	125.	15.47	0.80		14.95	1.17		16.10	1.03		13.53	1.22		12.41	1.35		19.79	0.42	
9	150.	14.50	0.73		14.23	1.10		14.82	0.92		12.63	1.11		11.74	1.24		17.64	0.55	
10	200.	12.70	0.61		12.76	0.94		12.63	0.72		11.37	0.95		10.74	1.08		14.91	0.70	
11	250.	11.27	0.51		11.37	0.78		11.15	0.60		10.48	0.85		9.94	0.96		13.53	0.76	
12	300.	10.15	0.43		10.20	0.65		10.10	0.53		9.81	0.77		9.30	0.87		12.69	0.78	
13	400.	8.38	0.32		8.29	0.46		8.48	0.42		8.79	0.67		8.29	0.74		11.61	0.80	
14	500.	7.02	0.24		6.93	0.34		7.13	0.32		7.99	0.60		7.51	0.65		10.75	0.73	
15	600.	6.04	0.18		6.04	0.27		6.04	0.24		7.33	0.54		6.86	0.59		10.09	0.74	
16	700.	5.34	0.15		5.39	0.23		5.27	0.19		6.65	0.49		6.18	0.52		9.41	0.71	
17	800.	4.77	0.13		4.83	0.20		4.69	0.15		5.98	0.43		5.51	0.44		8.72	0.67	
18	900.	4.30	0.11		4.36	0.17		4.23	0.13		5.31	0.38		4.86	0.37		8.02	0.60	
19	1000.	3.91	0.10		3.94	0.15		3.87	0.11		4.71	0.33		4.28	0.31		7.36	0.55	
20	1100.	3.57	0.08		3.58	0.13		3.56	0.10		4.23	0.29		3.82	0.27		6.71	0.43	
21	1200.	3.28	0.07		3.27	0.12		3.28	0.08		3.83	0.26		3.46	0.24		6.12	0.31	
22	1300.	3.03	0.07		3.01	0.10		3.06	0.09		3.50	0.23		3.17	0.21		5.57	0.26	
23	1400.	2.81	0.06		2.78	0.09		2.85	0.08		3.22	0.21		2.93	0.19		5.04	0.21	
24	1500.	2.62	0.06		2.59	0.08		2.65	0.08		2.96	0.19		2.71	0.18		4.54	0.18	
25	1750.	2.24	0.05		2.22	0.07		2.26	0.07		2.45	0.14		2.30	0.14		3.46	0.14	
26	2000.	1.96	0.05		1.95	0.07		1.97	0.06		2.08	0.12		1.98	0.13		2.72	0.12	
27	2500.	1.61	0.04		1.60	0.06		1.63	0.06		1.58	0.11		1.53	0.12		1.93	0.08	
28	3000.	1.40	0.04		1.38	0.06		1.43	0.06		1.20	0.11		1.16	0.12		1.54	0.03	
29*	3500.	1.22	0.04		1.17	0.06		1.28	0.06		0.89	0.11		0.84	0.12		1.32	0.06	
30	4000.	1.06	0.04		0.95	0.08		1.17	0.03		0.63	0.12		0.58	0.13		1.19	0.09	
31*	4500.	0.95	0.05		0.73	0.08		1.10	0.04		0.44	0.15		0.41	0.15		0.99	0.09	
32	5000.	0.93	0.06		0.64	0.09		1.06	0.04		0.50	0.19		0.50	0.19		0.91	0.03	
33*	5500.	1.04	0.07		0.82	0.37		1.08	0.04		0.70	0.01		0.70	0.01				

* These are not standard NODC levels. The data used are interpolations from observed levels.

Table 57a.—Annual mean salinity (‰) basin means and standard errors for the world ocean and Atlantic Ocean as a function of depth.

Standard Level	Depth	World Ocean		Southern Hemisphere Ocean		Northern Hemisphere Ocean		Atlantic Ocean		South Atlantic Ocean		North Atlantic Ocean	
		Mean	Standard Error	Mean	Standard Error	Mean	Standard Error	Mean	Standard Error	Mean	Standard Error	Mean	Standard Error
1	0.	34.63	0.12	34.87	0.08	34.31	0.25	34.75	0.35	35.10	0.22	34.48	0.60
2	10.	34.69	0.11	34.89	0.08	34.41	0.23	34.88	0.32	35.14	0.21	34.67	0.55
3	20.	34.75	0.10	34.91	0.08	34.53	0.21	35.02	0.29	35.16	0.21	34.91	0.48
4	30.	34.80	0.09	34.93	0.08	34.64	0.19	35.14	0.26	35.19	0.21	35.10	0.44
5	50.	34.90	0.08	34.96	0.07	34.81	0.17	35.31	0.23	35.23	0.21	35.37	0.38
6	75.	34.97	0.07	34.99	0.07	34.95	0.14	35.41	0.19	35.22	0.20	35.57	0.29
7	100.	35.02	0.07	35.01	0.07	35.03	0.13	35.47	0.17	35.19	0.19	35.69	0.26
8	125.	35.03	0.07	35.02	0.07	35.05	0.13	35.46	0.16	35.14	0.17	35.73	0.24
9	150.	35.03	0.06	35.01	0.06	35.06	0.12	35.44	0.15	35.08	0.15	35.76	0.22
10	200.	34.99	0.06	34.96	0.05	35.02	0.11	35.38	0.13	34.97	0.11	35.75	0.20
11	250.	34.93	0.05	34.89	0.04	34.98	0.11	35.32	0.12	34.89	0.09	35.71	0.18
12	300.	34.87	0.05	34.82	0.04	34.93	0.10	35.25	0.12	34.82	0.08	35.65	0.18
13	400.	34.76	0.04	34.70	0.03	34.85	0.10	35.12	0.11	34.69	0.05	35.52	0.17
14	500.	34.68	0.04	34.62	0.02	34.78	0.09	35.00	0.10	34.58	0.04	35.40	0.16
15	600.	34.63	0.04	34.56	0.02	34.74	0.08	34.90	0.10	34.51	0.03	35.28	0.16
16	700.	34.61	0.03	34.53	0.02	34.72	0.08	34.84	0.10	34.47	0.03	35.20	0.15
17	800.	34.60	0.03	34.52	0.02	34.72	0.07	34.81	0.09	34.46	0.03	35.15	0.15
18	900.	34.60	0.03	34.52	0.01	34.73	0.07	34.81	0.09	34.48	0.03	35.12	0.15
19	1000.	34.61	0.03	34.53	0.01	34.74	0.06	34.82	0.09	34.51	0.03	35.12	0.14
20	1100.	34.63	0.03	34.55	0.01	34.75	0.06	34.85	0.08	34.56	0.03	35.13	0.14
21	1200.	34.65	0.03	34.57	0.01	34.76	0.06	34.87	0.08	34.61	0.03	35.14	0.14
22	1300.	34.67	0.02	34.60	0.01	34.77	0.06	34.89	0.08	34.66	0.03	35.14	0.14
23	1400.	34.68	0.02	34.62	0.01	34.77	0.06	34.91	0.08	34.70	0.03	35.13	0.13
24	1500.	34.70	0.02	34.64	0.01	34.78	0.05	34.92	0.07	34.73	0.03	35.12	0.13
25	1750.	34.72	0.02	34.69	0.01	34.78	0.05	34.94	0.07	34.78	0.02	35.09	0.13
26	2000.	34.74	0.02	34.71	0.01	34.77	0.05	34.93	0.06	34.81	0.02	35.06	0.12
27	2500.	34.75	0.02	34.73	0.01	34.77	0.04	34.91	0.05	34.83	0.02	35.02	0.11
28	3000.	34.74	0.01	34.73	0.01	34.76	0.03	34.88	0.04	34.82	0.02	34.96	0.07
29*	3500.	34.74	0.01	34.73	0.01	34.75	0.02	34.86	0.03	34.80	0.02	34.93	0.01
30	4000.	34.73	0.01	34.72	0.01	34.74	0.01	34.83	0.02	34.77	0.02	34.91	0.01
31*	4500.	34.73	0.01	34.72	0.01	34.74	0.02	34.81	0.02	34.75	0.03	34.89	0.01
32	5000.	34.73	0.01	34.71	0.01	34.74	0.02	34.80	0.03	34.73	0.04	34.88	0.01
33*	5500.	34.72	0.02	34.70	0.01	34.73	0.03	34.82	0.06	34.68	0.02	34.86	0.01

*These are not standard NODC levels. The data used are interpolations from observed levels.

Table 58a.—Annual mean potential density (10^{-3}g/cm^3) basin means and standard errors for the world ocean and the Atlantic Ocean as a function of depth.

Standard Level	Depth	World Ocean		Southern Hemisphere Ocean		Northern Hemisphere Ocean		Atlantic Ocean		South Atlantic Ocean		North Atlantic Ocean	
		Mean	Standard Error	Mean	Standard Error	Mean	Standard Error	Mean	Standard Error	Mean	Standard Error	Mean	Standard Error
1	0.	24.53	0.14	25.06	0.17	23.81	0.25	25.19	0.36	25.69	0.26	24.79	0.40
2	10.	24.59	0.14	25.09	0.17	23.90	0.22	25.30	0.24	25.73	0.26	24.96	0.39
3	20.	24.67	0.14	25.13	0.16	24.04	0.21	25.45	0.22	25.79	0.25	25.17	0.34
4	30.	24.77	0.13	25.19	0.16	24.20	0.21	25.61	0.21	25.87	0.24	25.39	0.32
5	50.	25.02	0.13	25.35	0.16	24.56	0.20	25.90	0.19	26.06	0.22	25.78	0.30
6	75.	25.35	0.11	25.60	0.14	25.00	0.18	26.22	0.15	26.28	0.19	26.17	0.23
7	100.	25.65	0.10	25.84	0.13	25.39	0.16	26.46	0.13	26.48	0.16	26.45	0.19
8	125.	25.91	0.09	26.04	0.11	25.73	0.14	26.63	0.11	26.61	0.14	26.65	0.17
9	150.	26.12	0.07	26.21	0.10	26.00	0.12	26.75	0.10	26.71	0.13	26.79	0.15
10	200.	26.44	0.06	26.48	0.07	26.38	0.09	26.93	0.09	26.86	0.11	26.99	0.13
11	250.	26.64	0.05	26.67	0.06	26.59	0.08	27.03	0.08	26.95	0.10	27.10	0.12
12	300.	26.77	0.04	26.81	0.05	26.72	0.07	27.10	0.08	27.04	0.09	27.16	0.12
13	400.	26.96	0.03	26.99	0.04	26.91	0.06	27.21	0.07	27.16	0.08	27.25	0.11
14	500.	27.09	0.03	27.11	0.03	27.00	0.05	27.30	0.06	27.25	0.07	27.35	0.11
15	600.	27.19	0.02	27.19	0.03	27.18	0.04	27.38	0.06	27.33	0.06	27.43	0.10
16	700.	27.27	0.02	27.26	0.03	27.29	0.04	27.45	0.05	27.39	0.05	27.51	0.09
17	800.	27.35	0.02	27.33	0.02	27.37	0.03	27.51	0.05	27.44	0.05	27.59	0.08
18	900.	27.41	0.02	27.39	0.02	27.45	0.03	27.57	0.04	27.48	0.04	27.65	0.07
19	1000.	27.47	0.02	27.44	0.02	27.51	0.03	27.62	0.04	27.53	0.04	27.71	0.07
20	1100.	27.52	0.02	27.50	0.02	27.56	0.03	27.67	0.04	27.57	0.03	27.76	0.06
21	1200.	27.57	0.01	27.54	0.01	27.60	0.03	27.71	0.04	27.62	0.03	27.80	0.06
22	1300.	27.61	0.01	27.59	0.01	27.64	0.03	27.75	0.03	27.66	0.03	27.83	0.06
23	1400.	27.64	0.01	27.62	0.01	27.67	0.03	27.78	0.03	27.70	0.02	27.86	0.05
24	1500.	27.67	0.01	27.66	0.01	27.69	0.02	27.80	0.03	27.73	0.02	27.87	0.05
25	1750.	27.73	0.01	27.72	0.01	27.74	0.02	27.84	0.03	27.79	0.01	27.90	0.05
26	2000.	27.76	0.01	27.76	0.01	27.77	0.02	27.86	0.02	27.82	0.01	27.91	0.05
27	2500.	27.80	0.01	27.80	0.00	27.80	0.02	27.89	0.02	27.86	0.00	27.92	0.04
28	3000.	27.82	0.01	27.83	0.00	27.82	0.01	27.89	0.01	27.87	0.00	27.92	0.03
29*	3500.	27.84	0.00	27.84	0.00	27.82	0.01	27.89	0.00	27.89	0.00	27.92	0.02
30	4000.	27.85	0.00	27.86	0.00	27.83	0.01	27.90	0.00	27.89	0.00	27.91	0.01
31*	4500.	27.85	0.00	27.87	0.00	27.84	0.01	27.90	0.01	27.89	0.00	27.91	0.01
32	5000.	27.85	0.01	27.87	0.00	27.84	0.01	27.90	0.01	27.89	0.01	27.92	0.00
33*	5500.	27.84	0.01	27.85	0.01	27.84	0.02	27.91	0.02	27.87	0.00	27.92	0.01

*These are not standard NODC levels. The data used are interpolations from observed levels.

Table 58b.—Annual mean potential density (10^{-3}g/cm^3) basin means and standard errors for the Pacific Ocean and Indian Ocean as a function of depth.

Standard Level	Depth	Pacific Ocean		South Pacific Ocean		North Pacific Ocean		Indian Ocean		South Indian Ocean		North Indian Ocean	
		Mean	Standard Error	Mean	Standard Error	Mean	Standard Error	Mean	Standard Error	Mean	Standard Error	Mean	Standard Error
1	0.	24.11	0.18	24.78	0.24	23.31	0.23	24.58	0.34	25.00	0.34	22.33	0.58
2	10.	24.15	0.18	24.81	0.24	23.36	0.22	24.61	0.33	25.02	0.34	22.42	0.54
3	20.	24.21	0.18	24.85	0.24	23.45	0.22	24.66	0.33	25.06	0.33	22.53	0.52
4	30.	24.29	0.18	24.90	0.23	23.57	0.22	24.72	0.32	25.11	0.33	22.67	0.50
5	50.	24.53	0.17	25.05	0.23	23.92	0.22	24.94	0.30	25.28	0.31	23.05	0.46
6	75.	24.87	0.16	25.28	0.21	24.37	0.21	25.28	0.26	25.58	0.26	23.68	0.38
7	100.	25.18	0.14	25.50	0.20	24.79	0.19	25.66	0.21	25.87	0.22	24.46	0.30
8	125.	25.47	0.12	25.71	0.18	25.18	0.16	25.98	0.17	26.12	0.18	25.16	0.22
9	150.	25.73	0.11	25.90	0.15	25.51	0.13	26.22	0.14	26.31	0.15	25.68	0.18
10	200.	26.12	0.08	26.23	0.12	25.99	0.09	26.54	0.10	26.58	0.12	26.30	0.14
11	250.	26.38	0.06	26.47	0.09	26.27	0.08	26.73	0.08	26.76	0.09	26.59	0.13
12	300.	26.56	0.05	26.65	0.07	26.44	0.06	26.86	0.07	26.88	0.08	26.76	0.12
13	400.	26.81	0.04	26.90	0.05	26.69	0.05	27.01	0.06	27.02	0.07	26.95	0.11
14	500.	26.98	0.03	27.05	0.04	26.88	0.04	27.10	0.06	27.11	0.06	27.07	0.08
15	600.	27.10	0.02	27.14	0.03	27.04	0.03	27.18	0.05	27.17	0.06	27.18	0.08
16	700.	27.19	0.02	27.21	0.03	27.16	0.02	27.25	0.05	27.24	0.06	27.27	0.06
17	800.	27.27	0.02	27.28	0.03	27.25	0.01	27.32	0.04	27.31	0.05	27.35	0.05
18	900.	27.34	0.01	27.34	0.03	27.33	0.01	27.39	0.04	27.38	0.04	27.42	0.04
19	1000.	27.40	0.01	27.40	0.02	27.40	0.01	27.45	0.03	27.45	0.04	27.49	0.03
20	1100.	27.45	0.01	27.45	0.02	27.45	0.01	27.51	0.03	27.50	0.03	27.54	0.02
21	1200.	27.50	0.01	27.50	0.02	27.49	0.00	27.55	0.03	27.55	0.03	27.58	0.01
22	1300.	27.54	0.01	27.55	0.02	27.53	0.01	27.60	0.02	27.59	0.03	27.62	0.01
23	1400.	27.57	0.01	27.59	0.01	27.56	0.01	27.63	0.02	27.63	0.02	27.66	0.01
24	1500.	27.61	0.01	27.62	0.01	27.59	0.01	27.66	0.02	26.66	0.02	27.69	0.01
25	1750.	27.67	0.01	27.68	0.01	27.65	0.01	27.73	0.01	27.73	0.01	27.74	0.01
26	2000.	27.71	0.01	27.72	0.01	27.69	0.01	27.77	0.01	27.77	0.01	27.78	0.01
27	2500.	27.76	0.01	27.77	0.01	27.74	0.01	27.82	0.00	27.82	0.01	27.81	0.00
28	3000.	27.78	0.01	27.80	0.01	27.77	0.01	27.84	0.00	27.84	0.00	27.82	0.00
29*	3500.	27.80	0.00	27.82	0.01	27.79	0.01	27.85	0.00	27.85	0.00	27.83	0.00
30	4000.	27.82	0.00	27.84	0.01	27.81	0.00	27.86	0.00	27.86	0.00	27.84	0.00
31*	4500.	27.83	0.00	27.85	0.01	27.81	0.00	27.87	0.00	27.87	0.00	27.85	0.00
32	5000.	27.83	0.00	27.86	0.01	27.82	0.00	27.86	0.00	27.86	0.00	27.85	0.00
33*	5500.	27.82	0.00	27.84	0.03	27.82	0.00	27.86	0.00	27.86	0.00	—	—

*These are not standard NODC levels. The data used are interpolations from observed levels.

Table 59a.—Annual mean dissolved oxygen (ml/l) basin means and standard errors for the world ocean and Atlantic Ocean as a function of depth.

Standard Level	Depth	World Ocean		Southern Hemisphere Ocean		Northern Hemisphere Ocean		Atlantic Ocean		South Atlantic Ocean		North Atlantic Ocean	
		Mean	Standard Error	Mean	Standard Error	Mean	Standard Error	Mean	Standard Error	Mean	Standard Error	Mean	Standard Error
1	0.	5.62	0.09	5.78	0.12	5.41	0.14	5.98	0.19	6.03	0.27	5.94	0.27
2	10.	5.62	0.09	5.78	0.12	5.41	0.14	5.98	0.19	6.02	0.27	5.94	0.28
3	20.	5.62	0.09	5.77	0.12	5.40	0.14	5.96	0.19	6.01	0.27	5.92	0.27
4	30.	5.59	0.09	5.75	0.12	5.37	0.14	5.90	0.19	5.96	0.27	5.86	0.26
5	50.	5.50	0.09	5.70	0.12	5.23	0.14	5.76	0.19	5.84	0.27	5.70	0.26
6	75.	5.28	0.10	5.55	0.13	4.92	0.16	5.54	0.19	5.68	0.29	5.43	0.25
7	100.	5.03	0.12	5.35	0.14	4.57	0.19	5.33	0.20	5.49	0.30	5.20	0.26
8	125.	4.76	0.12	5.11	0.15	4.26	0.20	5.14	0.20	5.27	0.30	5.03	0.27
9	150.	4.55	0.13	4.92	0.15	4.00	0.21	4.98	0.20	5.07	0.30	4.90	0.28
10	200.	4.23	0.13	4.63	0.15	3.64	0.21	4.73	0.21	4.76	0.30	4.71	0.29
11	250.	4.02	0.13	4.44	0.15	3.40	0.22	4.58	0.21	4.56	0.30	4.59	0.30
12	300.	3.86	0.14	4.31	0.16	3.20	0.22	4.44	0.22	4.41	0.30	4.48	0.31
13	400.	3.67	0.14	4.19	0.16	2.88	0.23	4.30	0.22	4.26	0.29	4.34	0.32
14	500.	3.55	0.14	4.18	0.15	2.61	0.22	4.25	0.21	4.25	0.26	4.26	0.32
15	600.	3.45	0.14	4.16	0.14	2.39	0.22	4.26	0.19	4.31	0.22	4.21	0.31
16	700.	3.35	0.14	4.08	0.13	2.25	0.22	4.28	0.18	4.38	0.19	4.19	0.31
17	800.	3.27	0.13	3.98	0.13	2.20	0.22	4.33	0.17	4.42	0.16	4.24	0.30
18	900.	3.22	0.13	3.89	0.12	2.22	0.22	4.39	0.16	4.41	0.13	4.37	0.28
19	1000.	3.21	0.12	3.81	0.11	2.30	0.23	4.48	0.14	4.39	0.11	4.56	0.26
20	1100.	3.22	0.12	3.75	0.10	2.41	0.23	4.59	0.13	4.39	0.09	4.78	0.24
21	1200.	3.25	0.12	3.72	0.10	2.53	0.24	4.70	0.12	4.42	0.06	4.99	0.22
22	1300.	3.29	0.12	3.72	0.09	2.64	0.24	4.83	0.11	4.48	0.05	5.18	0.20
23	1400.	3.35	0.12	3.73	0.09	2.76	0.24	4.95	0.11	4.55	0.06	5.35	0.18
24	1500.	3.41	0.11	3.76	0.09	2.88	0.24	5.06	0.11	4.64	0.07	5.49	0.17
25	1750.	3.58	0.11	3.88	0.09	3.11	0.23	5.25	0.10	4.86	0.08	5.66	0.14
26	2000.	3.73	0.10	4.00	0.09	3.30	0.22	5.37	0.09	5.02	0.08	5.75	0.12
27	2500.	3.95	0.09	4.19	0.08	3.56	0.20	5.45	0.08	5.18	0.07	5.75	0.11
28	3000.	4.10	0.09	4.32	0.08	3.75	0.18	5.46	0.08	5.24	0.07	5.74	0.11
29*	3500.	4.26	0.08	4.47	0.08	3.92	0.16	5.45	0.08	5.24	0.08	5.71	0.10
30*	4000.	4.38	0.08	4.62	0.08	4.05	0.16	5.41	0.08	5.23	0.08	5.66	0.12
31*	4500.	4.50	0.09	4.82	0.08	4.12	0.16	5.41	0.09	5.25	0.11	5.62	0.10
32	5000.	4.46	0.12	4.82	0.11	4.15	0.18	5.38	0.11	5.20	0.16	5.57	0.11
33*	5500.	4.20	0.22	4.81	0.24	4.06	0.26	5.33	0.15	5.28	0.26	5.35	0.17

*These are not standard NODC levels. The data used are interpolations from observed levels.

1988 716 007 81809

Table 59b.—Annual mean dissolved oxygen (ml/l) basin means and standard errors for the Pacific Ocean and Atlantic Ocean as a function of depth.

Standard Level	Depth	Pacific Ocean		South Pacific Ocean		North Pacific Ocean		Indian Ocean		South Indian Ocean		North Indian Ocean	
		Mean	Standard Error	Mean	Standard Error	Mean	Standard Error	Mean	Standard Error	Mean	Standard Error	Mean	Standard Error
1	0.	5.39	0.11	5.59	0.16	5.15	0.13	5.67	0.21	5.88	0.23	4.53	0.05
2	10.	5.39	0.11	5.58	0.16	5.15	0.13	5.67	0.21	5.88	0.23	4.53	0.04
3	20.	5.39	0.11	5.58	0.16	5.17	0.14	5.66	0.21	5.88	0.23	4.48	0.06
4	30.	5.38	0.11	5.56	0.16	5.16	0.15	5.65	0.21	5.88	0.22	4.39	0.10
5	50.	5.31	0.12	5.51	0.16	5.07	0.17	5.59	0.21	5.86	0.22	4.09	0.19
6	75.	5.12	0.14	5.38	0.18	4.80	0.21	5.32	0.25	5.70	0.24	3.25	0.27
7	100.	4.87	0.16	5.19	0.20	4.48	0.24	4.97	0.30	5.46	0.27	2.27	0.34
8	125.	4.59	0.17	4.97	0.21	4.12	0.25	4.65	0.32	5.21	0.28	1.56	0.33
9	150.	4.33	0.17	4.76	0.22	3.81	0.25	4.46	0.33	5.05	0.28	1.19	0.32
10	200.	3.92	0.18	4.41	0.24	3.32	0.26	4.27	0.31	4.85	0.26	1.03	0.32
11	250.	3.64	0.19	4.17	0.25	2.99	0.26	4.20	0.29	4.76	0.23	1.04	0.32
12	300.	3.41	0.20	3.99	0.26	2.71	0.26	4.17	0.28	4.72	0.21	1.05	0.33
13	400.	3.13	0.20	3.83	0.26	2.26	0.25	4.12	0.28	4.67	0.20	0.95	0.29
14	500.	2.97	0.20	3.89	0.25	1.85	0.21	4.00	0.28	4.55	0.21	0.83	0.23
15	600.	2.86	0.20	3.94	0.23	1.52	0.17	3.83	0.28	4.35	0.22	0.74	0.17
16	700.	2.73	0.19	3.88	0.22	1.31	0.13	3.65	0.28	4.15	0.22	0.70	0.14
17	800.	2.62	0.19	3.79	0.20	1.19	0.12	3.50	0.27	3.96	0.22	0.71	0.13
18	900.	2.54	0.17	3.67	0.18	1.16	0.11	3.39	0.25	3.83	0.21	0.79	0.14
19	1000.	2.49	0.16	3.57	0.16	1.18	0.11	3.34	0.24	3.74	0.21	0.88	0.15
20	1100.	2.48	0.15	3.49	0.15	1.24	0.11	3.31	0.23	3.69	0.20	1.00	0.16
21	1200.	2.47	0.14	3.43	0.14	1.30	0.10	3.31	0.22	3.67	0.19	1.14	0.17
22	1300.	2.49	0.14	3.39	0.13	1.38	0.10	3.34	0.20	3.67	0.17	1.30	0.17
23	1400.	2.51	0.13	3.37	0.12	1.47	0.10	3.38	0.19	3.69	0.16	1.47	0.17
24	1500.	2.56	0.12	3.37	0.12	1.57	0.10	3.45	0.18	3.73	0.15	1.67	0.17
25	1750.	2.70	0.11	3.42	0.10	1.83	0.09	3.63	0.15	3.86	0.13	2.17	0.16
26	2000.	2.86	0.10	3.51	0.10	2.09	0.07	3.82	0.13	4.01	0.12	2.57	0.15
27	2500.	3.15	0.08	3.67	0.09	2.54	0.05	4.10	0.12	4.25	0.10	3.06	0.13
28	3000.	3.38	0.07	3.82	0.09	2.89	0.04	4.28	0.11	4.40	0.10	3.35	0.13
29*	3500.	3.63	0.07	4.03	0.09	3.20	0.03	4.45	0.12	4.56	0.12	3.57	0.13
30	4000.	3.85	0.07	4.27	0.10	3.46	0.04	4.57	0.12	4.64	0.12	3.78	0.28
31*	4500.	4.01	0.09	4.59	0.07	3.63	0.05	4.75	0.15	4.77	0.15	4.12	0.53
32	5000.	4.01	0.11	4.64	0.09	3.74	0.07	4.70	0.20	4.70	0.21	4.40	0.30
33*	5500.	3.80	0.14	4.37	0.42	3.71	0.11	4.55	0.03	4.55	0.03		

Sydney Levitus

*These are not standard NODC levels. The data used are interpolations from observed levels.

OXYGEN (%)

TABLE 60a

Table 60a.—Annual mean oxygen-saturation (%) basin means and standard errors for the world ocean and Atlantic Ocean as a function of depth.

Standard Level	Depth	World Ocean		Southern Hemisphere Ocean		Northern Hemisphere Ocean		Atlantic Ocean		South Atlantic Ocean		North Atlantic Ocean	
		Mean	Standard Error	Mean	Standard Error	Mean	Standard Error	Mean	Standard Error	Mean	Standard Error	Mean	Standard Error
1	0.	101.	0.2	101.	0.3	101.	0.3	101.	0.4	102.	0.8	101.	0.4
2	10.	101.	0.2	101.	0.3	101.	0.3	101.	0.4	101.	0.8	101.	0.5
3	20.	101.	0.3	101.	0.3	101.	0.4	101.	0.5	101.	0.9	101.	0.6
4	30.	100.	0.4	100.	0.5	99.	0.6	99.	0.8	100.	1.3	99.	0.9
5	50.	97.	0.7	98.	0.8	96.	1.3	96.	1.4	97.	2.3	96.	1.7
6	75.	92.	1.2	94.	1.3	88.	2.0	91.	1.9	92.	3.1	91.	2.4
7	100.	85.	1.5	89.	1.6	80.	2.7	87.	2.3	87.	3.7	86.	2.8
8	125.	80.	1.7	84.	1.9	73.	3.0	83.	2.4	83.	3.9	82.	3.0
9	150.	75.	1.8	80.	2.0	68.	3.2	80.	2.6	79.	4.1	80.	3.2
10	200.	68.	2.0	74.	2.2	60.	3.4	75.	2.8	73.	4.3	76.	3.5
11	250.	64.	2.0	70.	2.3	55.	3.5	71.	2.9	69.	4.4	73.	3.8
12	300.	60.	2.1	67.	2.4	51.	3.5	69.	3.1	66.	4.5	71.	4.0
13	400.	56.	2.1	63.	2.3	45.	3.4	65.	3.1	62.	4.3	68.	4.2
14	500.	52.	2.0	61.	2.2	39.	3.3	63.	2.8	60.	3.7	65.	4.1
15	600.	50.	2.0	60.	2.1	35.	3.1	61.	2.5	60.	3.1	63.	3.9
16	700.	48.	1.9	58.	1.9	33.	3.0	61.	2.3	60.	2.7	61.	3.7
17	800.	46.	1.8	56.	1.8	31.	3.0	60.	2.1	60.	2.3	61.	3.6
18	900.	45.	1.8	54.	1.6	31.	3.0	61.	1.9	59.	1.9	62.	3.3
19	1000.	44.	1.7	52.	1.4	32.	3.1	61.	1.7	59.	1.5	64.	3.0
20	1100.	44.	1.6	51.	1.3	34.	3.2	63.	1.6	59.	1.1	67.	2.7
21	1200.	44.	1.6	50.	1.2	35.	3.2	64.	1.5	59.	0.8	69.	2.4
22	1300.	44.	1.6	50.	1.2	36.	3.3	66.	1.4	60.	0.6	72.	2.1
23	1400.	45.	1.5	50.	1.2	38.	3.3	67.	1.4	61.	0.8	74.	1.9
24	1500.	46.	1.5	50.	1.1	39.	3.3	68.	1.4	62.	1.0	75.	1.7
25	1750.	47.	1.5	51.	1.1	42.	3.2	71.	1.3	65.	1.1	77.	1.4
26	2000.	49.	1.4	52.	1.1	44.	3.0	72.	1.2	66.	1.2	78.	1.2
27	2500.	52.	1.3	54.	1.1	47.	2.7	72.	1.1	68.	1.1	77.	1.0
28	3000.	53.	1.2	56.	1.0	49.	2.4	72.	1.0	68.	1.1	76.	1.2
29*	3500.	55.	1.1	57.	1.0	51.	2.2	70.	1.3	68.	1.1	74.	2.2
30	4000.	56.	1.1	59.	1.0	52.	2.1	70.	1.2	66.	1.0	74.	1.5
31*	4500.	57.	1.2	61.	0.9	53.	2.2	69.	1.3	66.	1.3	73.	1.3
32	5000.	57.	1.5	60.	1.0	54.	2.4	69.	1.8	65.	1.9	73.	1.5
33*	5500.	55.	2.5	59.	1.9	53.	3.0	68.	2.5	65.	2.8	69.	2.8

*These are not standard NODC levels. The data used are interpolations from observed levels.

Table 60b.—Annual mean oxygen-saturation (%) basin means and standard errors for the Pacific Ocean and Indian Ocean as a function of depth.

Standard Level	Depth	Pacific Ocean		South Pacific Ocean		North Pacific Ocean		Indian Ocean		South Indian Ocean		North Indian Ocean	
		Mean	Standard Error	Mean	Standard Error	Mean	Standard Error	Mean	Standard Error	Mean	Standard Error	Mean	Standard Error
1	0.	101.	0.3	101.	0.3	101.	0.4	101.	0.3	101.	0.3	101.	0.9
2	10.	101.	0.3	101.	0.3	101.	0.4	101.	0.3	101.	0.3	100.	0.8
3	20.	101.	0.3	100.	0.5	101.	0.5	101.	0.3	101.	0.3	100.	1.4
4	30.	100.	0.5	100.	0.7	100.	0.8	100.	0.6	100.	0.4	97.	2.6
5	50.	97.	1.1	98.	1.3	96.	1.8	98.	1.1	99.	0.6	89.	4.6
6	75.	92.	1.7	94.	2.0	89.	3.0	91.	2.2	95.	1.6	70.	6.0
7	100.	86.	2.2	90.	2.5	81.	3.7	82.	3.4	89.	2.6	47.	7.0
8	125.	80.	2.5	85.	2.8	73.	4.1	75.	4.2	83.	3.2	30.	6.7
9	150.	74.	2.7	80.	3.1	66.	4.3	71.	4.6	80.	3.5	22.	6.2
10	200.	65.	2.9	72.	3.5	56.	4.4	67.	4.6	76.	3.5	18.	5.6
11	250.	58.	3.0	67.	3.7	49.	4.4	66.	4.4	74.	3.4	17.	5.6
12	300.	54.	3.0	62.	3.8	43.	4.3	65.	4.4	73.	3.4	17.	5.4
13	400.	47.	2.9	57.	3.8	35.	3.9	63.	4.3	71.	3.3	16.	4.7
14	500.	44.	2.8	57.	3.5	27.	3.2	60.	4.3	68.	3.4	13.	3.7
15	600.	41.	2.8	57.	3.3	22.	2.5	56.	4.3	64.	3.5	11.	2.9
16	700.	39.	2.7	55.	3.1	19.	1.8	53.	4.0	60.	3.4	11.	2.3
17	800.	37.	2.5	53.	2.8	17.	1.5	50.	3.8	56.	3.2	11.	2.1
18	900.	35.	2.4	51.	2.5	16.	1.4	47.	3.6	53.	3.0	12.	2.2
19	1000.	34.	2.2	49.	2.2	16.	1.4	46.	3.2	51.	2.8	13.	2.3
20	1100.	34.	2.0	47.	1.9	17.	1.4	45.	3.0	50.	2.5	15.	2.4
21	1200.	33.	1.9	46.	1.8	18.	1.3	45.	2.8	49.	2.4	16.	2.5
22	1300.	33.	1.8	45.	1.6	19.	1.3	45.	2.6	49.	2.2	19.	2.5
23	1400.	34.	1.7	45.	1.5	20.	1.3	45.	2.4	49.	2.0	21.	2.3
24	1500.	34.	1.6	45.	1.4	21.	1.2	46.	2.2	49.	1.9	24.	2.3
25	1750.	35.	1.4	45.	1.3	24.	1.1	48.	1.8	51.	1.6	30.	2.1
26	2000.	37.	1.2	45.	1.2	27.	0.9	50.	1.6	52.	1.4	35.	1.9
27	2500.	41.	1.0	47.	1.1	33.	0.6	53.	1.4	55.	1.3	40.	1.7
28	3000.	44.	0.9	49.	1.0	37.	0.4	55.	1.3	56.	1.2	44.	1.7
29*	3500.	47.	0.8	51.	1.1	41.	0.4	56.	1.3	58.	1.3	46.	1.7
30	4000.	49.	0.9	54.	1.2	45.	0.4	58.	1.3	59.	1.3	49.	3.0
31*	4500.	51.	1.0	58.	0.7	47.	0.6	59.	1.5	59.	1.6	53.	1.4
32	5000.	52.	1.2	59.	0.9	48.	0.8	58.	1.0	58.	1.0	56.	4.0
33*	5500.	51.	1.6	59.	2.2	49.	1.1	58.	0.4	58.	0.4	—	—

*These are not standard NODC levels. The data used are interpolations from observed levels.

Table 61.—Area, volume, per cent volume contribution of each standard level to total basin volume, and the number of points (N_I) used in the standard error computation for the world ocean as a function of depth.

Standard Level	Depth (m)	World Ocean				Southern Hemisphere Ocean				Northern Hemisphere Ocean			
		Area (10^4 km^2)	Volume (10^4 km^3)	% Volume	N_I	Area (10^4 km^2)	Volume (10^4 km^3)	% Volume	N_I	Area (10^4 km^2)	Volume (10^4 km^3)	% Volume	N_I
1	0.	35013.	175.065	0.14	187.5	20176.	100.878	0.13	108.0	14837.	74.187	0.14	79.5
2	10.	34934.	349.343	0.27	187.1	20149.	201.486	0.26	107.9	14786.	147.858	0.28	79.2
3	20.	34854.	348.543	0.27	186.6	20121.	201.214	0.26	107.7	14733.	147.330	0.28	78.9
4	30.	34765.	521.474	0.40	186.2	20102.	301.527	0.39	107.6	14663.	219.946	0.42	78.5
5	50.	34354.	772.959	0.60	184.0	19967.	449.268	0.58	106.9	14386.	323.691	0.62	77.0
6	75.	34162.	854.059	0.66	182.9	19928.	498.200	0.65	106.7	14234.	355.859	0.68	76.2
7	100.	33735.	843.378	0.65	180.6	19799.	494.978	0.64	106.0	13936	348.400	0.67	74.6
8	125.	33665.	841.618	0.65	180.3	19790.	494.743	0.64	106.0	13875.	346.874	0.67	74.3
9	150.	33496.	1256.081	0.97	179.4	19757.	740.891	0.96	105.8	13738.	515.190	0.99	73.6
10	200.	33182.	1659.075	1.28	177.7	19690.	984.510	1.28	105.4	13491.	674.565	1.30	72.2
11	250.	33104.	1655.194	1.28	177.3	19677.	983.849	1.28	105.4	13427.	671.345	1.29	71.9
12	300.	32879.	2465.921	1.91	176.1	19612.	1470.894	1.91	105.0	13267.	995.027	1.91	71.0
13	400.	32692.	3269.179	2.53	175.1	19545.	1954.508	2.53	104.7	13147.	1314.671	2.52	70.4
14	500.	32418.	3241.796	2.51	173.6	19409.	1940.871	2.52	103.9	13009.	1300.925	2.50	69.7
15	600.	32267.	3226.672	2.50	172.8	19346.	1934.640	2.51	103.6	12920.	1292.032	2.48	69.2
16	700.	32114.	3211.354	2.49	172.0	19287.	1928.708	2.50	103.3	12826.	1282.646	2.46	68.7
17	800.	31910.	3191.035	2.47	170.9	19197.	1919.680	2.49	102.8	12714.	1271.355	2.44	68.1
18	900.	31803.	3180.335	2.46	170.3	19143.	1914.267	2.48	102.5	12661.	1266.067	2.43	67.8
19	1000.	31494.	3149.393	2.44	168.6	19008.	1900.754	2.46	101.8	12486.	1248.638	2.40	66.9
20	1100.	31390.	3139.006	2.43	168.1	18966.	1896.563	2.46	101.6	12424.	1242.442	2.39	66.5
21	1200.	31203.	3120.323	2.41	167.1	18882.	1888.157	2.45	101.1	12322.	1232.166	2.37	66.0
22	1300.	31067.	3106.675	2.40	166.4	18824.	1882.374	2.44	100.8	12243.	1224.301	2.35	65.6
23	1400.	30981.	3098.105	2.40	165.9	18778.	1877.824	2.43	100.6	12203.	1220.281	2.34	65.3
24	1500.	30721.	5376.156	4.16	164.5	18644.	3262.778	4.23	99.8	12076.	2113.381	4.06	64.7
25	1750.	30438.	7609.547	5.89	163.0	18498.	4624.383	5.99	99.1	11941.	2985.166	5.73	63.9
26	2000.	29694.	11135.242	8.62	159.0	18142.	6803.121	8.82	97.1	11552.	4332.121	8.32	61.9
27	2500.	28546.	14273.078	11.05	152.9	17547.	8773.437	11.37	94.0	10999.	5499.637	10.56	58.9
28	3000.	26476.	13238.090	10.24	141.8	16290.	8145.172	10.56	87.2	10186.	5092.918	9.78	54.5
29	3500.	23056.	11527.777	8.92	123.5	14019.	7009.414	9.09	75.1	9037.	4518.363	8.68	48.4
30	4000.	18419.	9209.492	7.13	98.6	10854.	5426.957	7.03	58.1	7565.	3782.533	7.26	40.5
31	4500.	12569.	6284.676	4.86	67.3	6850.	3425.191	4.44	36.7	5719.	2859.488	5.49	30.6
32	5000.	6828.	3414.201	2.64	36.6	3172.	1585.889	2.06	17.0	3657.	1828.311	3.51	19.6
33	5500.	1911.	477.844	0.37	10.2	506.	126.453	0.16	2.7	1406.	351.391	0.67	7.5

* Definition 's given in text.

** Per cent volume at each level is computed as the per cent contribution with respect to total volume of basin.

*** Number of independent data points used in the computation of basin wide standard errors. Definition given in text.

Table 62.—Area, volume, per cent volume contribution of each standard level to total basin volume, and the number of points (N_I) used in the standard error computation for the Atlantic Ocean as a function of depth.

Standard Level	Depth (m)	Atlantic Ocean				South Atlantic Ocean				North Atlantic Ocean			
		Area (10^4 km^2)	Volume* (10^4 km^3)	% Volume**	N_I ***	Area (10^4 km^2)	Volume (10^4 km^3)	% Volume	N_I	Area (10^4 km^2)	Volume (10^4 km^3)	% Volume	N_I
1	0.	10204.	51.021	0.15	54.6	4489.	22.447	0.13	24.0	5715.	28.574	0.18	30.6
2	10.	10172.	101.722	0.30	54.5	4486.	44.865	0.26	24.0	5686.	56.857	0.35	30.4
3	20.	10144.	101.443	0.30	54.3	4486.	44.858	0.26	24.0	5658.	56.584	0.35	30.3
4	30.	10117.	151.757	0.45	54.2	4484.	67.254	0.38	24.0	5633.	84.502	0.52	30.2
5	50.	9925.	223.302	0.66	53.1	4447.	100.052	0.57	23.8	5478.	123.250	0.76	29.3
6	75.	9849.	246.223	0.73	52.7	4443.	111.075	0.63	23.8	5406.	135.148	0.84	28.9
7	100.	9617.	240.434	0.71	51.5	4394.	109.852	0.63	23.5	5223.	130.581	0.81	28.0
8	125.	9562.	239.047	0.71	51.2	4389.	109.722	0.62	23.5	5173.	129.326	0.80	27.7
9	150.	9408.	352.791	1.05	50.4	4361.	163.544	0.93	23.4	5047.	189.246	1.17	27.0
10	200.	9202.	460.093	1.36	49.3	4342.	217.108	1.24	23.3	4860.	242.985	1.50	26.0
11	250.	9141.	457.031	1.35	48.9	4335.	216.736	1.23	23.2	4806.	240.295	1.49	25.7
12	300.	9008.	675.563	2.00	48.2	4319.	323.942	1.84	23.1	4688.	351.621	2.17	25.1
13	400.	8890.	889.038	2.63	47.6	4293.	429.338	2.44	23.0	4597.	459.701	2.84	24.6
14	500.	8798.	879.804	2.61	47.1	4266.	426.593	2.43	22.8	4532.	453.211	2.80	24.3
15	600.	8720.	872.005	2.58	46.7	4253.	425.341	2.42	22.8	4467.	446.664	2.76	23.9
16	700.	8650.	865.050	2.56	46.3	4240.	424.042	2.41	22.7	4410.	441.008	2.73	23.6
17	800.	8559.	855.879	2.54	45.8	4213.	421.317	2.40	22.6	4346.	434.562	2.69	23.3
18	900.	8517.	851.665	2.52	45.6	4206.	420.663	2.39	22.5	4310.	431.031	2.66	23.1
19	1000.	8409.	840.889	2.49	45.0	4193.	419.292	2.39	22.5	4216.	421.597	2.61	22.6
20	1100.	8372.	837.185	2.48	44.8	4184.	418.364	2.38	22.4	4188.	418.821	2.59	22.4
21	1200.	8291.	829.083	2.46	44.4	4160.	416.032	2.37	22.3	4131.	413.051	2.55	22.1
22	1300.	8233.	823.317	2.44	44.1	4151.	415.135	2.36	22.2	4082.	408.181	2.52	21.9
23	1400.	8203.	820.337	2.43	43.9	4148.	414.772	2.36	22.2	4056.	405.565	2.51	21.7
24	1500.	8123.	1421.582	4.21	43.5	4131.	722.918	4.11	22.1	3992.	698.664	4.32	21.4
25	1750.	8019.	2004.722	5.94	42.9	4109.	1027.307	5.85	22.0	3910.	977.415	6.04	20.9
26	2000.	7764.	2911.646	8.63	41.6	4064.	1523.981	8.67	21.8	3700.	1387.665	8.58	19.8
27	2500.	7348.	3673.845	10.89	39.3	3961.	1980.657	11.27	21.2	3386.	1693.188	10.47	18.1
28	3000.	6693.	3346.599	9.92	35.8	3707.	1853.379	10.55	19.8	2986.	1493.220	9.23	16.0
29	3500.	5793.	2896.726	8.58	31.0	3263.	1631.725	9.29	17.5	2530.	1265.001	7.82	13.5
30	4000.	4592.	2296.243	6.80	24.6	2627.	1313.680	7.48	14.1	1965.	982.563	6.07	10.5
31	4500.	3182.	1591.039	4.71	17.0	1787.	893.708	5.09	9.6	1395.	697.331	4.31	7.5
32	5000.	1688.	844.231	2.50	9.0	877.	438.380	2.50	4.7	812.	405.851	2.51	4.3
33	5500.	386.	96.411	0.29	2.1	84.	21.086	0.12	0.5	301.	75.325	0.47	1.6

*Definition is given in text.

**Per cent volume at each level is computed as the per cent contribution with respect to total volume of basin.

***Number of independent data points used in the computation of basin wide standard errors. Definition given in text.

Table 63.—Area, volume, per cent volume contribution of each standard level to total basin volume, and the number of points (N_I) used in the standard error computation for the Pacific Ocean as a function of depth.

Standard Level	Depth (m)	Pacific Ocean				South Pacific Ocean				North Pacific Ocean			
		Area (10^4 km^2)	Volume* (10^4 km^3)	% Volume**	N_I ***	Area (10^4 km^2)	Volume (10^4 km^3)	% Volume	N_I	Area (10^4 km^2)	Volume (10^4 km^3)	% Volume	N_I
1	0.	17403.	87.016	0.13	93.2	9467.	47.337	0.13	50.7	7936.	39.679	0.12	42.5
2	10.	17360.	173.603	0.26	93.0	9445.	94.450	0.27	50.6	7915.	79.153	0.24	42.4
3	20.	17320.	173.201	0.25	92.7	9424.	94.242	0.27	50.5	7896.	78.958	0.24	42.3
4	30.	17262.	258.923	0.38	92.4	9407.	141.110	0.40	50.4	7854.	117.813	0.36	42.1
5	50.	17114.	385.071	0.57	91.6	9346.	210.285	0.59	50.0	7768.	174.786	0.54	41.6
6	75.	17006.	425.162	0.62	91.1	9315.	232.887	0.66	49.9	7691.	192.275	0.59	41.2
7	100.	16891.	422.265	0.62	90.4	9284.	232.089	0.65	49.7	7607.	190.176	0.58	40.7
8	125.	16878.	421.937	0.62	90.4	9281.	232.032	0.65	49.7	7596.	189.906	0.58	40.7
9	150.	16873.	632.730	0.93	90.4	9280.	347.992	0.98	49.7	7593.	284.739	0.88	40.7
10	200.	16808.	840.382	1.23	90.0	9258.	462.925	1.30	49.6	7549.	377.457	1.16	40.4
11	250.	16793.	839.633	1.23	89.9	9254.	462.707	1.30	49.6	7539.	376.926	1.16	40.4
12	300.	16731.	1254.859	1.84	89.6	9227.	692.025	1.95	49.4	7504.	562.834	1.73	40.2
13	400.	16682.	1668.238	2.45	89.3	9205.	920.460	2.59	49.3	7478.	747.778	2.30	40.0
14	500.	16582.	1658.204	2.44	88.8	9141.	914.092	2.57	48.9	7441.	744.112	2.29	39.8
15	600.	16532.	1653.241	2.43	88.5	9108.	910.772	2.56	48.8	7425.	742.469	2.28	39.8
16	700.	16469.	1646.884	2.42	88.2	9072.	907.238	2.55	48.6	7396.	739.645	2.27	39.6
17	800.	16378.	1637.757	2.41	87.7	9020.	902.025	2.54	48.3	7357.	735.731	2.26	39.4
18	900.	16328.	1632.800	2.40	87.4	8984.	898.376	2.53	48.1	7344.	734.424	2.26	39.3
19	1000.	16199.	1619.888	2.38	86.7	8908.	890.751	2.51	47.7	7291.	729.137	2.24	39.0
20	1100.	16146.	1614.559	2.37	86.5	8885.	888.500	2.50	47.6	7261.	726.059	2.23	38.9
21	1200.	16073.	1607.315	2.36	86.1	8842.	884.235	2.49	47.4	7231.	723.079	2.22	38.7
22	1300.	16015.	1601.498	2.35	85.8	8808.	880.828	2.48	47.2	7207.	720.669	2.22	38.6
23	1400.	15974.	1597.431	2.35	85.5	8781.	878.052	2.47	47.0	7194.	719.378	2.21	38.5
24	1500.	15875.	2778.053	4.08	85.0	8716.	1525.231	4.29	46.7	7159.	1252.822	3.85	38.3
25	1750.	15747.	3936.820	5.79	84.3	8629.	2157.125	6.07	46.2	7119.	1779.694	5.47	38.1
26	2000.	15422.	5783.145	8.50	82.6	8424.	3158.888	8.89	45.1	6998.	2624.256	8.07	37.5
27	2500.	14989.	7494.387	11.01	80.3	8143.	4071.459	11.46	43.6	6846.	3422.928	10.53	36.7
28	3000.	14087.	7043.465	10.35	75.4	7546.	3773.241	10.62	40.4	6540.	3270.226	10.06	35.0
29	3500.	12485.	6242.625	9.17	66.9	6481.	3240.327	9.12	34.7	6005.	3002.300	9.23	32.2
30	4000.	10077.	5038.547	7.40	54.0	4802.	2400.771	6.76	25.7	5276.	2637.778	8.11	28.3
31	4500.	7042.	3520.978	5.17	37.7	2820.	1410.079	3.97	15.1	4222.	2110.898	6.49	22.6
32	5000.	4079.	2039.301	3.00	21.8	1252.	625.885	1.76	6.7	2827.	1413.416	4.35	15.1
33	5500.	1278.	319.550	0.47	6.8	174.	43.483	0.12	0.9	1104.	276.066	0.85	5.9

* Definition is given in text.

** Per cent volume at each level is computed as the per cent contribution with respect to total volume of basin.

*** Number of independent data points used in the computation of basin wide standard errors. Definition given in text.

Table 64.—Area, volume, per cent volume contribution of each standard level to total basin volume, and the number of points (N_I) used in the standard error computation for the Indian Ocean as a function of depth.

Standard Level	Depth (m)	Indian Ocean				South Indian Ocean				North Indian Ocean			
		Area (10^4 km^2)	Volume* (10^4 km^3)	% Volume**	N_I ***	Area (10^4 km^2)	Volume (10^4 km^3)	% Volume	N_I	Area (10^4 km^2)	Volume (10^4 km^3)	% Volume	N_I
1	0.	7433.	37.166	0.13	39.8	6262.	31.310	0.13	35.5	1171.	5.856	0.17	6.3
2	10.	7429.	74.293	0.27	39.8	6260.	62.603	0.26	33.5	1169.	11.689	0.35	6.3
3	20.	7420.	74.201	0.27	39.7	6253.	62.534	0.26	33.5	1167.	11.668	0.35	6.2
4	30.	7416.	111.246	0.40	39.7	6253.	93.793	0.39	33.5	1164.	17.453	0.52	6.2
5	50.	7350.	165.383	0.60	39.4	6217.	139.877	0.58	33.3	1134.	25.505	0.75	6.1
6	75.	7343.	183.575	0.67	39.3	6212.	155.289	0.64	33.3	1131.	28.285	0.84	6.1
7	100.	7266.	181.646	0.66	38.9	6162.	154.058	0.64	33.0	1104.	27.588	0.82	5.9
8	125.	7264.	181.599	0.66	38.9	6160.	154.011	0.64	33.0	1104.	27.588	0.82	5.9
9	150.	7254.	272.010	0.99	38.8	6157.	230.886	0.96	33.0	1097.	41.124	1.22	5.9
10	200.	7213.	360.651	1.31	38.6	6130.	306.519	1.27	32.8	1083.	54.132	1.60	5.8
11	250.	7212.	360.580	1.31	38.6	6129.	306.448	1.27	32.8	1083.	54.132	1.60	5.8
12	300.	7181.	538.574	1.96	38.5	6107.	457.991	1.90	32.7	1074.	80.583	2.38	5.8
13	400.	7160.	716.003	2.60	38.3	6088.	608.795	2.52	32.6	1072.	107.208	3.17	5.7
14	500.	7075.	707.523	2.57	37.9	6038.	603.789	2.50	32.3	1037.	103.734	3.07	5.6
15	600.	7052.	705.160	2.56	37.8	6021.	602.129	2.49	32.2	1030.	103.031	3.05	5.5
16	700.	7030.	703.035	2.55	37.6	6010.	601.031	2.49	32.2	1020.	102.005	3.02	5.5
17	800.	7010.	701.014	2.55	37.5	5999.	599.940	2.48	32.1	1011.	101.074	2.99	5.4
18	900.	6995.	699.485	2.54	37.5	5989.	598.861	2.48	32.1	1006.	100.624	2.98	5.4
19	1000.	6915.	691.511	2.51	37.0	5938.	593.834	2.46	31.8	977.	97.677	2.89	5.2
20	1100.	6900.	690.038	2.51	37.0	5928.	592.822	2.45	31.7	972.	97.215	2.88	5.2
21	1200.	6865.	686.460	2.49	36.8	5909.	590.892	2.45	31.6	956.	95.569	2.83	5.1
22	1300.	6846.	684.631	2.49	36.7	5894.	589.412	2.44	31.6	952.	95.219	2.82	5.1
23	1400.	6831.	683.108	2.48	36.6	5880.	588.003	2.43	31.5	951.	95.105	2.81	5.1
24	1500.	6748.	1180.953	4.29	36.1	5827.	1019.673	4.22	31.2	922.	161.280	4.77	4.9
25	1750.	6700.	1674.923	6.08	35.9	5789.	1447.157	5.99	31.0	911.	227.766	6.74	4.9
26	2000.	6533.	2449.924	8.90	35.0	5680.	2130.159	8.82	30.4	853.	319.765	9.46	4.6
27	2500.	6234.	3116.854	11.32	33.4	5467.	2733.333	11.31	29.3	767.	383.521	11.35	4.1
28	3000.	5716.	2858.232	10.38	30.6	5058.	2528.758	10.47	27.1	659.	329.474	9.75	3.5
29	3500.	4792.	2396.229	8.70	25.7	4290.	2145.165	8.88	23.0	502.	251.065	7.43	2.7
30	4000.	3760.	1880.104	6.83	20.1	3436.	1717.911	7.11	18.4	324.	162.193	4.80	1.7
31	4500.	2353.	1176.266	4.27	12.6	2250.	1125.008	4.66	12.0	103.	51.259	1.52	0.5
32	5000.	1067.	533.672	1.94	5.7	1049.	524.628	2.17	5.6	18.	9.044.	0.27	0.1
33	5500.	249.	62.185	0.23	1.3	249.	62.185	0.26	1.3	--	--	--	--

* Definition is given in text.

** Per cent volume at each level is computed as the per cent contribution with respect to total volume of basin.

*** Number of independent data points used in the computation of basin wide standard errors. Definition given in text.

Table 65.—Volume means of potential temperature, salinity, potential density, oxygen, and oxygen-saturation for the major ocean basins and the volume of each basin. Values in parentheses are those computed by Montgomery (1958), Cochrane (1958), and Pollack (1958).

	Volume (10^4 km^3)	Potential Temperature ($^{\circ}\text{C}$)	Salinity (‰)	Potential Density (g/cm^3)	Oxygen (ml/l)	Oxygen Saturation (%)
Pacific	68 049	3.49 (3.36)*	34.62 (34.62)	27.45	3.24	44.2
South Pacific	35 531	3.55 (3.36)	34.65 (34.64)	27.47	3.86	52.6
North Pacific	32 517	3.44 (3.38)	34.58 (34.59)	27.43	2.56	35.1
Indian	27 538	3.67 (3.72)	34.75 (34.76)	27.53	4.04	54.7
South Indian	24 158	3.34	34.72	27.55	4.30	58.1
North Indian	3 379	6.03	34.97	27.37	2.20	31.0
Atlantic	33 747	3.85 (3.73)	34.93 (34.90)	27.66	5.10	69.5
South Atlantic	17 569	2.90	34.75	27.64	4.93	65.9
North Atlantic	16 178	4.87	35.12	27.68	5.29	73.4
Globe	129 222	3.62 (3.52)	34.73 (34.72)	27.53	3.90	53.1
Southern Hemisphere	77 143	3.33	34.70	27.54	4.24	57.3
Northern Hemisphere	52 079	4.05	34.77	27.50	3.38	46.7

* Values in parentheses are the volume means computed by Montgomery (1958), Cochrane (1958), and Pollack (1958).

Table A1.—Response function of the test analysis.

WAVELENGTH (KM)	AMPLITUDE (‰)
1650	97
1320	94
1100	88
880	75
660	41
550	19
440	5

Table E1.—Listing of microfiche contents.

Fiche	Total Number of Frames on Fiche	Parameter	Quantity Presented	Location on Fiche
F-01	200	a) In situ temperature based on NODC Station Data, MBT, and XBT file observations	a) Annual mean statistics by 5° squares at all standard levels from the sea-surface through 500 m depth	Frames 1-84
		b) Potential temperature based on NODC Station Data file observations	b) Annual mean statistics by 5° squares at all standard levels from 600 m through 5500 m depth	Frames 85-198
F-02	200	Salinity based on NODC Station Data file observations	Annual mean statistics by 5° squares at all standard levels from the sea-surface through 5500 m depth	Frames 1-198
F-03	200	Dissolved oxygen based on NODC Station Data file observations	Annual mean statistics by 5° squares at all standard levels from the sea-surface through 5500 m depth	Frames 1-198
F-04	200	Dissolved oxygen saturation based on NODC Station Data file observations	Annual mean statistics by 5° squares at all standard levels from the sea-surface through 5500 m depth	Frames 1-198
F-05	200	Potential density based on NODC Station Data file observations	Annual mean statistics by 5° squares at all standard levels from the sea-surface through 5500 m depth	Frames 1-198
F-06	200	Anomaly of specific volume based on NODC Station Data file observations	Annual mean statistics by 5° squares at all standard levels from the sea-surface through 5500 m depth	Frames 1-198
F-07	200	a) In situ temperature based on NODC Station Data, MBT, and XBT file observations	a) Winter (Feb., Mar., Apr.) mean statistics by 5° squares at all standard levels from the sea-surface through 250 m depth	Frames 1-66
		b) In situ temperature based on NODC Station Data, MBT, and XBT file observations	b) Spring (May, Jun., Jul.) mean statistics by 5° squares at all standard levels from the sea-surface through 250 m depth	Frames 68-133
		c) In situ temperature based on NODC Station Data, MBT, and XBT file observations	c) Summer (Aug., Sep., Oct.) mean statistics by 5° squares at all standard levels from the sea-surface through 250 m depth	Frames 135-200

Table E1.—Listing of microfiche contents—Continued

Fiche	Total Number of Frames on Fiche	Parameter	Quantity Presented	Location on Fiche
F-08	200	a) In situ temperature based on NODC Station Data, MBT, and XBT file observations	a) Fall (Nov., Dec., Jan.) mean statistics by 5° squares at all standard levels from the sea-surface through 250 m depth	Frames 1-66
		b) Salinity based on NODC Station Data file observations	b) Winter (Feb., Mar., Apr.) mean statistics by 5° squares at all standard levels from the sea-surface through 250 m depth	Frames 68-133
		c) Salinity based on NODC Station Data file observations	c) Spring (May, Jun., Jul.) mean statistics by 5° squares at all standard levels from the sea-surface through 250 m depth	Frames 135-200
F-09	200	a) Salinity based on NODC Station Data file observations	a) Summer (Aug., Sep., Oct.) mean statistics by 5° squares at all standard levels from the sea-surface through 250 m depth	Frames 1-66
		b) Salinity based on NODC Station Data file observations	b) Fall (Nov., Dec., Jan.) mean statistics by 5° squares at all standard levels from the sea-surface through 250 m depth	Frames 68-133
		c) Dissolved oxygen based on NODC Station Data file observations	c) Winter (Feb., Mar., Apr.) mean statistics by 5° squares at all standard levels from the sea-surface through 250 m depth	Frames 135-200
F-10	200	a) Dissolved oxygen based on NODC Station Data file observations	a) Spring (May, Jun., Jul.) mean statistics by 5° squares at all standard levels from the sea-surface through 250 m depth	Frames 1-66
		b) Dissolved oxygen based on NODC Station Data file observations	b) Summer (Aug., Sep., Oct.) mean statistics by 5° squares at all standard levels from the sea-surface through 250 m depth	Frames 68-133
		c) Dissolved oxygen based on NODC Station Data file observations	c) Fall (Nov., Dec., Jan.) mean statistics by 5° squares at all standard levels from the sea-surface through 250 m depth	Frames 135-200

Table E1.—Listing of microfiche contents—Continued

Fiche	Total Number of Frames on Fiche	Parameter	Quantity Presented	Location on Fiche
F-11	200	a) Dissolved oxygen saturation based on NODC Station Data file observations	a) Winter (Feb., Mar., Apr.) mean statistics by 5° squares at all standard levels from the sea-surface through 250 m depth	Frames 1-66
		b) Dissolved oxygen saturation based on NODC Station Data file observations	b) Spring (May, Jun., Jul.) mean statistics by 5° squares at all standard levels from the sea-surface through 250 m depth	Frames 68-133
		c) Dissolved oxygen saturation based on NODC Station Data file observations	c) Summer (Aug., Sep., Oct.) mean statistics by 5° squares at all standard levels from the sea-surface through 250 m depth	Frames 135-200
F-12		a) Dissolved oxygen saturation based on NODC Station Data file observations	a) Fall (Nov., Dec., Jan.) mean statistics by 5° squares at all standard levels from the sea-surface through 250 m depth	Frames 1-66
		b) Potential density based on NODC Station Data file observations	b) Winter (Feb., Mar., Apr.) mean statistics by 5° squares at all standard levels from the sea-surface through 250 m depth	Frames 68-133
		c) Potential density based on NODC Station Data file observations	c) Spring (May, Jun., Jul.) mean statistics by 5° squares at all standard levels from the sea-surface through 250 m depth	Frames 135-200
F-13	200	a) Potential density based on NODC Station Data file observations	a) Summer (Aug., Sep., Oct.) mean statistics by 5° squares at all standard levels from the sea-surface through 250 m depth	Frames 1-66
		b) Potential density based on NODC Station Data file observations	b) Fall (Nov., Dec., Jan.) mean statistics by 5° squares at all standard levels from the sea-surface through 250 m depth	Frames 68-133
		c) Anomaly of specific volume based on NODC Station Data file observations	c) Winter (Feb., Mar., Apr.) mean statistics by 5° squares at all standard levels from the sea-surface through 250 m depth	Frames 135-200

Table E1.—Listing of microfiche contents—Continued

Fiche	Total Number of Frames on Fiche	Parameter	Quantity Presented	Location on Fiche
F-14	200	a) Anomaly of specific volume based on NODC Station Data file observations	a) Spring (May, Jun., Jul.) mean statistics by 5° squares at all standard levels from the sea-surface through 250 m depth	Frames 1-66
		b) Anomaly of specific volume based on NODC Station Data file observations	b) Summer (Aug., Sep., Oct.) mean statistics by 5° squares at all standard levels from the sea-surface through 250 m depth	Frames 68-133
		c) Anomaly of specific volume based on NODC Station Data file observations	c) Fall (Nov., Dec., Jan.) mean statistics by 5° squares at all standard levels from the sea-surface through 250 m depth	Frames 135-200
F-15	170	a) Potential temperature	a) Annual mean objectively analyzed field on a 1° latitude-longitude grid at all standard levels from the sea-surface through 5500 m depth	Frames 1-33
		b) Salinity	b) Annual mean objectively analyzed field on a 1° latitude-longitude grid at all standard levels from the sea-surface through 5500 m depth	Frames 35-67
		c) Potential density	c) Annual mean objectively analyzed field on a 1° latitude-longitude grid at all standard levels from the sea-surface through 5500 m depth	Frames 69-101
		d) Dissolved oxygen	d) Annual mean objectively analyzed field on a 1° latitude-longitude grid at all standard levels from the sea-surface through 5500 m depth	Frames 103-135
		e) Dissolved oxygen saturation	e) Annual mean objectively analyzed field on a 1° latitude-longitude grid at all standard levels from the sea-surface through 5500 m depth	Frames 137-169

Sydney Levitus

Table E1.—Listing of microfiche contents—Continued

Fiche	Total Number of Frames on Fiche	Parameter	Quantity Presented	Location on Fiche
F-16	170	a) Brunt-Väisälä frequency	a) Annual mean objectively analyzed field on a 1° latitude-longitude grid at all standard levels from the sea-surface through 5000 m depth	Frames 1-32
		b) Potential temperature	b) Winter (Feb., Mar., Apr.) mean objectively analyzed fields on a 1° latitude-longitude grid at all standard levels from the sea-surface through 250 m depth	Frames 35-45
		c) Potential temperature	c) Spring (May, Jun., Jul.) mean objectively analyzed fields on a 1° latitude-longitude grid at all standard levels from the sea-surface through 250 m depth	Frames 52-62
		d) Potential temperature	d) Summer (Aug., Sep., Oct.) mean objectively analyzed fields on a 1° latitude-longitude grid at all standard levels from the sea-surface through 250 m depth	Frames 69-79
		e) Potential temperature	e) Fall (Nov., Dec., Jan.) mean objectively analyzed fields on a 1° latitude-longitude grid at all standard levels from the sea-surface through 250 m depth	Frames 86-96
		f) Salinity	f) Winter (Feb., Mar., Apr.) mean objectively analyzed fields on a 1° latitude-longitude grid at all standard levels from the sea-surface through 250 m depth	Frames 103-113
		g) Salinity	g) Spring (May, Jun., Jul.) mean objectively analyzed fields on a 1° latitude-longitude grid at all standard levels from the sea-surface through 250 m depth	Frames 120-130
		h) Salinity	h) Summer (Aug., Sep., Oct.) mean objectively analyzed fields on a 1° latitude-longitude grid at all standard levels from the sea-surface through 250 m depth	Frames 137-147

Table E1.—Listing of microfiche contents—Continued

Fiche	Total Number of Frames on Fiche	Parameter	Quantity Presented	Location on Fiche
F-16		i) Salinity	i) Fall (Nov., Dec., Jan.) mean objectively analyzed fields on a 1° latitude-longitude grid at all standard levels from the sea-surface through 250 m depth	Frames 154-164
F-17	170	a) Temperature observations based on NODC Station Data, MBT and XBT files	a) Annual distribution of temperature observations on a 1° latitude-longitude grid at all standard levels from the sea-surface through 5500 m depth	Frames 1-33
		b) Salinity observations based on NODC Station Data file	b) Annual distribution of salinity observations on a 1° latitude-longitude grid at all standard levels from the sea-surface through 5500 m depth	Frames 35-67
		c) Oxygen observations based on NODC Station Data file	c) Annual distribution of oxygen observations on a 1° latitude-longitude grid at all standard levels from the sea-surface through 5500 m depth	Frames 69-101
		d) Temperature observations based on NODC Station Data, MBT, and XBT files	d) Seasonal distributions of temperature observations on a 1° latitude-longitude grid at the sea-surface and 250 m depth	Frames 103-110
		e) Salinity observations based on NODC Station Data file	e) Seasonal distribution of salinity observations on a 1° latitude-longitude grid at the sea-surface and 250 m depth	Frames 112-119
		f) Oxygen observations based on NODC Station Data file	f) Seasonal distribution of oxygen observations on a 1° latitude-longitude grid at the sea-surface and 250 m depth	Frames 120-127
		g) Temperature observations based on NODC Station Data, MBT, and XBT files	g) Monthly distribution of temperature observations on a 1° latitude-longitude grid at the sea-surface and 250 m depth	Frames 129-152
		h) Salinity observations based on NODC Station Data file	h) Monthly distribution of observations on a 1° latitude-longitude grid at the sea-surface	Frames 154-165

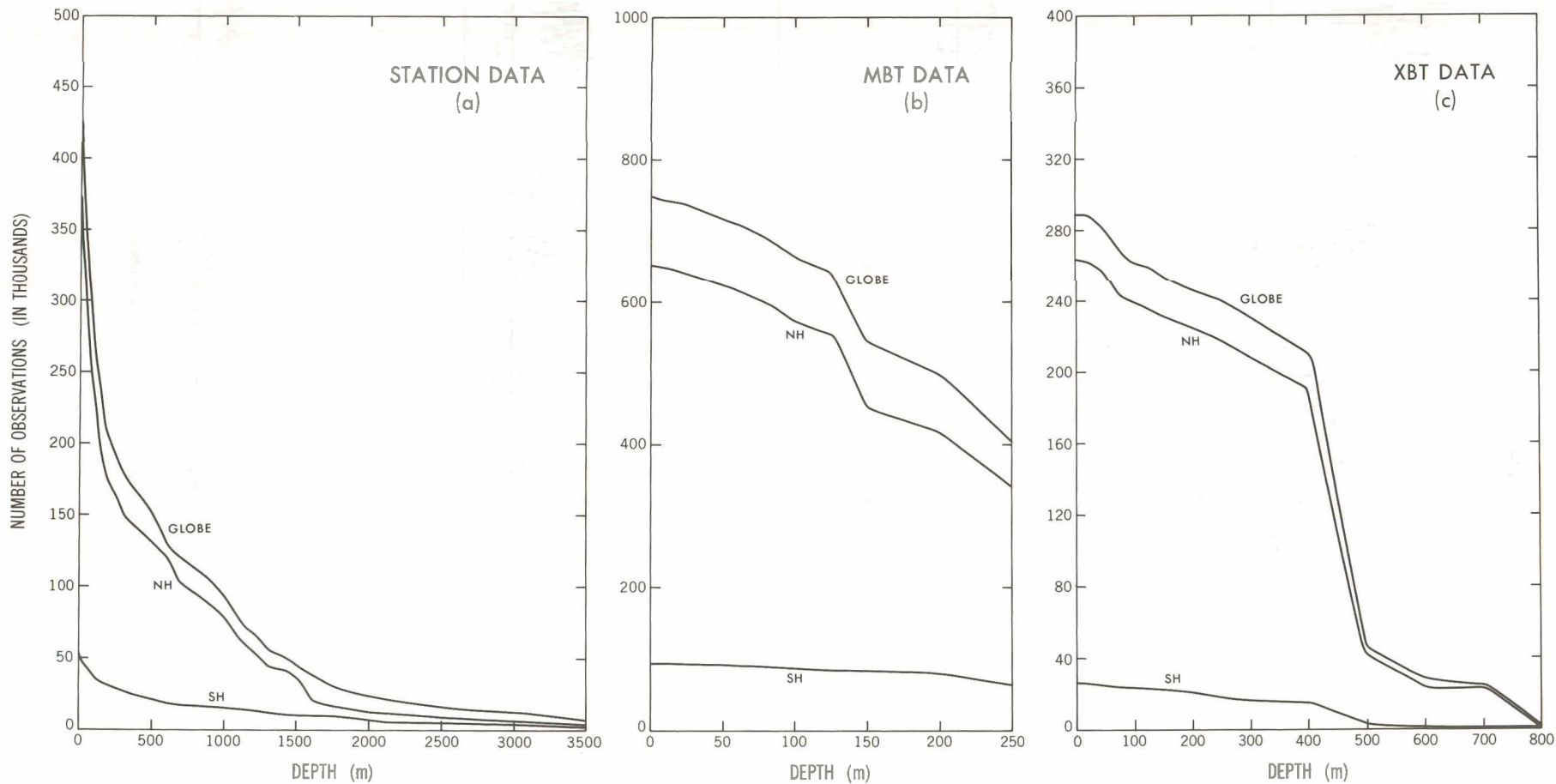


Figure 1.—Distribution of (a) SD temperature observations, (b) MBT observations, and (c) XBT observations as a function of depth for the globe and the Northern and Southern Hemispheres.

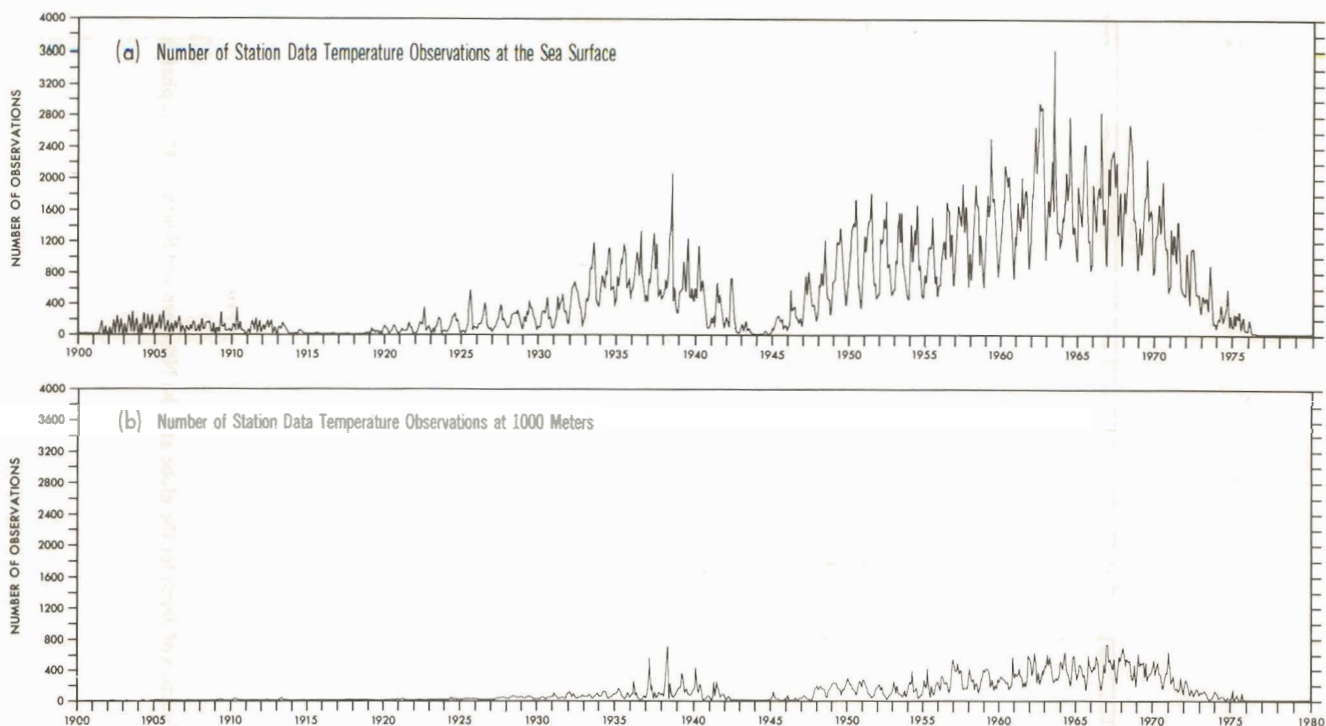


Figure 2.—Time series of Station Data temperature observations.

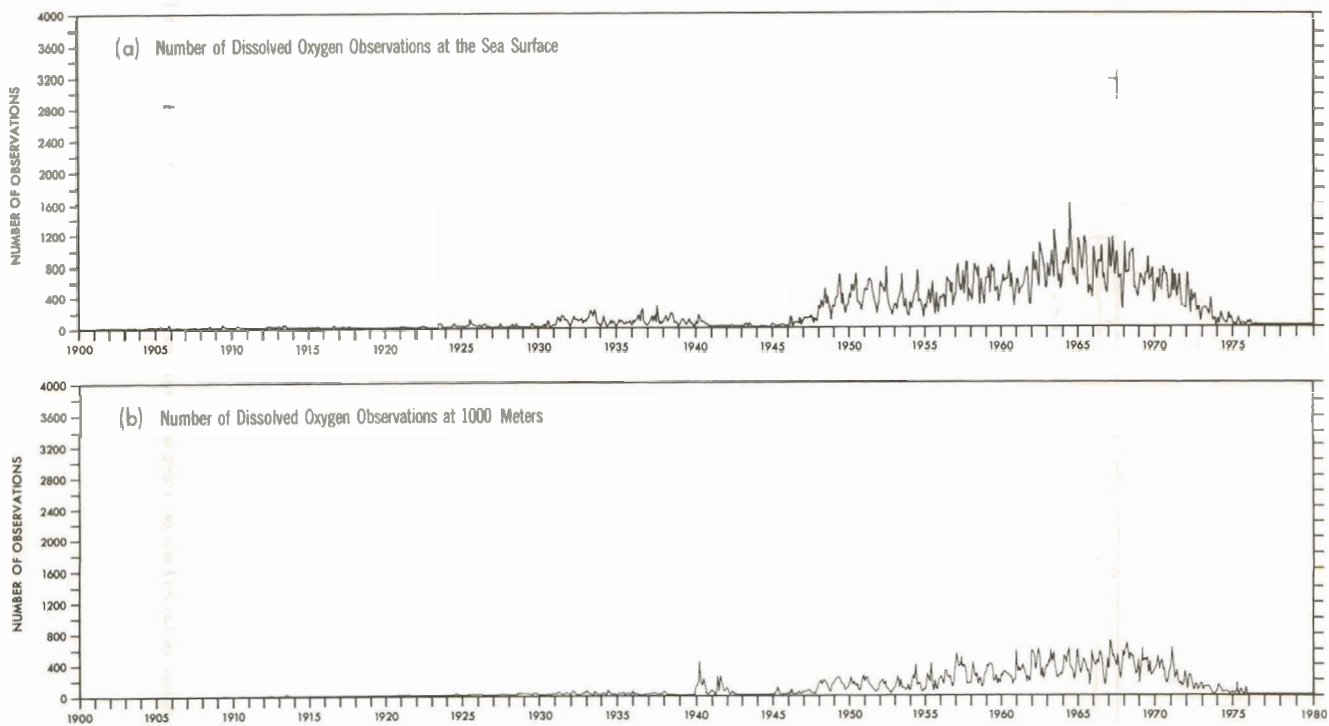


Figure 3.—Time series of Station Data oxygen observations.

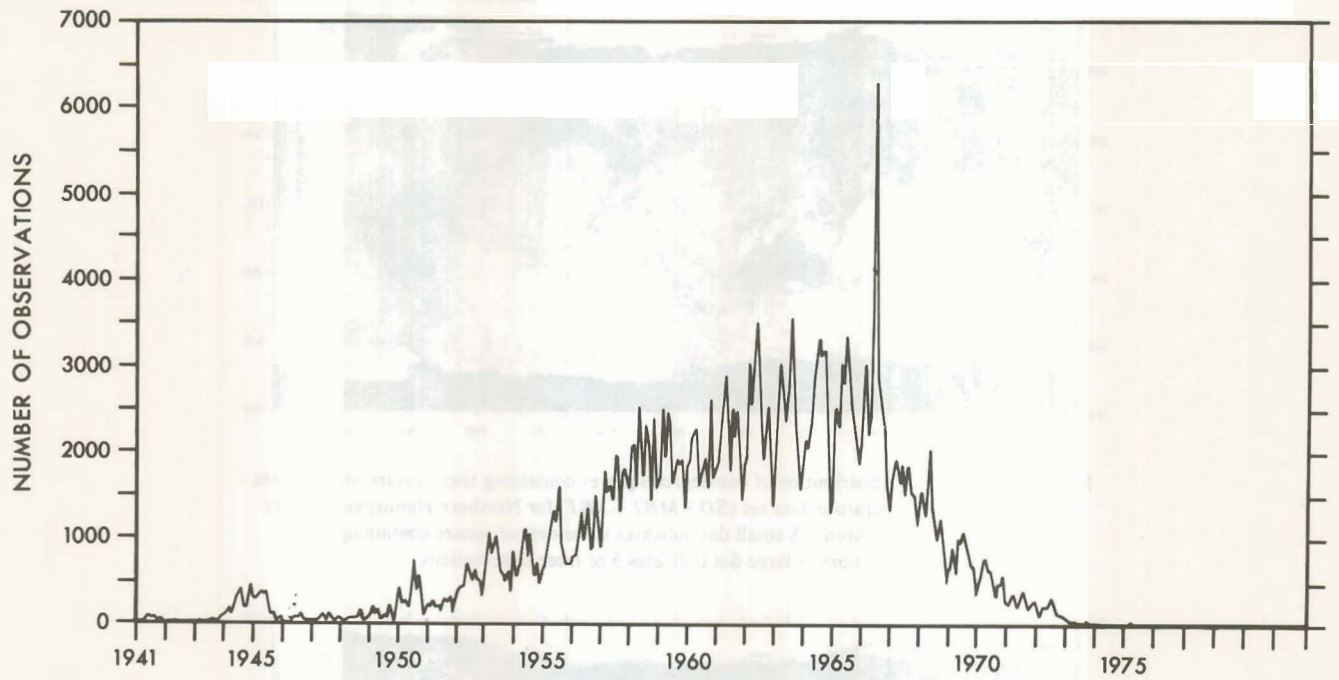


Figure 4.—Time series of MBT casts.

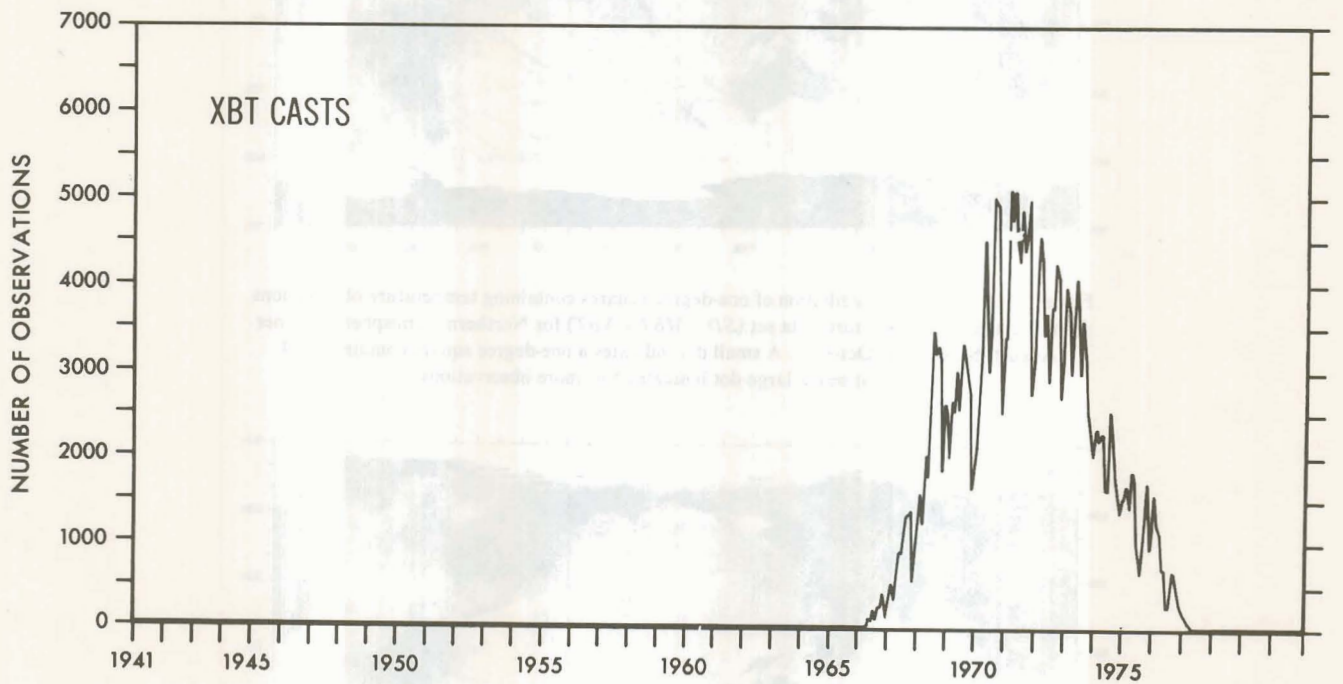


Figure 5.—Time series of XBT casts.

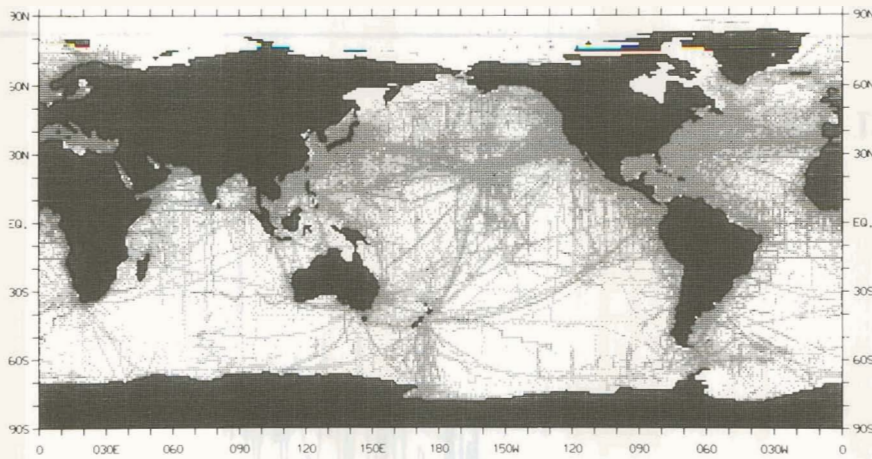


Figure 6.—Sea surface distribution of one-degree squares containing temperature observations from the merged temperature data set ($SD+MBT+XBT$) for Northern Hemisphere winter (February, March, April). A small dot indicates a one-degree square containing 1-4 observations, a large dot indicates 5 or more observations.

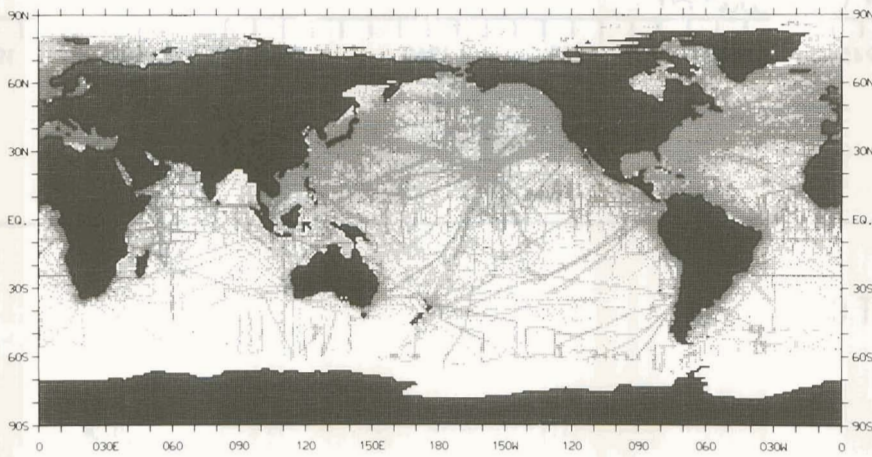


Figure 7.—Sea surface distribution of one-degree squares containing temperature observations from the merged temperature data set ($SD+MBT+XBT$) for Northern Hemisphere summer (August, September, October). A small dot indicates a one-degree square containing 1-4 observations, a large dot indicates 5 or more observations.

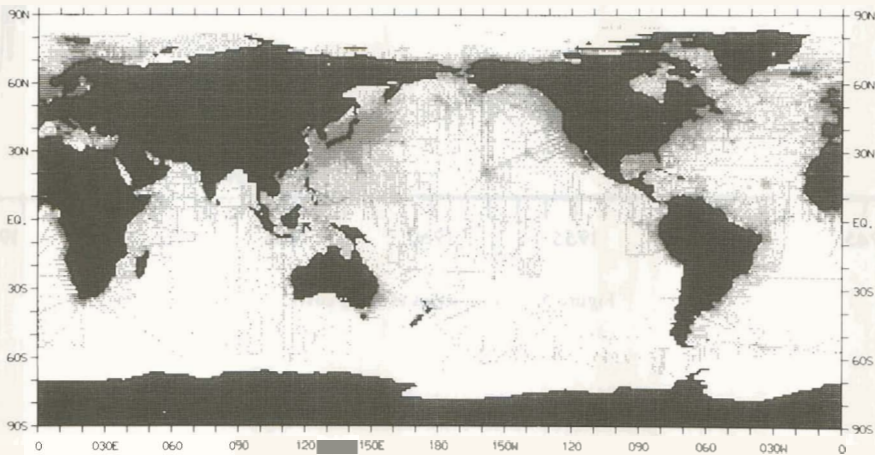


Figure 8.—Sea surface distribution of one-degree squares containing salinity observations for Northern Hemisphere summer (August, September, October). A small dot indicates a one-degree square containing 1-4 observations, a large dot indicates 5 or more observations.

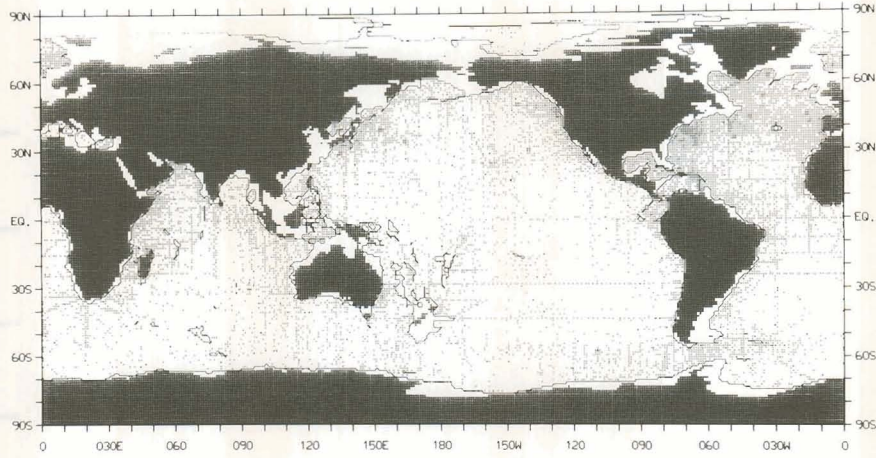


Figure 9.—Distribution of one-degree squares containing salinity observations at a depth of 2000 m for the annual period. A small dot indicates a one-degree square containing 1-9 observations, a large dot indicates 10 or more observations.

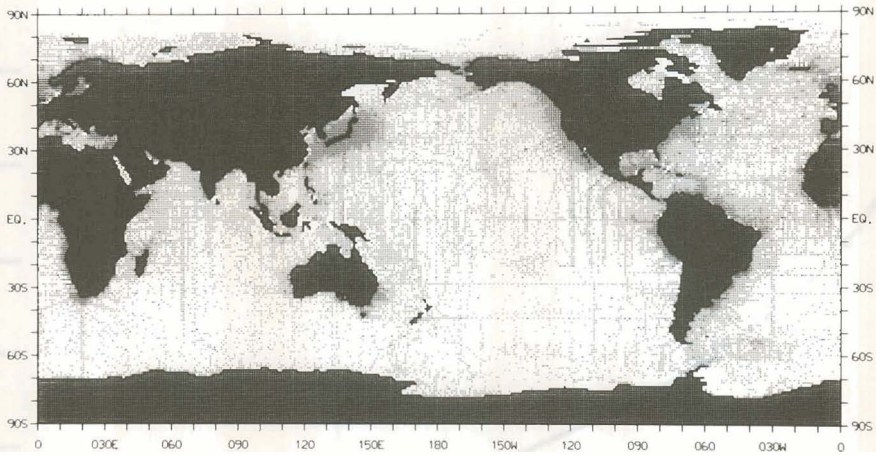
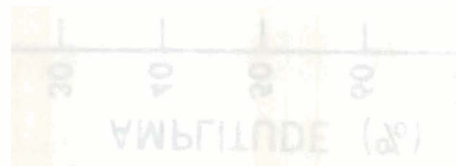


Figure 10.—Sea surface distribution of one-degree squares containing oxygen observations for the annual period. A small dot indicates a square containing 1-9 observations, a large dot indicates 10 or more observations.



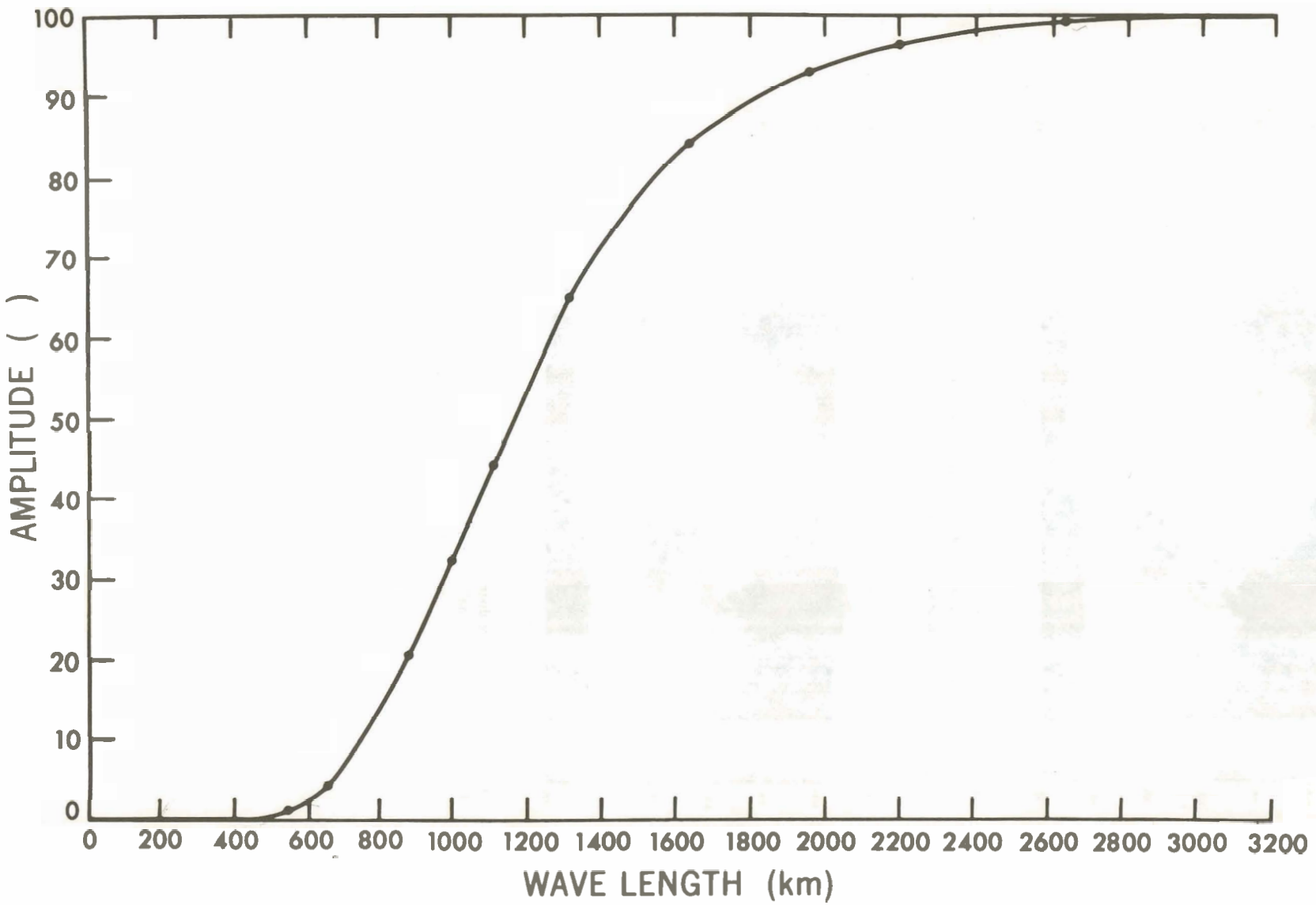


Figure 11.—Response function of the objective analysis.

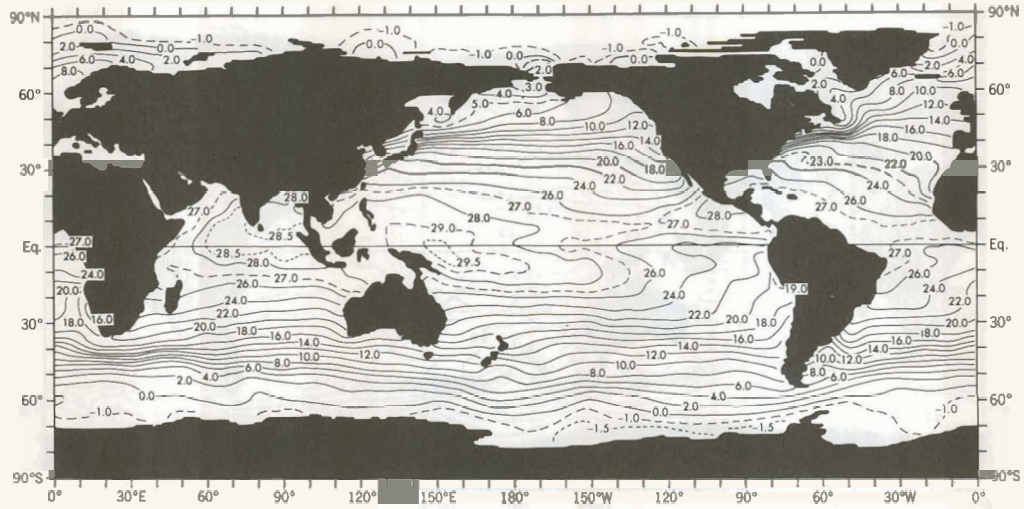


Figure 12.—Annual mean potential temperature (°C) at the sea surface.

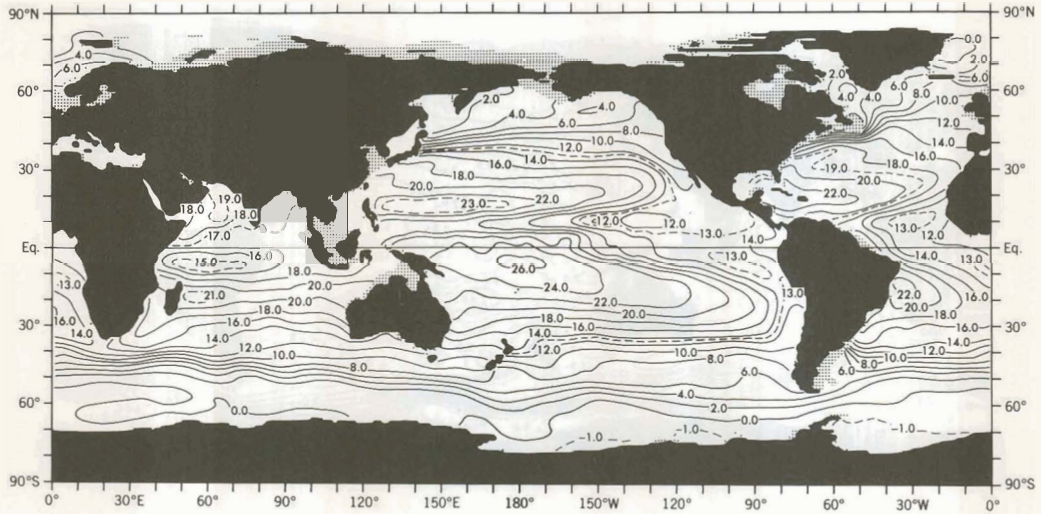


Figure 13.—Annual mean potential temperature (°C) at 150 m depth.

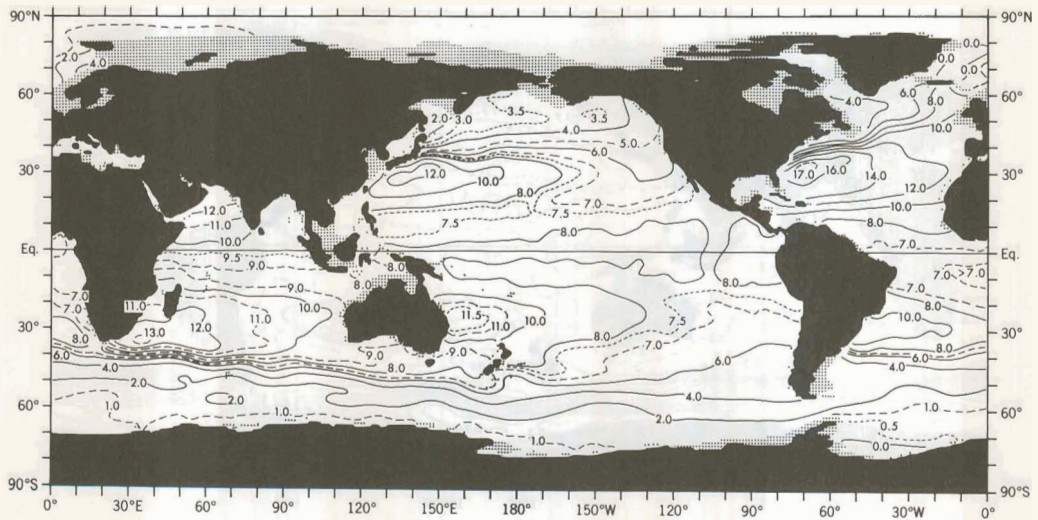


Figure 14.—Annual mean potential temperature (°C) at 500 m depth.

Climatological Atlas of the World Ocean

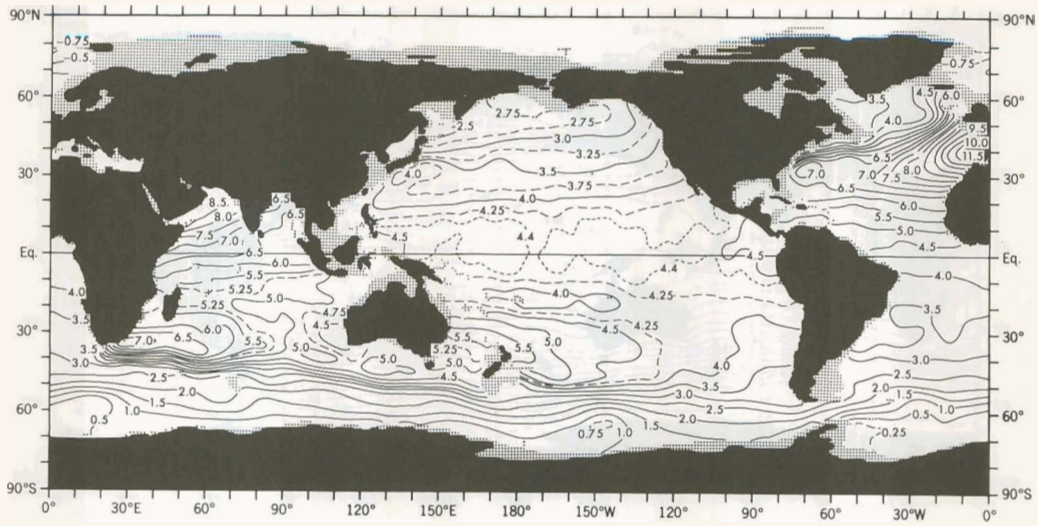


Figure 15.—Annual mean potential temperature ($^{\circ}$ C) at 1000 m depth.

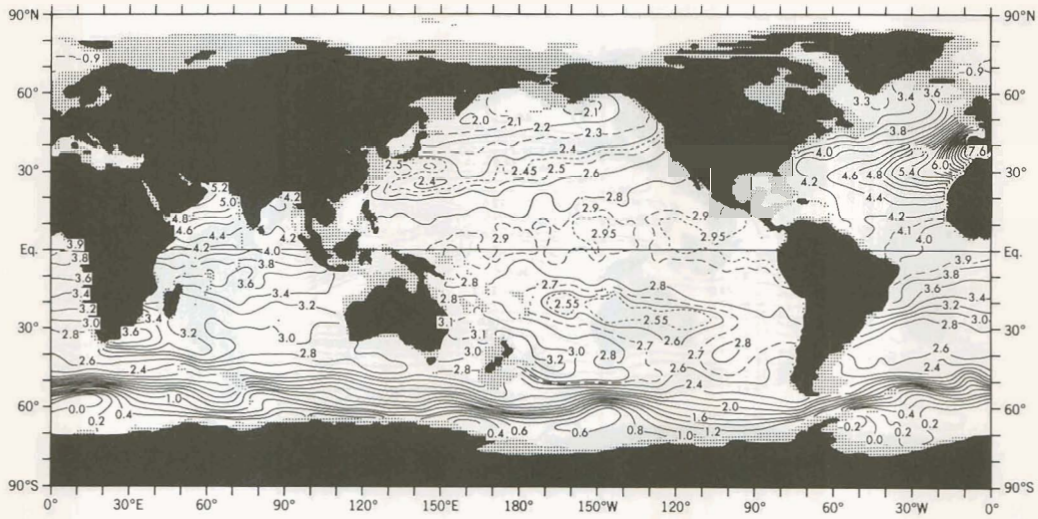


Figure 16.—Annual mean potential temperature ($^{\circ}$ C) at 1500 m depth.

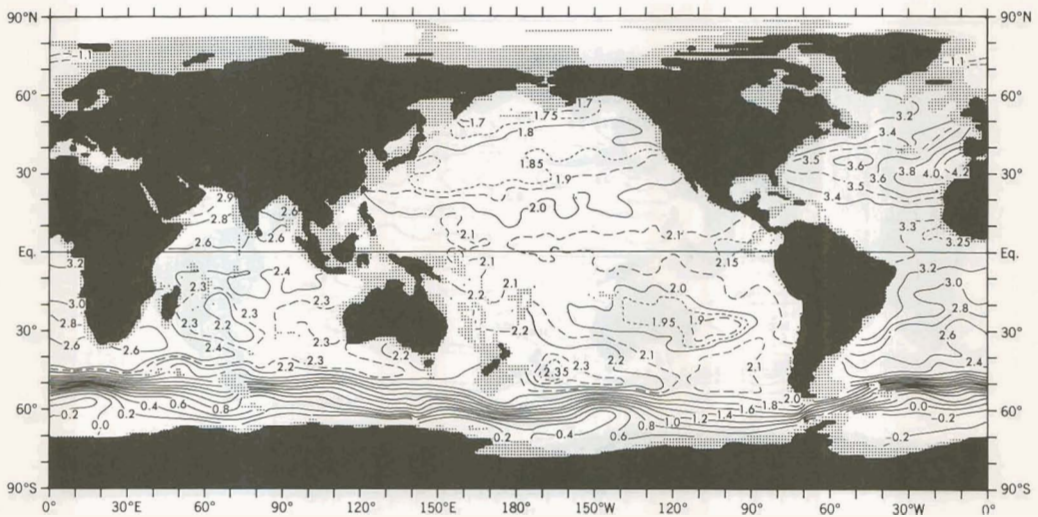


Figure 17.—Annual mean potential temperature ($^{\circ}$ C) at 2000 m depth.

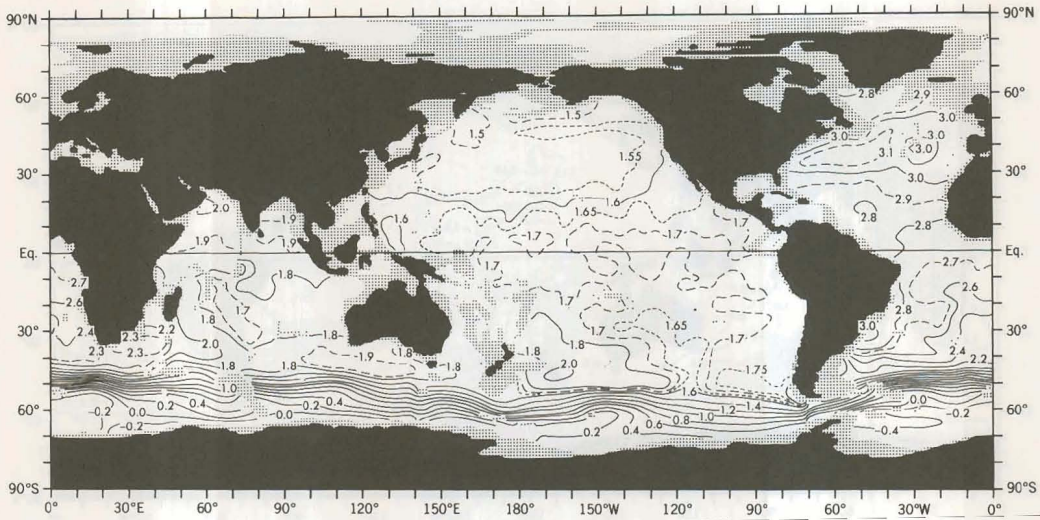


Figure 18.—Annual mean potential temperature ($^{\circ}$ C) at 2500 m depth.

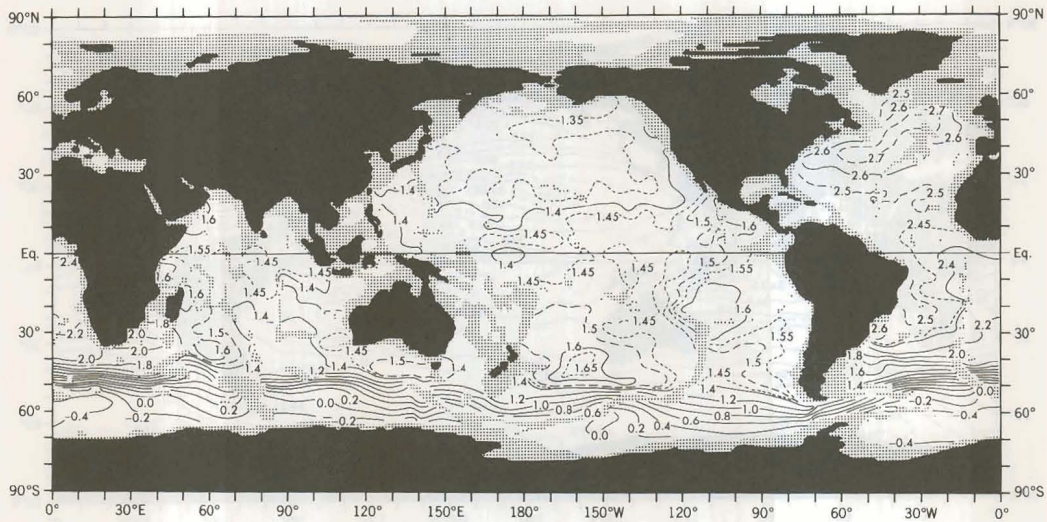


Figure 19.—Annual mean potential temperature ($^{\circ}$ C) at 3000 m depth.

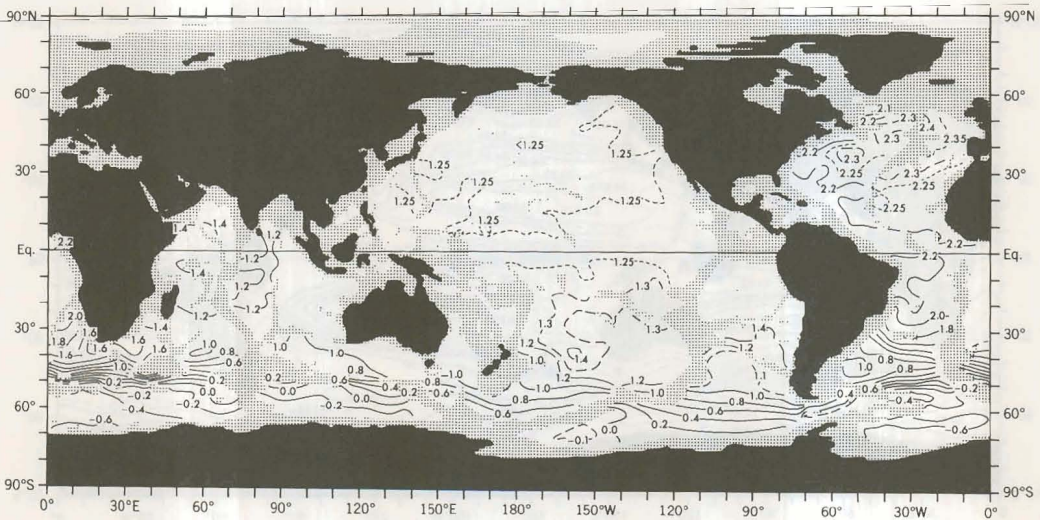


Figure 20.—Annual mean potential temperature ($^{\circ}$ C) at 3500 m depth.

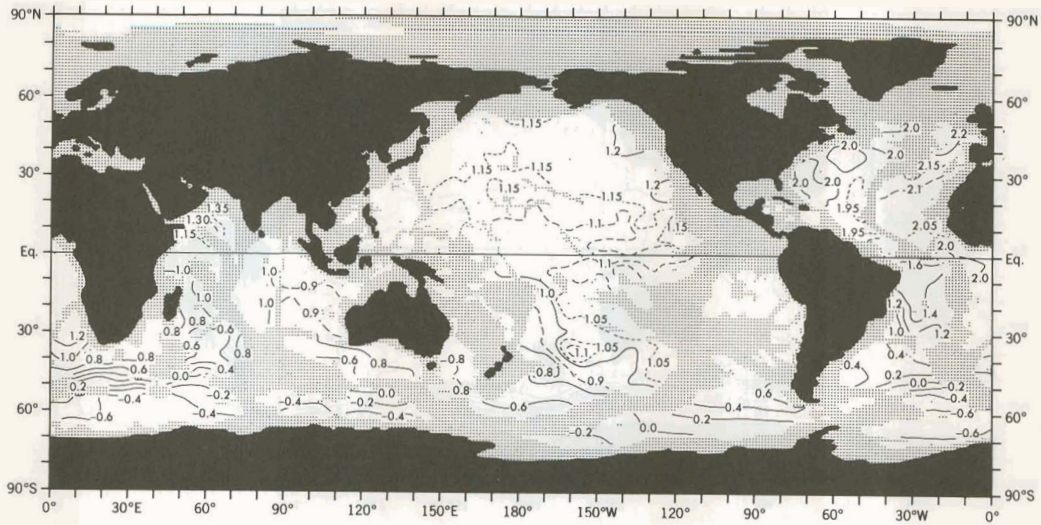


Figure 21.—Annual mean potential temperature ($^{\circ}\text{C}$) at 4000 m depth.

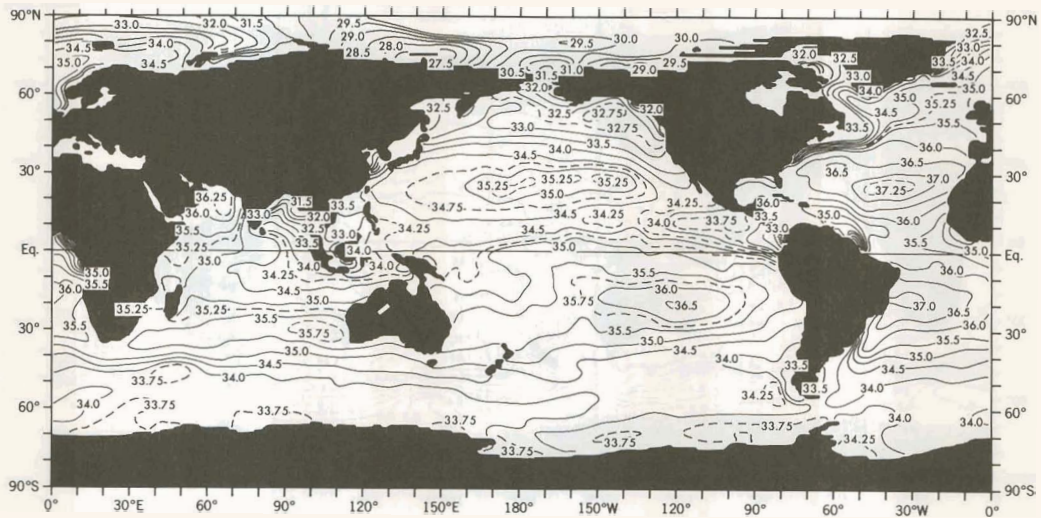


Figure 22.—Annual mean salinity (‰) at the sea surface.

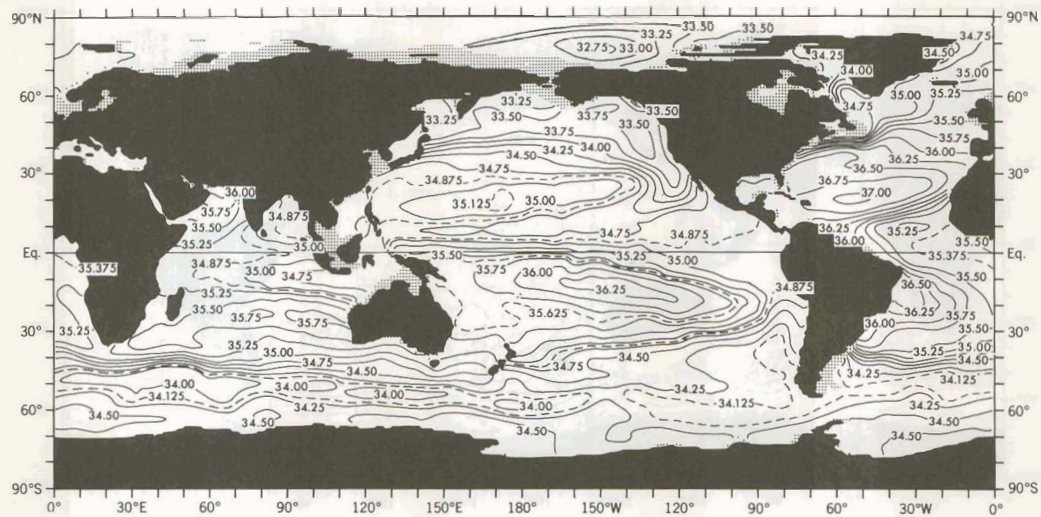


Figure 23.—Annual mean salinity (‰) at 150 m depth.

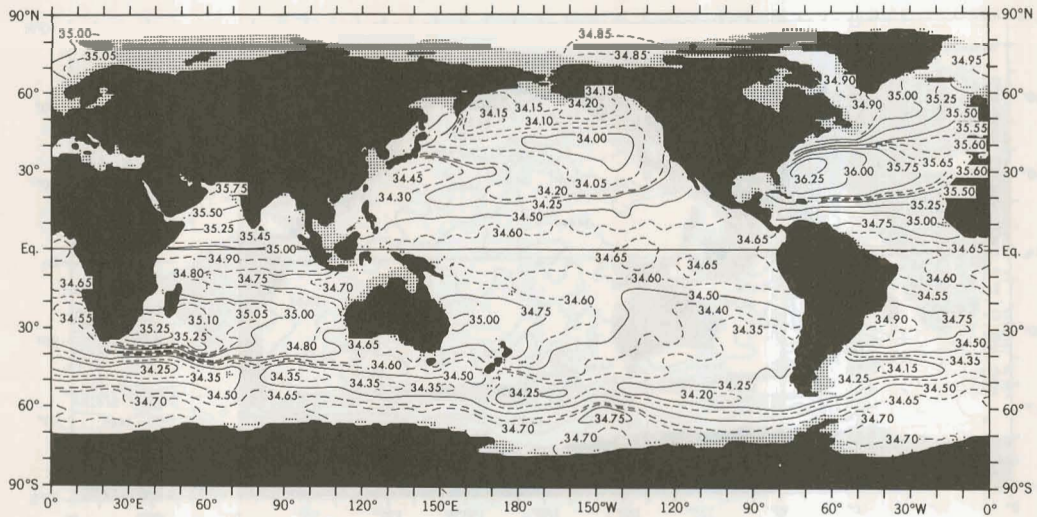


Figure 24.—Annual mean salinity (‰) at 500 m depth.

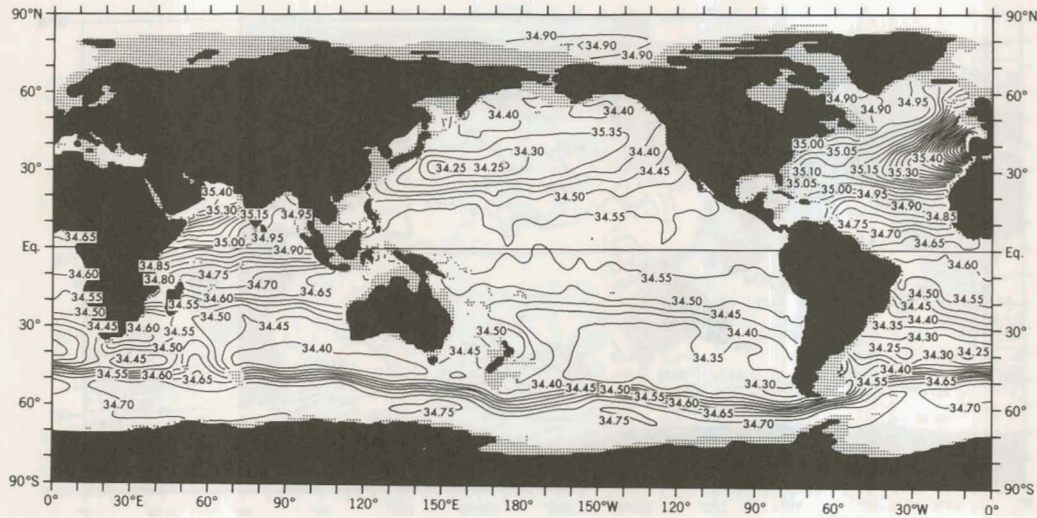


Figure 25.—Annual mean salinity (‰) at 1000 m depth.

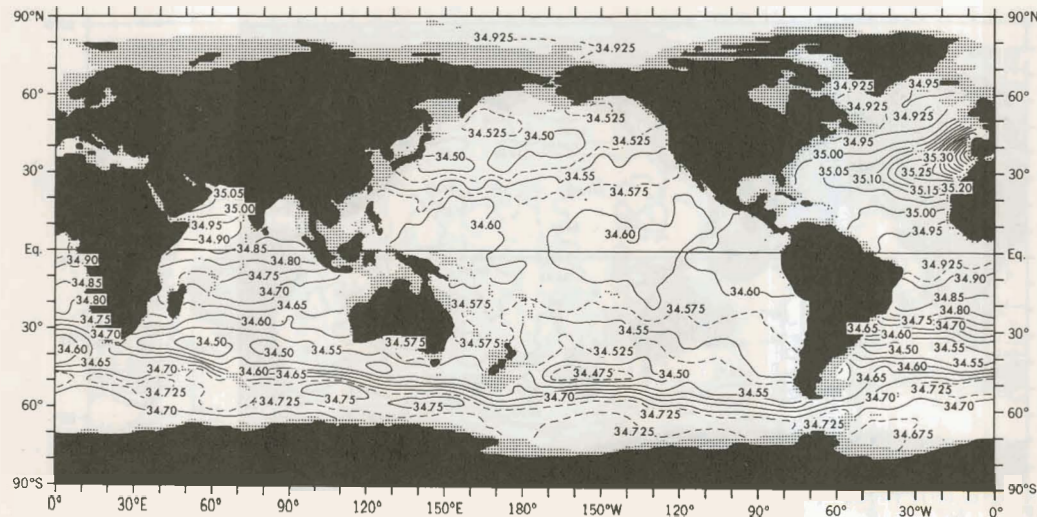


Figure 26.—Annual mean salinity (‰) at 1500 m depth.

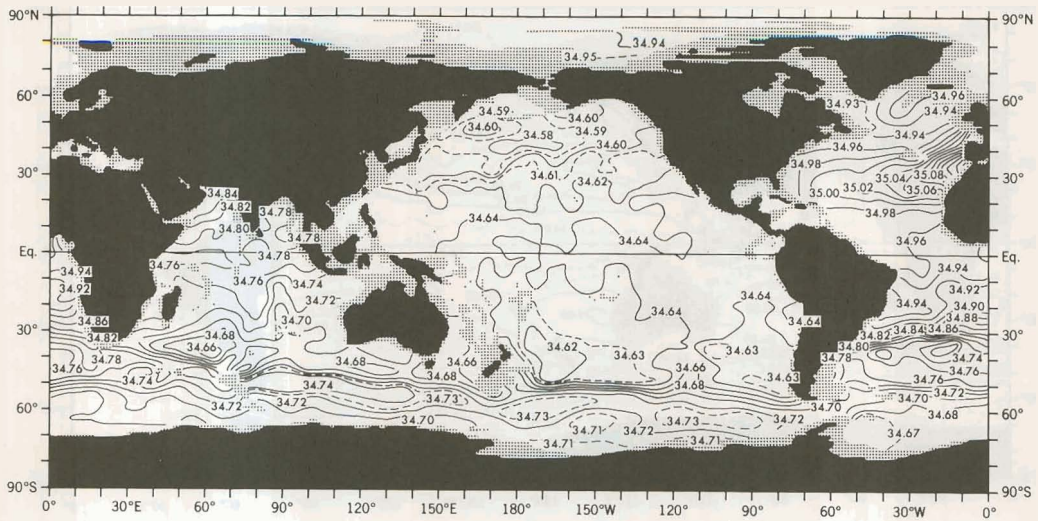


Figure 27.—Annual mean salinity (‰) at 2000 m depth.

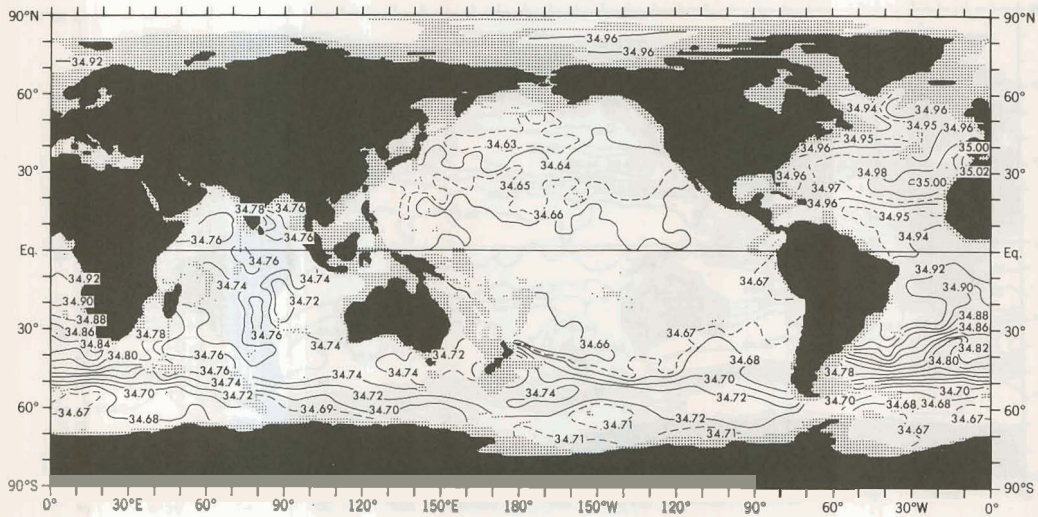


Figure 28.—Annual mean salinity (‰) at 2500 m depth.

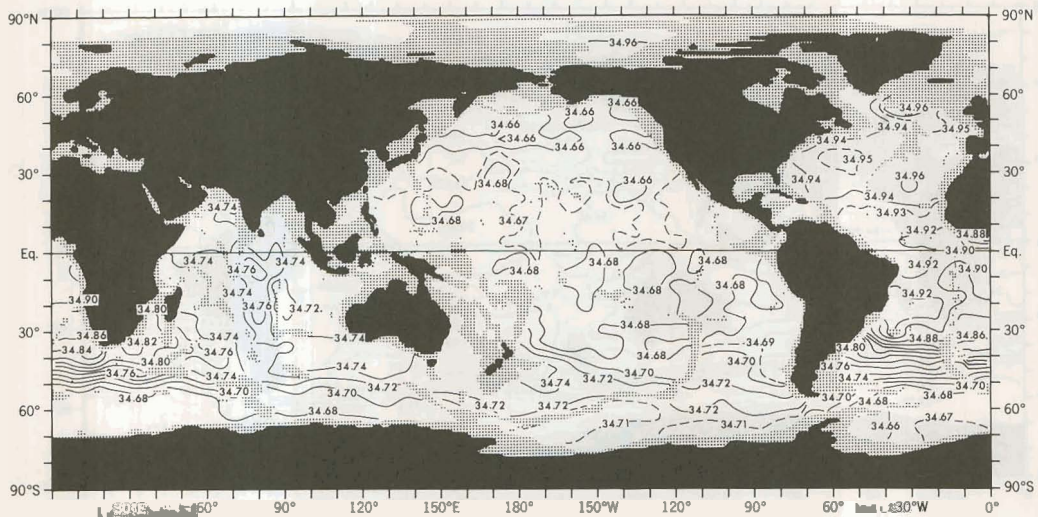


Figure 29.—Annual mean salinity (‰) at 3000 m depth.

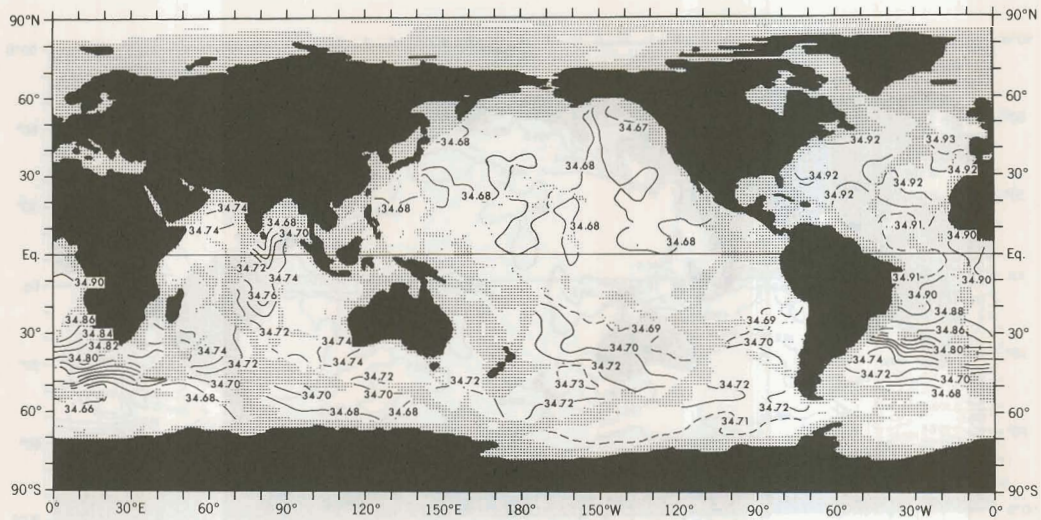


Figure 30.—Annual mean salinity (‰) at 3500 m depth.

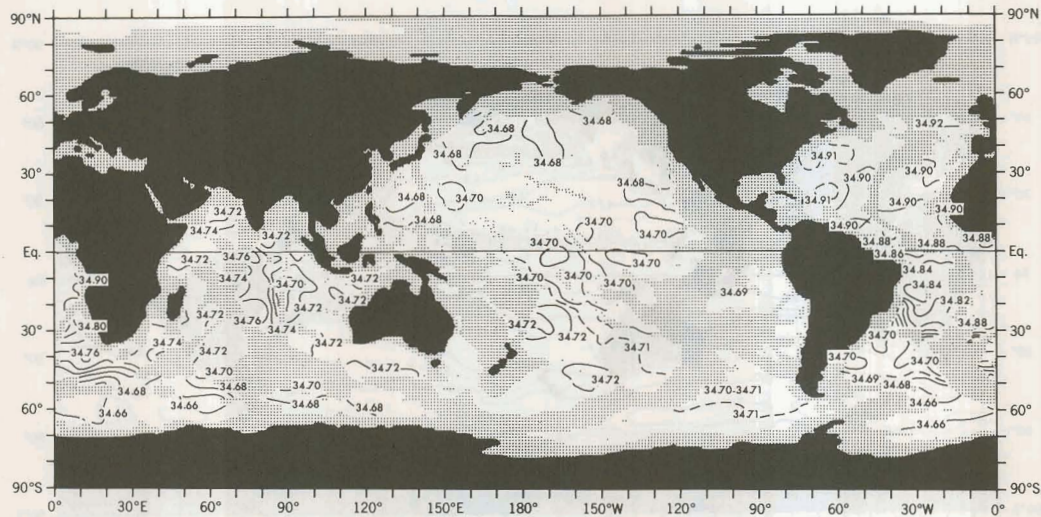


Figure 31.—Annual mean salinity (‰) at 4000 m depth.

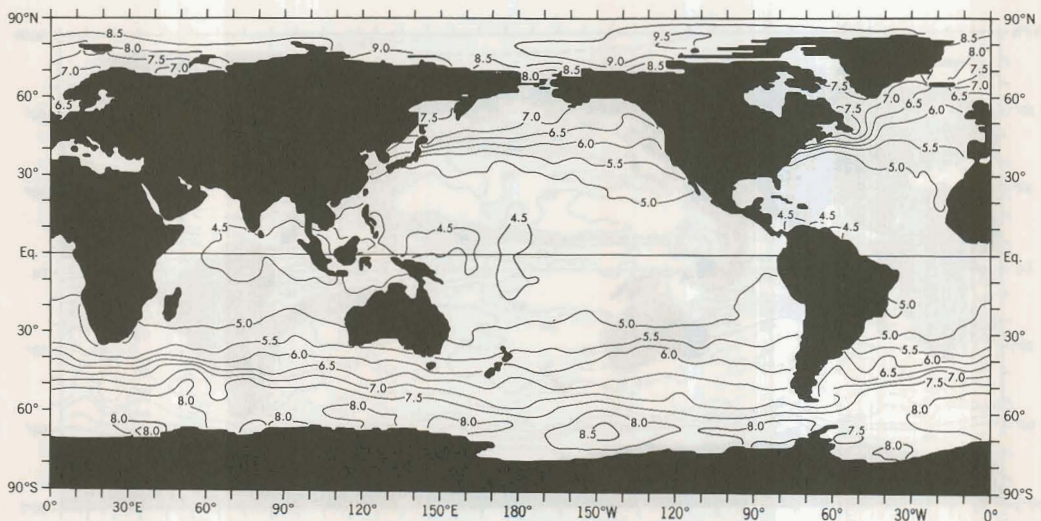


Figure 32.—Annual mean oxygen (ml/l) at the sea surface.

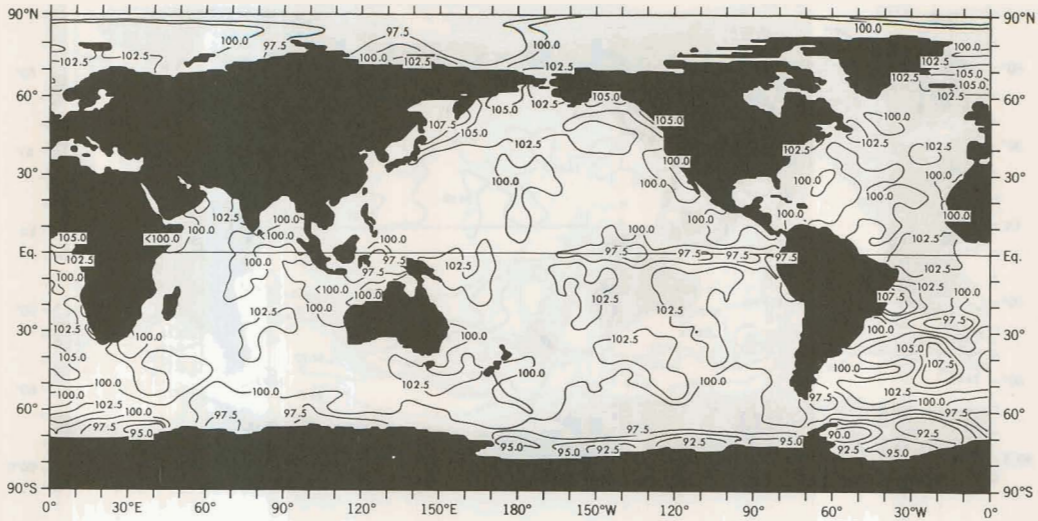


Figure 33.—Annual mean oxygen-saturation (%) at the sea surface.

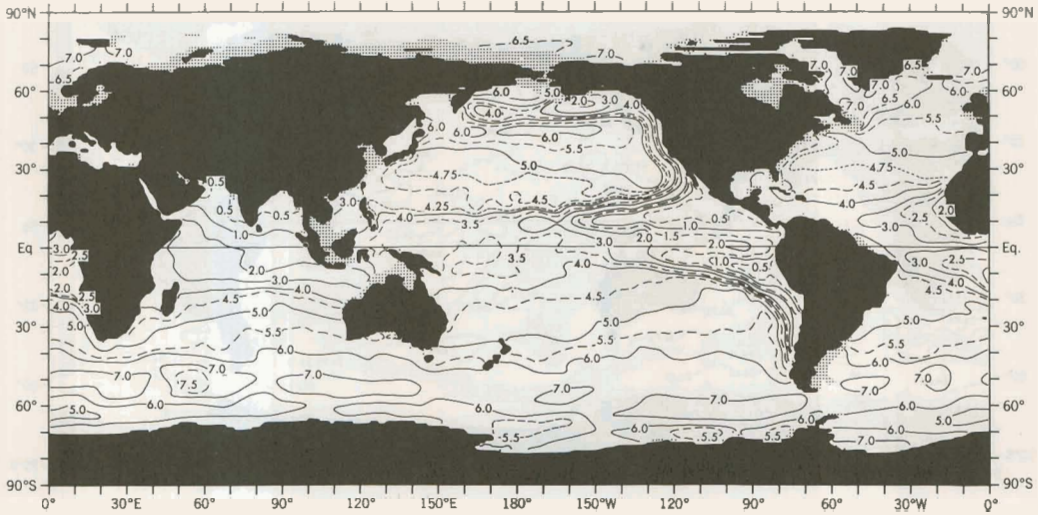


Figure 34.—Annual mean oxygen (ml/l) at 150 m depth.

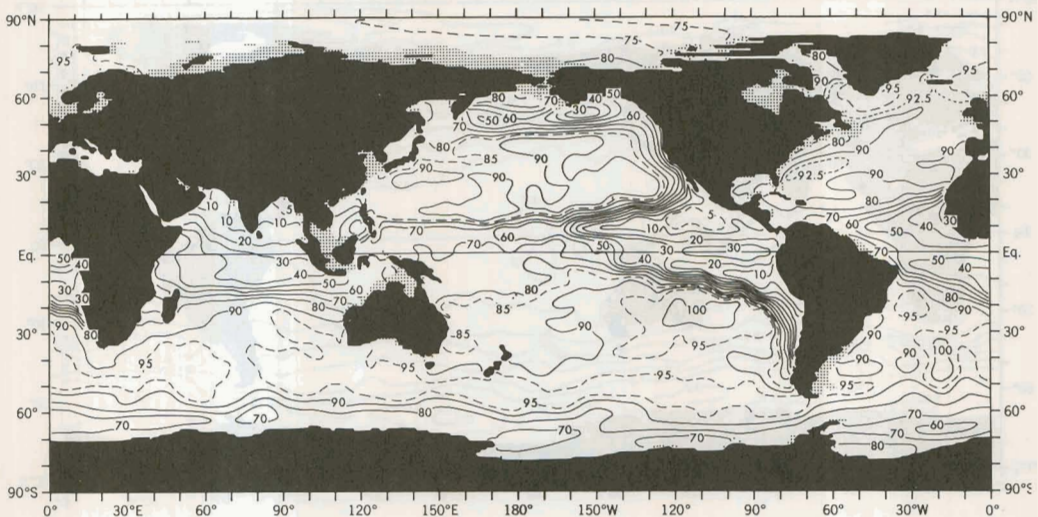


Figure 35.—Annual mean oxygen-saturation (%) at 150 m depth.

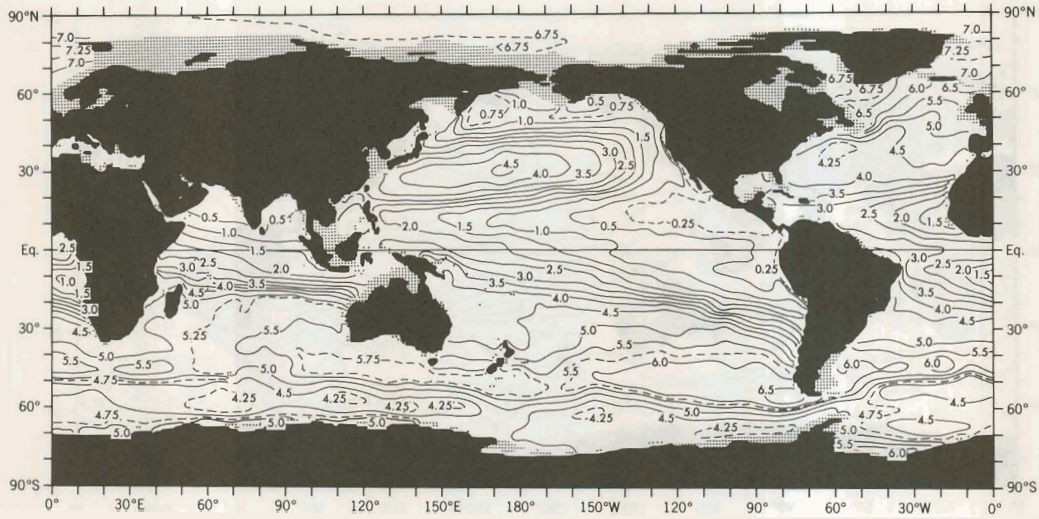


Figure 36.—Annual mean oxygen (ml/l) at 500 m depth.

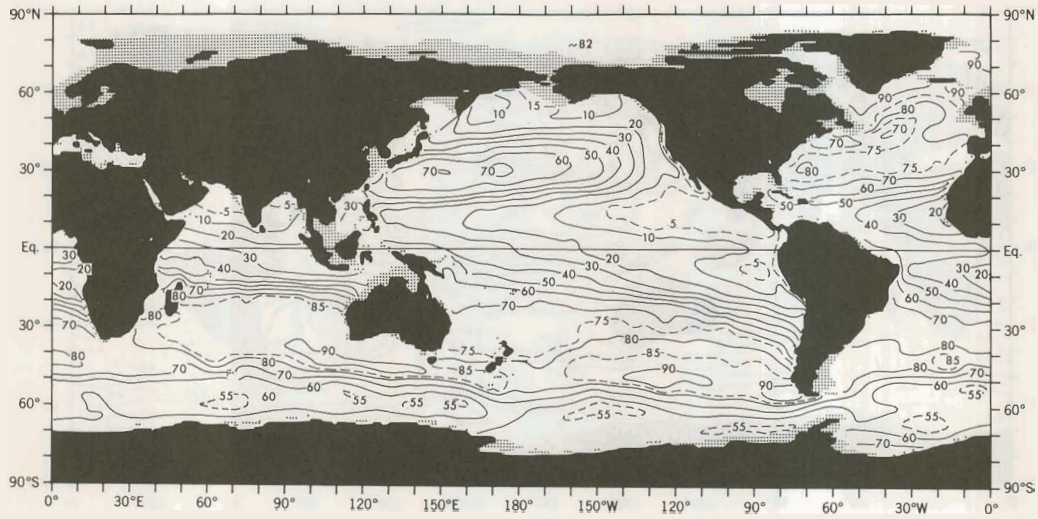


Figure 37.—Annual mean oxygen-saturation (%) at 500 m depth.

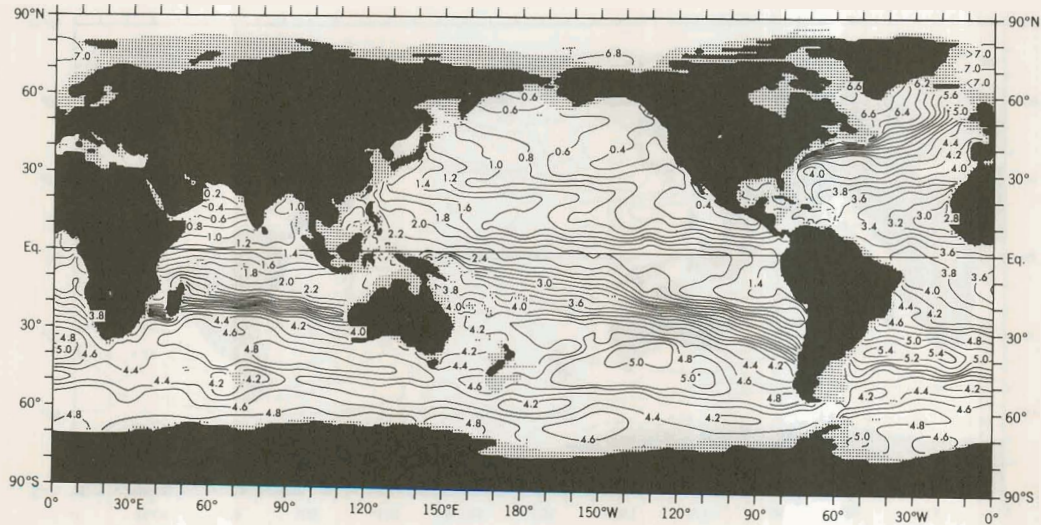


Figure 38.—Annual mean oxygen (ml/l) at 1000 m depth.

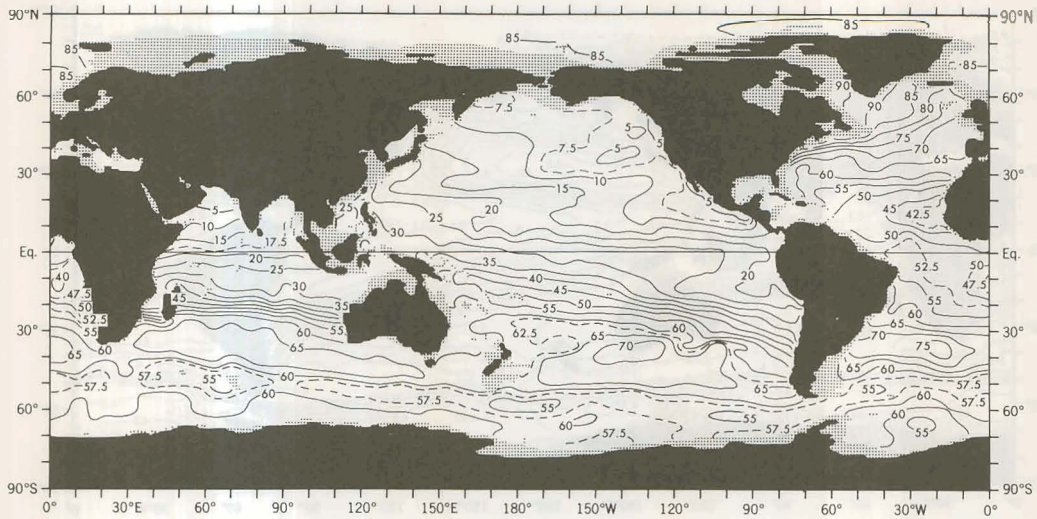


Figure 39.—Annual mean oxygen-saturation (%) at 1000 m depth.

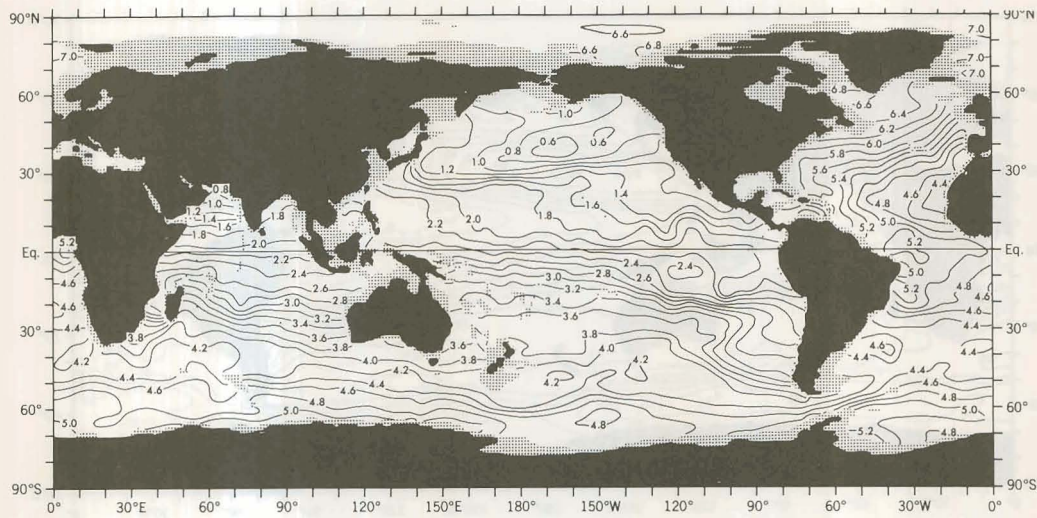


Figure 40.—Annual mean oxygen (ml/l) at 1500 m depth.

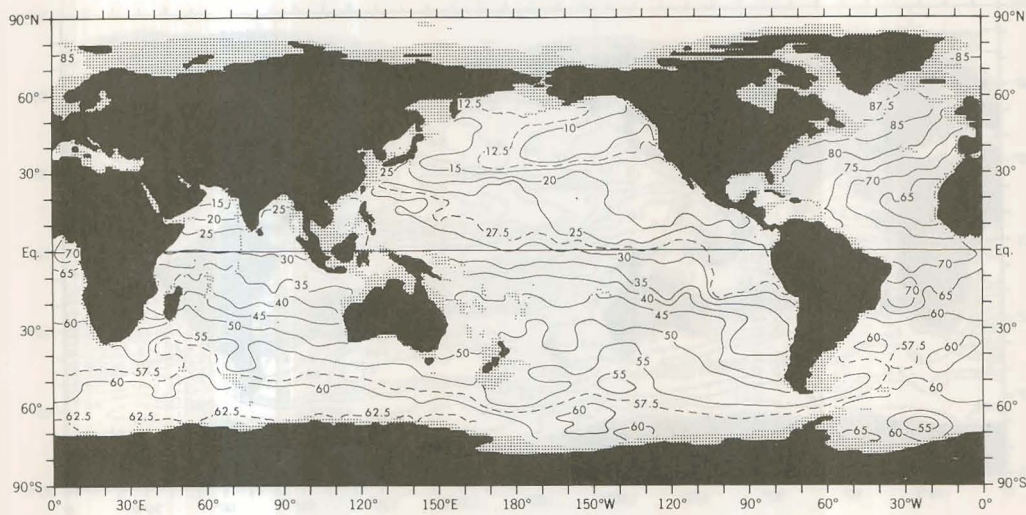


Figure 41.—Annual mean oxygen-saturation (%) at 1500 m depth.

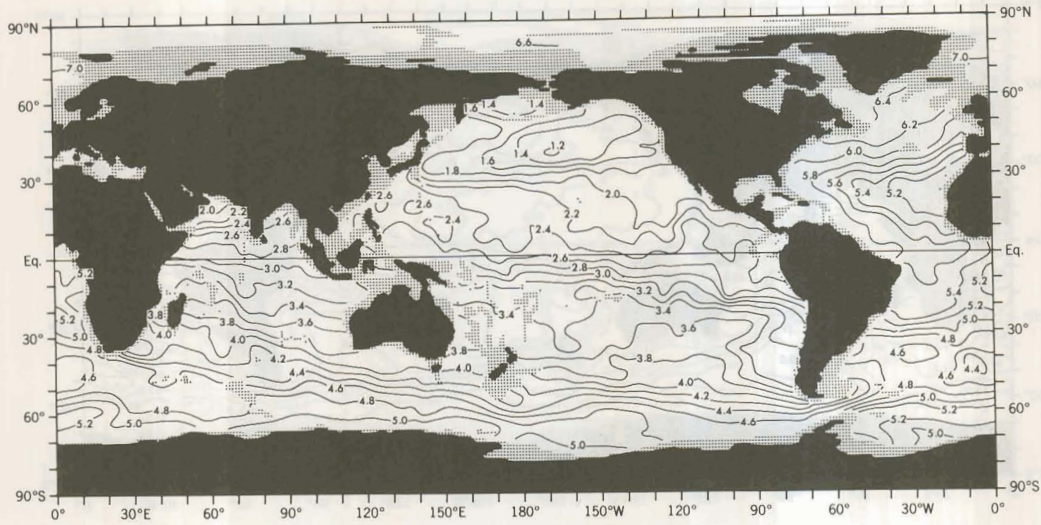


Figure 42.—Annual mean oxygen (ml/l) at 2000 m depth.

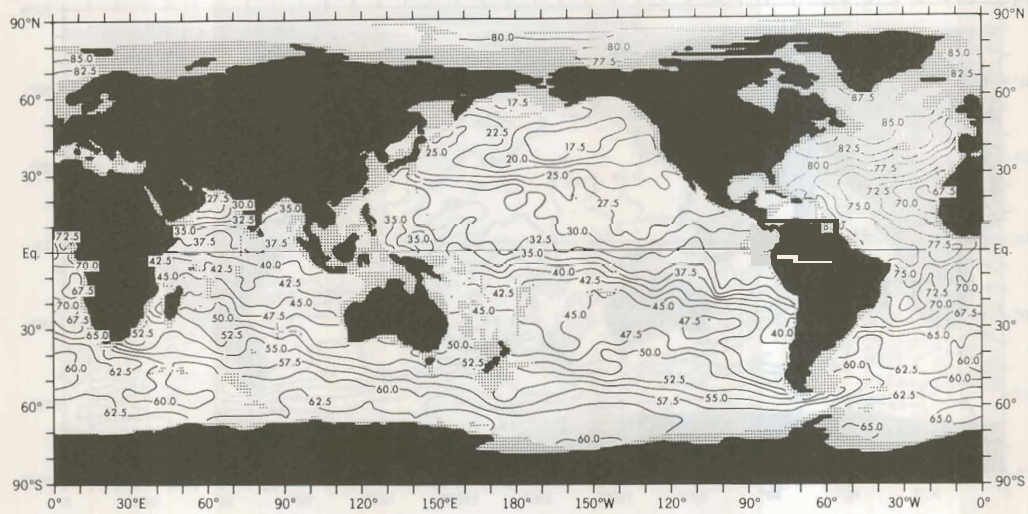


Figure 43.—Annual mean oxygen-saturation (%) at 2000 m depth.

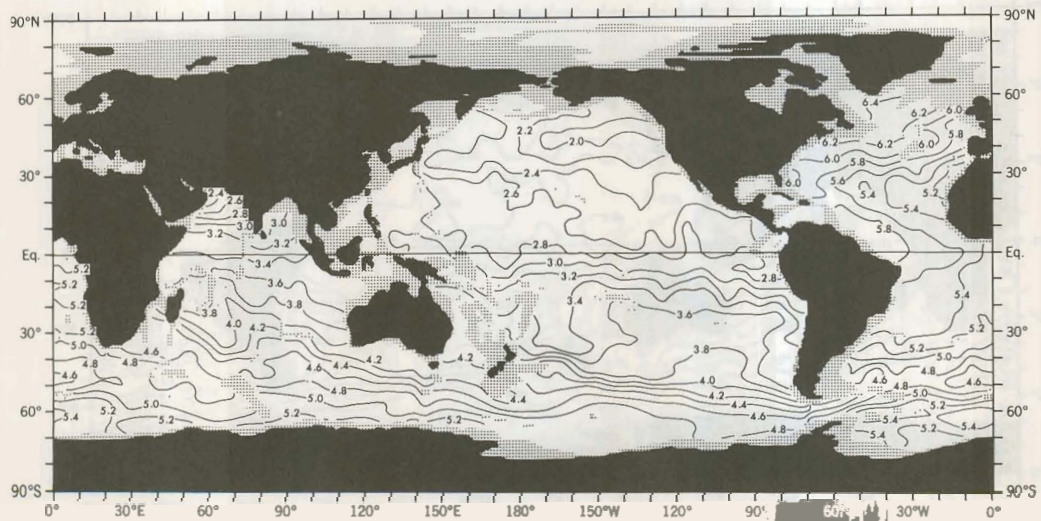


Figure 44.—Annual mean oxygen (ml/l) at 2500 m depth.

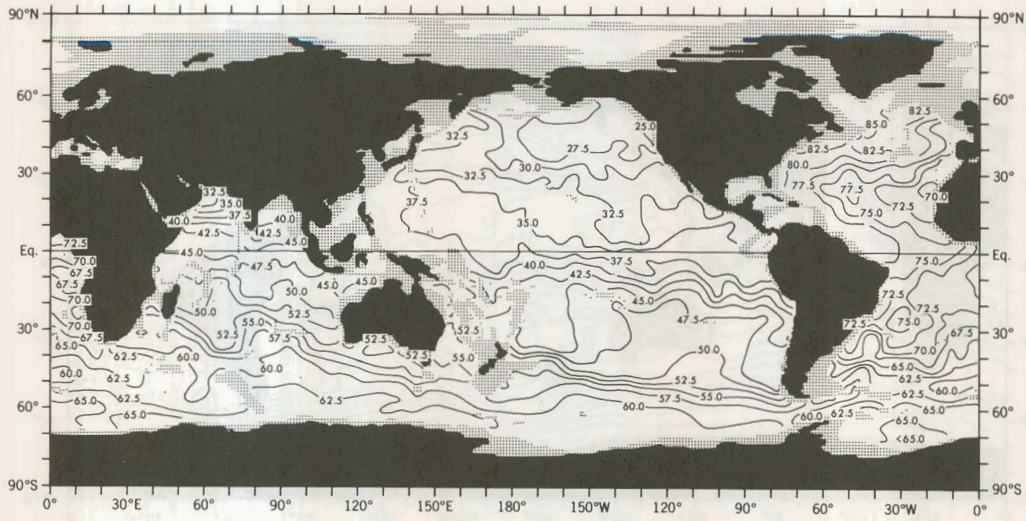


Figure 45.—Annual mean oxygen-saturation (%) at 2500 m depth.

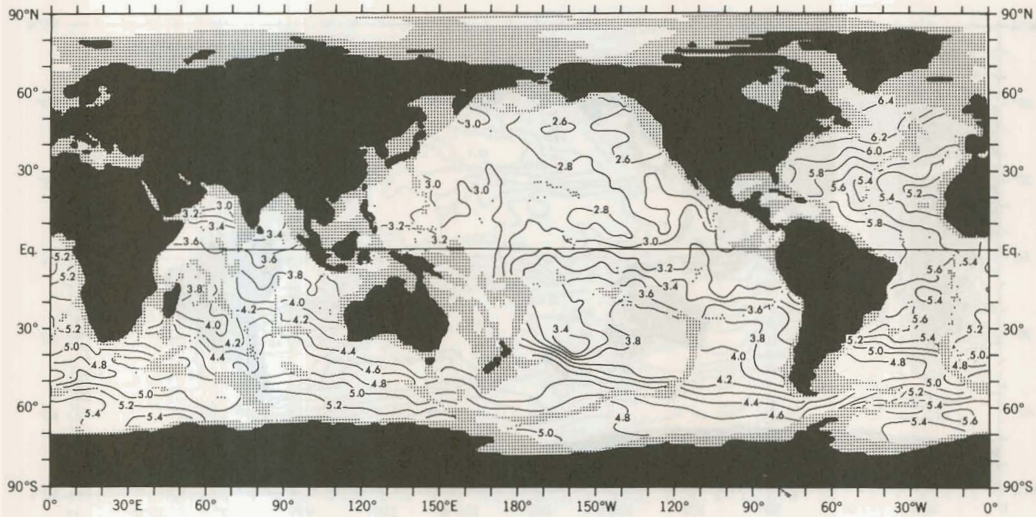


Figure 46.—Annual mean oxygen (ml/l) at 3000 m depth.

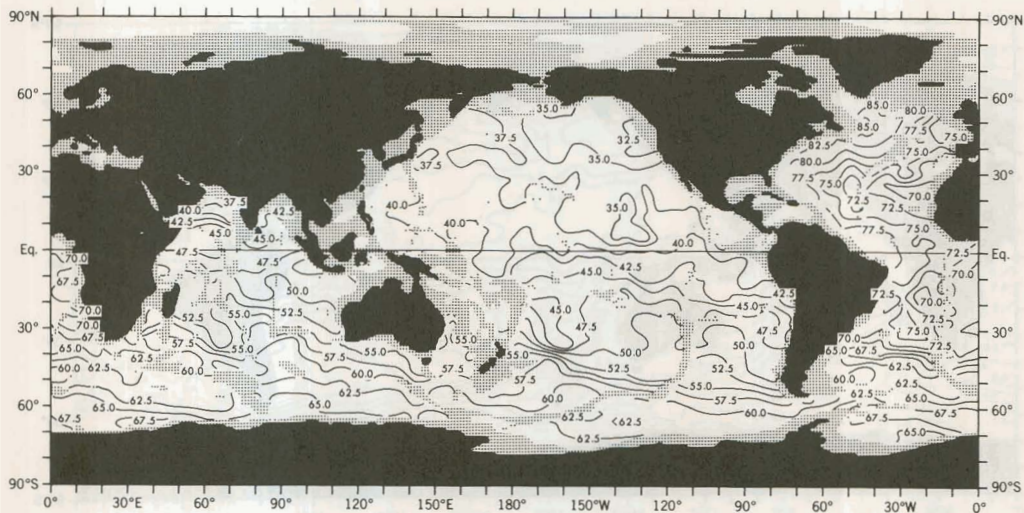


Figure 47.—Annual mean oxygen-saturation (%) at 3000 m depth.

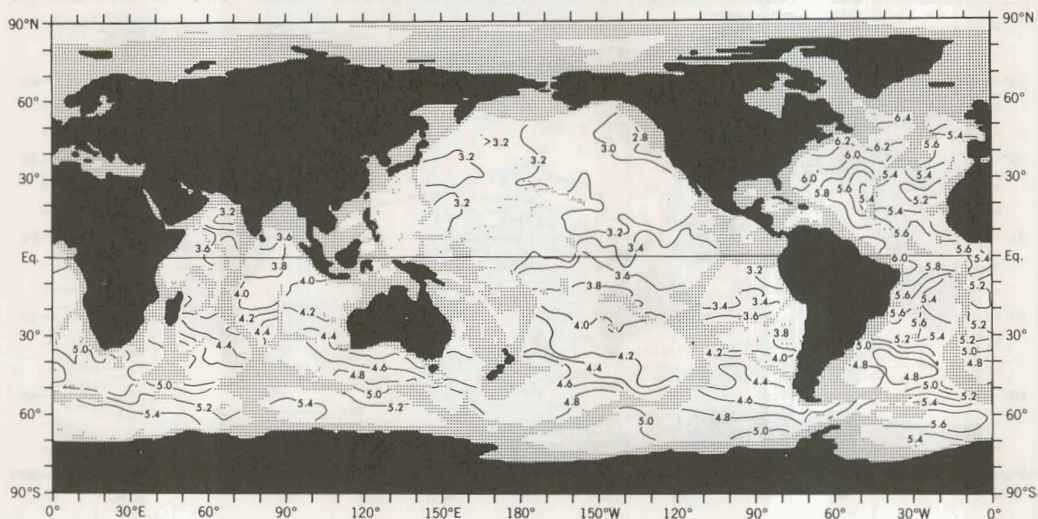


Figure 48.—Annual mean oxygen (ml/l) at 3500 m depth.

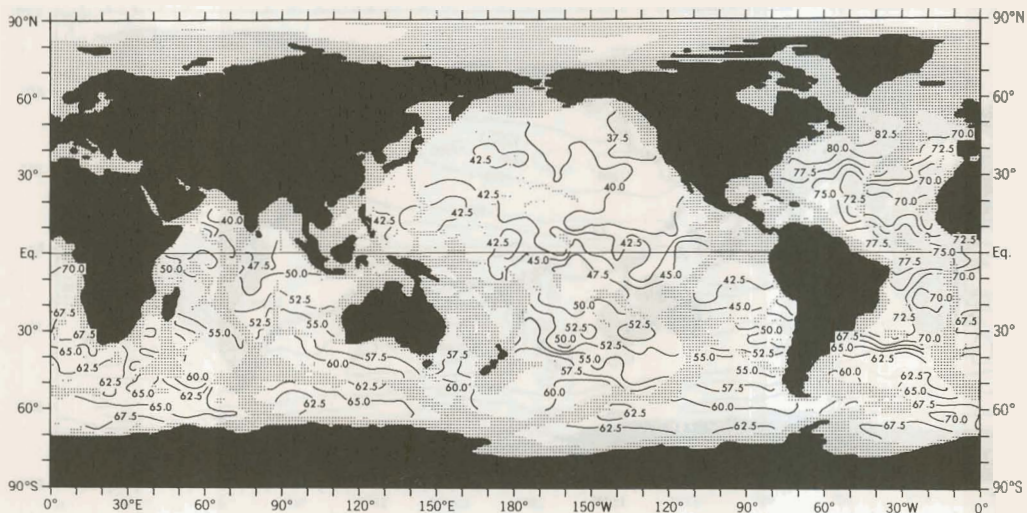


Figure 49.—Annual mean oxygen-saturation (%) at 3500 m depth.

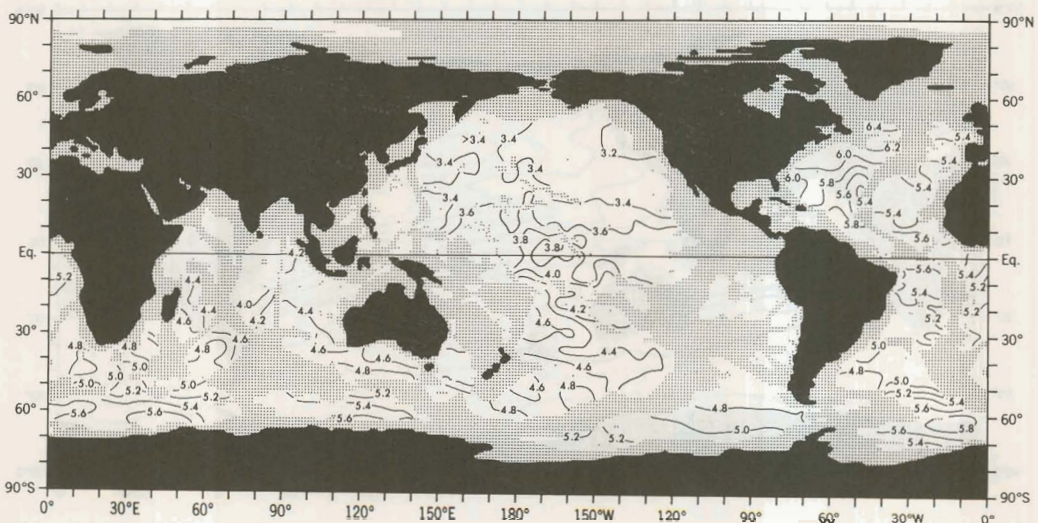


Figure 50.—Annual mean oxygen (ml/l) at 4000 m depth.

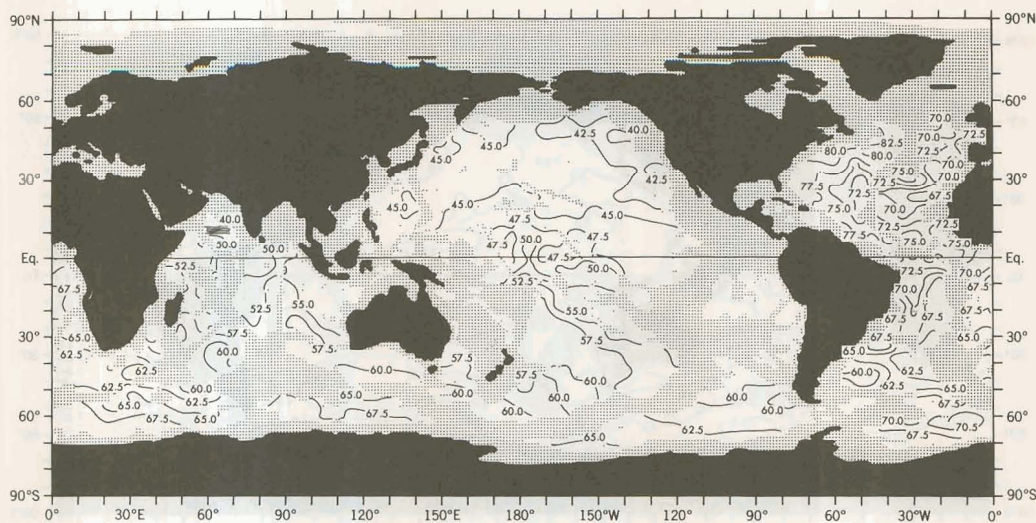


Figure 51.—Annual mean oxygen-saturation (%) at 4000 m depth.

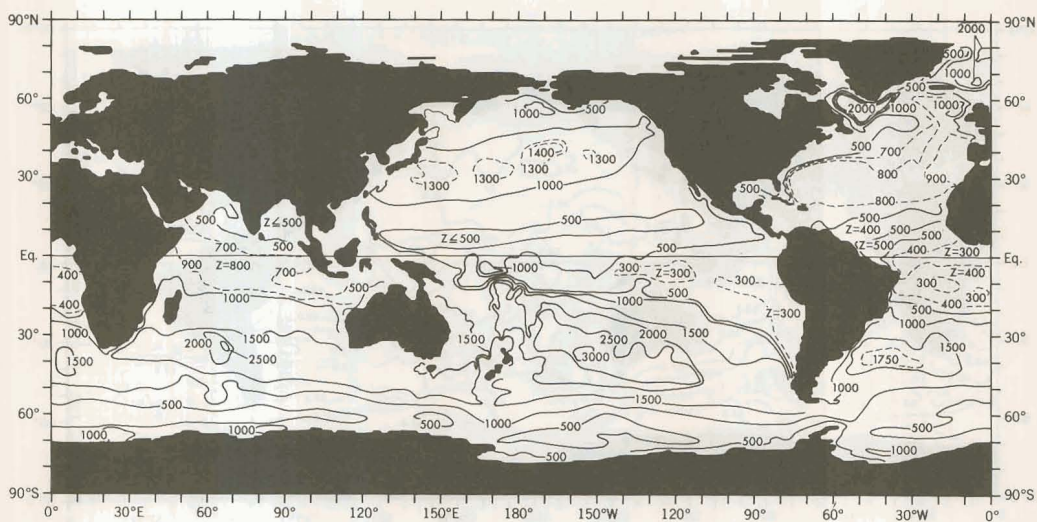


Figure 52.—Annual mean depth (m) of the absolute oxygen minimum surface with respect to the vertical.

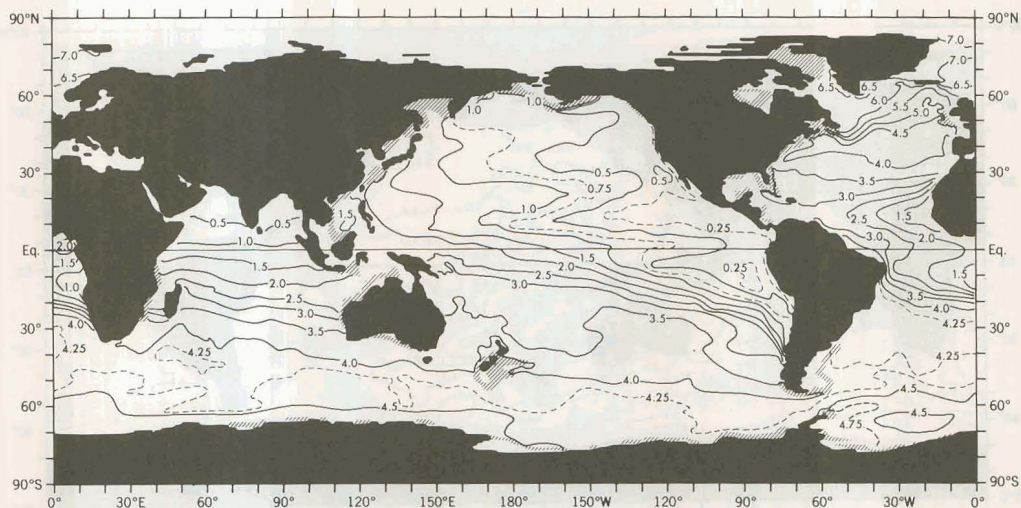


Figure 53.—Annual mean oxygen (ml/l) on the absolute oxygen minimum surface. Hatching indicates areas where gradients are too large to contour.

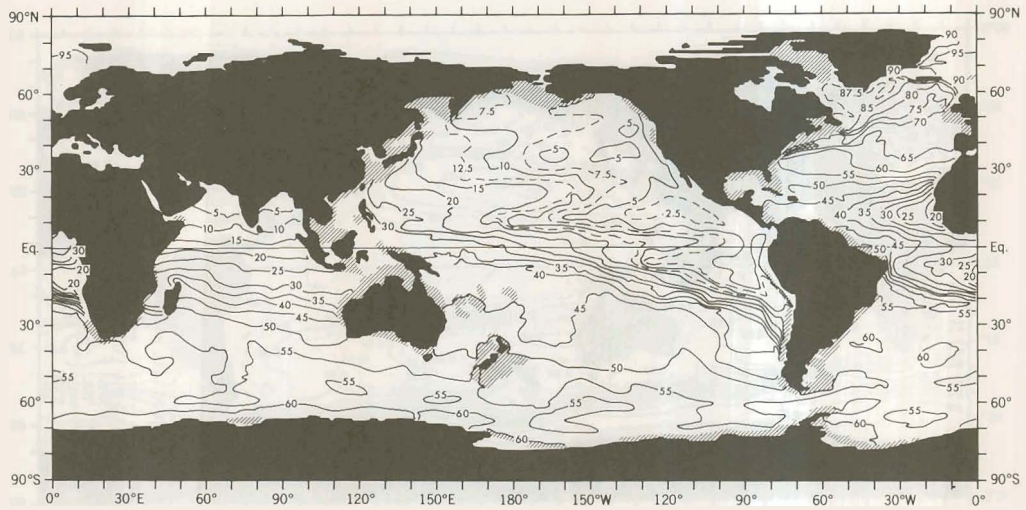


Figure 54.—Annual mean oxygen-saturation (%) on the absolute oxygen minimum surface. Hatching indicates areas where gradients are too large to contour.

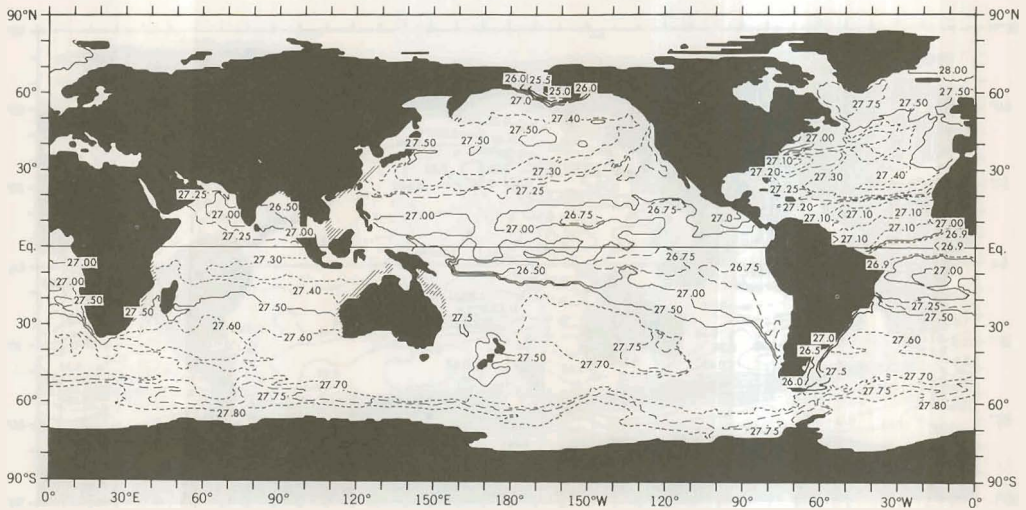


Figure 55.—Annual mean potential density (10^{-3}g/cm^3) on the absolute oxygen minimum surface. Hatching indicates areas where gradients are too large to contour.

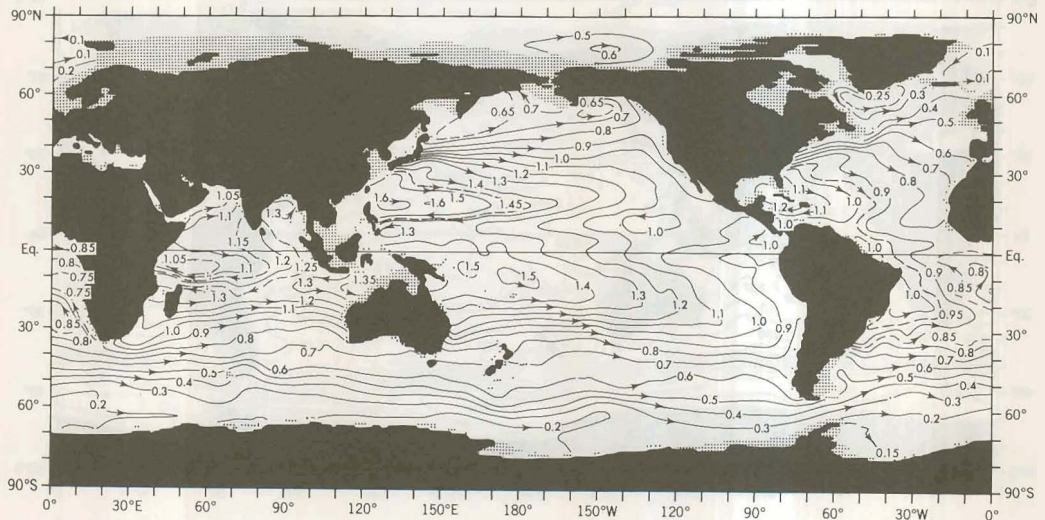


Figure 56.—Annual mean anomaly of geopotential thickness ($10\text{ m}^2/\text{sec}^2$) of the 0-500 m layer.

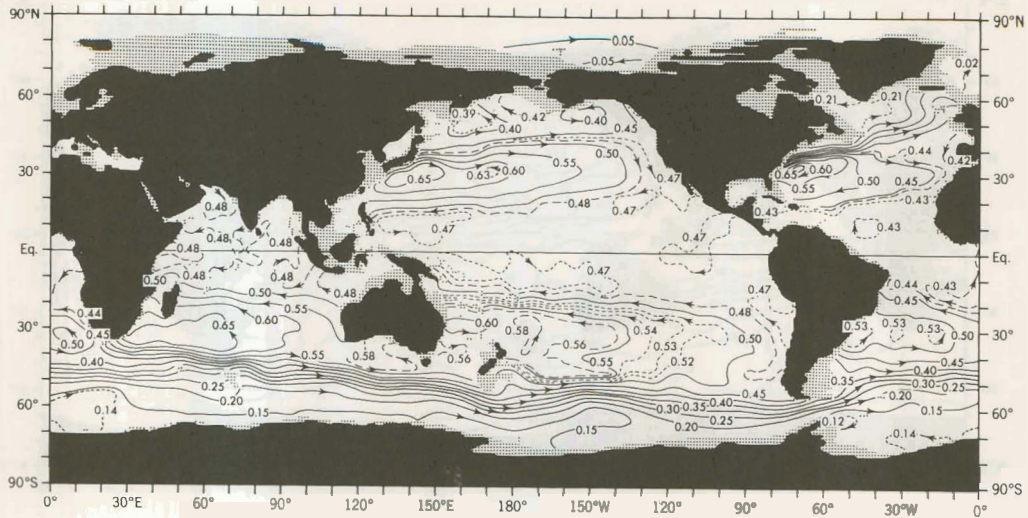


Figure 57.—Annual mean anomaly of geopotential thickness ($10 \text{ m}^2/\text{sec}^2$) of the 500-1000 m layer.

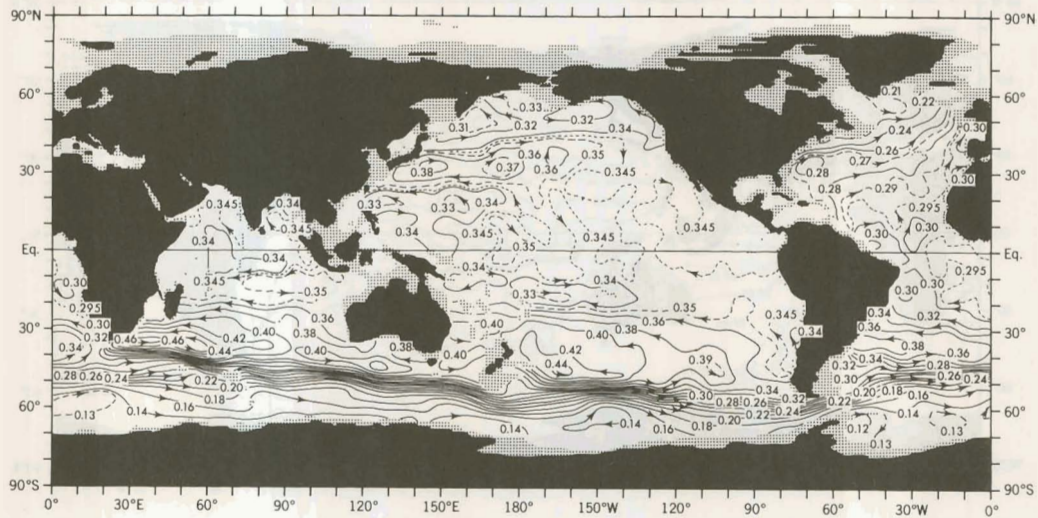


Figure 58.—Annual mean anomaly of geopotential thickness ($10 \text{ m}^2/\text{sec}^2$) of the 1000-1500 m layer.



Figure 59.—Annual mean anomaly of geopotential thickness ($10 \text{ m}^2/\text{sec}^2$) of the 1500-2000 m layer.

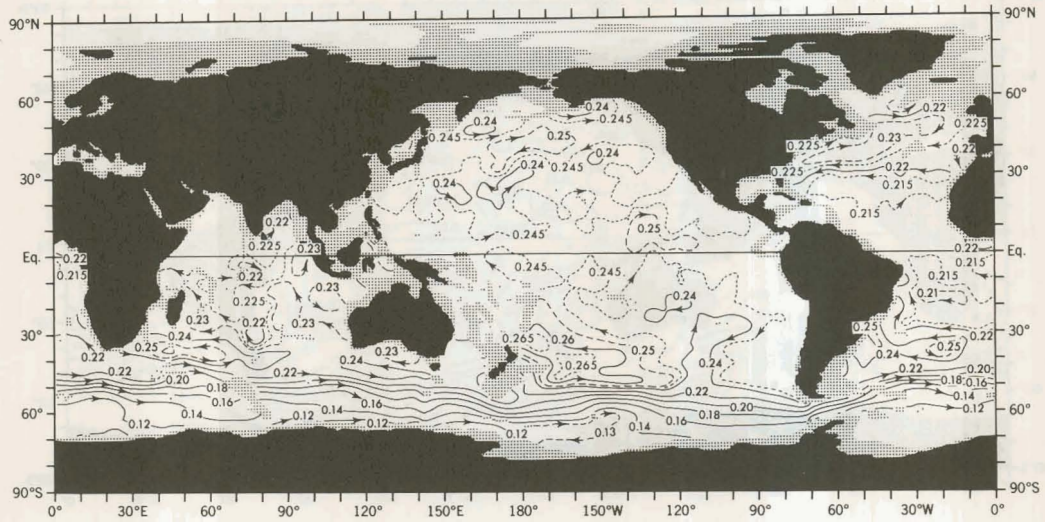


Figure 60.—Annual mean anomaly of geopotential thickness ($10 \text{ m}^2/\text{sec}^2$) of the 2000-2500 m layer

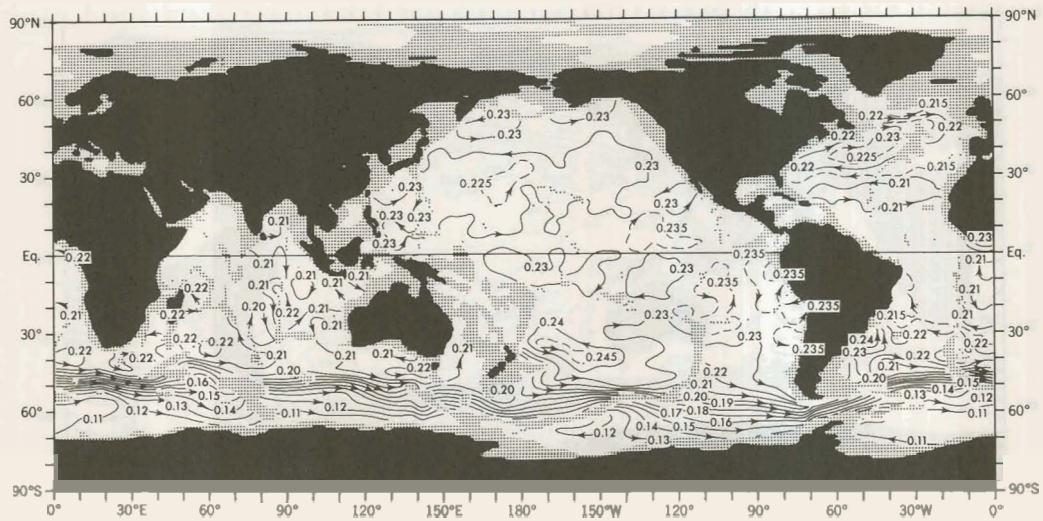


Figure 61.—Annual mean anomaly of geopotential thickness ($10 \text{ m}^2/\text{sec}^2$) of the 2500-3000 m layer.

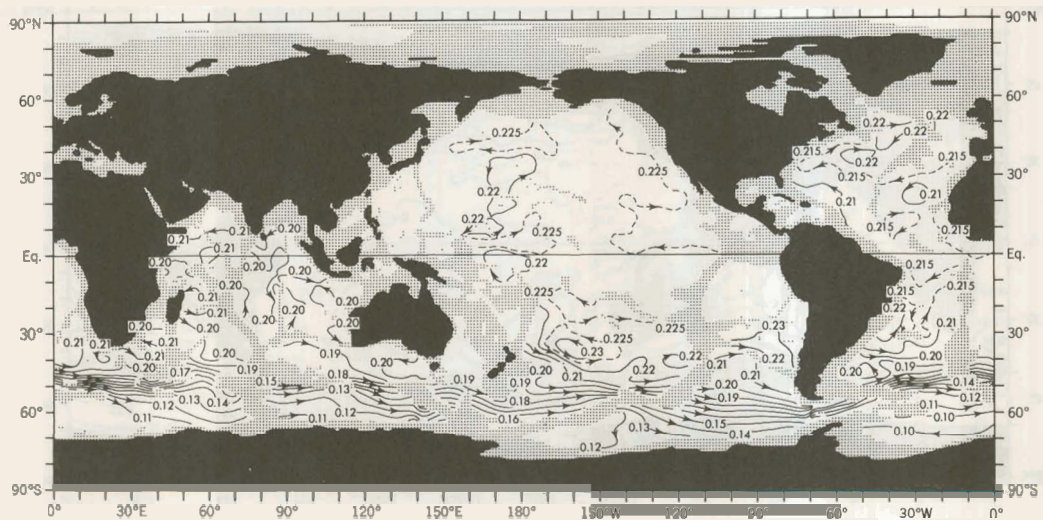


Figure 62.—Annual mean anomaly of geopotential thickness ($10 \text{ m}^2/\text{sec}^2$) of the 3000-3500 m layer.

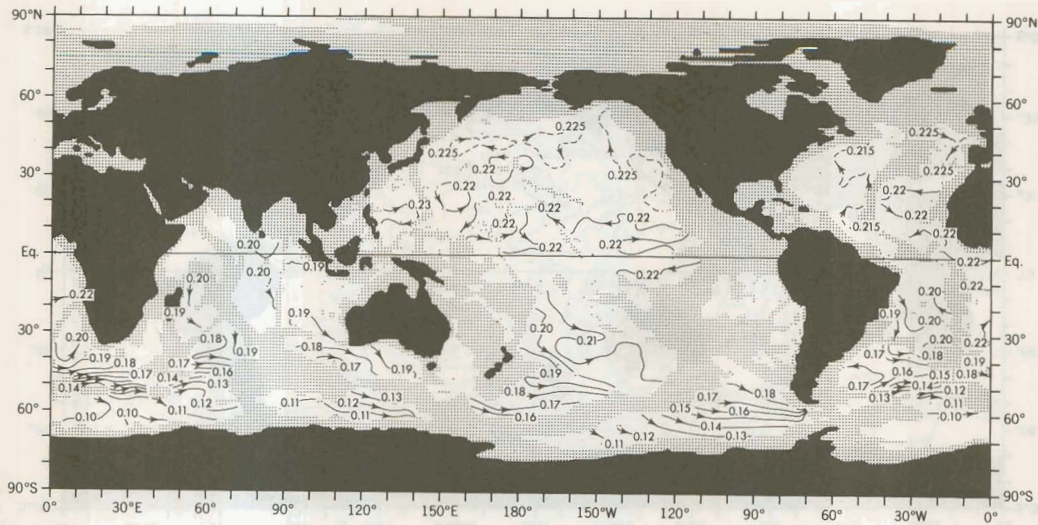


Figure 63.—Annual mean anomaly of geopotential thickness ($10 \text{ m}^2/\text{sec}^2$) of the 3500-4000 m layer.

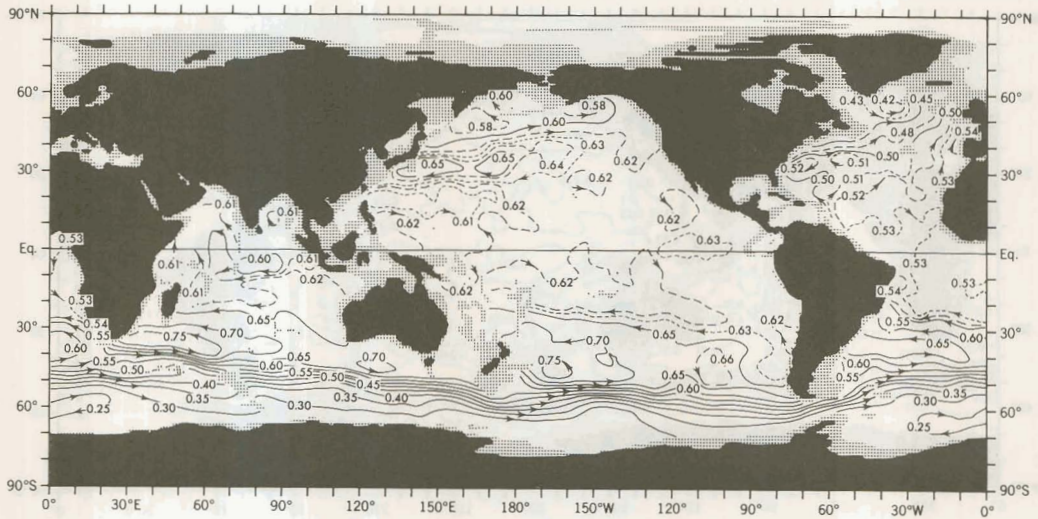


Figure 64.—Annual mean anomaly of geopotential thickness ($10 \text{ m}^2/\text{sec}^2$) of the 1000-2000 m layer.

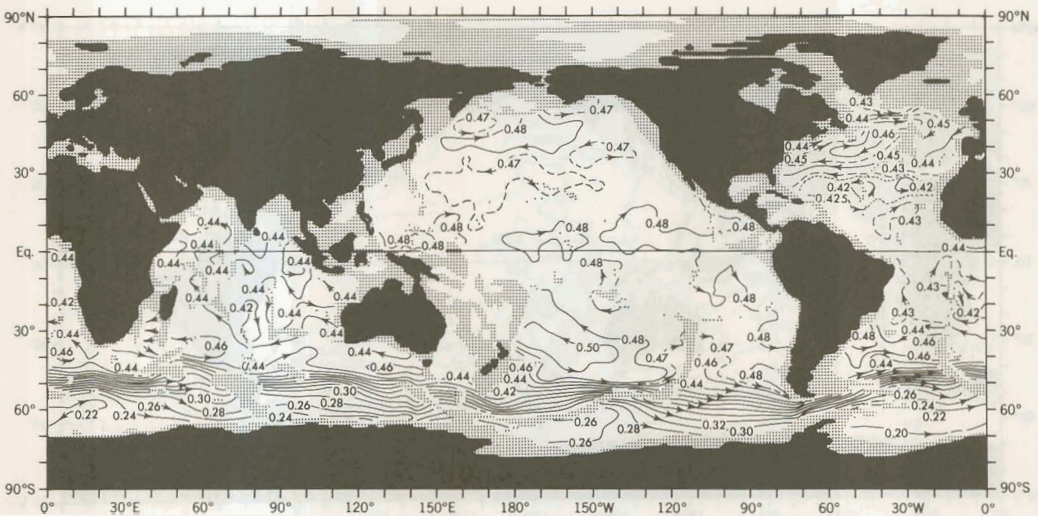


Figure 65.—Annual mean anomaly of geopotential thickness ($10 \text{ m}^2/\text{sec}^2$) of the 2000-3000 m layer.

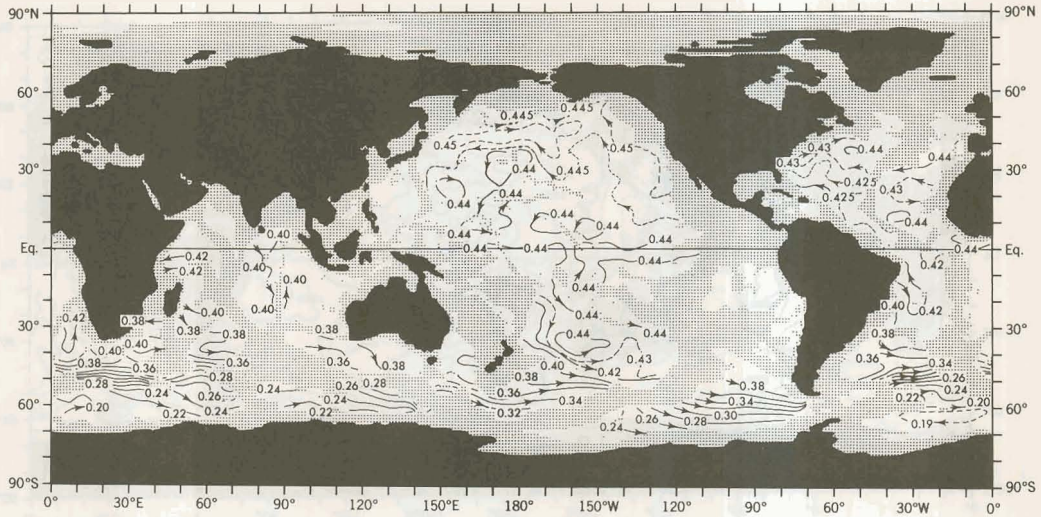


Figure 66.—Annual mean anomaly of geopotential thickness ($10 \text{ m}^2/\text{sec}^2$) of the 3000-4000 m layer.

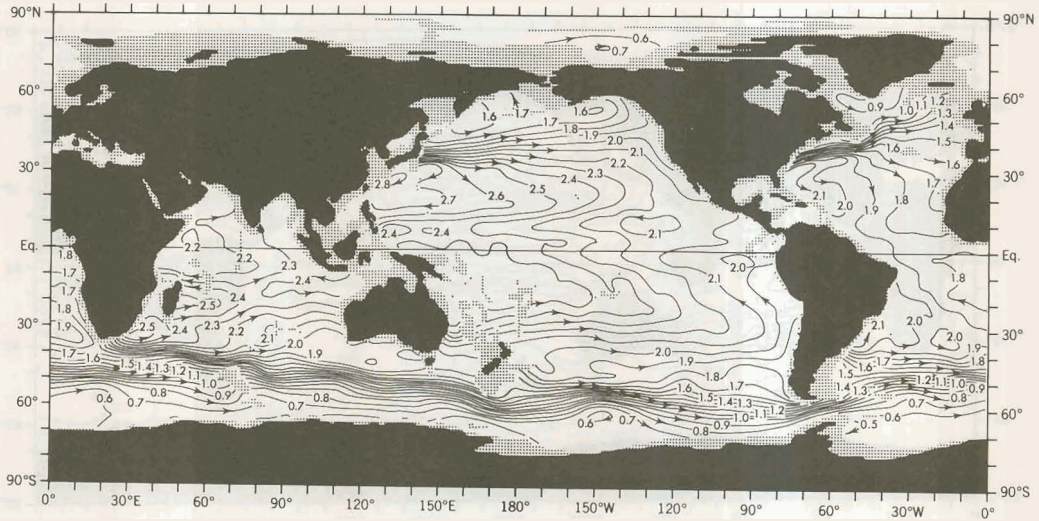


Figure 67.—Annual mean anomaly of geopotential thickness ($10 \text{ m}^2/\text{sec}^2$) of the 0-2000 m layer.

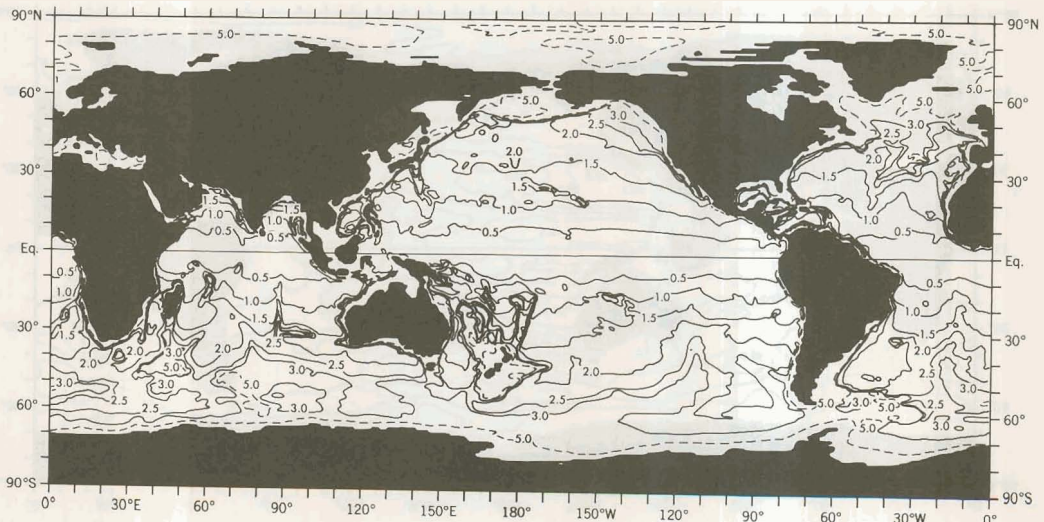


Figure 68.—Planetary vorticity (f/H) ($10^{-8} \text{ m}^{-1} \text{ sec}^{-1}$).

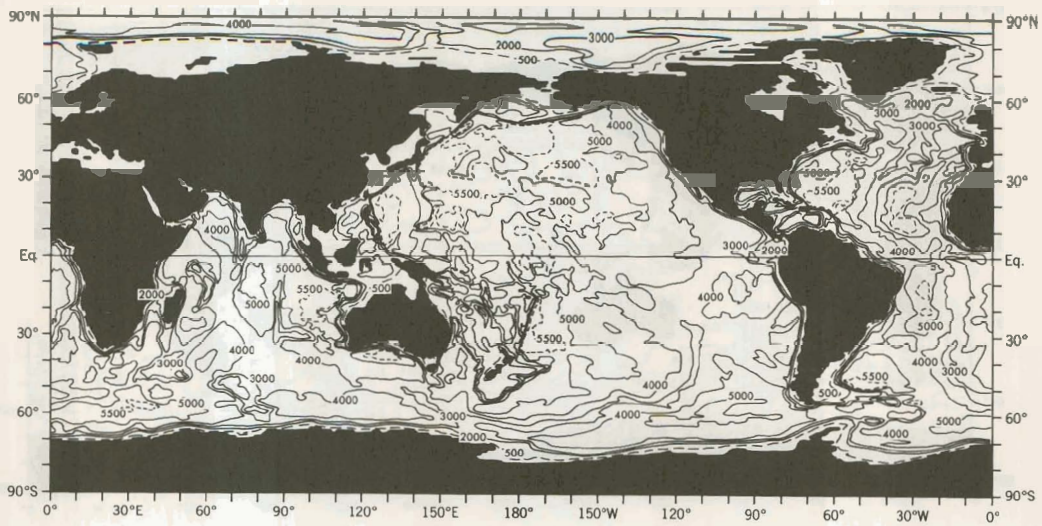


Figure 69.—Depth of the world ocean (meters).

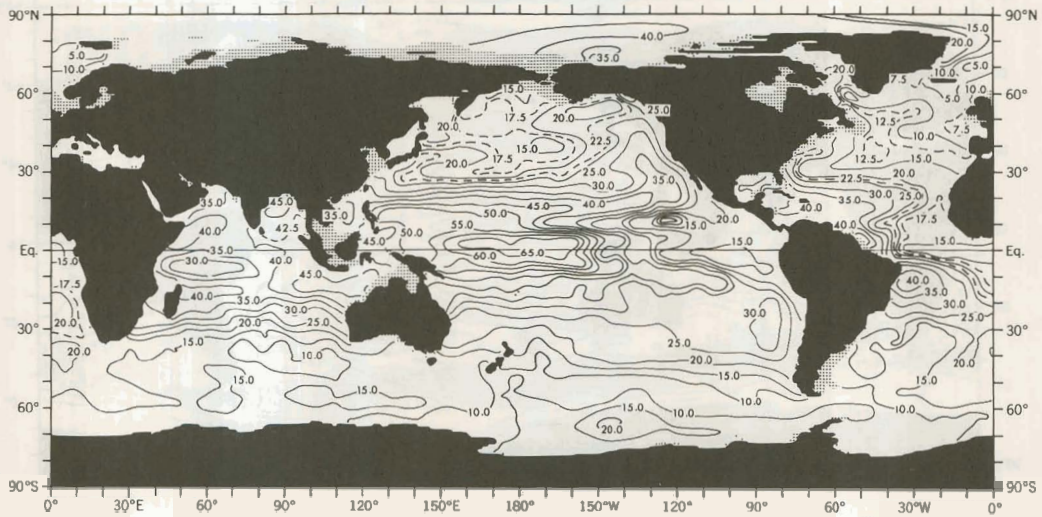


Figure 70.—Annual mean Brunt-Väisälä frequency (cycles/hr) at 150 m depth.

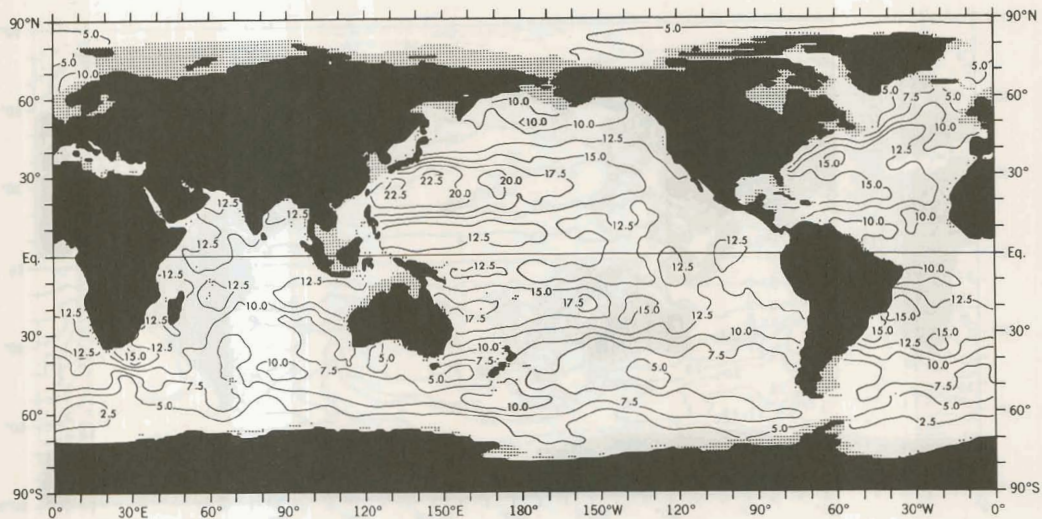


Figure 71.—Annual mean Brunt-Väisälä frequency (cycles/hr) at 500 m depth.

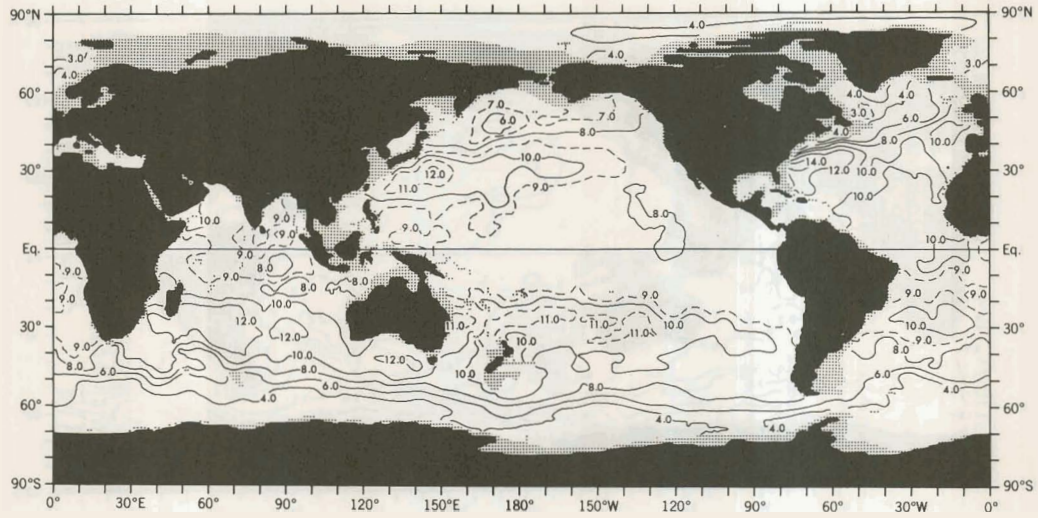


Figure 72.—Annual mean Brunt-Väisälä frequency (cycles/hr) at 1000 m depth.

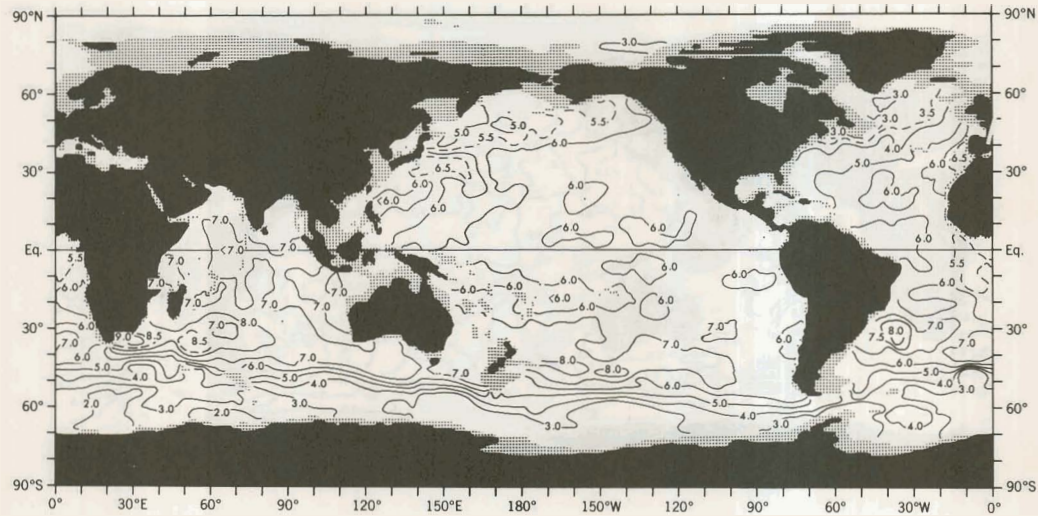


Figure 73.—Annual mean Brunt-Väisälä frequency (cycles/hr) at 1500 m depth.

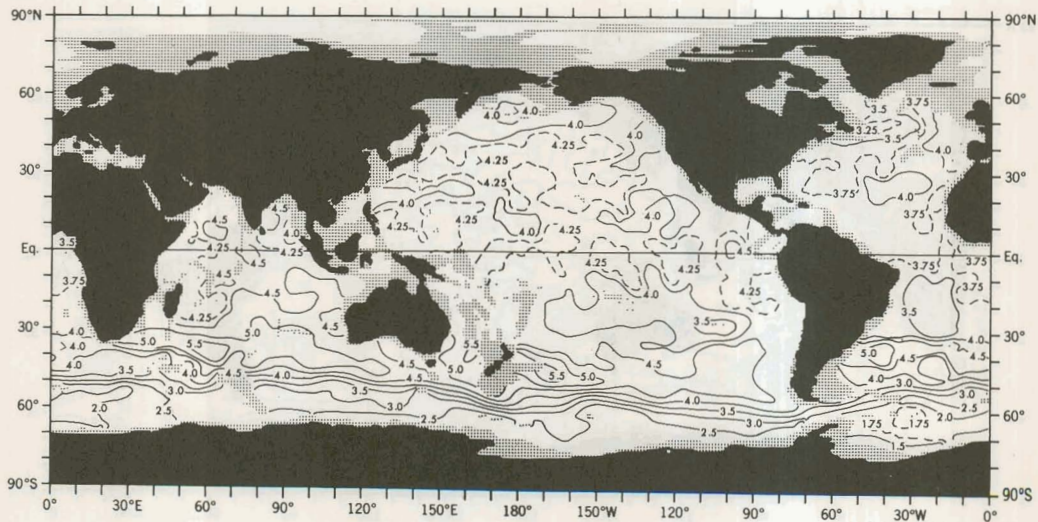


Figure 74.—Annual mean Brunt-Väisälä frequency (cycles/hr) at 2000 m depth.

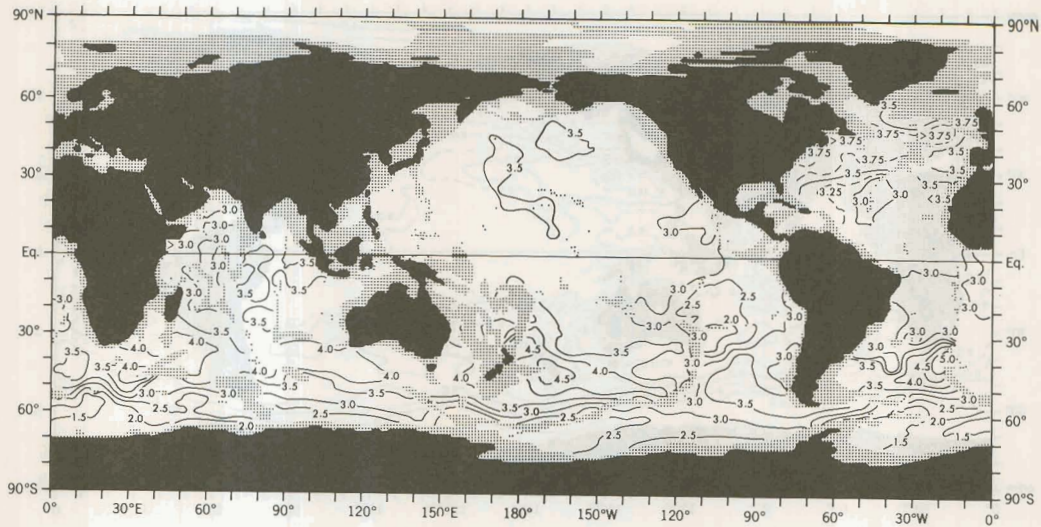


Figure 75.—Annual mean Brunt-Väisälä frequency (cycles/hr) at 2500 m depth.

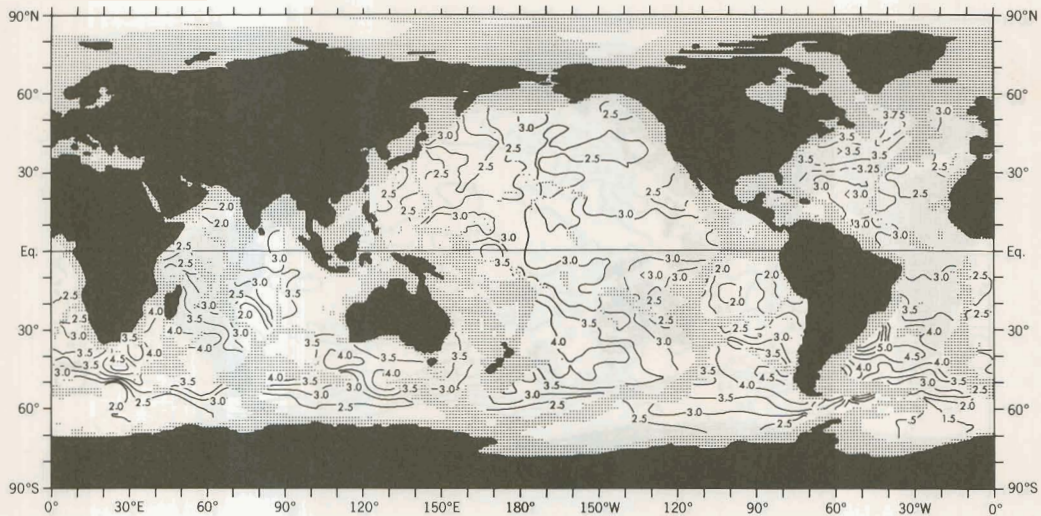


Figure 76.—Annual mean Brunt-Väisälä frequency (cycles/hr) at 3000 m depth.

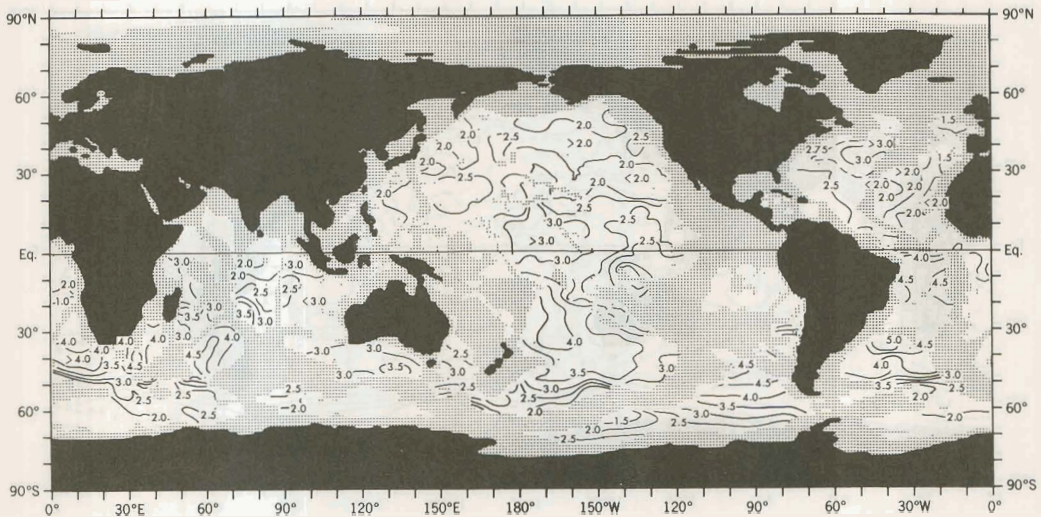


Figure 77.—Annual mean Brunt-Väisälä frequency (cycles/hr) at 3500 m depth.

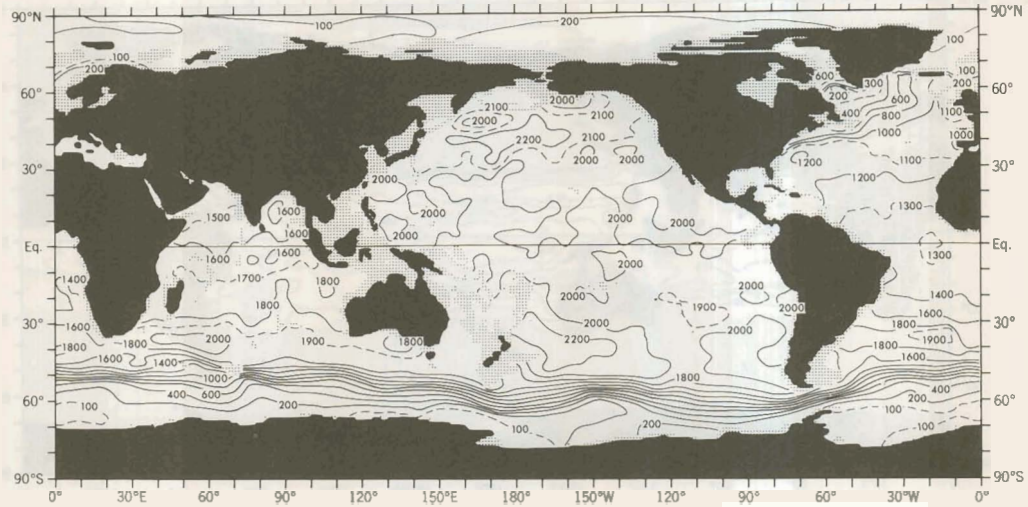


Figure 78.—Annual mean depth (meters) of the 27.7 potential density surface.

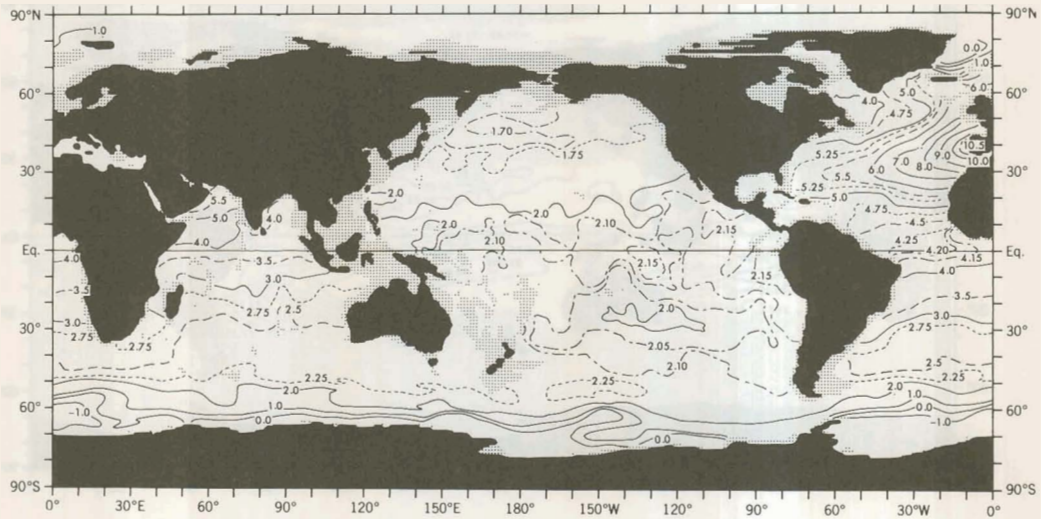


Figure 79.—Potential temperature (°C) on the annual mean 27.7 potential density surface.

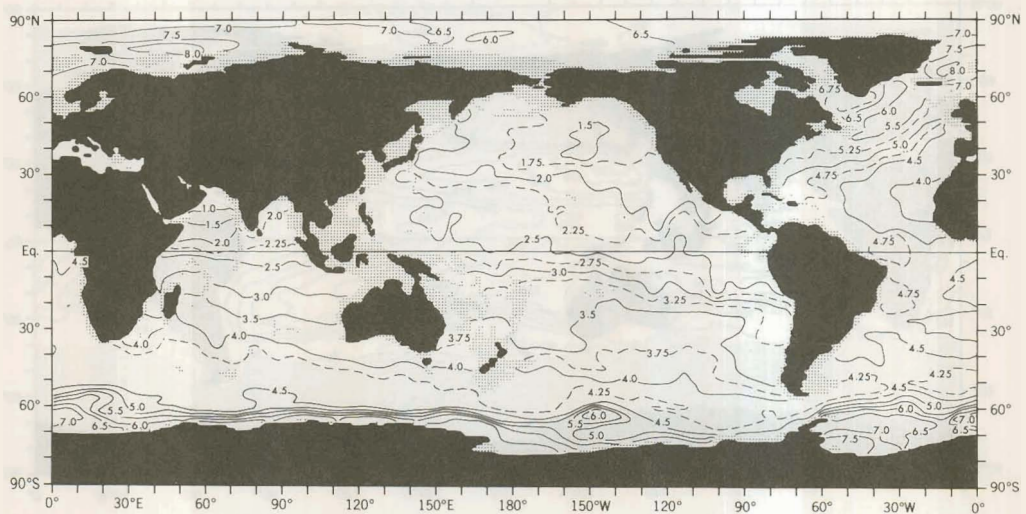


Figure 80.—Oxygen (ml/l) on the annual mean 27.7 potential density surface.

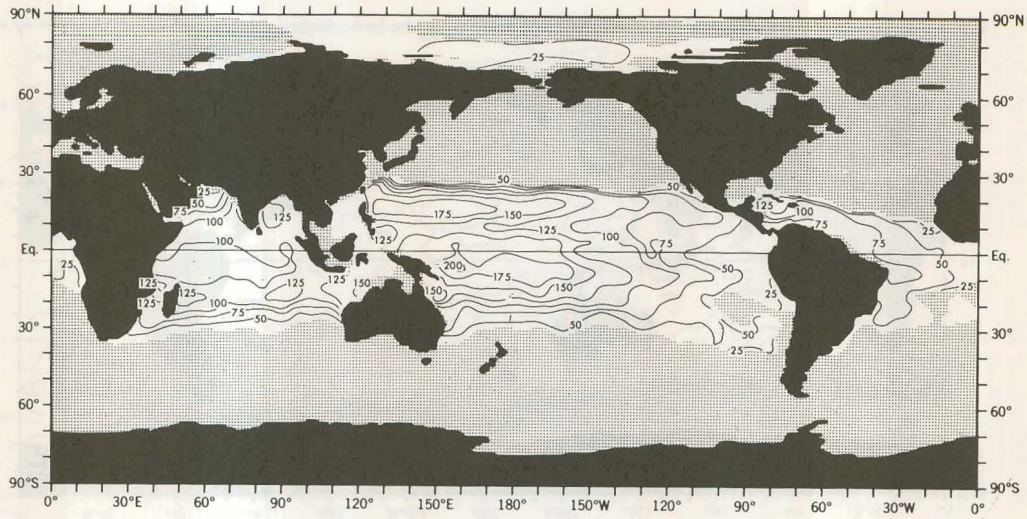


Figure 81.—Northern Hemisphere winter (February, March, April) depth (meters) of the 24.5 potential density surface.

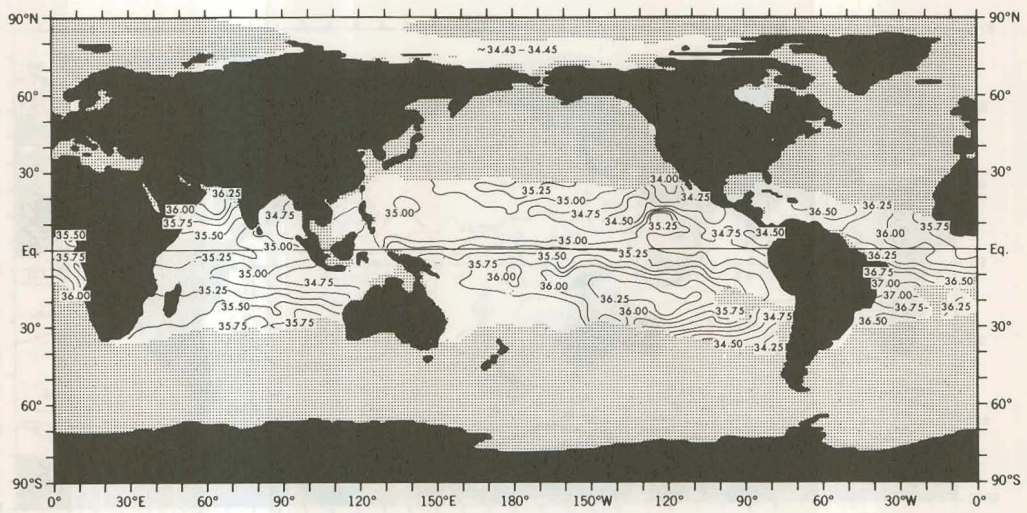


Figure 82.—Salinity (‰) on the Northern Hemisphere winter (February, March, April) 24.5 potential density surface.

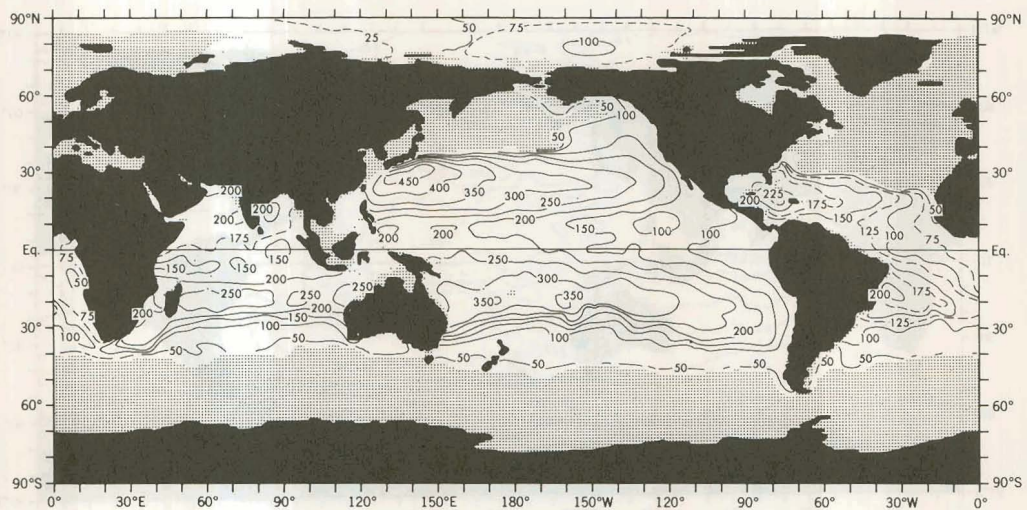


Figure 83.—Northern Hemisphere winter (February, March, April) depth (meters) of the 26.0 potential density surface.

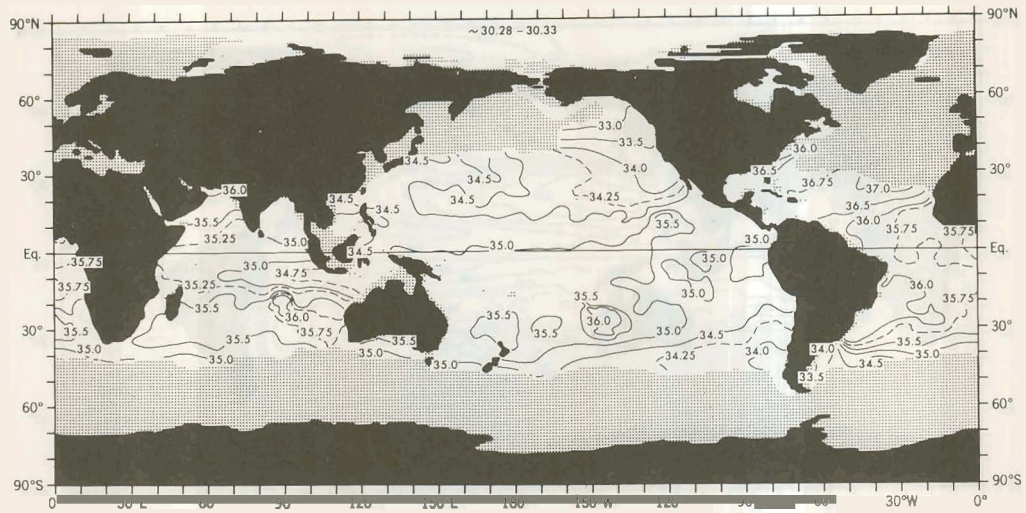


Figure 84.—Salinity (‰) on the Northern Hemisphere winter (February, March, April) 26.0 potential density surface.

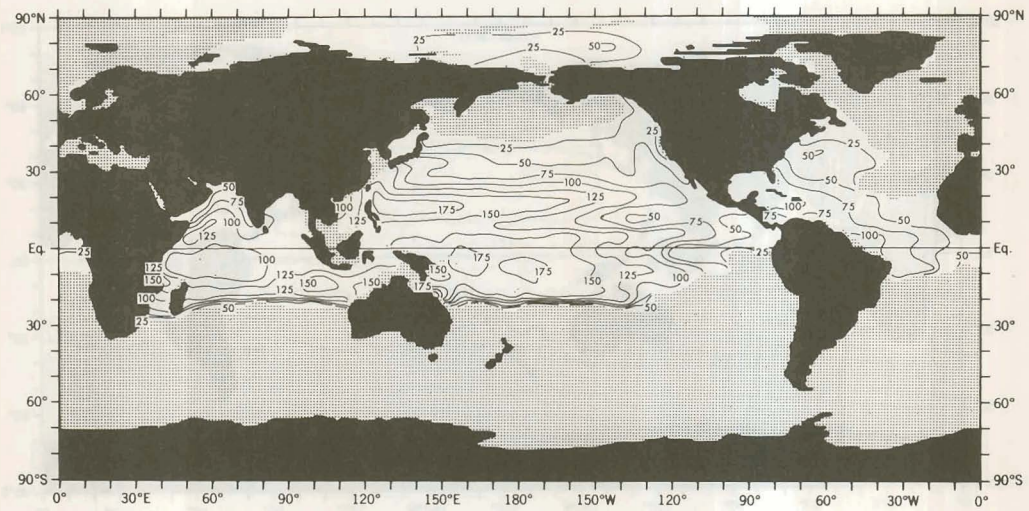


Figure 85.—Northern Hemisphere summer (August, September, October) depth (meters) of the 24.5 potential density surface.

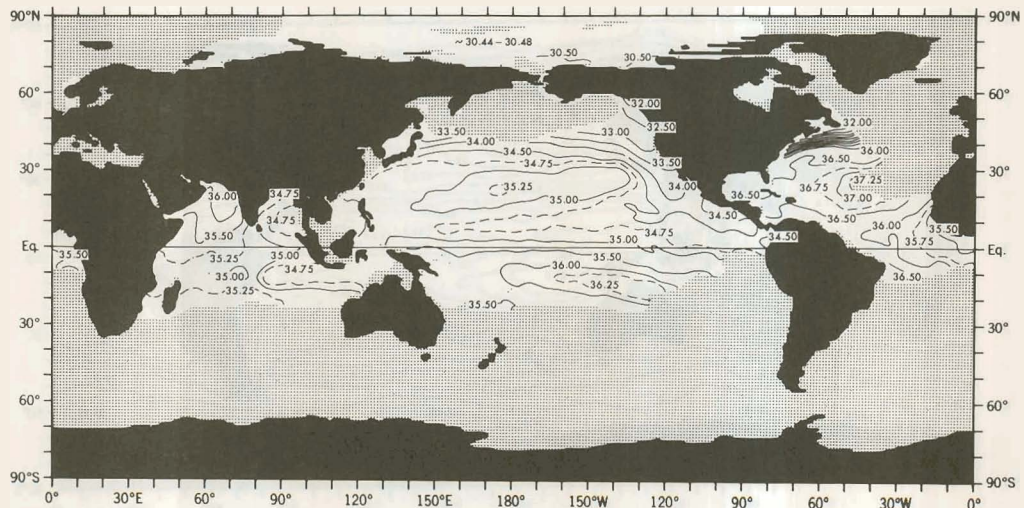


Figure 86.—Salinity (‰) on the Northern Hemisphere summer (August, September, October) 24.5 potential density surface.

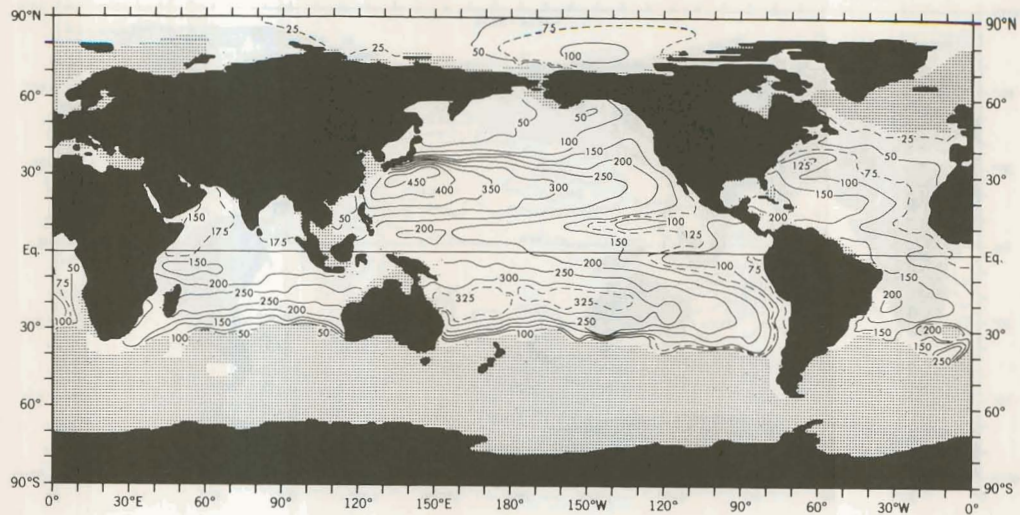


Figure 87.—Northern Hemisphere summer (August, September, October) depth (meters) of the 26.0 potential density surface.

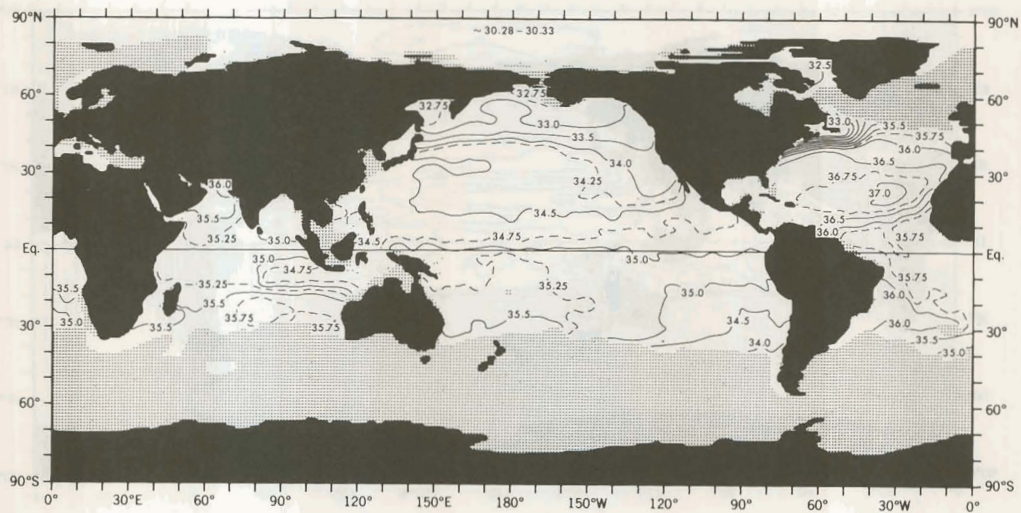


Figure 88.—Salinity (‰) on the Northern Hemisphere summer (August, September, October) 26.0 potential density surface.

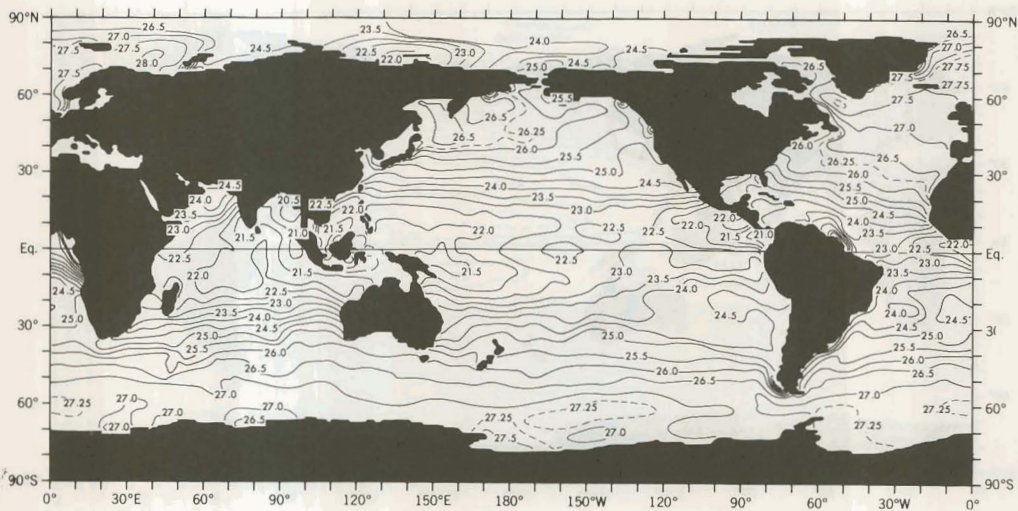


Figure 89.—Northern Hemisphere winter (February, March, April) sea surface density σ_t (10^{-3}g/cm^3).

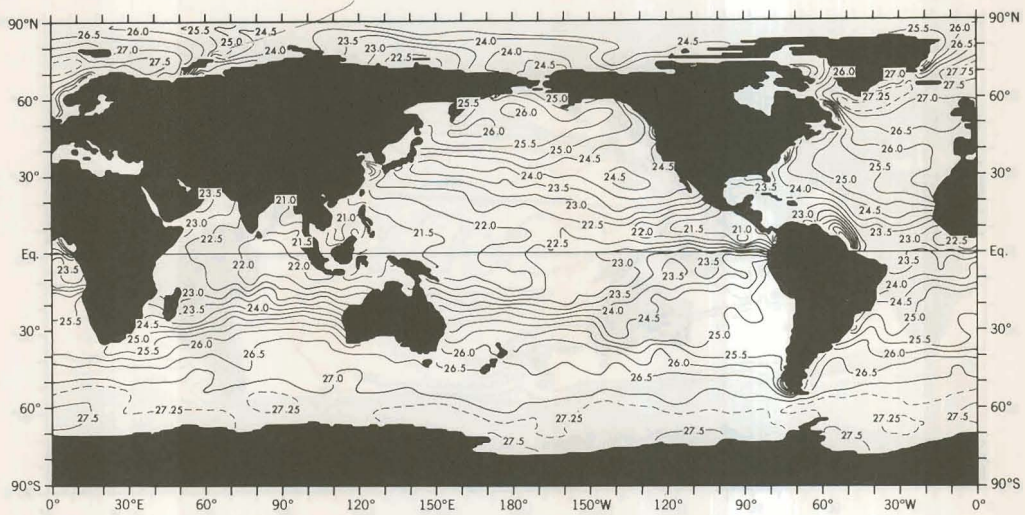


Figure 90.—Northern Hemisphere spring (May, June, July) sea surface density, sigma-t (10^{-3}g/cm^3).

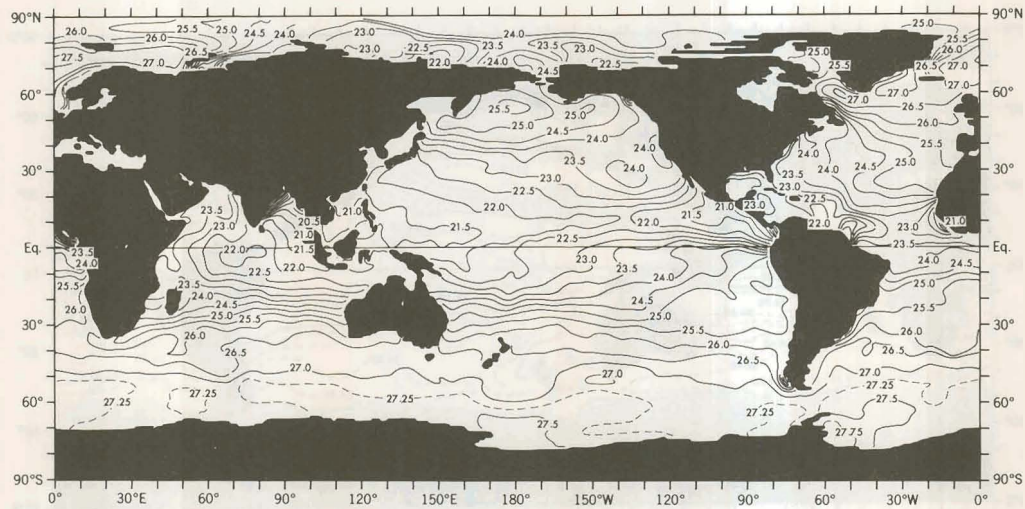


Figure 91.—Northern Hemisphere summer (August, September, October) sea surface density, sigma-t (10^{-3}g/cm^3).

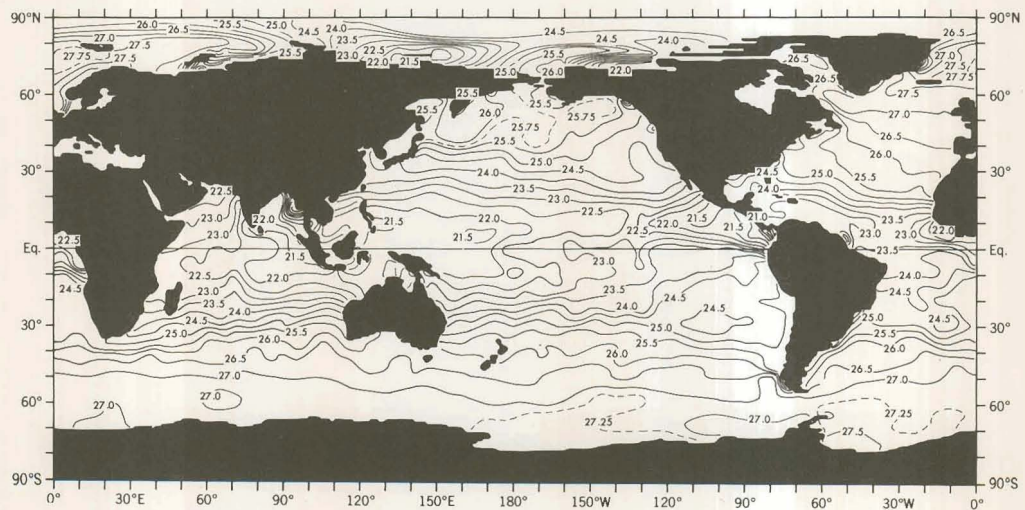


Figure 92.—Northern Hemisphere fall (November, December, January) sea surface density, sigma-t (10^{-3}g/cm^3).

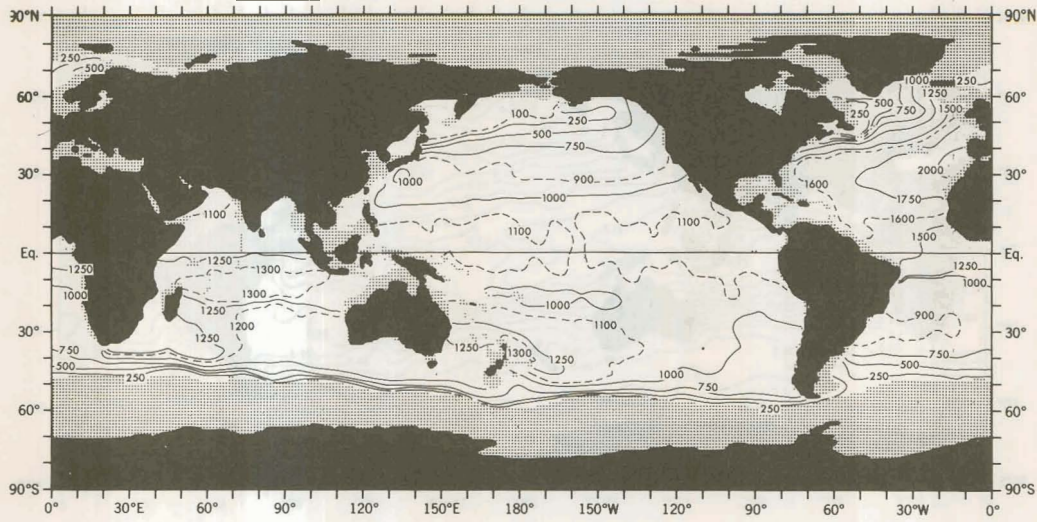


Figure 93.—Annual mean depth (meters) of the 4°C potential temperature surface.

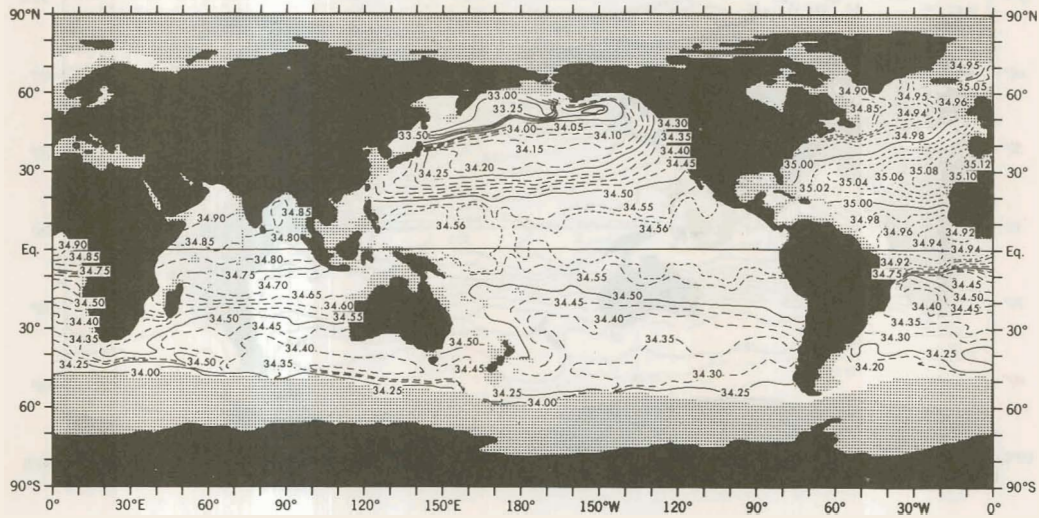


Figure 94.—Salinity (‰) on the annual mean 4°C potential temperature surface.

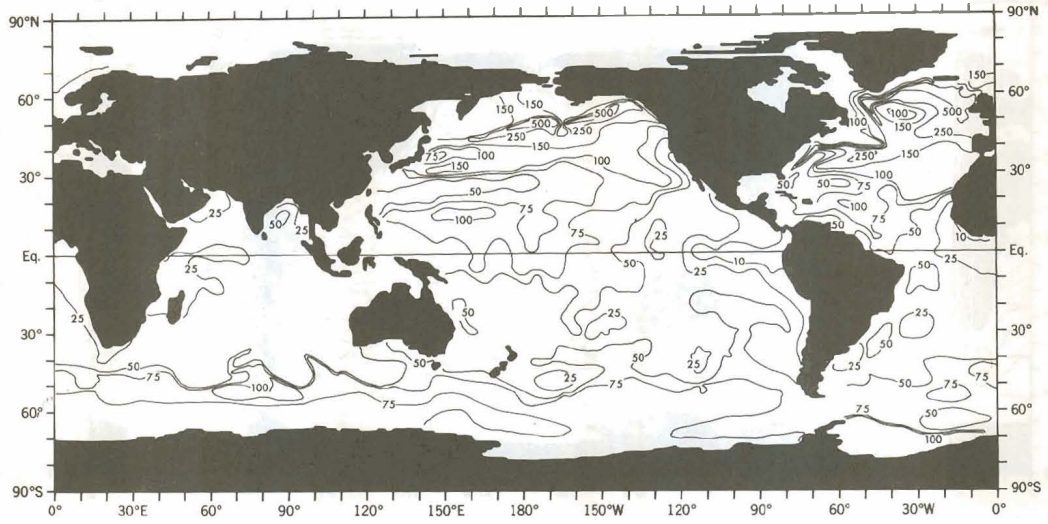


Figure 95a.—March mixed-layer depths based on a temperature criterion of 0.5°C.

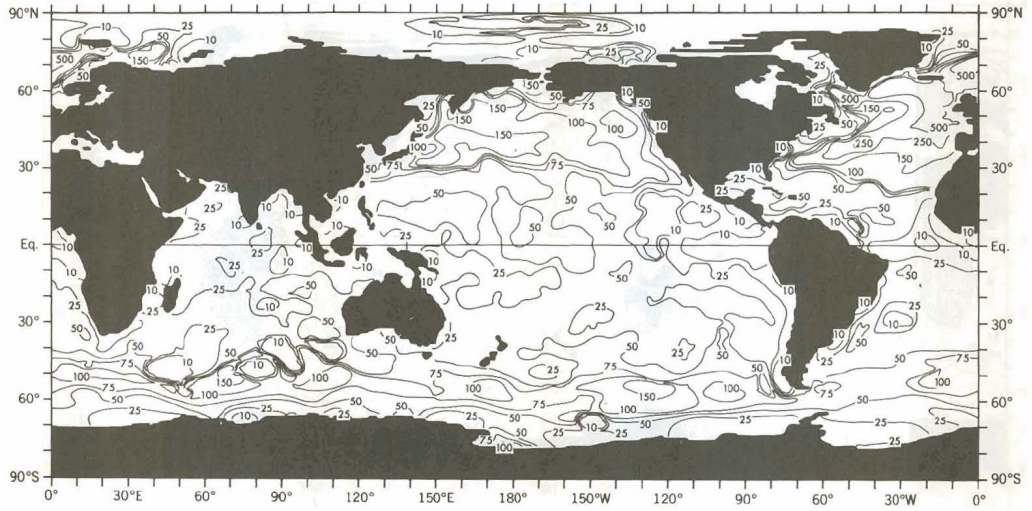


Figure 95b.—March mixed-layer depths based on a sigma-t criterion of 0.125.

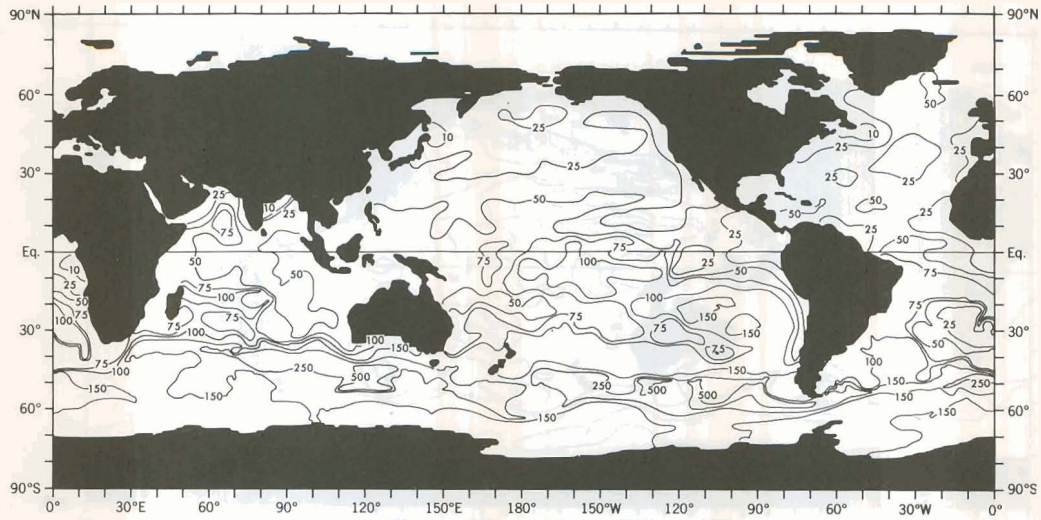


Figure 96a.—September mixed-layer depths based on a temperature criterion of 0.5°C.

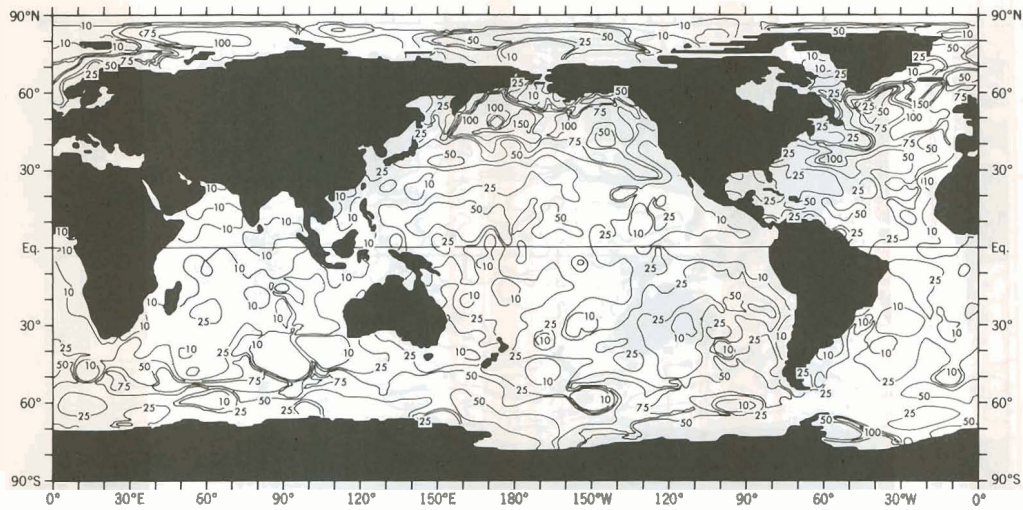


Figure 96b.—September mixed-layer depths based on a sigma-t criterion of 0.125.

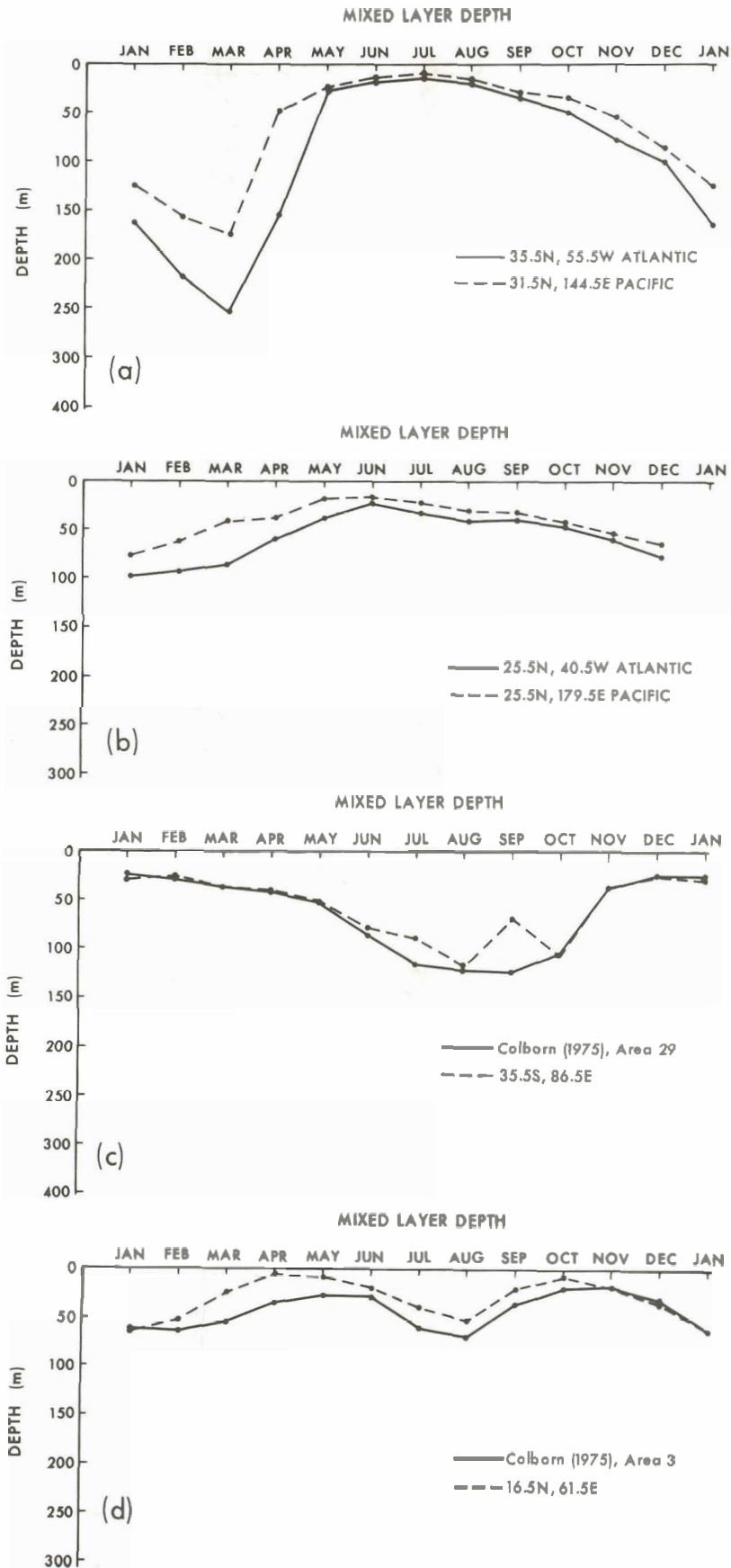


Figure 97.—Annual cycle of mixed-layer depths based on temperature for selected regions in the world ocean.

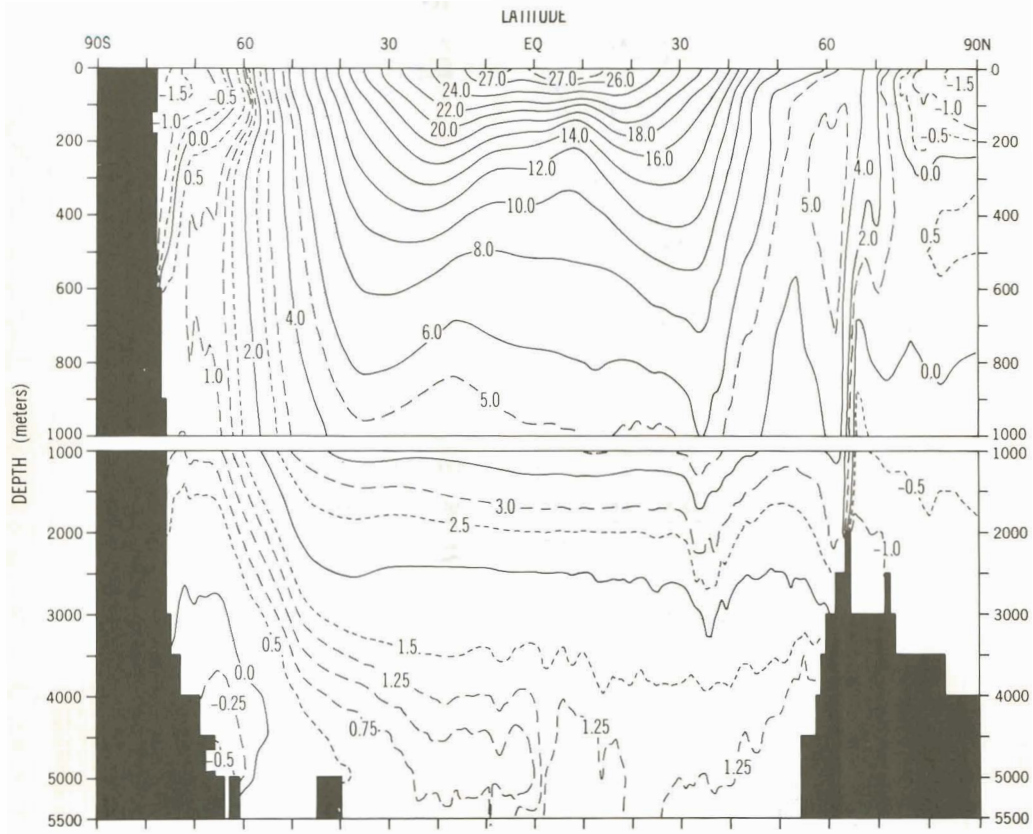


Figure 98.—Annual mean global zonal average (by one-degree squares) of potential temperature ($^{\circ}\text{C}$).

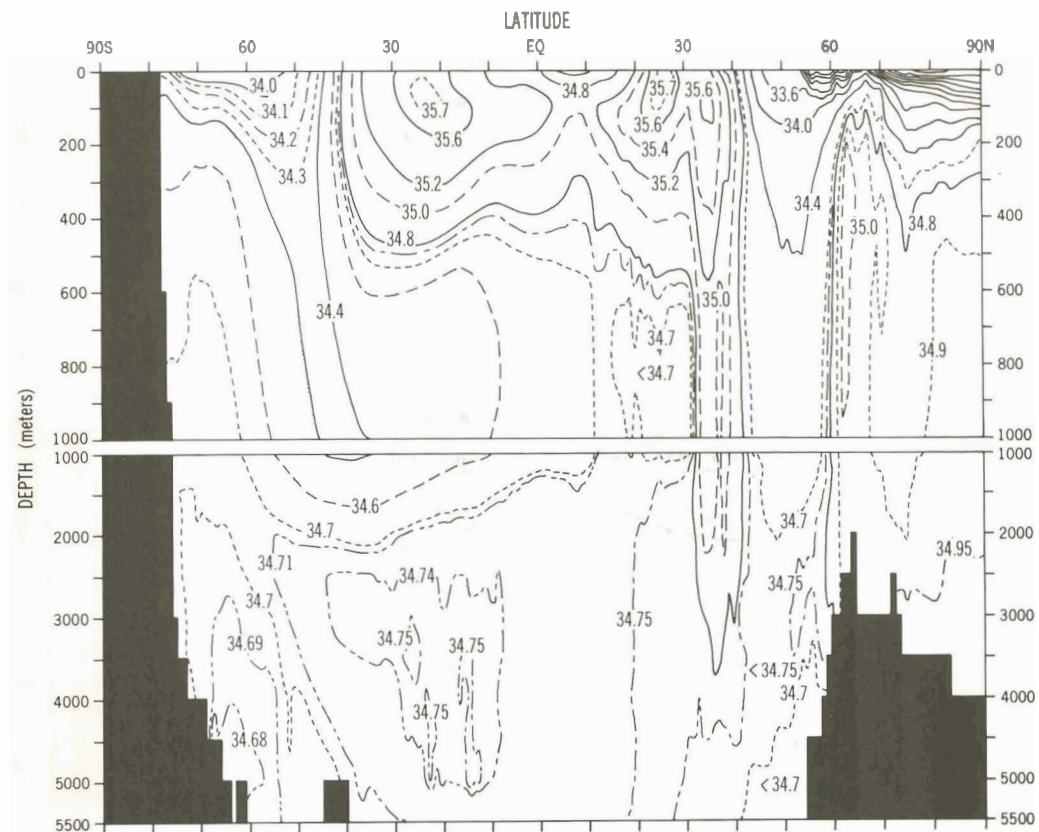


Figure 99.—Annual mean global zonal average (by one-degree squares) of salinity (‰).

Sydney Levitus

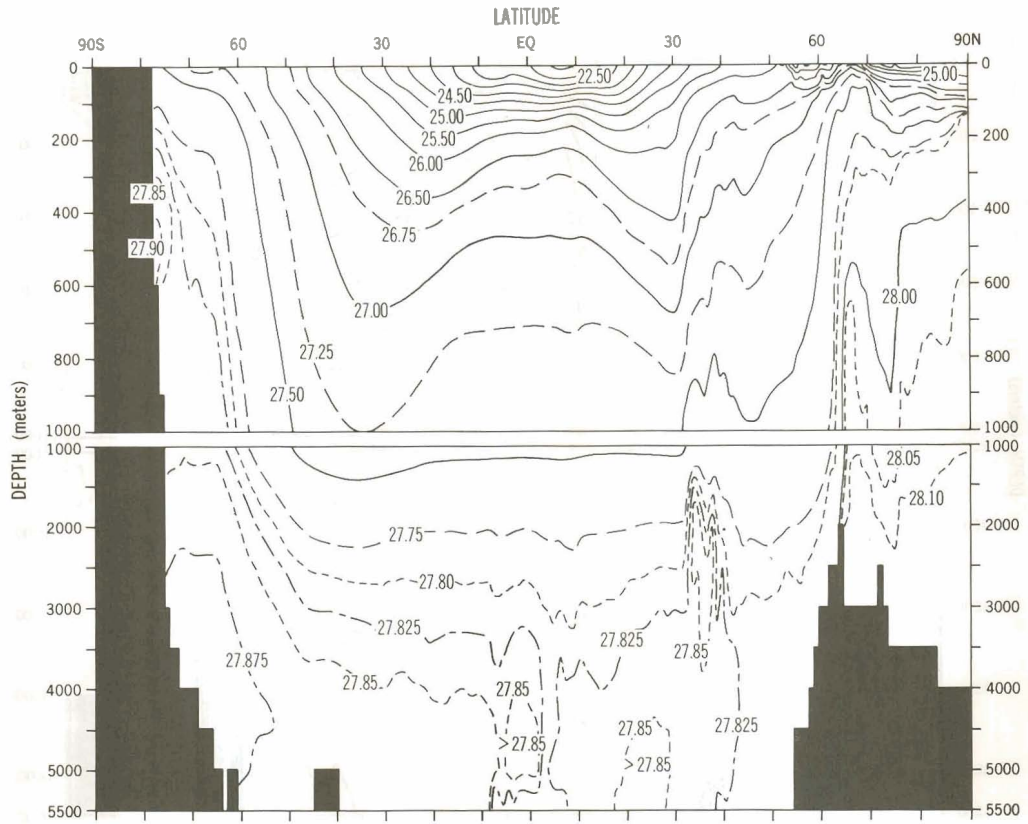


Figure 100.—Annual mean global zonal average (by one-degree squares) of potential density (10^{-3}g/cm^3).

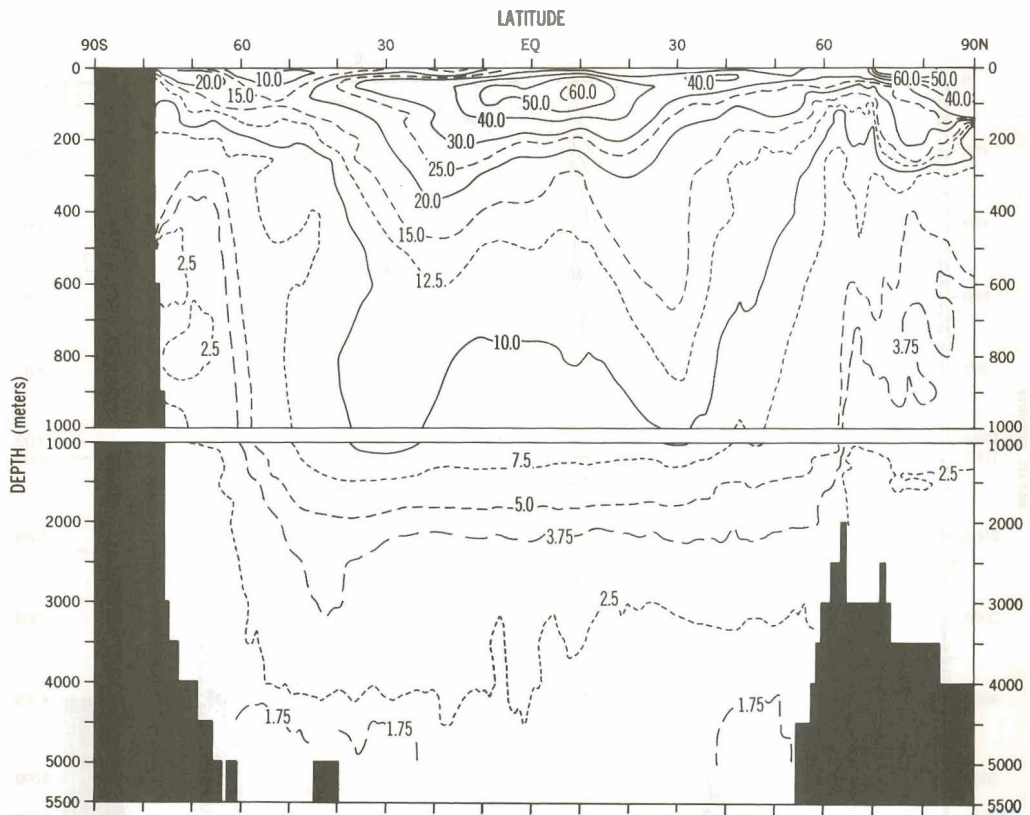


Figure 101.—Annual mean global zonal average (by one-degree squares) of Brunt-Väisälä frequency (cycles/hr).

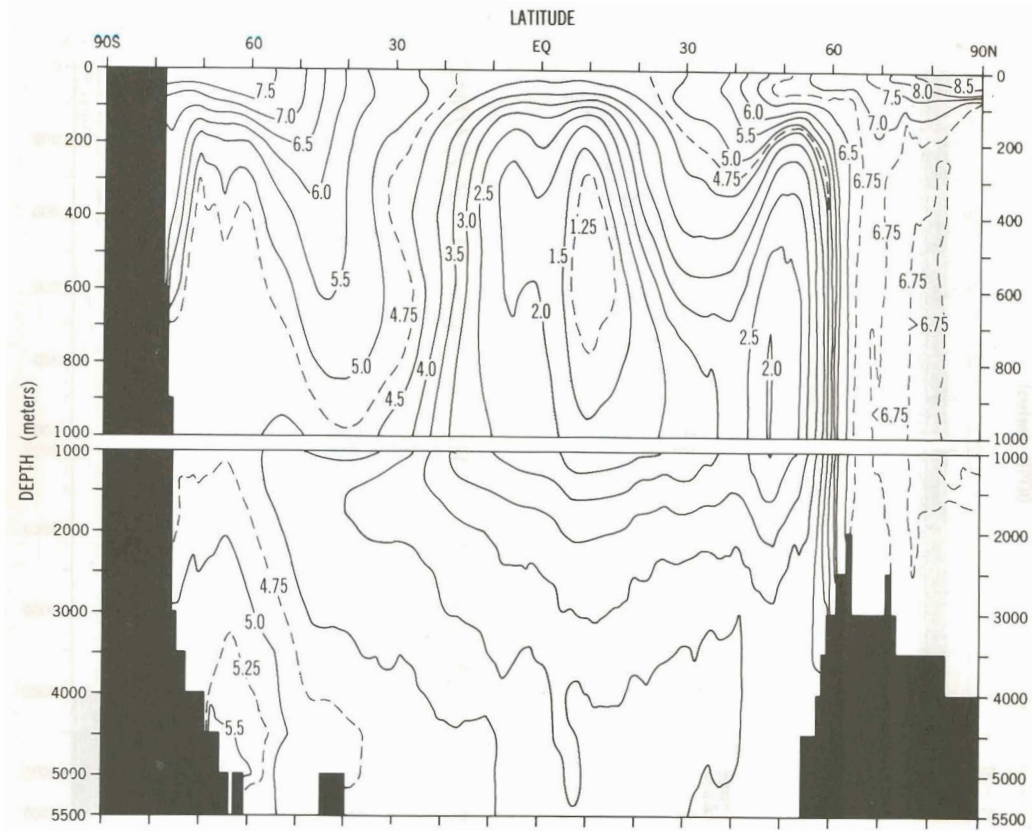


Figure 102.—Annual mean global zonal average (by one-degree squares) of oxygen (ml/l).

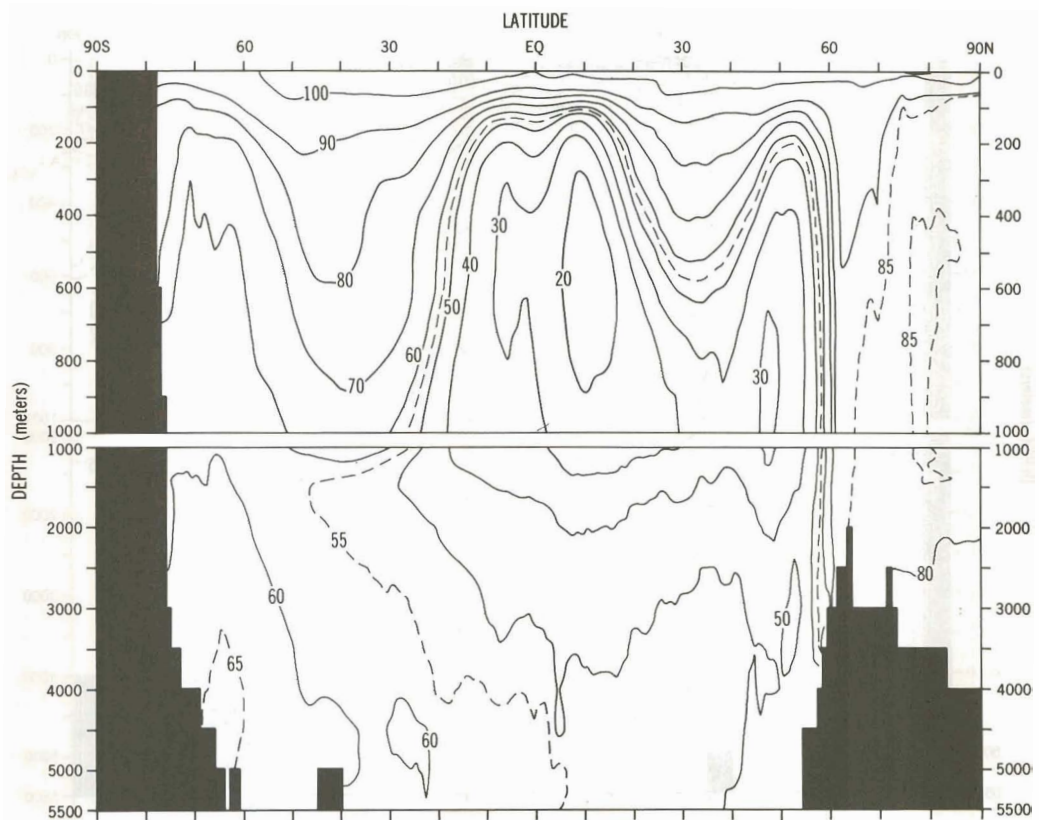


Figure 103.—Annual mean global zonal average (by one-degree squares) of oxygen-saturation (%).

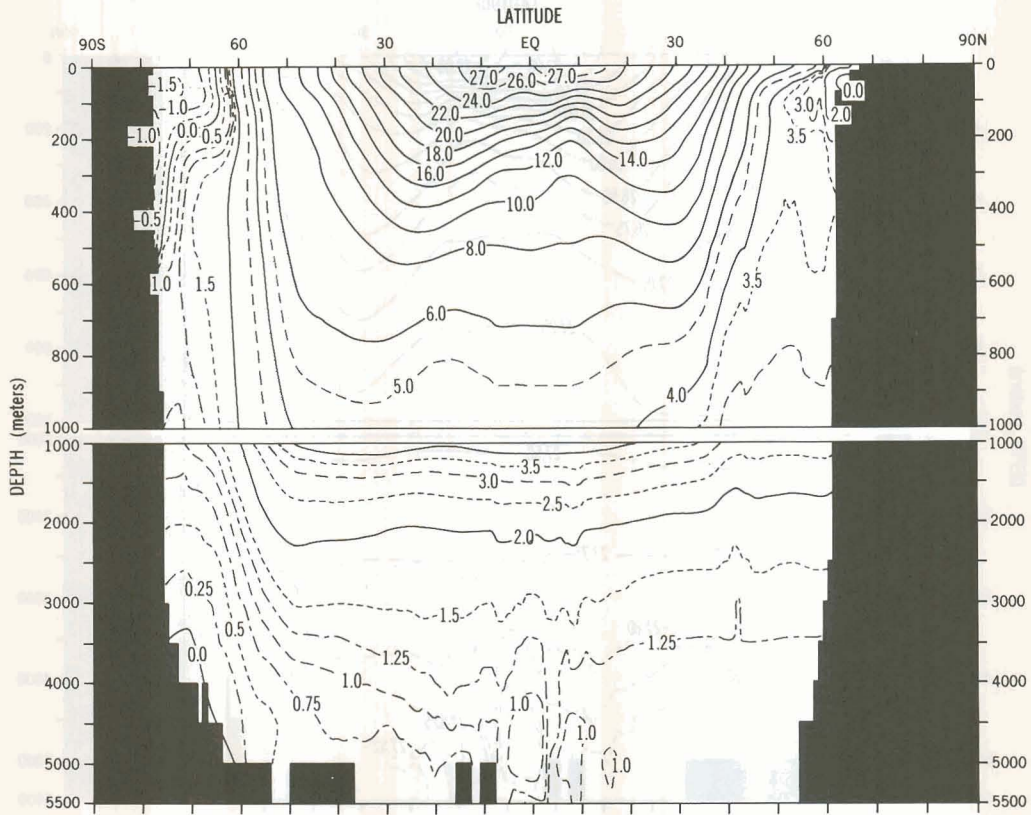


Figure 104.—Annual mean Pacific zonal average (by one-degree squares) of potential temperature ($^{\circ}\text{C}$).

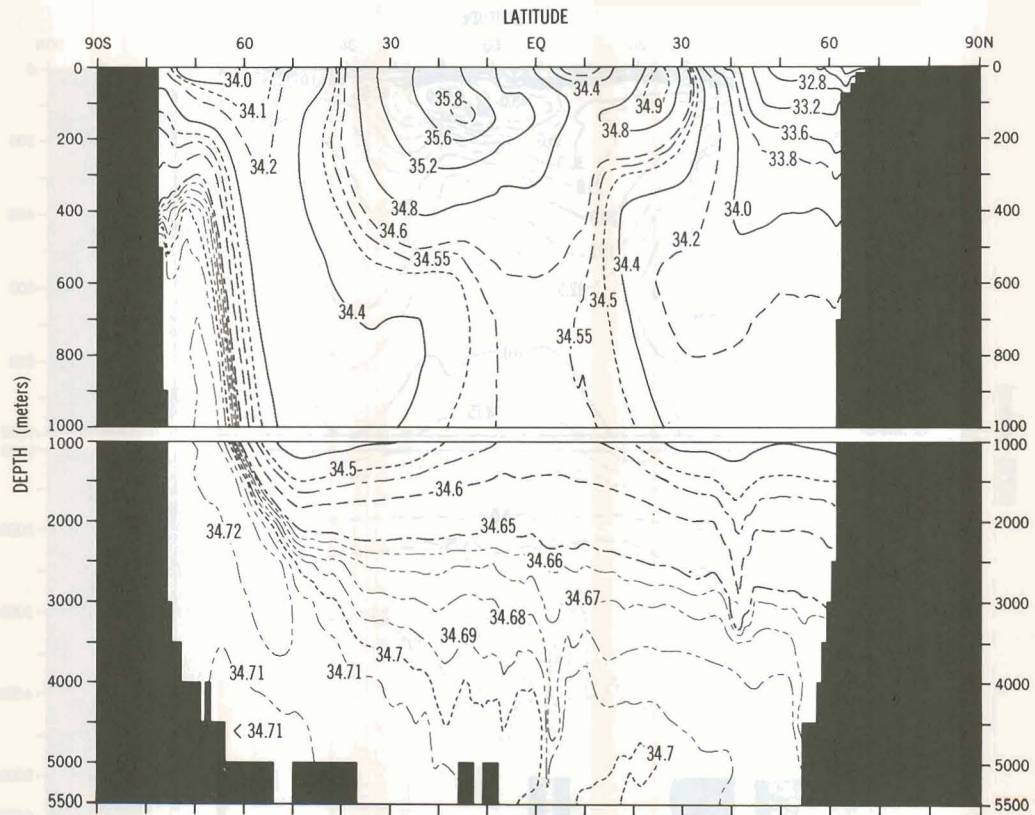


Figure 105.—Annual mean Pacific zonal average (by one-degree squares) of salinity (‰).

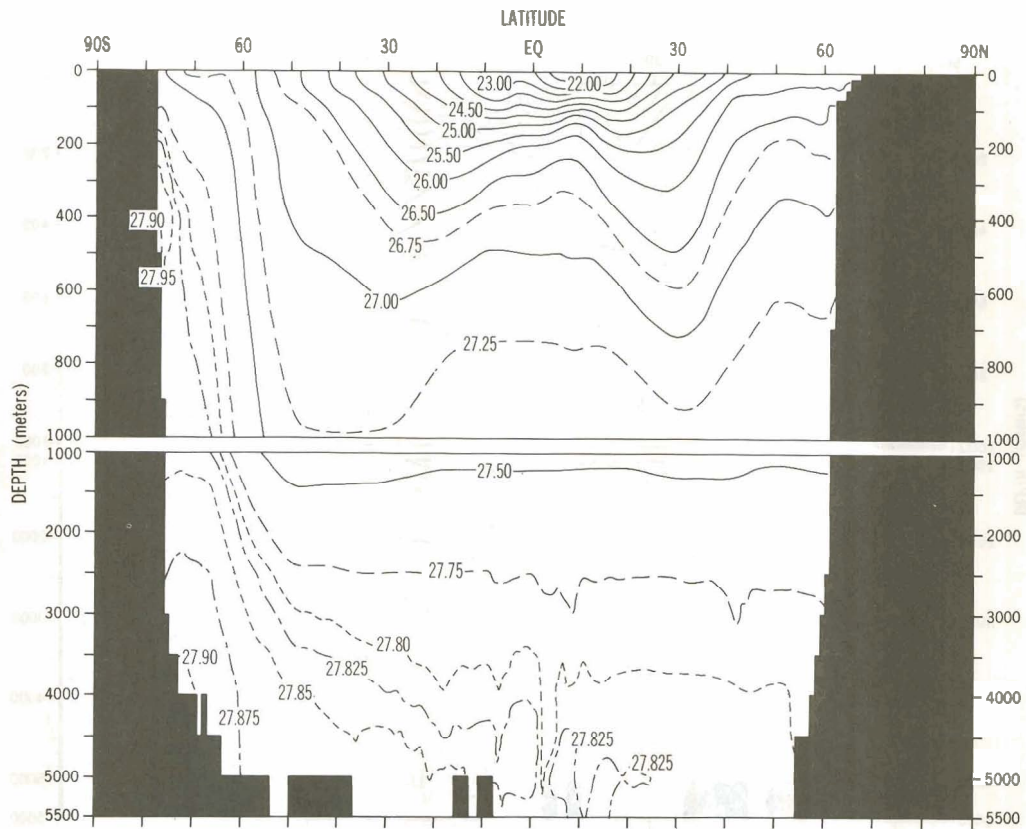


Figure 106.—Annual mean Pacific zonal average (by one-degree squares) of potential density (10^{-3}g/cm^3).

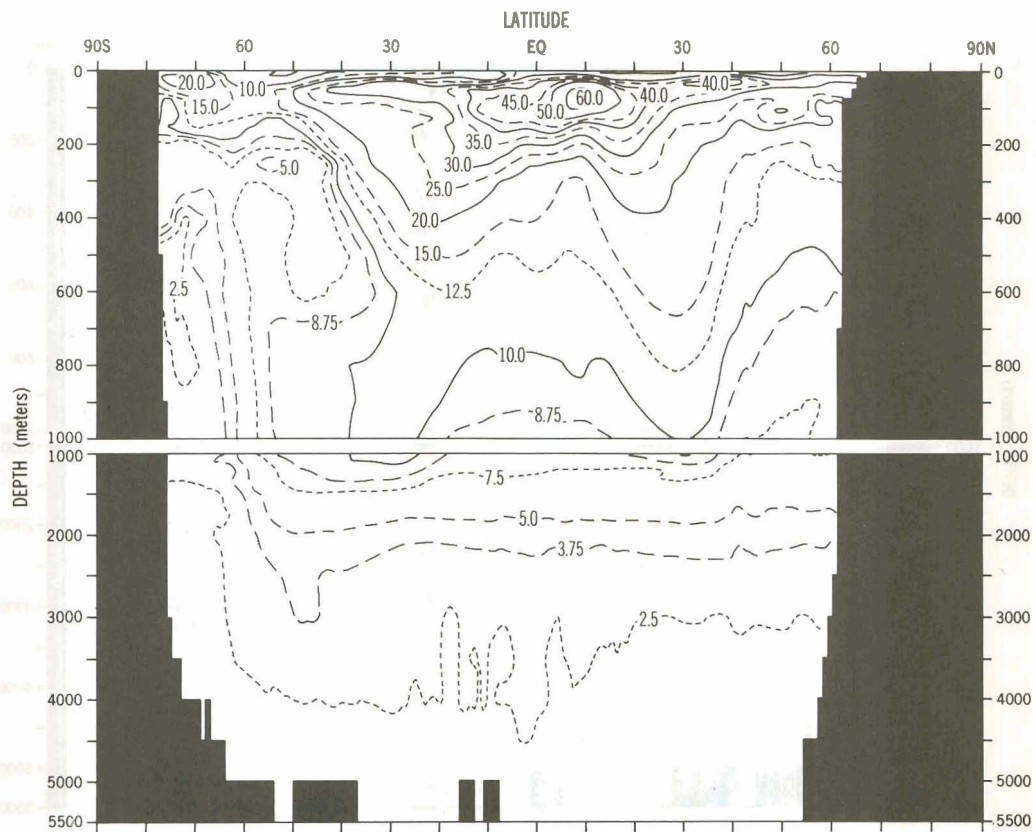


Figure 107.—Annual mean Pacific zonal average (by one-degree squares) of Brunt-Väisälä frequency (cycles/hr).

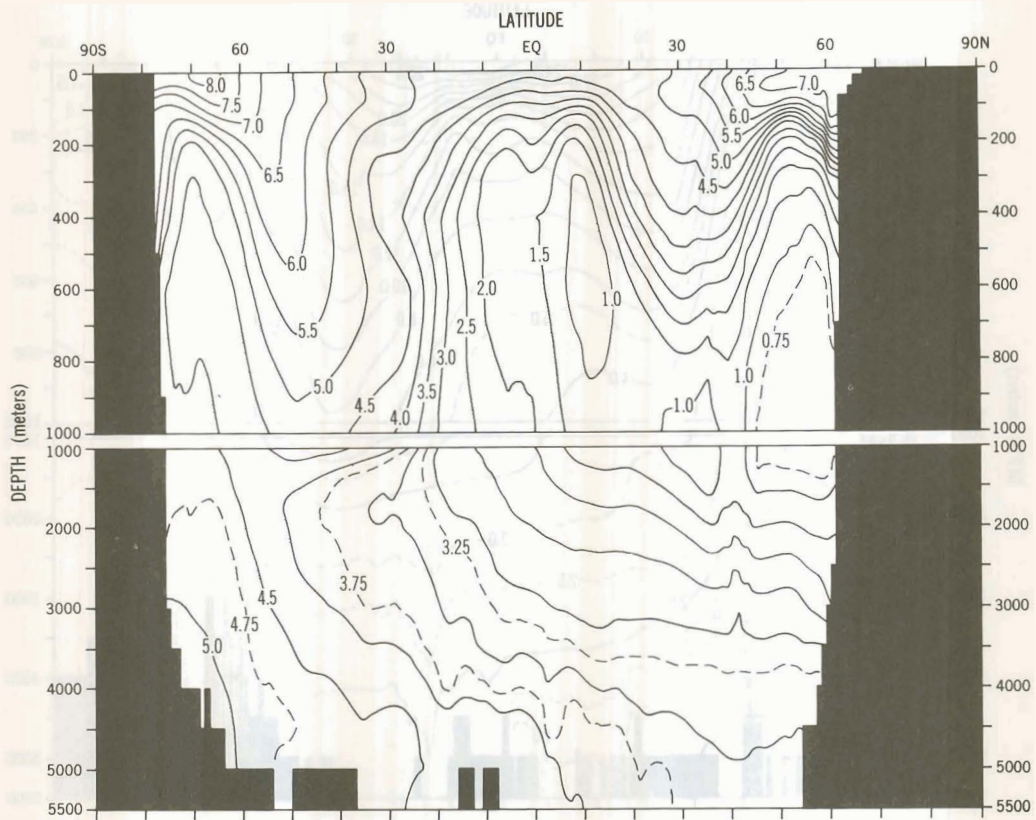


Figure 108.—Annual mean Pacific zonal average (by one-degree squares) of oxygen (ml/l).

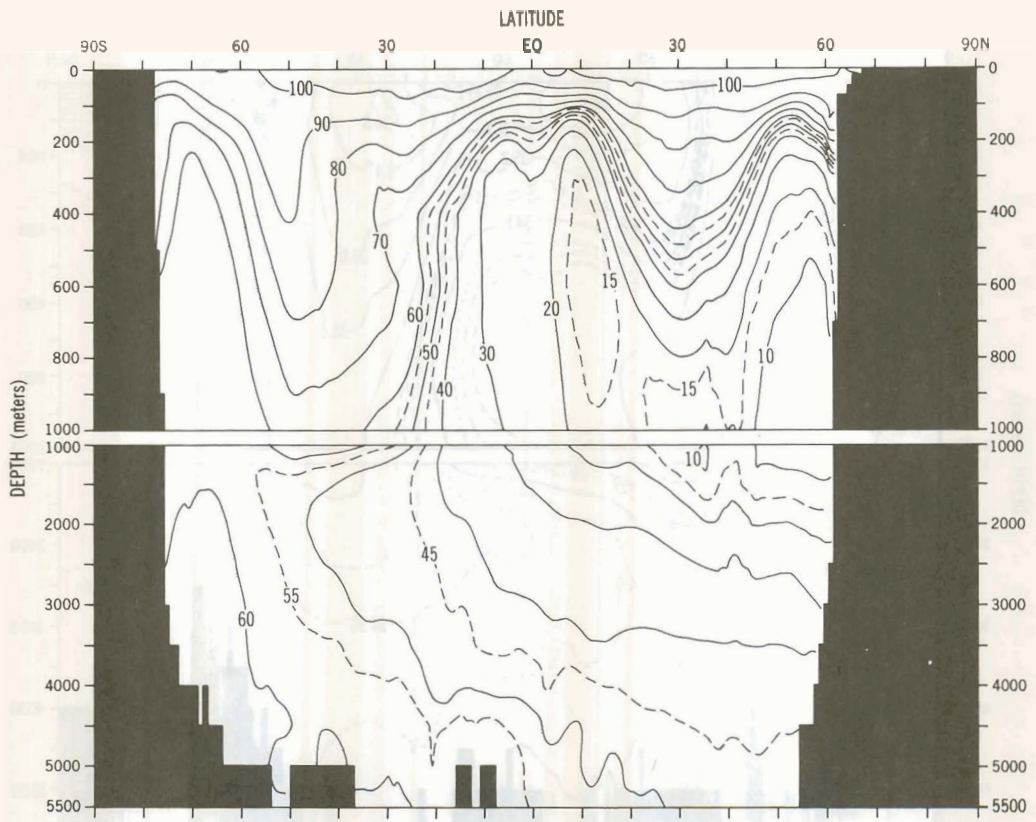


Figure 109.—Annual mean Pacific zonal average (by one-degree squares) of oxygen-saturation (%).

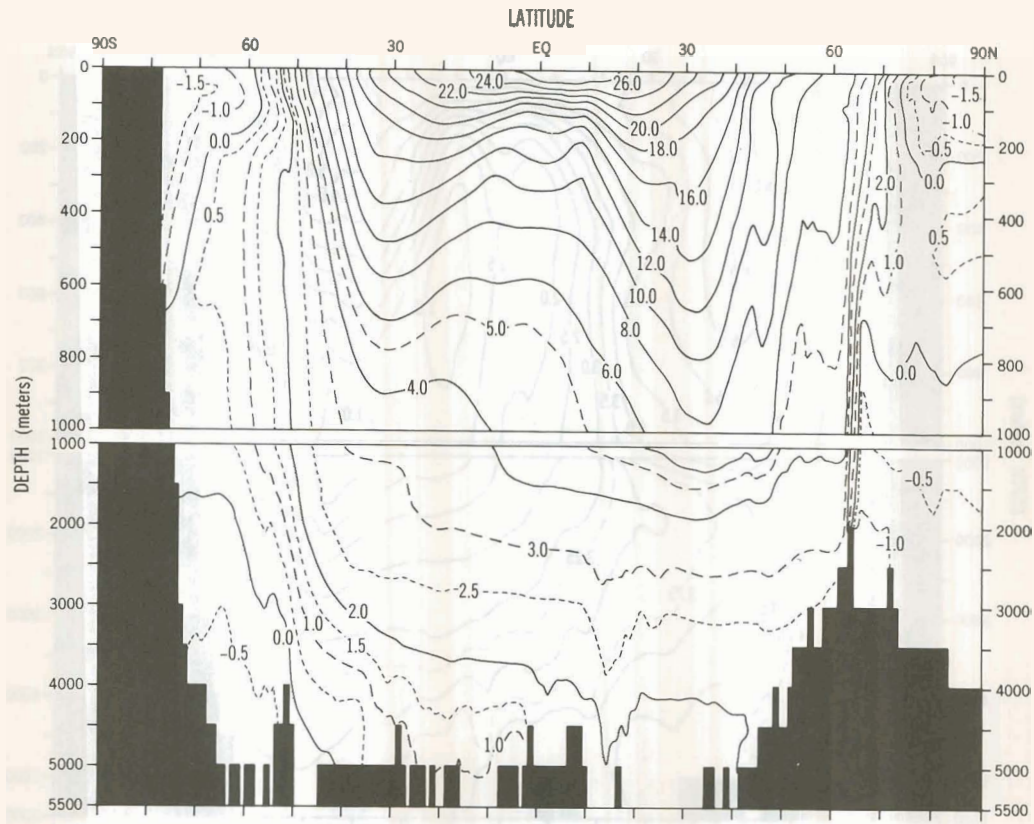


Figure 110.—Annual mean Atlantic zonal average (by one-degree squares) of potential temperature (°C).

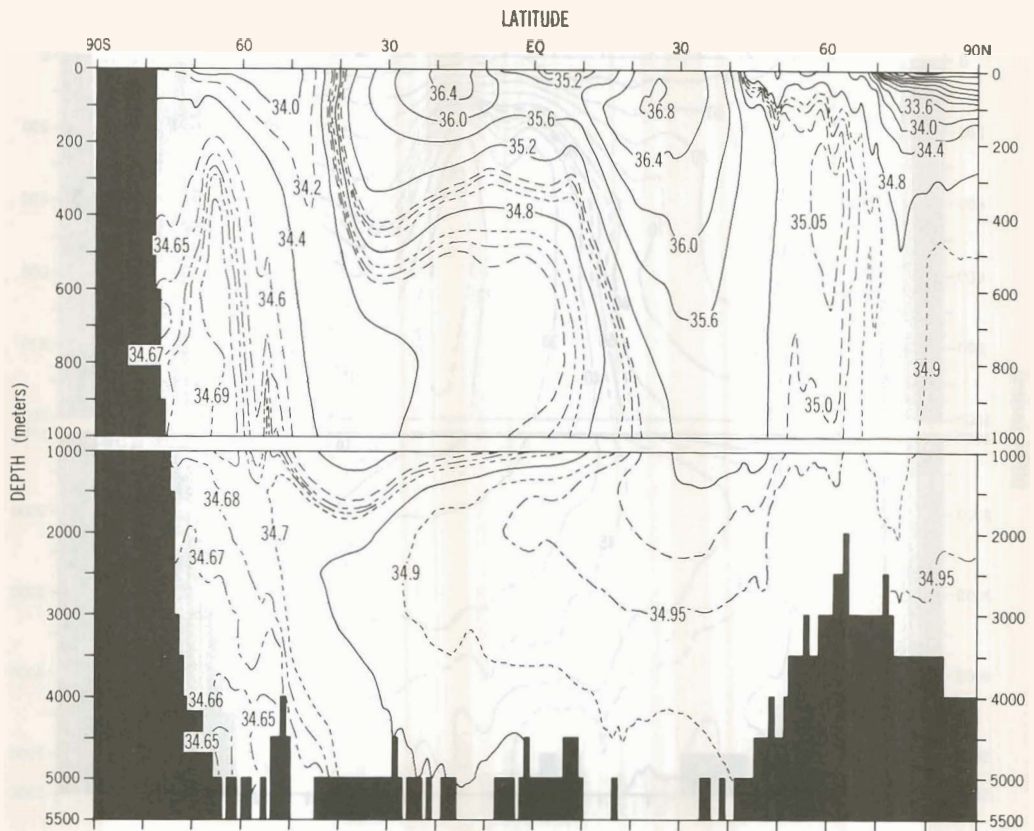


Figure 111.—Annual mean Atlantic zonal average (by one-degree squares) of salinity (‰)

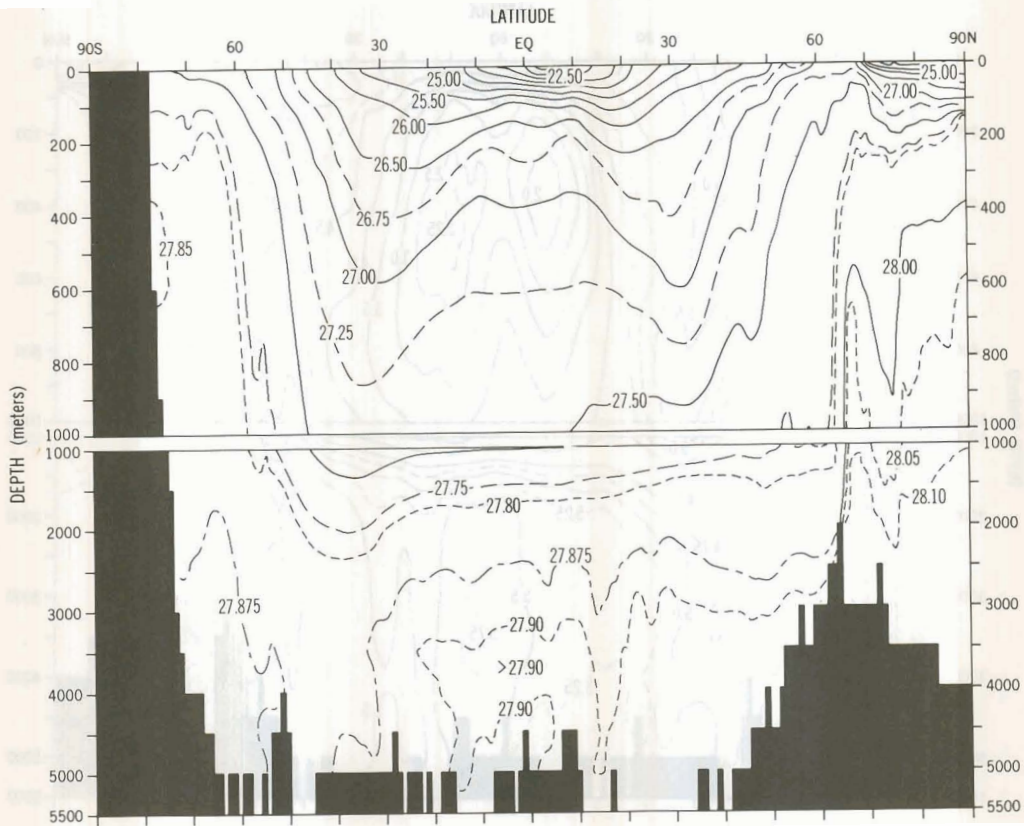


Figure 112.—Annual mean Atlantic zonal average (by one-degree squares) of potential density (10^{-3}g/cm^3).

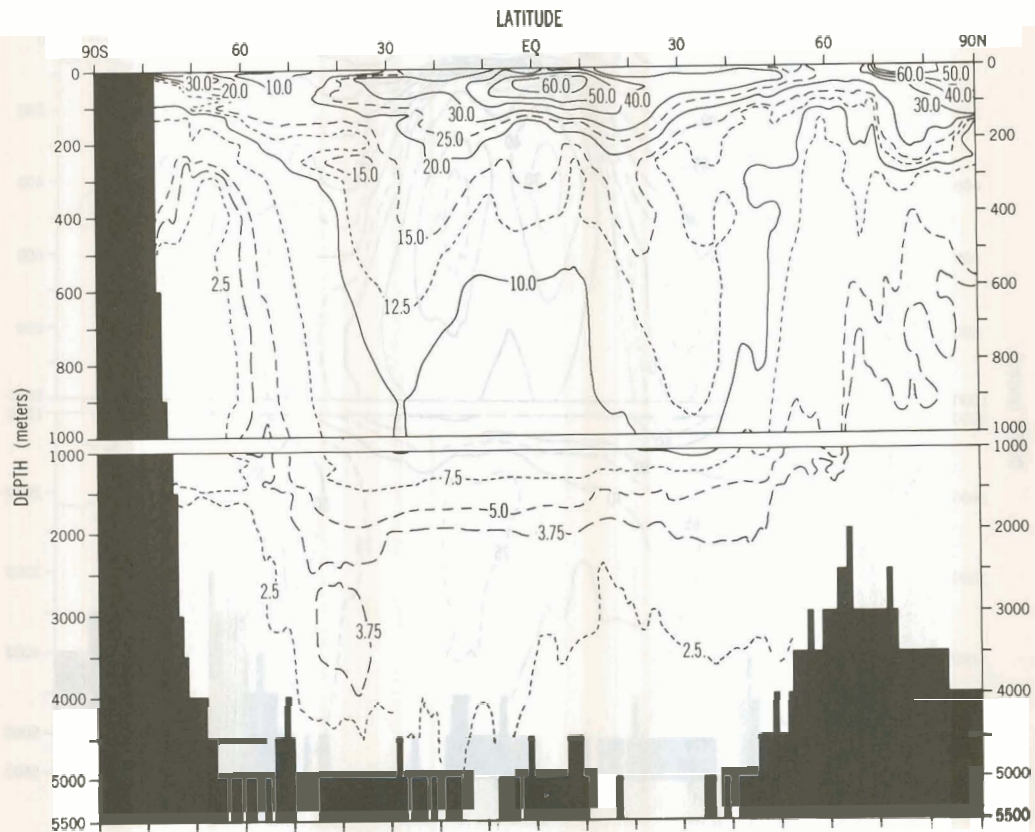


Figure 113.—Annual mean Atlantic zonal average (by one-degree squares) of Brunt-Väisälä frequency (cycles/hr).

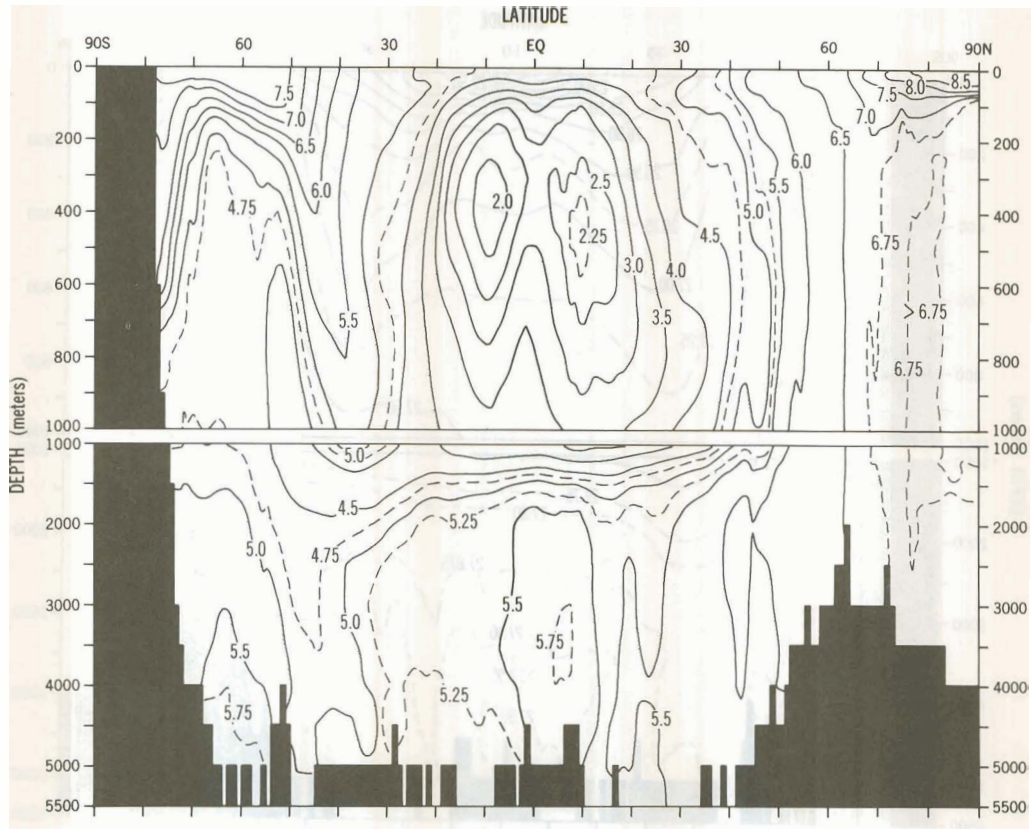


Figure 114.—Annual mean Atlantic zonal average (by one-degree squares) of oxygen (ml/l).

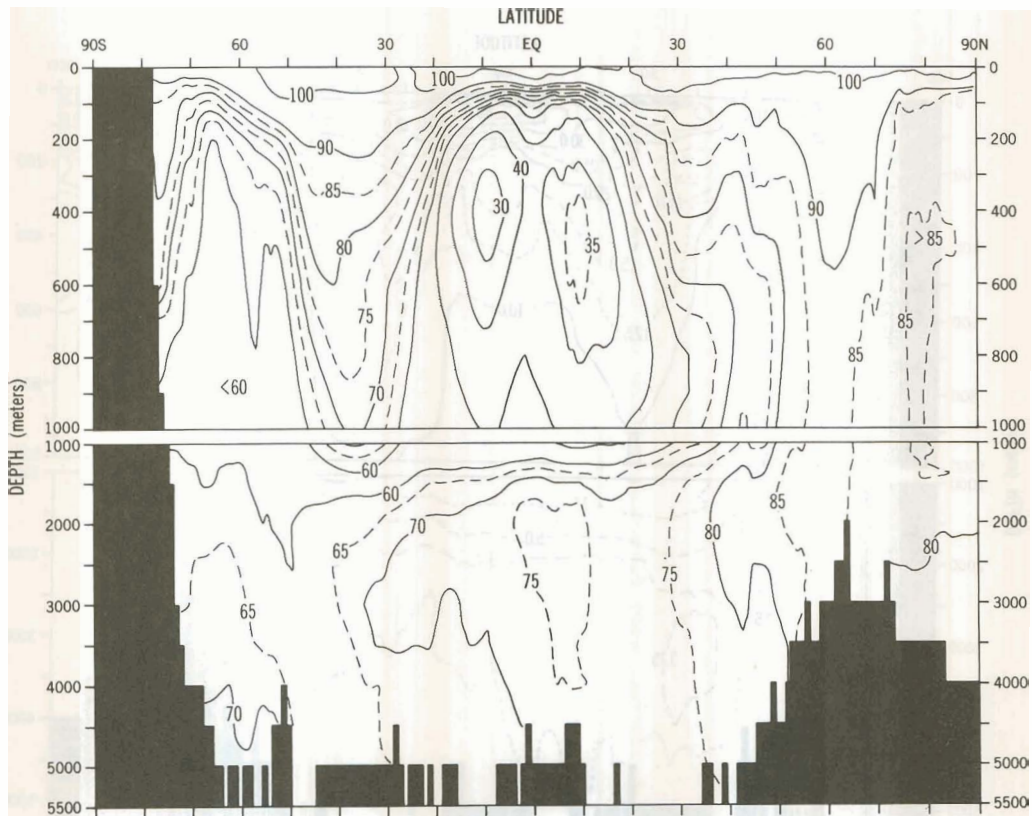


Figure 115.—Annual mean Atlantic zonal average (by one-degree squares) of oxygen-saturation (%).

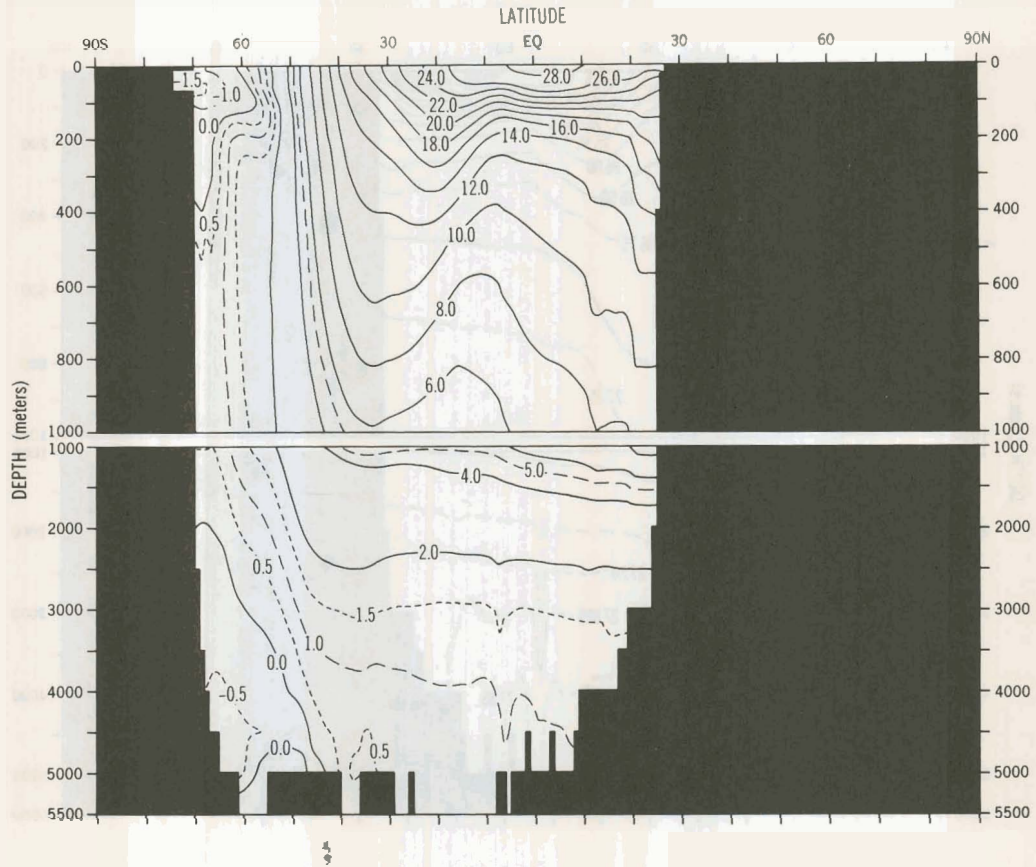


Figure 116.—Annual mean Indian zonal average (by one-degree squares) of potential temperature ($^{\circ}\text{C}$).

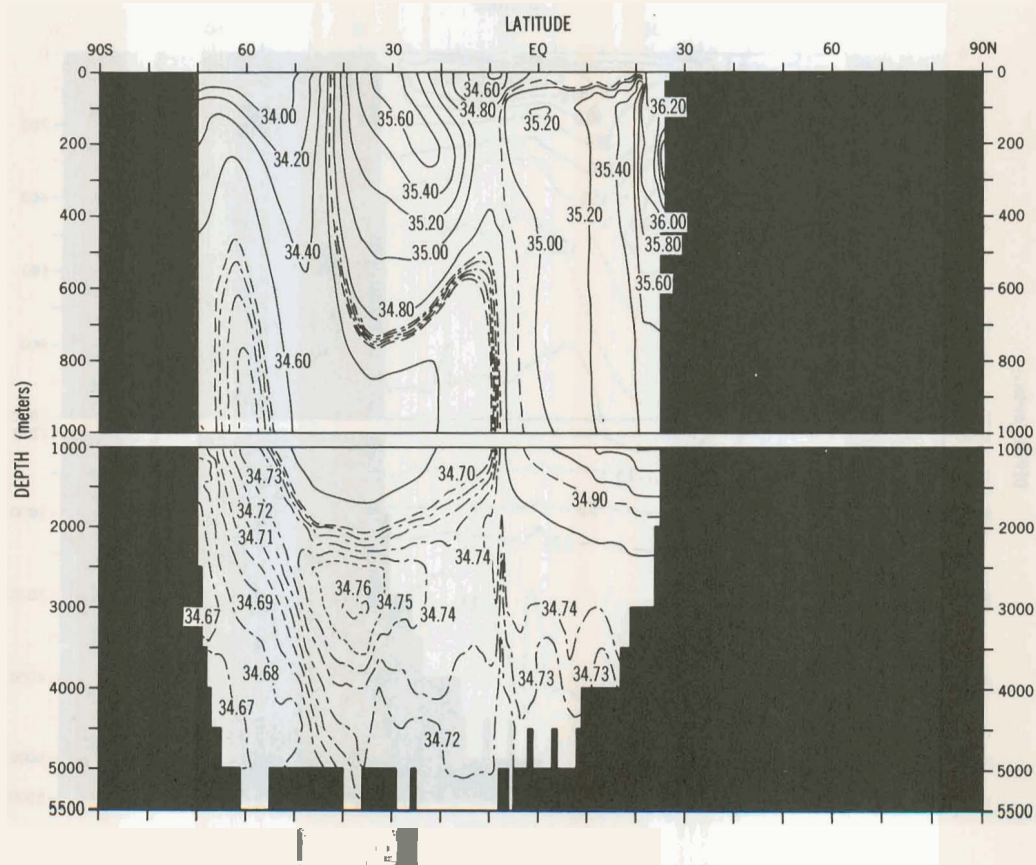


Figure 117.—Annual mean Indian zonal average (by one-degree squares) of salinity (‰).

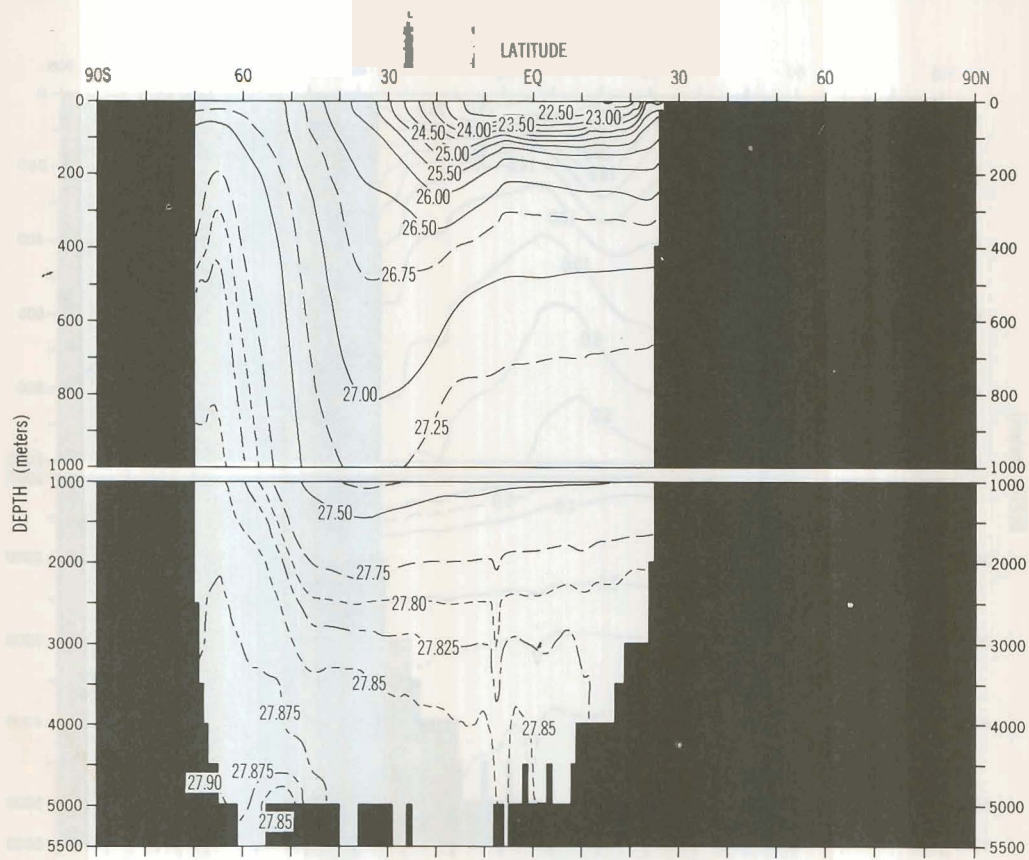


Figure 118.—Annual mean Indian zonal average (by one-degree squares) of potential density (10^{-3}g/cm^3).

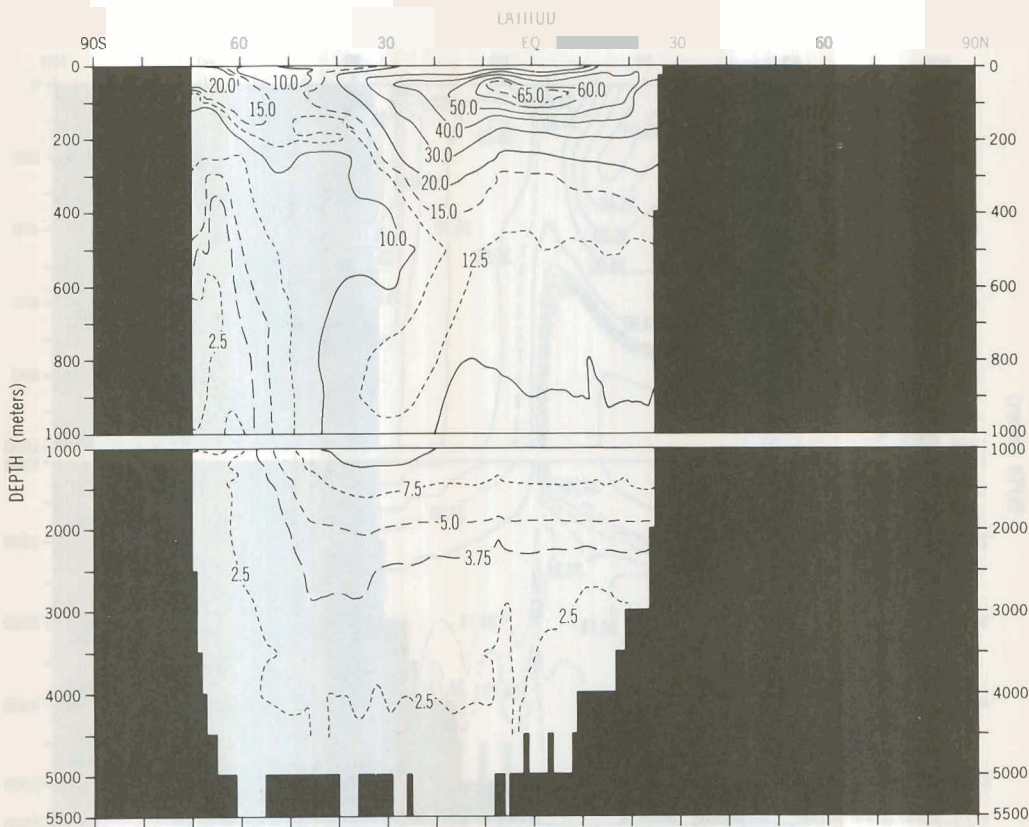


Figure 119.—Annual mean Indian zonal average (by one-degree squares) of Brunt-Vaisala frequency (cycles/hr).

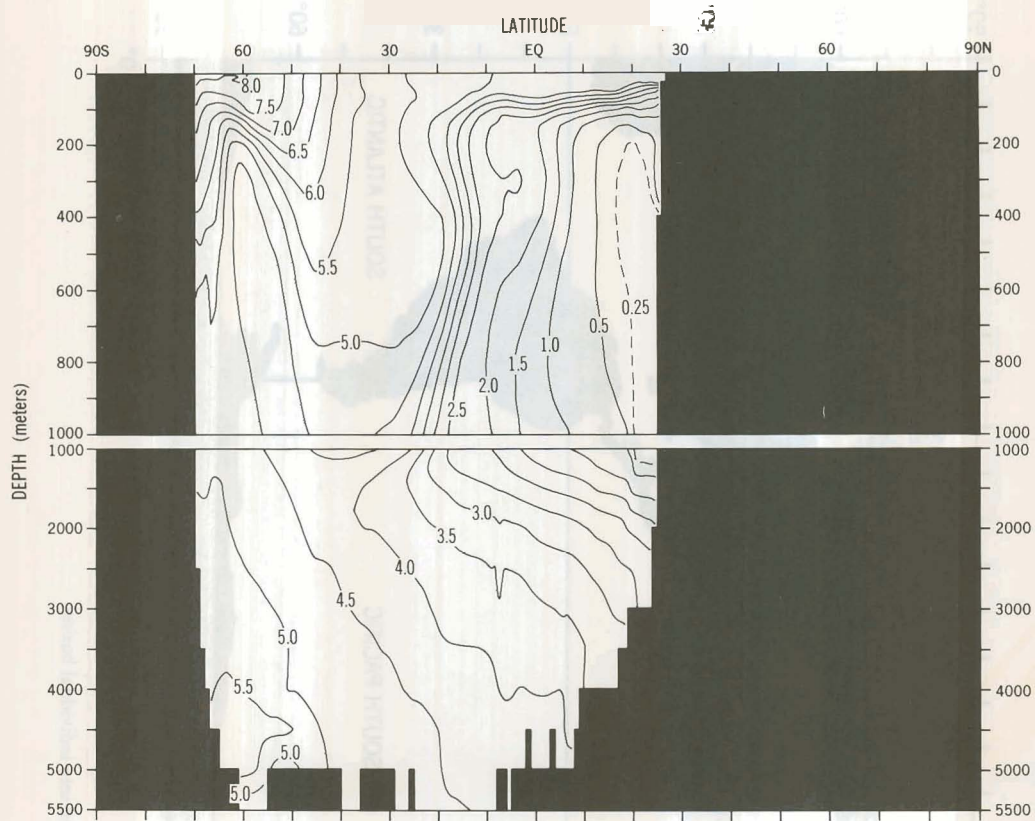


Figure 120.—Annual mean Indian zonal average (by one-degree squares) of oxygen (ml/l).

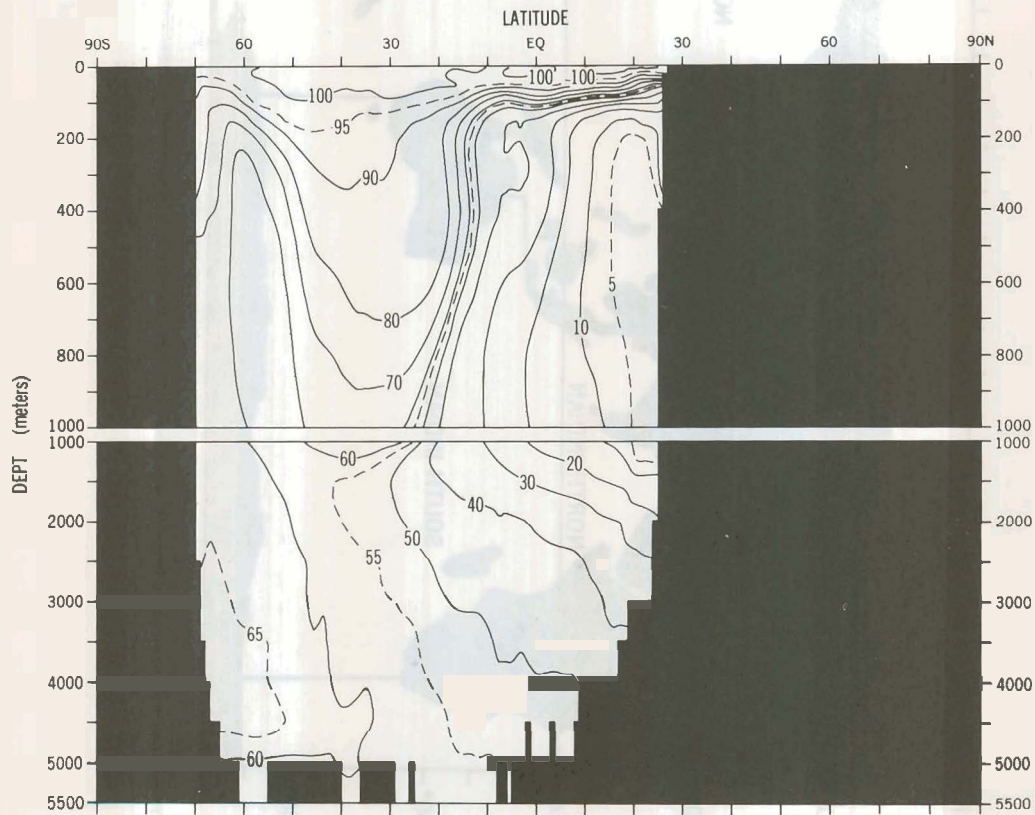


Figure 121.—Annual mean Indian zonal average (by one-degree squares) of salinity (‰).

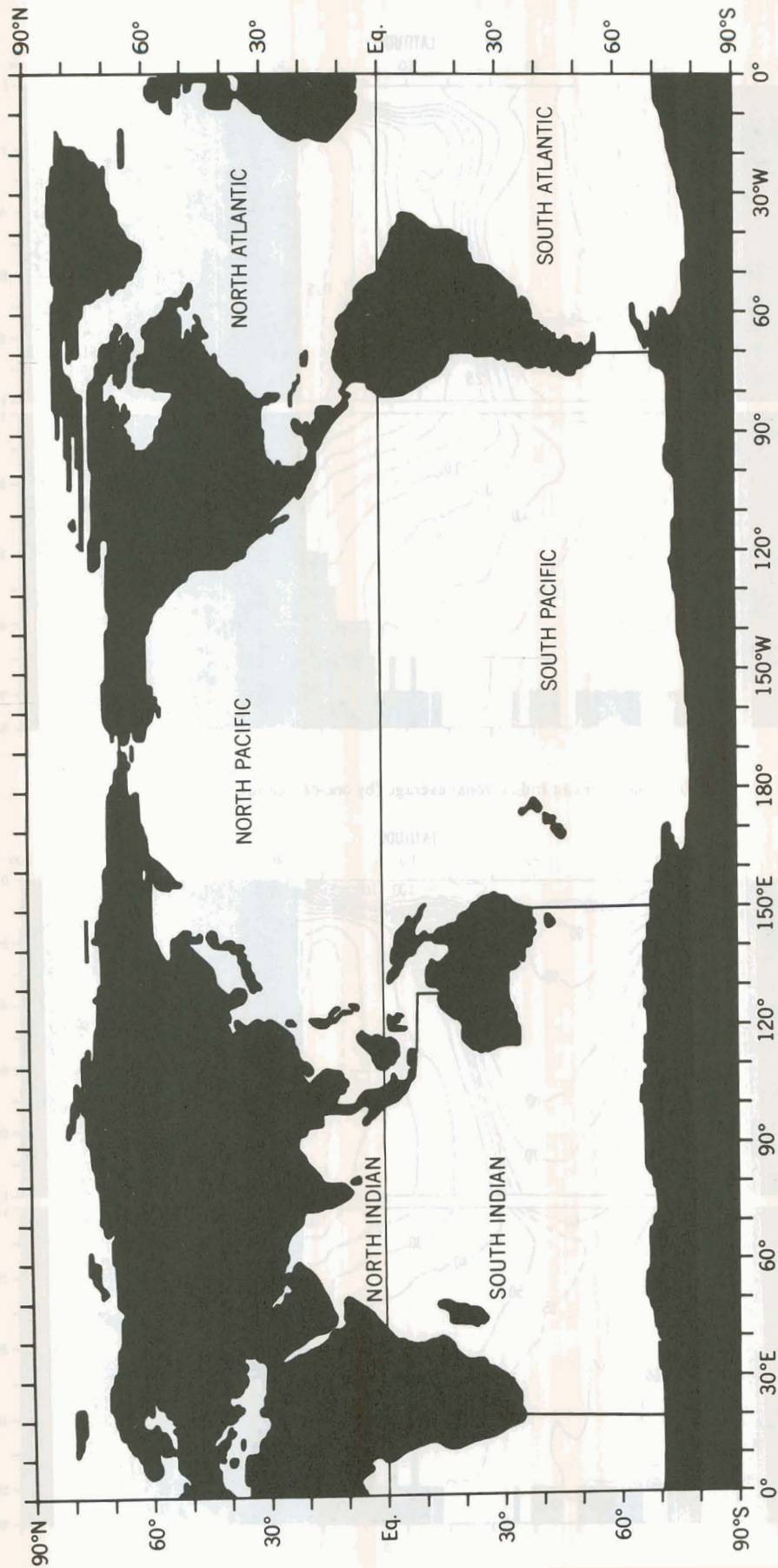


Figure 122.—Division of world ocean into individual basins.

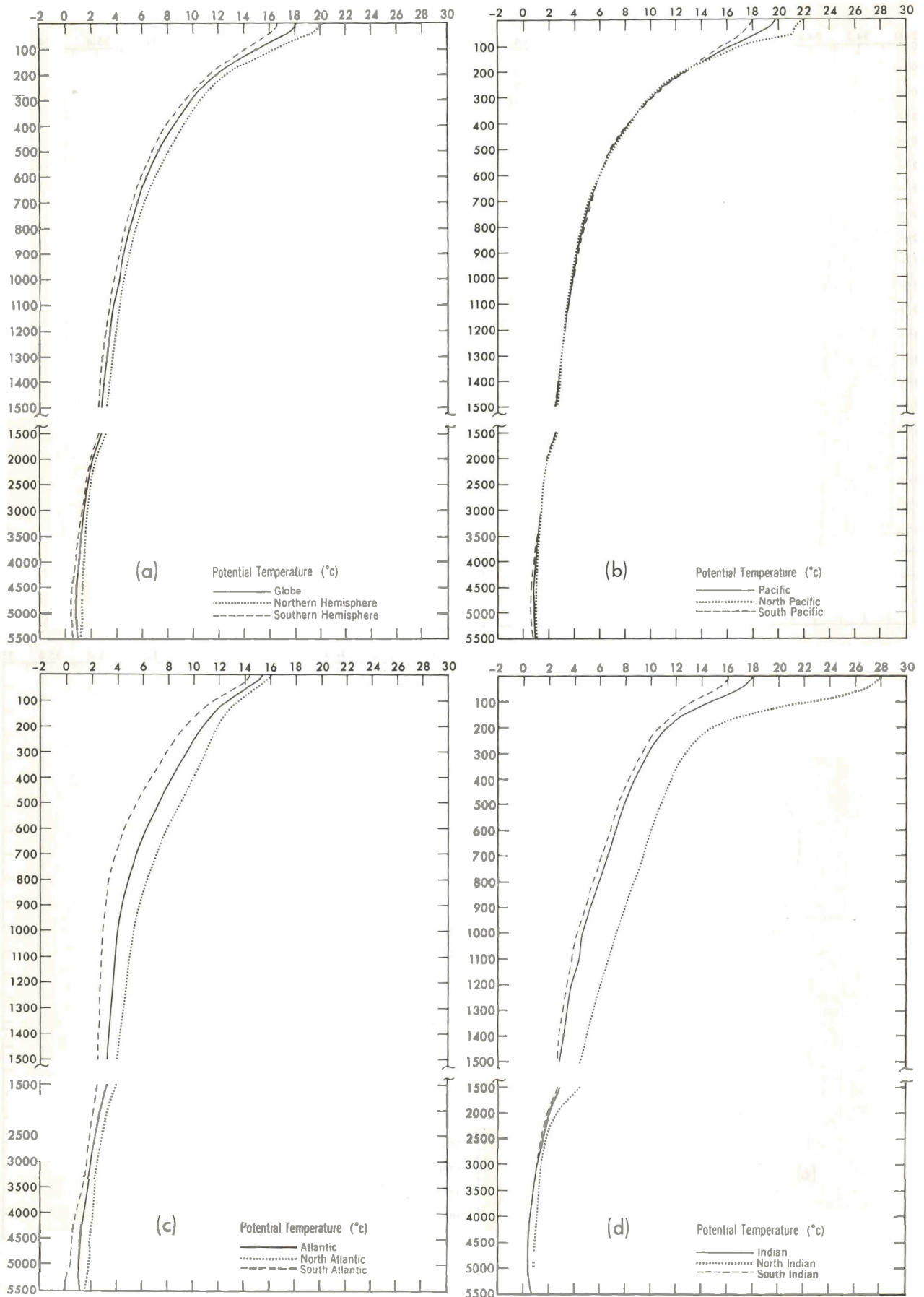


Figure 123.—Basin means of potential temperature (°C) as a function of depth.

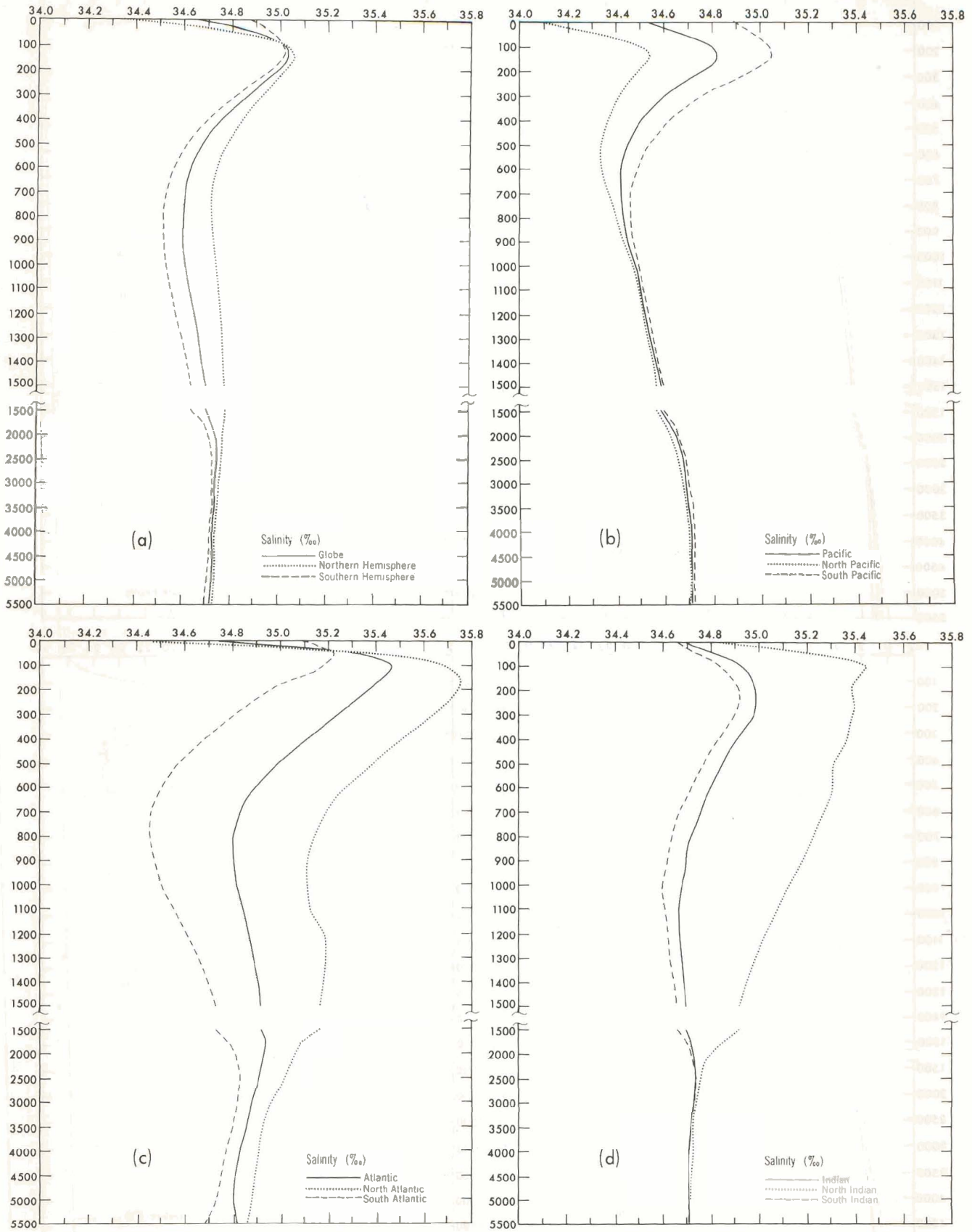


Figure 124.—Basin means of salinity (‰) as a function of depth.

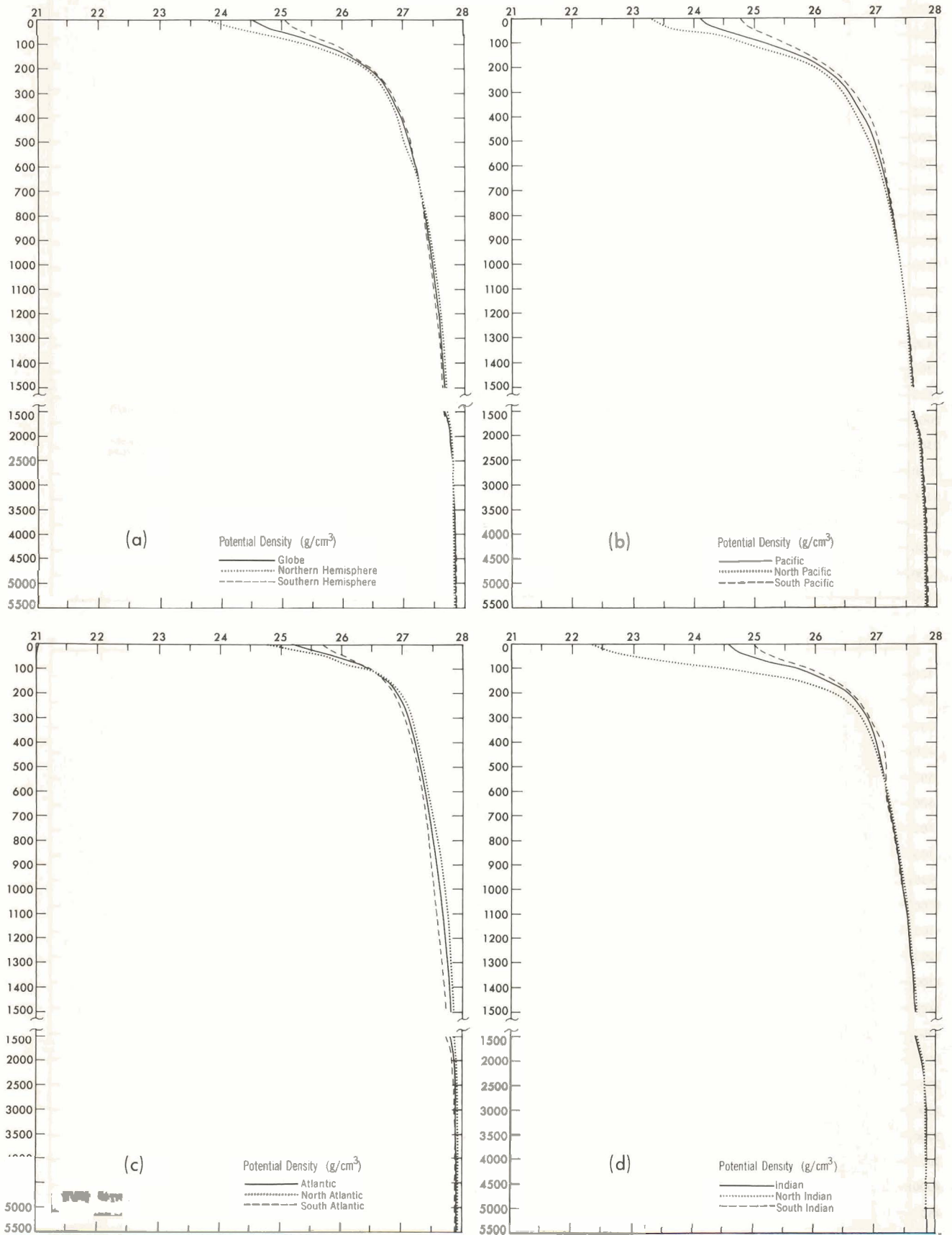


Figure 125.—Basin means of potential density (10^{-3} g/cm^3) as a function of depth.

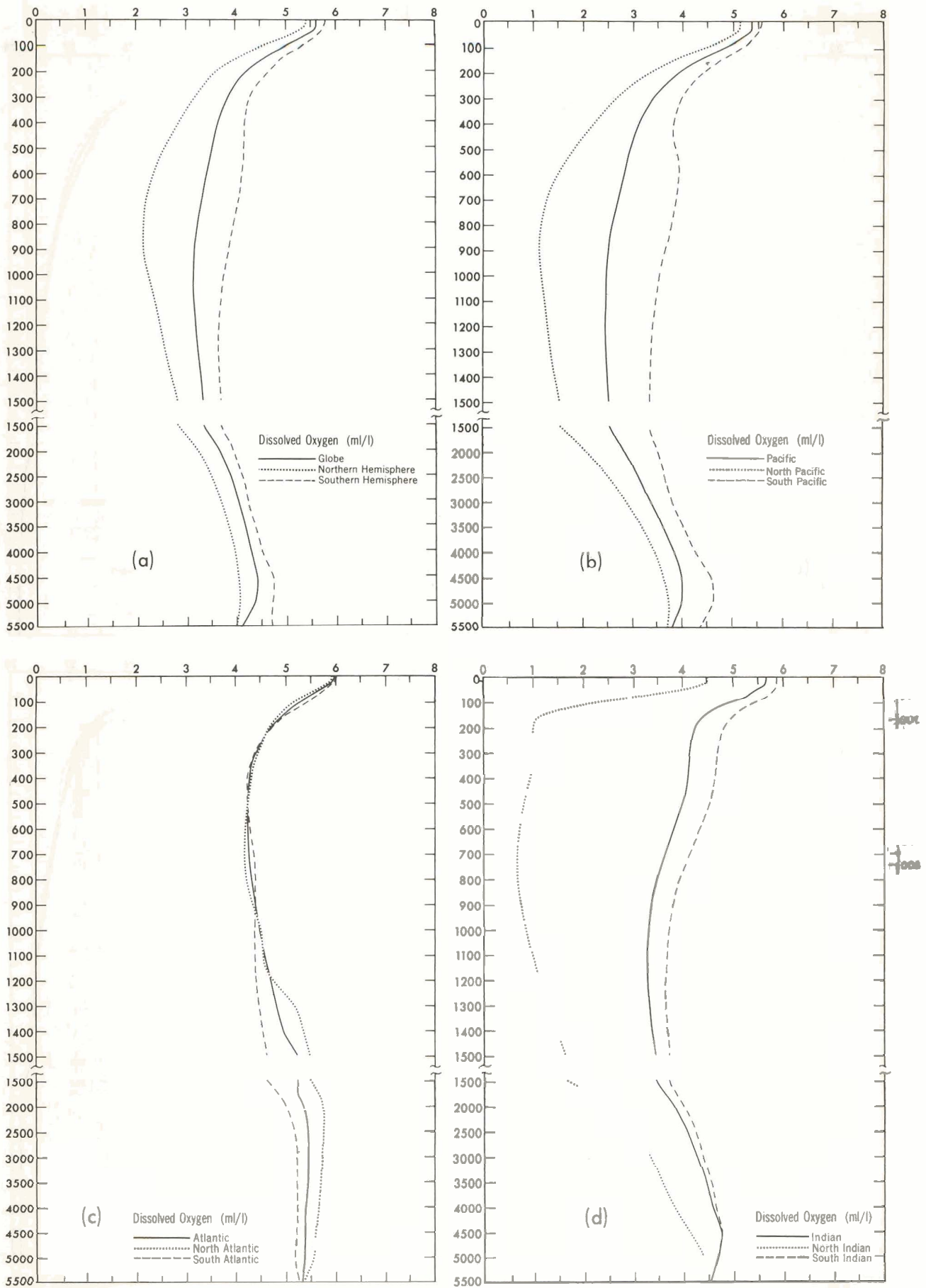


Figure 126.—Basin means of dissolved oxygen (ml/l) as a function of depth.

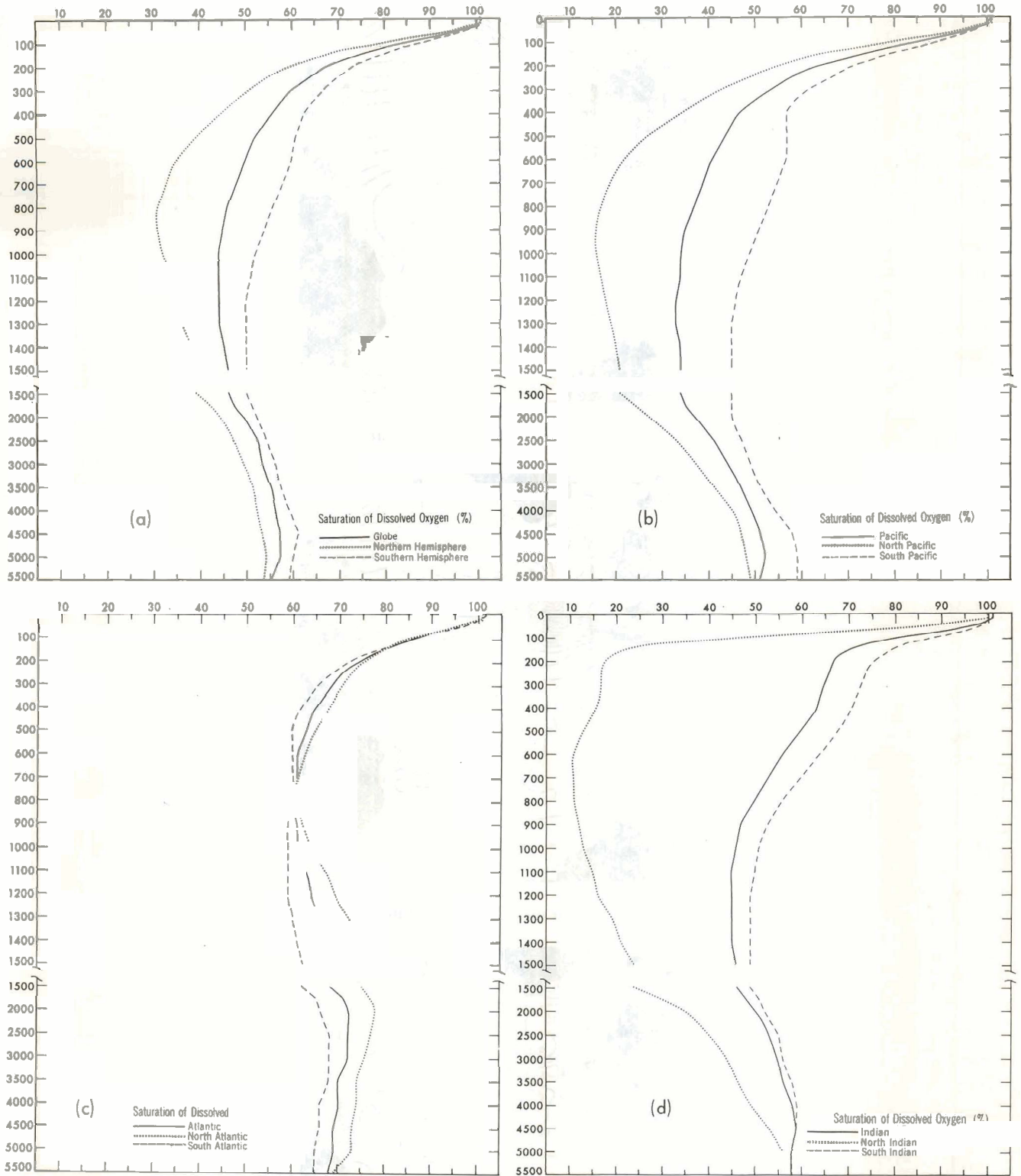


Figure 127.—Basin means of saturation of dissolved oxygen (%) as a function of depth.

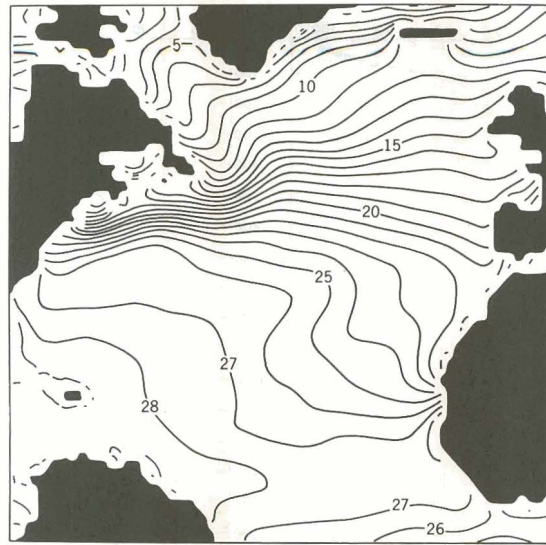


Figure A1.—Standard summer sea surface temperature (°C) analysis.

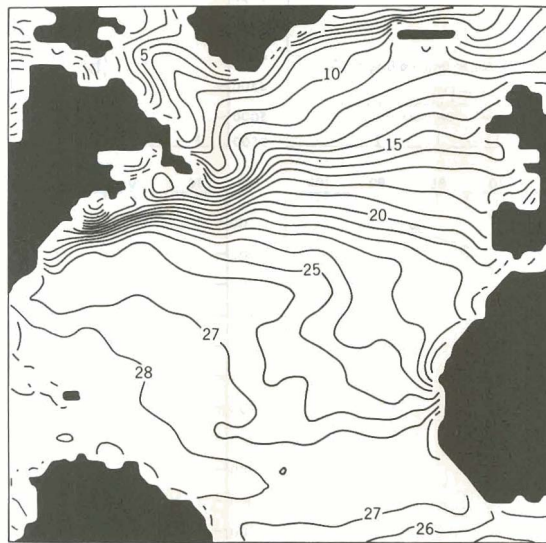


Figure A2.—Test summer sea surface temperature (°C) analysis.

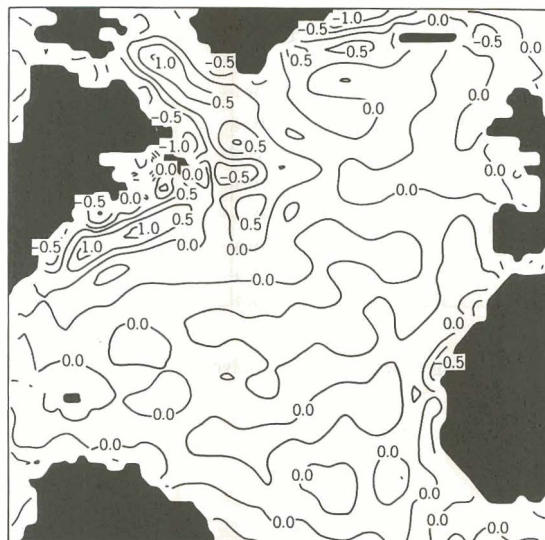


Figure A3.—Test analysis minus standard analysis (°C).

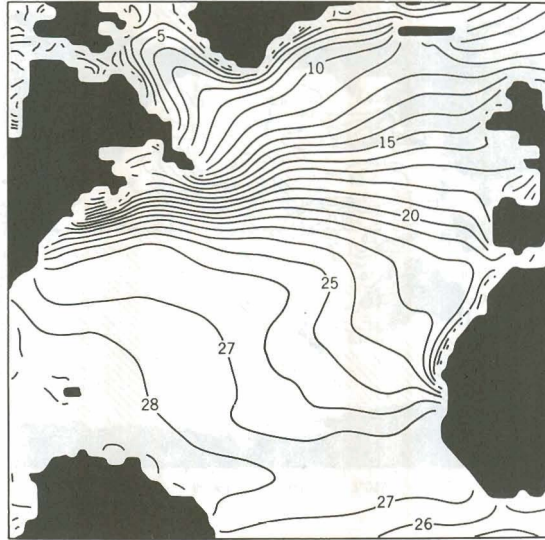


Figure B1.—First guess summer sea surface test analysis ($^{\circ}\text{C}$).

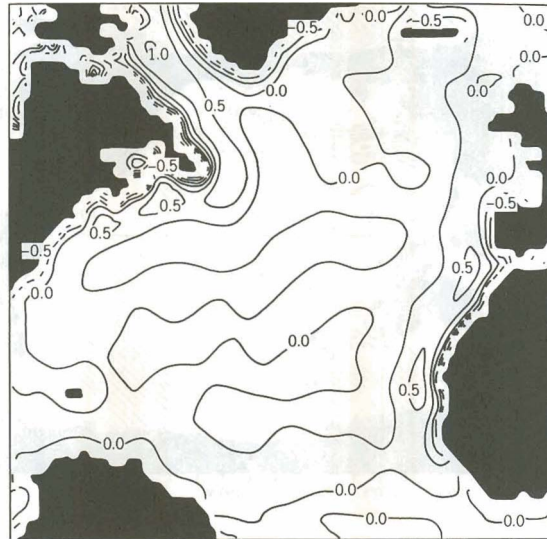


Figure B2.—First guess summer sea surface test analysis minus standard analysis ($^{\circ}\text{C}$).

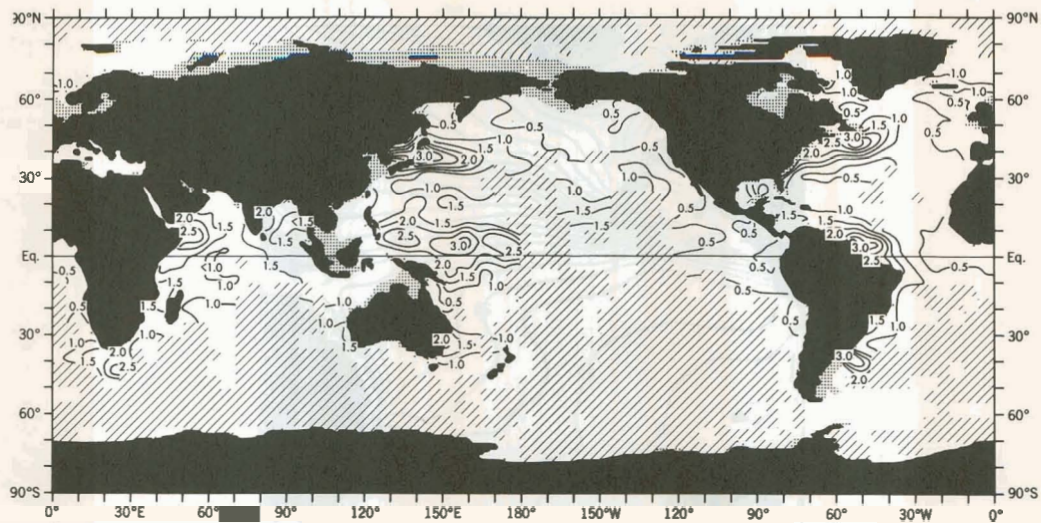


Figure D1.—Annual mean standard deviation of temperature ($^{\circ}$ C) at 150 m.

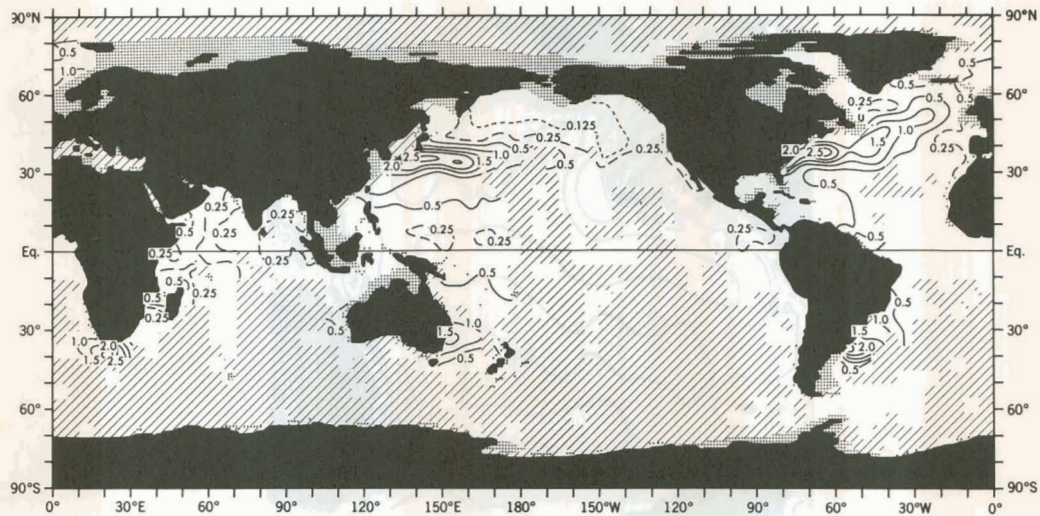


Figure D2.—Annual mean standard deviation of temperature ($^{\circ}$ C) at 500 m.

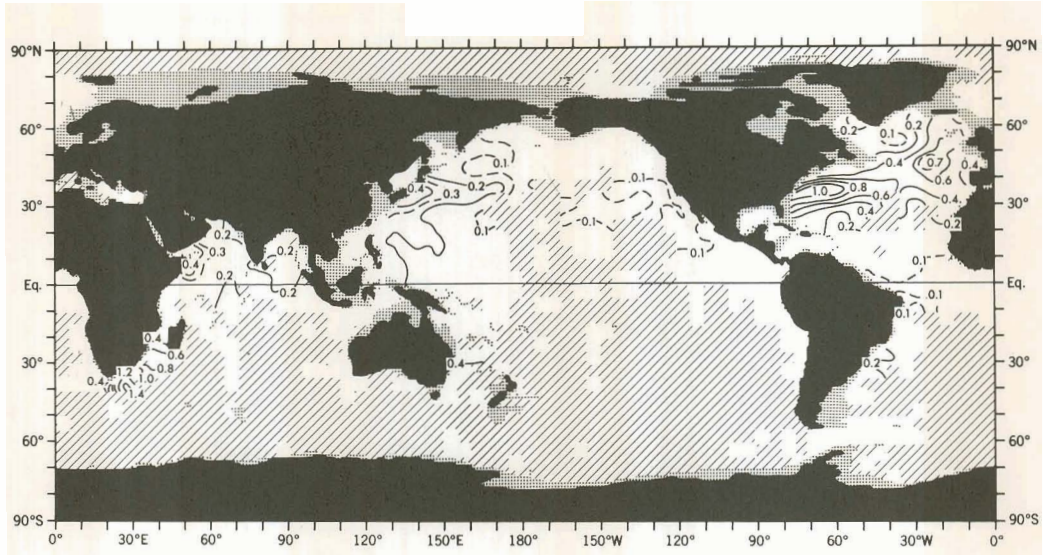


Figure D3.—Annual mean standard deviation of temperature ($^{\circ}$ C) at 1000 m.

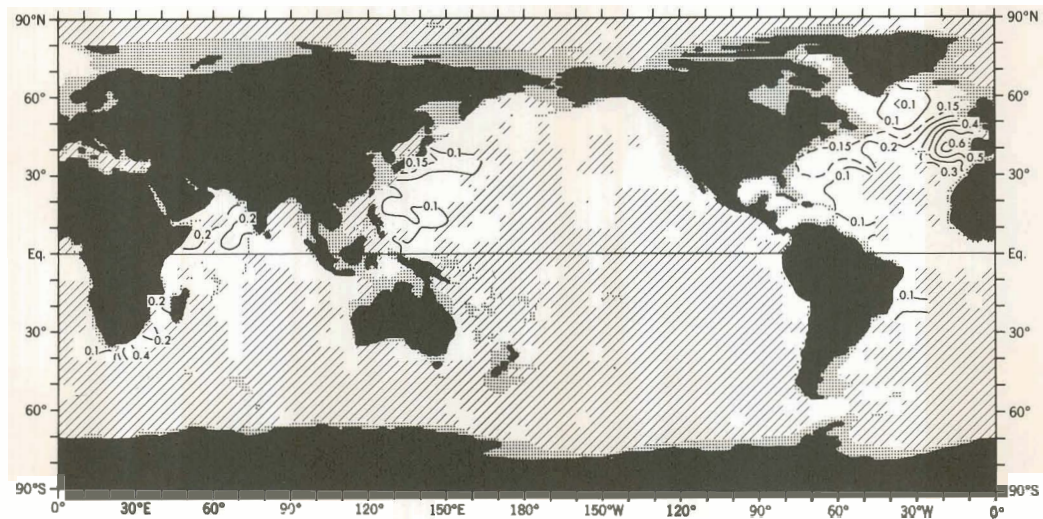


Figure D4.—Annual mean standard deviation of temperature ($^{\circ}$ C) at 1500 m.

